Development and application of a comprehensive methodology for the analysis of global and local emissions of energy systems

ScuDo
Scuola di Dottorato ~ Doctoral School
WHAT YOU ARE, TAKES YOU FAR

Doctoral Dissertation
Doctoral Program in Environmental Engineering (29th Cycle)

Development and application of a comprehensive methodology for the analysis of global and local emissions of energy systems

By

Marco Ravina

******

Supervisors
Prof. M.C. Zanetti, Supervisor
Prof. D. Panepinto, Co-Supervisor

Doctoral Examination Committee:
Prof. L. Lombardi, Referee, Università degli Studi Niccolò Cusano, Roma
Prof. G. Venkatesh, Referee, Karlstad University, Sweden

Politecnico di Torino
2016

Declaration

I hereby declare that, the contents and organization of this dissertation constitute my own original work and does not compromise in any way the rights of third parties, including those relating to the security of personal data.

Marco Ravina

2016

* This dissertation is presented in partial fulfillment of the requirements for **Ph.D. degree** in the Graduate School of Politecnico di Torino (ScuDo).

A mia moglie Laura, che ha condiviso con me questo periodo lungo ed intenso.

Al mio piccolo Dario, che è da poco entrato a far parte della nostra famiglia per scaldare i cuori e infondere energia.

Ai miei genitori, per avermi lasciato fare.

Al prof. Giuseppe Genon, che è stato per me un esempio di rigore scientifico e nobiltà di animo. Un leone dal cuore gentile.

Acknowledgment

Ringrazio le Prof. Mariachiara Zanetti e Deborah Panepinto che mi hanno seguito e sostenuto con professionalità e disponibilità. Sono orgoglioso di averle avute come tutors accademici.

Ringrazio il gruppo SEA del Dipartimento di Energia del Politecnico di Torino, nelle persone di: Alberto Poggio, Michel Noussan, Giulio Cerino e Matteo Jarre, per l'aiuto e i dati forniti sulla parte di modellazione energetica.

Ringrazio il Dipartimento Sitemi Previsionali di ARPA Piemonte, nelle persone di: Anna Maria Gaffodio, Roberta Demaria, Cinzia Cascone, Stefano Bande, Mauro Grosa, per i dati meteo-climatici che mi hanno fornito;

Ringrazio Annamaria Senor e Marco Poggio, per le dritte su AERMOD, SURFER e CALPUFF;

Ringrazio i miei suoceri e mio cognato Sandro per avermi dato la possibilità di sostenere economicamente questo periodo.

Abstract

The energy sector is a source of economic and social progress, but it is also the main responsible of air pollution resulting from human activity, mainly from the combustion of fossil fuels and bioenergy. The impacts on atmosphere may be divided into global effects, due to change in concentration of greenhouse gases, and regional/local effects, due to the dispersion of SO_2, NO_x, particulates and other gases. The aim of this thesis is the development and application of a methodology for calculating the emissions in atmosphere associated with energy management interventions. The methodology aims to characterize and quantify the environmental impacts affecting both the local and global scale. The pollutants involving local effects considered in this study are nitrogen oxides and particulate matter. Globally, the emission of greenhouse gases is considered, by quantifying the equivalent CO_2 (CO_{2eq}) emitted. The environmental impact of an energy option is quantified in terms of its emission balance, i.e. by comparing the present situation with one (or more) future scenarios. The study at the local scale also considers the dispersion of pollutants using modelling tools. The methodology is applied to two case studies located in the Italian Metropolitan City of Turin, characterized by different application contexts and different scales of operation. The first case study is represented by a system for the production and conversion of biogas and biomethane. The analysis of global emissions considers four different operating scenarios. The results show a CO_2 reduction of 1426 t/y for biogas combustion in full cogeneration mode (generation of both heat and electricity). Biomethane for transports scenario provides a similar result (1379

t/y). If biogas combustion with partial cogeneration is considered (generation of electricity only), the CO_2 balance approaches to zero. The evaluation of local impacts is made with two different dispersion models. The application of an Octave-based Gaussian model provides an average increase of concentration both for NO_x and TSP, in the order of units of $\mu g/m^3$. The results of CALPUFF model simulations show a slight decrease of concentration in the order of 10^{-2} $\mu g/m^3$. The second case study consists of a potential extension of the district heating network in the urban area of Turin. The production of local emissions is calculated considering the operation of the main power plants in response to the estimated heat demand. Avoided emissions are calculated simulating the heat production of centralized residential heaters. The results of CALPUFF model simulations show a potential reduction of NO_x average concentration between 1 and 6 $\mu g/m^3$. The results of global emissions show an unfavorable balance in the order of 10^4 t/y of CO_2, that varies depending on the assumptions on the emission factors of the power units.

A comprehensive final discussion is reported after the analysis of the two case studies. The calculation of two indicators (the "thermal benefit vs. local emission indicator" and the "local to global emission ratio") is also included to discuss a possible standardization of the proposed methodology.

This study provides important information on the effects on air quality resulting from the modification of the energetic management of an area or settlement. The employed methodology is consistent and comprehensive in identifying the potential optimal solutions for energy production and management, as well as identifying the consequences to a given scenario under an environmental point of view.

Contents

Abbreviations

ARPA Piedmont Region's Environmental Protection Agency

AwR alkaline with regeneration carbon mineralization

BABIU bottom ash for biogas upgrading

BAT best available techniques

CH_4 methane

CHP combined heat and power

CO_2 carbon dioxide

CO_{2eq} equivalent carbon dioxide

COP21 21st Conference of Parties

CRY cryogenic separation

dLUC direct land use change

GHG greenhouse gas

GWP global warming potential

H_2S hydrogen sulfide

IEA International Energy Agency

iLUC indirect land use change

INDC intended nationally determined contributions

IREA Piedmont Region's emission to atmosphere inventory

L Monin-Obukhov length

LCA life cycle assessment

LPG liquefied petroleum gases

MB membrane permeation

MEA chemical absorption with amine solutions

NG natural gas

NH_3 ammonia

NO_x nitrous oxides

PGT Pasquill – Gifford stability class

PLC programmable logic controller

PM particulate matter

$PM_{2.5}$ particulate matter $\leq$ 2.5 μm

PM_{10} particulate matter $\leq$ 10 μm

PSA pressure swing absorption

PV photovoltaic

PWS pressurized water scrubbing

SCR selective catalytic removal

SO_2 sulfur dioxide

toe ton of oil equivalent

TO-E Torino Est power plant

TO-N Torino Nord power plant

VOC volatile organic compounds

VS volatile solids

WHO World Health Organization

u*surface friction velocity

w*convective velocity scale

z_i mixing height

ρ_a air density

λ excess air-to-fuel ratio

Part 1

General introduction

Chapter 1

Energy production and environment

The use of energy resources and systems will continue to increase in the future to support the world's growing population. These resources must be used in an efficient way, reducing their impacts on human health and the environment, and reflecting other priorities of communities. The economic development is based on the safe and sufficient availability of energy sources, and development is necessary for achieving the standard of living to which most people in the world aspire. However, growth and development must be sustainable. A generally accepted definition of sustainable development is "development which meets the needs of present generations without compromising the ability of future generations to meet their own needs" (WCED, 1987). Sustainable energy development applies the principles of sustainable development to the energy sector.

Sustainable energy development means that the planning and use of energy options should involve human health and environmental impacts, resource exploitation and social equity implications together with the traditional economic and technical issues. This means that economic development and environmental protection objectives should be pursued as for common and strongly linked targets. Global concern over the level of environmental degradation is nowadays of paramount interest, and people expect that economic development should not be pursued causing the deterioration of natural resources.

The production and consumption of heat and electricity generates environmental impacts which must be considered in selecting and developing energy systems. The key to moving towards sustainable energy development is to find the balance between environmental, economic and social objectives of society, and integrating them at the earliest stages of project planning, program development and policy making. Thus, environmental issues must be integrated more effectively into all aspects of energy planning and decision making, to take environmentally clean, economically efficient and socially equitable actions.

Environmental degradation is a problem affecting different scales: local, regional, and global. All forms of energy generation and all steps of the fuel chain, have positive and negative impacts (Figure 1.1). Comparative assessment can be used to match and evaluate impacts of existing and potential energy conversion facilities. The results of comparative assessment can also be useful in the development of energy policies for a country or a region. Several studies have been undertaken in recent years on the environmental effects of fuel chains. These studies provide a basis for a generally accepted framework for comparative assessments, and for the identification of technical issues and uncertainties in the process. The studies have been also addressed towards the identification and quantification of the external costs, i.e. the economic value of health and environmental impacts (IAEA,1999).

In general, assessment and integration of information on health and environmental impacts may contribute to (Table 1.1):

- aware decision making, based on the characterization of potential environmental implications of alternative energy systems;
- improvement of environmental compatibility, e.g. by helping in the identification of optimal areas for reducing emissions, based on a comparative assessment of environmental issues;
- more explicit consideration of environmental effects within a broader decision process;
- information and education of players and people in environmental matters;
- influencing of international environmental policy.

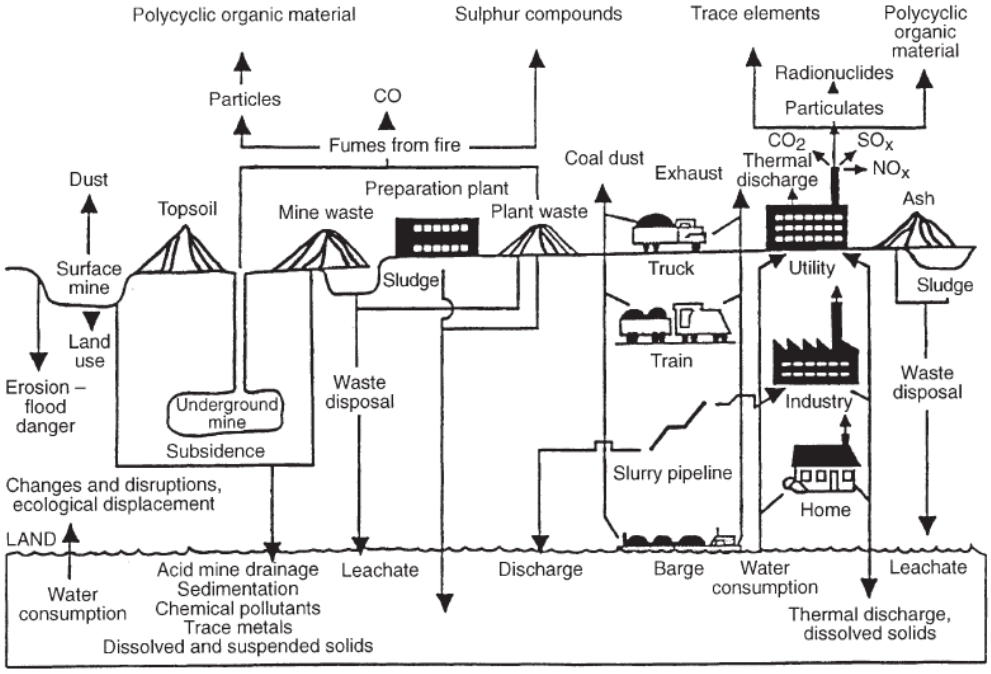

Figure 1.1. Fuel chain concept and its related environmental impacts (source: Oak Ridge National Laboratory, 1992)

The effect of emission on the environment represents an important issue. Since an impact is influenced by the concentration of an emission, the factors by which emissions are dispersed in the environment are relevant. Thus, for emissions into the air, the height of the release, the atmospheric turbulence, the distance to the receptors, the topographic features between the emission source and the receptor, as well as the meteorological factors are all important.

To make possible a comparison of environmental effects of different energy options, there is a need for comprehensive and quantitative indicators of environmental impacts. Such indicators can be needed in different contexts, such as:

- selection of technologies;
- selection between alternative fuel cycles using the same generation technology;
- analysis of impact trends with time;
- comparison between alternative technologies for the reduction in pollution;
- comparison of impacts between different locations.

Primary indicators of health and environmental impacts are estimates of the specific effects themselves, such as increased rates of respiratory illness or damage to trees. The magnitude of pollutant emissions is instead the most common indirect indicator (e.g. tons of NO_x emitted).

The geographical definition of the environmental indicators has a significant relevance. Under this point of view, impacts may be divided into:

- global effects, due to change in concentration of greenhouse gases;
- regional, local and site-specific effects from NO_x, SO_2, particulate and other gases.

The definition and characterization of these impacts is subjected to boundary conditions. The temporal boundary is chosen to assess the period during which the impacts take place. This period can be classified as short term (few years), medium term (a human generation) or long term (many generations). Air pollution is expected to show both short term acute effects and medium term effects (over a lifetime). The second boundary condition is represented by the physical limits within the assessment takes place. Such a boundary can be classified in terms of distance from the energy plant (or from another phase of the associated fuel cycle), differentiating between local (up to 100 km), regional (100-1000 km) or global scale. Local impacts are the effects of emissions acting on the immediate surrounding of the plant. A gaseous plume can instead have an effect many hundreds or thousands of kilometers downwind, generating a regional impact. The emission of carbon dioxide, on the other hand, contributes globally towards global climate change.

The general approach for estimating environmental impact indicators is based on all these aspects and, in particular, on their contribution to the development of the impact pathway approach. Current worldwide studies follow this approach. Some of the advances made in the more recent studies include:

- an explicit life cycle approach and a consideration of the whole fuel chain, rather than analysis on the only energy generation phase;
- greater use of numerical analysis through atmospheric dispersion modeling, to estimate the spatial distribution of the impacts;
- more comprehensive and dedicated engineering analysis for estimating emissions from power plants, rather than relying on previous estimates or default references;

- complete consideration of different impact evolution scenarios;

If the objective of a study is the comparison of environmental impacts, it is important to conduct the analysis in a consistent way. The preferred approach for comparative assessment of environmental impacts is the assessment of the full fuel cycle. This implies evaluating the major effects associated with the production of fuel used to produce energy, construction of the generation facility, operation of the facility, decommissioning, transportation, and disposal of wastes. In many cases, the level of the objective to be pursued will define the level of detail in the comparative assessment. Nevertheless, it must be considered that if assessments are being undertaken for comparative purposes, then all options being considered must be assessed on the basis of the same temporal and spatial boundaries.

Identification, quantification and localization of environmental impacts are subjected to a great deal of uncertainty, that must be estimated at each step in the methodology. Often, estimated impacts can cover a wide range, depending on the initial assumptions. Uncertainty in all steps of the methodology, input data and final results must be considered so that better decisions are made. Thus, it is important that information on uncertainty is clearly included in the presentation of results.

Table 1.1. Use of information on environmental effects (source: modified from IAEA, 1999)

Action	Use of environmental information
Planning	Identify levels of demand side management program to address societal issues (e.g. greenhouse gas reduction)
	Evaluate external impacts and costs associated with imports and exports of energy
	Compare alternative plans and generation options based on environmental damage
Investment/decision making	Evaluate investment alternatives which reflect consideration making of environmental, economic and social factors
	Contribute to decisions about retiring or rehabilitating existing plants
	Compare alternative sites and generation options based on environmental damage and other criteria
Selection of environmental protection technologies	Assess the marginal cost of damages in comparison with the marginal cost of control associated with control technologies, to aid in decisions about economically efficient control technologies
System dispatch	Assess the environmental implications of the order of dispatch of energy generation options for the system
Policy making	Develop regional, national and/or international targets and/or policies with the goal of enhancing environmental performance and minimizing environmental degradation
	Contribute to assessment of optimal reference starting points for emission trading schemes (locally, regionally, nationally and/or internationally, based on potential environmental damages)
	Evaluate the benefits and costs of new proposed environmental regulations

1.1 Air pollution: global and local emissions

The energy sector is a push of economic and social progress, but it is also the largest source of air pollution resulting from human activity, mainly from the combustion of fossil fuels and bioenergy. Air pollution is often considered an urban issue, as economic activities and energy demand are concentrated in cities, where the critical situations are usually detected. But air pollution does not affect only the urban areas, as emission sources might be found almost everywhere, even in rural areas. Moreover, pollutants dispersion may interest large distances in the atmosphere, causing regional and global impacts.

The global energy mix is still dominated by fossil fuels. Despite the increased attention given to low-carbon sources of energy, the overall share of oil, coal and natural gas in global energy consumption has been substantially stable over the last 25 years (IEA, 2015). Fossil fuels accounted for 81% of total energy use in 1989, the same percentage as in 2014 (IPCC, 2014). Over this period, the use of natural gas increased even more, from 19% to 21%; coal consumption also raised from 25% to 28%, and the share of oil consumption declined from 37% to 31%. The role of bioenergy has remained steady, meeting around 10% of global energy needs.

The relationship between fuel production, their use and the resulting emissions is not direct. The quantity and quality of emission depend on fuel nature and use, and different grades or qualities of fuel contain substances in different quantities. Pollutants may be reduced or removed from the process at various stages before combustion (e.g. oil refining or coal washing), and the nature of the same combustion process can influence emissions levels (e.g. the temperature of combustion). Finally, post-combustion technologies may be used to chemically alter or limit harmful emissions (e.g. catalytic converters). This means that there is no single level of emissions per unit of a specific fuel but, rather, a range of emission factors depending on such variables.

Nitrogen oxides (NO_x), particulate matter (PM) and sulphur dioxide (SO_2) are between the most damaging of the air pollutants derived from energy activities and those for which the most reliable systematic data are available.

Power generation is one of the main sources of global sulfur dioxide emissions, accounting for around 27 Mt of SO_2 in 2015, one-third of the global total. NO_x emissions amount to 14% of the total, while particulate matter

emissions amount to 5% of the total (in terms of $PM_{2.5}$). Coal is the major fuel generating air pollution in the power sector: around three-quarters of the SO_2 emissions from the sector, 70% of NO_x emissions and over 90% of $PM_{2.5}$ emissions are attributable to this fuel. Oil-fired power generation accounts for 7% of the global emissions of SO_2, given the limited contribution (4%) to global electricity generation. Oil-fired emissions come mainly from obsolete power plants with minimal pollution control technology installed. Oil-related emissions also include significant quantities of NO_x and $PM_{2.5}$. Natural gas-fired plants generally emit fewer air pollutants than coal and oil-fired power plants. Data for 2015 reveal that gas-fired generation is responsible for around 20% of NO_x emissions from power generation, but not for SO_2 or $PM_{2.5}$. The low-sulfur emissions from gas-fired power generation are due to the usual treatment of natural gas (i.e. sulfur removal) before its commercialization. Biomass plays a negligible role in global power generation, accounting for around 2% of total output, thus contributing not much to air pollution. On the other hand, if relative terms are considered (emissions per unit of output), biomass performs only slightly better than coal-fired plants for NO_x emissions, moderately worse for $PM_{2.5}$ emissions, but is much better in terms of SO_2 emissions (Figure 1.2).

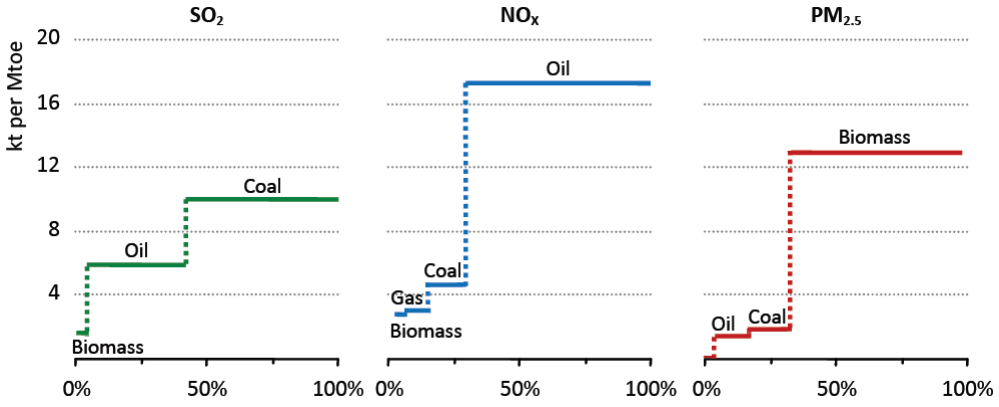

Figure 1.2. Global average emissions factors and share of major pollutant emissions by fuel, 2015 (source IEA, 2016).

The European power sector is subjected to a major transformation because of the last decisive energy and climate policies issued by the EU. The growth of

electricity demand is strongly hindered by a strong push towards energy efficiency.

Considering the projection trends to 2040 (IEA 2016), power generation from coal is expected to decrease by more than three-quarters, while the output from renewable energy technologies doubles. The growth in renewables is dominated by the deployment of wind and solar photovoltaics (PV), although biomass also improves strongly. Natural gas is still expected to constitute the backbone of Europe's power system, as it provides flexibility and reliability. In fact, the share of gas-fired power in the European power mix is expected to increase more by 2040, from 16% to 20%. The distribution of emissions between the different energy sectors is reported in Figure 1.3.

In the last years, the European Union issued a very stringent set of controls over the emissions from power stations. The directives plan the retirement of facilities that cannot comply with the regulation: in the period 2016-2023, plants can decide whether planning the adjustment to the emissions limit values or retire (EC, 2009). In terms of particulate matter, the limit for $PM_{2.5}$ is 10-30 mg/m^3, depending on the plant capacity and whether it is a new or existing facility. NO_x emissions limits are between 200 and 300 mg/m^3 for existing plants and between 150 and 300 mg/m^3 for new plants. For sulfur dioxide, new power stations must emit no more SO_2 than 150-400 mg/m^3, depending on the plant capacity, while the range for existing plants is between 200 and 400 mg/m^3 (Table 1.2).

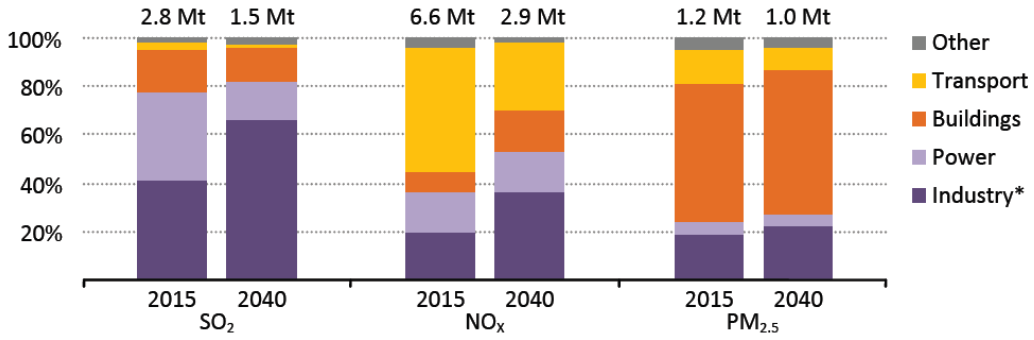

Figure 1.3. Emissions by air pollutant and by energy sector in the European Union, present situation and future projection (source: IEA, 2016).

The imposition of strict emissions standards for the main air pollutants fosters the installation of control equipment technologies in new plants, as well as new investments in existing plants to update control technologies. The abatement techniques for air pollutants in power generation can be divided into two categories (Figure 1.4):

- primary combustion technologies or measures that prevent the generation of an emission;
- end-of-pipe technologies that capture pollutants to avoid them being released into the environment.

Primary combustion technologies to reduce thermal NO_x emissions include improved combustion techniques and the installation of low-NO_x burners in process heaters and industrial heat and electricity generation plants. Low-NO_x burners operate by phasing air and fuel injection to achieve lower temperature flames, accounting the fact that there is an exponential positive relationship between combustion temperature and thermal generation of NO_x. Another primary combustion technology is fluidized-bed combustion technology for solid fuels that reduces the emission of both SO_2 and NO_x (Bell and Buckingham).

End-of-pipe technologies focus on the removal of SO_2, PM and NO_x from flue gases before release into the atmosphere, by means of either physical separation or chemical reactions. This group of technologies includes: electrostatic precipitators (to separate PM from gaseous streams); flue-gas desulfurization plants that use a sorbent (typically alkaline compounds such as limestone) to absorb and/or oxidize SO_2 into solid matter, which is then physically separated from the flue gases; and selective catalytic reduction systems (using ammonia) or selective non-catalytic reduction systems (using urea) that reduce the NO_x in the flue gas to nitrogen and water (IEA, 2016).

Table 1.2. Emission limits for existing and new power plants in selected countries/regions (mg/m^3) (source: IEA, 2016).

Region	Policy	SO_2		NO_x		PM	
		Existing	New	Existing	New	Existing	New
European Union	Industrial Emissions Directive	200-400	150-400	200-450	150-400	20-30	10-20
China	Emission standard of air pollutants for thermal power plants	200-400	100	200	100	30	30
United States	New Source Performance Standards	160-640	160	117-640	117	23	23
India	Environment Protection Amendment Rules, 2015	200-600	100	300-600	100	50-100	30
South Africa	The Minimum Emissions Standards are published by the government	3,500	500	1,100	750	100	50

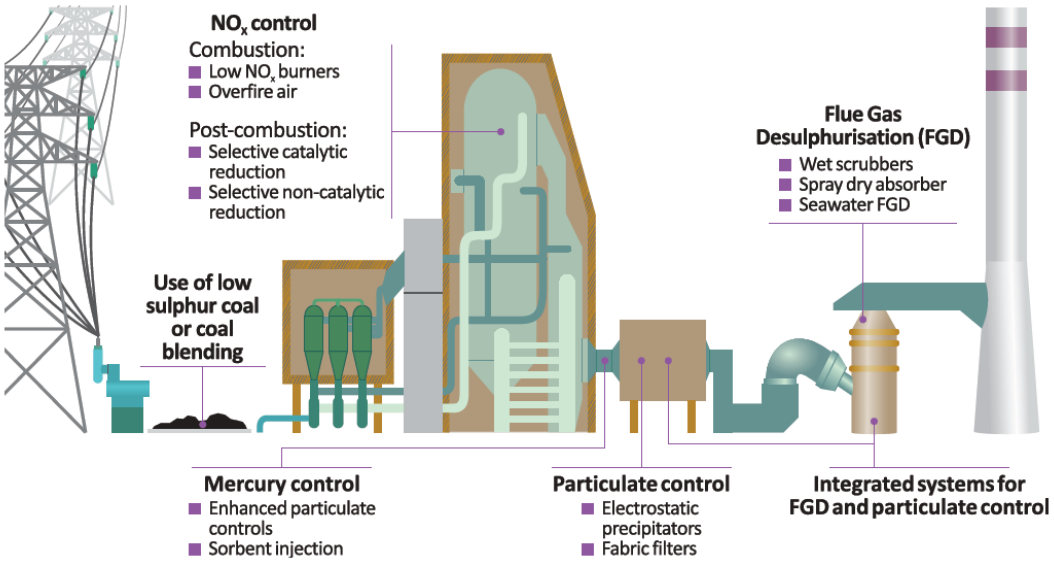

Figure 1.4. Typical emissions control systems for power plants (source: Moretti and Jones, 2012)

Greenhouse-gas emissions from the energy sector represent almost two-thirds of all anthropogenic greenhouse gas emissions. CO_2 emissions from the sector have increased over the last decades, to the highest levels ever. Effective action in the energy sector is thus essential to mitigating the problem of climate change. One clear indicator of the dimension of this challenge is the fact that the total volume of global CO_2 emissions from the energy sector over the past 27 years matched the total level of all previous years. In the period 2000-2014, the contribution of coal to energy-related CO_2 emissions has increased from 38% to 44%; the share of natural gas remained unchanged at 20%; that of oil declined from 42% to 35% (IPCC, 2014).

Methane (CH_4) and nitrous oxide (N_2O) are other powerful greenhouse gases emitted by the energy sector. Methane originates mainly from oil and gas extraction, transformation and distribution, and accounts for around 10% of energy sector emissions. Much of the remainder is nitrous oxide emissions from energy transformation, industry, transport and buildings (Figure 1.5).

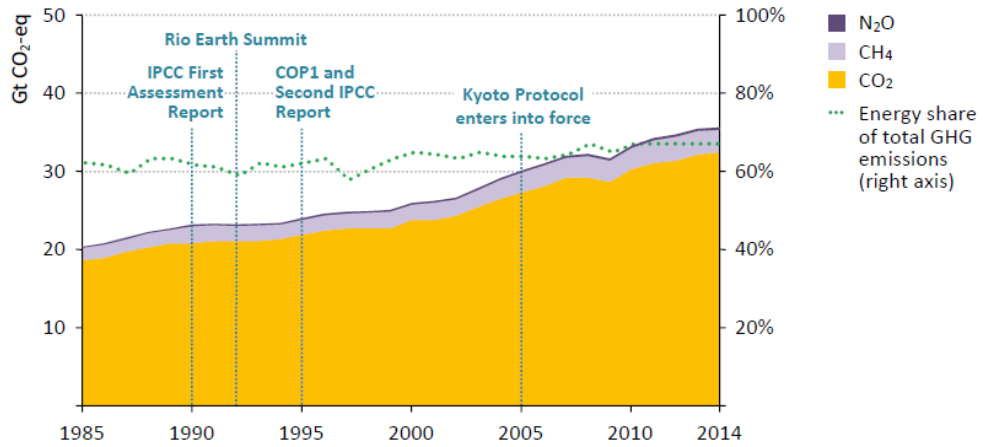

Notes: CO_2 = carbon dioxide, CH_4 = methane, N_2O = nitrous oxide. CH_4 has a global warming potential of 28 to 30 times that of CO_2, while the global warming potential of N_2O is 265 higher than that of CO_2.

Figure 1.5. Global anthropogenic energy-related greenhouse-gas emissions by type (source: IEA, 2015)

In 2014, the growing trend in global energy-related CO_2 emissions stalled, with an estimated total of 32.2 Gt, unchanged from the preceding year. Energy-related CO_2 emissions in the European Union decreased by more than 200 Mt (around 6%), because of the decline of fossil fuels demand. Power generation

from non-hydro renewables grew by 12%, as they continued to benefit from active decarbonisation policies, while natural gas demand declined by 12%, partly due to the mild winter. Analysts are detecting initial signs of a decoupling between energy-related emissions and economic growth in some parts of the world: in fact, for the first time in 40 years, a stop or reduction in total global emissions was not associated with an economic crisis. It is true that clear conclusions cannot be drawn from the data for a single year, but this datum represents a positive sign that a committed climate action has the potential to achieve such a decoupling.

The Intended Nationally Determined Contributions (INDC) of the EU countries include challenging targets to reduce domestic GHG emissions by at least 40% in 2030, compared with 1990 levels (Figure 1.6 and Table 1.3). This target is based on the 2030 framework for energy and climate policies issued by the European Union, which also sets out objectives to improve energy efficiency and increase the use of renewable sources of energy. The European Union's own assessment of the effects of the 2030 framework indicates that CO_2 emissions from the energy sector will fall by around 37% and non-CO_2 greenhouse gases by around 55% (PBL, 2014). The 2030 framework builds on the target to reduce EU GHG emissions by 20% by 2020, which the EU is on track to meet, with energy sector CO_2 emissions in 2014 being around 22% below 1990 levels. Both the 2020 and 2030 emissions targets represent important milestones towards the EU's long-term objective of cutting emissions by at least 80% by 2050.

If the INDC Scenario is considered, the CO_2 energy-related emission in the EU shifts from above 3.3 Gt in 2013 to 2.4 Gt by 2030, that means a decrease at nearly double the average annual rate observed since 2000. Renewables cover more than 50% of EU's power generation capacity in 2030. Natural gas-fired capacity increases by one-third, to reach 300 GW, while coal-fired capacity declines by nearly 40%, to stand at around 120 GW. The carbon intensity of the EU's power sector is expected to halve by 2030. Around one quarter of total generation is expected to come from variable renewables (wind and solar). The consequence is the need to invest in greater levels of interconnection, as well as in upgraded distribution networks and metering.

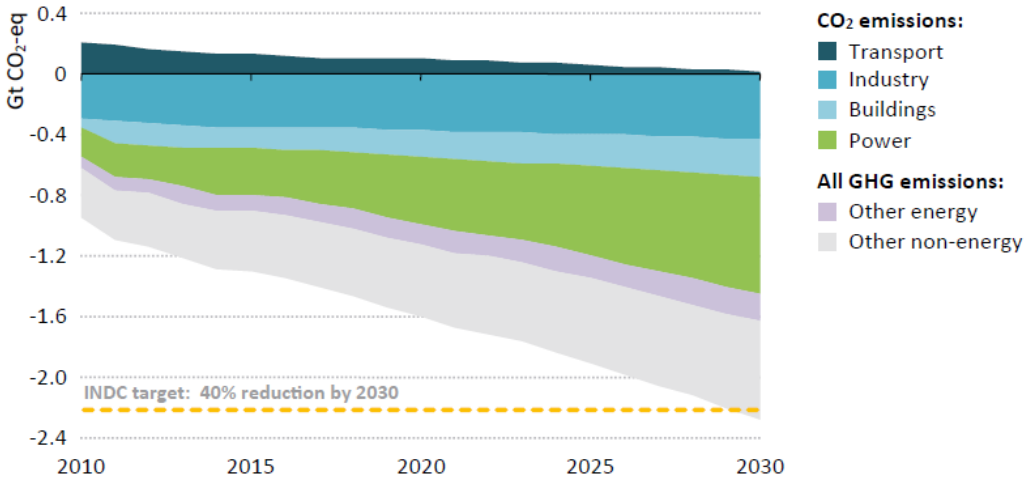

Figure 1.6. European Union energy-related greenhouse-gas emissions reductions relative to 1990 in the INDC Scenario (source IEA, 2015)

Table 1.3. Current and projected CO_2 emissions in the European Union by type of fuel (source: modified from IEA, 2015)

Fuel type	**CO_2 emissions (Mt)**				
	1990	**2013**	**2020**	**2025**	**2030**
Coal	1,172	914	648	443	278
Oil	197	60	35	22	17
Natural gas	128	258	276	309	294

Recently, the International Energy Agency (IEA, 2015) proposed a near-term strategy, based on available technology and proven policy measures. Adoption of these measures can improve the recently observed decoupling of emissions growth from economic growth. This represents an important first step towards the achievement of the long-term commitment discussed in the recent COP21 Conference held in Paris, that considers a maximum temperature rise of 2 °C. The proposed policy measures are:

- increasing energy efficiency in the industry, buildings and transport sectors.
- progressively reducing the use of the least-efficient coal-fired power plants and banning their construction.
- increasing investment in renewable energies to $400 billion in 2030.
- gradually phasing out subsidies to fossil-fuel consumption.
- reducing methane emissions from oil and gas production.

Existing national commitments and nations' engagement in this process is a clear signal of collective willingness to contribute to international climate objectives. But the extent of the proposed changes is not enough and more can still be done. But can it be joined with other government priorities, such as economic growth and energy security and affordability? And in what timescale?

While low-carbon technologies are nowadays becoming available and affordable, the pace of transformation needs to be accelerated and must overcome new challenges. This puts an important emphasis on bringing to maturity the most promising technologies in terms of emissions reductions in the future. The process of transformation in the energy sector (as for other sectors) can be very long, reflecting the need to redesign both the supply infrastructure and end-use energy equipment, while conforming to consumer preferences. In this perspective, low-carbon power generation technologies that have long been employed, such as hydropower (the largest source of low-carbon generation today), nuclear power (the second-largest source), bioenergy and geothermal continue to play an important role to decarbonise the power sector. But much of the transformational change needed in the energy sector to meet the 2 °C climate goal has still to be put in place (IEA, 2015). The achievement of this target requires coordinated national, regional and local action, regulated by appropriate policies and standards, and engagement of both public and private finance for low-carbon energy infrastructures and supply. A strong international framework is then needed to coordinate these national efforts and then progressively to amplify them until low-carbon energy investment becomes the global norm.

1.2 Air pollution effects on health and environment

Air pollution has many undesirable effects, the extent of which is determined by the levels of concentration of the different pollutants. There is a range of negative health impacts, adverse impacts on vegetation (leading to lower agricultural yields), acidification (leading to acid rain) and eutrophication. The

characteristics of different pollutants define their health impacts: even relatively slight exposure may come with high health risks for vulnerable segments of the population.

Existing studies of the economic impacts of air pollution differ in many aspects (e.g. geographic and sectoral coverage, methodology), but most conclude that the external costs of inaction are high and overstep the costs of taking mitigating measures. The costs associated with the health impacts tend to dominate any overall economic assessment.

The present study is focused on the emission of NO_x and particulate matter as local pollutants, as well as on the global contribution to the greenhouse effect. The main phenomenological features of the greenhouse effect and local pollution, and the effects the pollutants on health and environment is reported in the following paragraphs.

1.2.1 Contribution to greenhouse effect

The greenhouse effect is the process by which radiation from a planet's atmosphere warms the planet's surface to a temperature above what it would be without its atmosphere. Earth's natural greenhouse effect is critical to supporting life. Human activities, primarily the burning of fossil fuels and clearing of forests, have intensified the natural greenhouse effect, causing global warming.

Recent publications issued by the Intergovernmental Panel on Climate Change (IPCC, 2014), state that *"human influence on the climate change is clear. Warming of the climate system is unequivocal, and since the 1950s, many of the observed changes are unprecedented over decades to millennia. The atmosphere and ocean have warmed, the amounts of snow and ice have diminished, and sea level has risen"*.

In each of the last three decades, the surface of the Earth has been successively warmer than any preceding decade since 1850. The period 1983-2012 was very likely the warmest period of the last 800 years in the Northern Hemisphere, where such assessment is possible, and likely the warmest 30-year period of the last 1400 years.

In last 50 years, changes in climate have caused impacts on natural and human systems on all continents and across the oceans. Impacts are attributed to observed climate change and indicate the sensitivity of natural and human systems

to changing climate. The evidence of observed climate change impacts is strongest and most visible for natural systems. Some impacts on human systems may also be attributed to climate change, with a major or minor confidence depending on the aspects involved.

The cross-linked impacts observed across the world regions are briefly represented in Figure 1.7. This figure is based on the available scientific literature since the IPCC Fourth Assessment Report (AR4) and shows how there are substantially more impacts in recent decades now attributed to climate change. Attribution requires defined scientific evidence on the role of climate change. The publications supporting attributed impacts reflect a growing basic knowledge, but publications are still limited to many regions, systems and processes, highlighting gaps in data and studies.

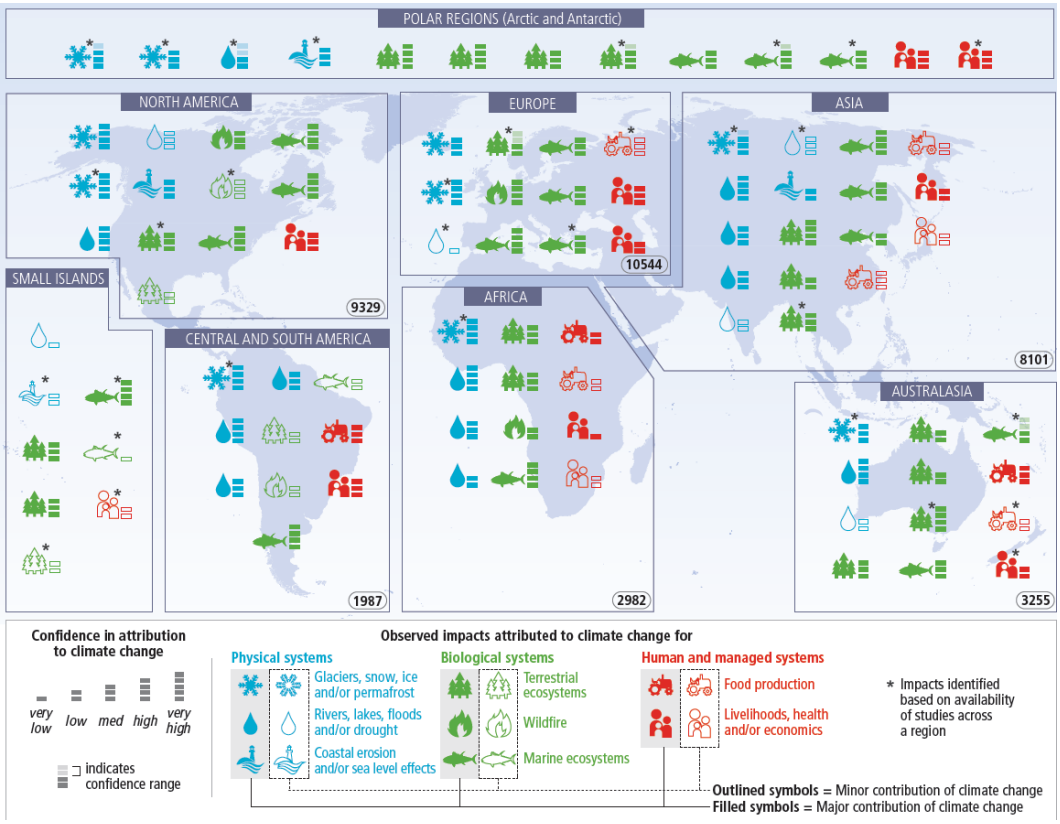

Figure 1.7. Widespread impacts attributed to climate change based on the available scientific literature since the IPCC AR4. Symbols indicate categories of attributed impacts, the relative contribution of climate change (major or minor) to the observed impact and confidence in attribution. Numbers in ovals indicate regional totals of climate change publications from 2001 to 2010, based on the Scopus bibliographic database for publications in English with individual countries mentioned in the title, abstract or keywords (source: IPCC).

In many regions, changes in precipitation rate or snow and ice melting are affecting **hydrological systems**, altering water resources in terms of quantity and quality. Glaciers continue to shrink almost worldwide due to climate change, with consequences for runoff and water resources downstream. Climate change is causing permafrost warming and thawing in high-latitude regions and in high-elevation regions.

Many **terrestrial and aquatic species** have shifted their activities, migration patterns, diffusion and species interactions in response to ongoing climate change. While only a few recent species extinctions have been attributed to climate change, natural global climate change at rates slower than current anthropogenic

climate change caused significant ecosystem shifts and species extinctions during the past millions of years.

Increased tree mortality, observed in many places worldwide, has been attributed to climate change in some regions. Increases in the frequency or intensity of **ecosystem disturbances** such as droughts, windstorms, fires have been detected in many parts of the world and, in some case, are attributed to climate change. Numerous observations over the last decades in all ocean basins show changes in abundance.

Some impacts of **ocean acidification** on marine organisms have been attributed to human influence, as the declining growth rates of corals. Oxygen minimum zones are progressively expanding in the tropical Pacific, Atlantic and Indian Oceans, due to reduced ventilation and O_2 solubility in warmer, more stratified oceans, and are constraining fish habitat.

Assessment of many studies covering a wide range of regions and crops shows that negative impacts of climate change on **crop yields** have been more common than positive impacts. The smaller number of studies showing positive impacts relate mainly to high-latitude regions. Climate change has negatively affected wheat and maize yields for many regions and in the global aggregate. Effects on rice and soybean yield have been smaller in major production regions and globally. Several periods of rapid food and cereal price increases following climate extremes in key producing regions indicate a sensitivity of current markets to climate extremes among other factors.

At present, the worldwide burden of **human ill-health** from climate change is relatively small compared with effects of other stressors and is not well quantified. However, there has been increased heat-related mortality and decreased cold-related mortality in some regions because of warming. Local changes in temperature and rainfall have altered the distribution of some waterborne illnesses and disease vectors.

Some **indirect impacts** of climate change are evident to intermediate systems and then to people (Figure 1.7). The changes in climate feeding into the cascade, in some cases, are linked to human drivers, while, in other cases, there is not sufficient information to establish the drivers.

Changes in many **extreme weather and climate events** have been observed since many decades. Some of these changes have been linked to human

influences, including a decrease in cold temperature extremes, an increase in warm temperature extremes, an increase in extreme high sea levels and an increase in the number of heavy precipitation events in several regions.

1.2.2 Local pollutant emission

As already mentioned, the effect of a pollutant on human health and ecosystems depend on its characteristics and concentration. For some substance, even relatively slight exposure may come with high risks for vulnerable segments of populations and ecosystems.

Nitrogen oxides formation occurs by three fundamentally different mechanisms. The principal mechanism of NO_x formation in natural gas combustion is thermal NO_x. The thermal NO_x mechanism occurs through the thermal dissociation and subsequent reaction of nitrogen (N_2) and oxygen (O_2) molecules in the combustion air. Most NO_x formed through the thermal NO_x mechanism occurs in the high-temperature flame zone near the burners. The formation of thermal NO_x is affected by three combustion factors:

- oxygen concentration;
- peak temperature;
- time of exposure at peak temperature.

As these three factors increase, NO_x emission levels increase. The emission trends due to changes in these factors are consistent for all types of natural gas-fired boilers and furnaces. Emission levels vary considerably with the type and size of the combustor and with operating conditions (e.g., combustion air temperature, volumetric heat release rate, load, and excess oxygen level).

The second mechanism of NO_x formation, called prompt NO_x, occurs through early reactions of nitrogen molecules in the combustion air and hydrocarbon radicals from the fuel. Prompt NO_x reactions occur within the flame and are usually negligible when compared to the amount of NO_x formed through the thermal NO_x mechanism. However, prompt NO_x levels may become significant with ultra-low-NO_x burners.

The third mechanism of NO_x formation, called fuel NO_x, stems from the evolution and reaction of fuel-bound nitrogen compounds with oxygen. Due to the characteristically low fuel nitrogen content of natural gas, NO_x formation through the fuel NO_x mechanism is insignificant.

Nitrogen dioxide (NO_2) is to be considered among the more hazardous air pollutants, both because it is an irritating substance, and because it generates, in the presence of strong sunlight, a series of photochemical reactions that lead to the formation of polluting substances (for example, ozone), generally indicated with the term *photochemical smog*. A fundamental contribution to pollution by nitrogen dioxide and photochemical derivatives is due, in cities, to the exhaust gases of motor vehicles.

Nitrogen dioxide is a toxic gas, irritating to mucous membranes, and is responsible for specific diseases affecting the respiratory system, with decreases in lung defense (bronchitis, allergies, irritation). Recent studies by the WHO have associated events such as mortality, hospital admissions and respiratory symptoms, with short and long term exposure to nitrogen dioxide in concentrations equal to or below the current EU limit values (ARPA, 2015).

Nitrogen oxides contribute to the formation of acid rain and favor the accumulation of nitrates in the soil that can cause alteration of environmental ecological balance. The limit values and the alarm threshold defined by Italian regulation for NO_2 and NO_x are reported in Table 1.4.

Table 1.4. Limit exposure values for nitrous oxides in Italian regulation (Legislative Decree n.155/2010)

Averaging period	Limit value (293 K, 101.3 kPa)	Note
1-hour mean	200 μg/m^3	Not to be exceeded more than 18 times a year
Annual mean	40 μg/m^3	Referred to NO_2
Annual mean	30 μg/m^3	Referred to NO_x
Alarm threshold	400 μg/m^3	Measured on 3 consecutive hours on at least 100 km^2.

Particulate matter is made from all suspended non-gaseous material, usually solid. The nature of airborne particles may be several: particulate may be composed of airborne dust, organic material dispersed by plants (pollens and plant

fragments), inorganic material produced by natural agents (wind and rain), soil or artifacts erosion, etc. In urban areas, the particulate matter may be originated from industrial processes (construction sites, foundries, cement factories), from degradation of asphalt, tires, brakes, and the exhaust emissions from motor vehicles, especially from diesel fueled vehicles.

Particulate matter may be either directly emitted into the atmosphere (primary particles) or formed in the atmosphere by chemical reactions (secondary particles.) The relative importance of primary and secondary particles depends mainly on the geographical location, with its specific mix of emissions, and on the prevailing atmospheric chemistry. As shown in Figure 1.8, secondary particles are formed through several pathways. Atmospheric particles may be either solid or liquid and have aerodynamic diameters between approximately 0.002 and 100 μm (Finlayson-Pitts and Pitts, 1986). The most important particles with respect to atmospheric chemistry, physics, and health effects related issues are smaller than 10 μm diameter.

Particle size fractions commonly measured by air quality monitors are illustrated in Figure 1.9 showing the relative concentration of particles as a function of particle diameter. The mass collected is proportional to the area under the distribution within each size range. The total suspended particulate (TSP) represents all particles in size fractions from 0 to approximately 40 μm, the PM_{10} fraction ranges from 0 to 10 μm, and the $PM_{2.5}$ size fraction ranges from 0 to 2.5 μm in aerodynamic diameter.

Particles in the fine particle ($PM_{2.5}$) size fraction have substantially longer residence times, and therefore greater potential to affect PM concentrations further from emissions sources, than particles with aerodynamic diameters exceeding 2 or 3 μm. In this regard, fine particles behave more like gases than coarse particles. Combustion processes (e.g., power plants) may produce particles not only in the nucleation range (less than approximately 0.08 μm) but also in the accumulation range.

Some of the gaseous species, by a series of chemical transformations, are converted into particles, forming secondary aerosols. Sulfates and nitrates are the most common secondary particles, though a fraction of organic carbon can also be formed via atmospheric reactions involving volatile organic compounds (VOC). In general, the gaseous precursors of most particulate sulfates and nitrates are SO_2, SO_3, oxides of nitrogen (NO and NO_2) and ammonia. Ambient

concentrations of sulfate and nitrate are not necessarily proportional to source emission rates since the rates at which they form may be limited by factors other than the concentration of the precursor gas (e.g., photo-chemical reactions).

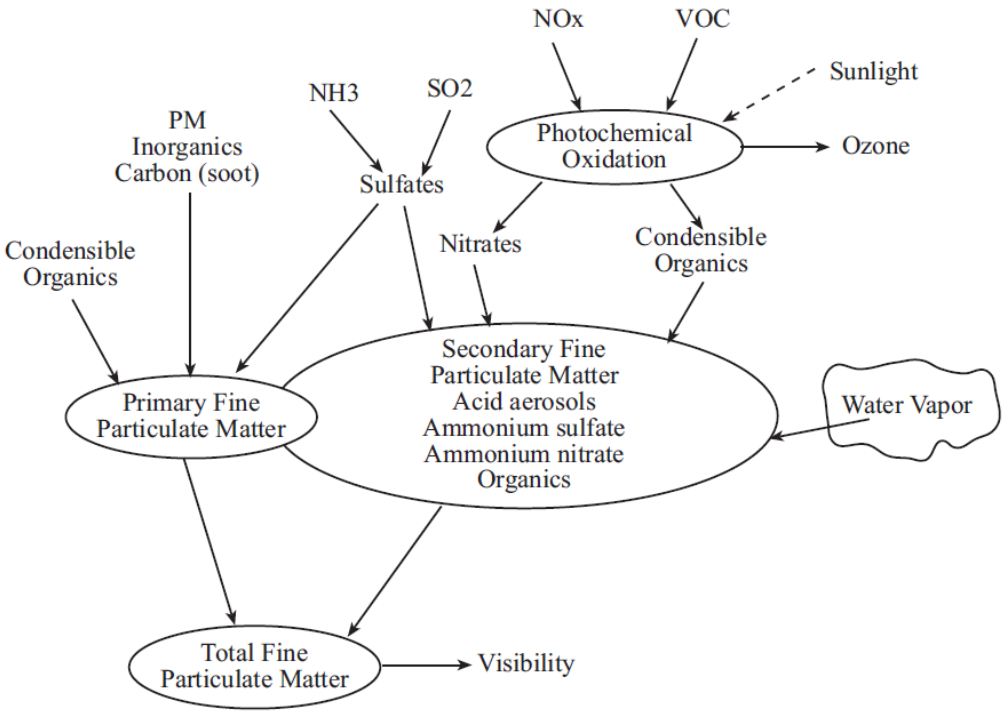

Figure 1.8. Fine particulate formation pathways (source: Chang and England)

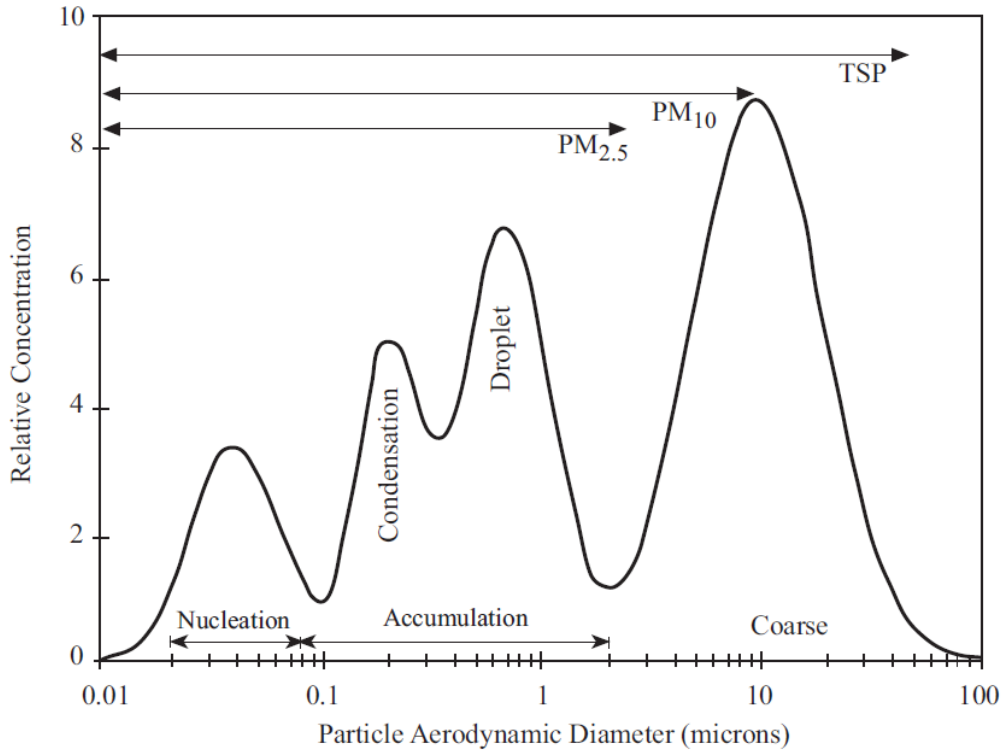

Figure 1.9. Idealized size distribution of particles in the ambient air (source: Chang and England).

Epidemiological studies have shown a correlation between the concentrations of dust in the air and manifestation of chronic respiratory diseases, especially asthma, bronchitis and emphysema. At the level of indirect effects, in addition, the fine particulate acts as a vehicle for substances with high toxicity, such as polycyclic aromatic hydrocarbons and metals.

The health risk associated with substances present in the form of particles suspended in the air depends not only on their concentration but also on the size of the particles. Smaller particles constitute a greater danger to human health, as they can penetrate deep into the respiratory system. In first approximation:

- particles with an aerodynamic diameter of 10 μm reach the upper respiratory tract;
- particles with an aerodynamic diameter between 5 and 10 μm reach the trachea and bronchi;

- particles with an aerodynamic diameter lower than 5 μm can reach the pulmonary alveoli.

The limit values and the alarm threshold defined by Italian regulation for PM_{10} and $PM_{2.5}$ are reported in Table 1.5.

Table 1.5. Limit exposure values for particulate matter in Italian regulation (Legislative Decree n.155/2010)

Averaging period	Limit value (293 K, 101.3 kPa)	Note
24-hour mean	50 μg/m^3	Referred to PM_{10}. Not to be exceeded more than 35 times a year
Annual mean	40 μg/m^3	Referred to PM_{10}
Annual mean	25 μg/m^3	Referred to $PM_{2.5}$

The limit exposure values issued by Italian regulation are consistent with other air quality guidelines proposed by international organizations. The most important set of air quality guidelines has been recently issued by the World Health Organization (WHO) for several air pollutants, including NO_2 and PM. The guidelines apply worldwide and are based on expert evaluation of the scientific evidence. Table 1.6 resumes the exposure limit issued by the WHO.

Table 1.6. WHO air quality guidelines for concentrations of particulate matter and nitrous oxides (source: WHO, 2006).

Averaging period	NO_2	$PM_{2.5}$	PM_{10}
1-hour mean	200 μg/m^3	-	-
24-hour mean	-	25 μg/m^3	50 μg/m^3
Annual mean	40 μg/m^3	10 μg/m^3	20 μg/m^3

Chapter 2

Objectives of the study

The aim of this study is the development and application of a methodology for calculating emissions into the atmosphere associated with energy management interventions. The methodology aims to characterize and quantify the environmental impacts in respect to the effects interesting both the local and global scale. The pollutants interesting the local effects considered in this study are the nitrogen oxides, calculated as total oxides (NO_x) and particulate matter, calculated as total suspended particulate (TSP). Globally, the emission of greenhouse gases is considered, by calculating the contribution to the greenhouse effect in terms of carbon footprint, i.e. quantifying the equivalent CO_2 (CO_{2eq}) emitted.

This study starts from considering one or more significant interventions involving a change in the configuration of energy management in a specific area, analyzing possible scenarios and alternatives of use. For each configuration, the intent is initially to characterize the processes in terms of mass and energy balance, and then quantifying the environmental aspects associated with them. The environmental impact is quantified in terms of changes in emissions, i.e. by comparing the present situation with one (or more) future scenarios, and calculating the possible improvement (or deterioration) brought by new energy configurations.

The ultimate objective of this study is then seeking the development of a conceptual framework that allows the objective comparison of different possible installation and/or management solutions, identifying the best compromise from

the environmental point of view, both in respect of the local population and in respect of globality. This comparison is achieved using a series of modeling tools.

The application of the methodology to real case studies is the mean to achieve relevant information on its validity: for this reason, it was chosen to study two significant real cases located in a specific geographic area, namely the metropolitan area of the city of Turin, Italy. The two case studies are characterized by different application contexts and different scales of operation, and for this reason they are expected to provide important information with respect of the achievement of goals. The first case study is represented by a system for the production and conversion of biogas and biomethane, located in the immediate suburbs of the metropolitan area of Turin. The second case study is represented by an operation of extension of the district heating network in the urban area of the city, connecting new households to the existing network. The intention is then, on the one hand to obtain separate results and findings for each case, to assess the actual local and global environmental sustainability of the single intervention (and its alternatives); on the other hand, through the joint analysis of the two cases, the intent is to obtain information on the validity of the adopted methodology, in view of a possible standardization of the same.

An efficient assessment methodology represents a potentially useful tool to administrations, utilities and other organizations that need to undertake comparative assessments of the health and environmental impacts of energy generation options.

In summary, the present study intends to take the following steps:

- characterizing a given energy intervention in terms of mass and energy flows, considering different possible design and operation alternatives;
- quantifying the emissions associated with each alternative, with respect to both the local dispersion of NO_x and TSP and the overall carbon footprint;
- identifying, for each case study, the best possible compromise in terms of environmental sustainability;
- obtaining, from the joint analysis of case studies considered, information about a possible extended application of the methodology adopted.

2.1 Thesis organization

This thesis is divided into four parts as follows:

- Part 1: General introduction. Part 1 includes the presentation of the main environmental issues connected to energy generation. The objectives of the study are then presented. The area of study, its energetic configuration and the related environmental critical issues is described. The two case studies are finally presented, as well as the methodological approach adopted for the pursuing of the objectives.
- Part 2: Biogas and biomethane case study. Part 2 reports the analysis made in the first case study considered, i.e. a facility for the production and conversion of biogas and biomethane located in the surroundings of the metropolitan area of Turin.
- Part 3: DH network extension case study. Part 3 reports the environmental study of a potential extension of the district heating network in the northern and eastern areas of Turin. The change in the operation of the main power units feeding the network, as well as the emissions from residential heaters is considered.
- Part 4: General discussion and conclusion. Part 4 provides a final joint discussion and conclusion on the entire study. Findings and results from the two case studies are compared and assessed, as well as the methodological approach adopted.

Chapter 3

The Metropolitan city of Turin and related energy and environmental issues

The Metropolitan city of Turin covers an area of 6,830 km^2 and is the one with the greatest number of municipalities in Piedmont (316 in total, Figure 1.10). The resident population is 2,306,676. It is concentrated in a few larger towns located in the plain territory. The population density varies within area borders: in the main urban centers, it is around 910 inhabitants/km^2, whereas in mountain areas is equal to 40 inhabitants/km^2. The average density value is about 328.6 inhabitants/km^2.

The economy of the area is characterized by a highly skilled workforce, innovative companies and well-known universities. The productive structure of the area is widely diversified, ranging from manufacturing to services activities. The manufacturing sector is mainly composed by automotive, engineering and aerospace industries. Although the industry sector is still strong, most employees are occupied in the services sector.

Figure 1.10. Location of the Metropolitan City of Turin (scale 1:400,000).

The main city, Turin, is located on the western bank of the Po River, in front of Susa Valley and surrounded by the western Alpine arch and by the Superga Hill. The population of the city is 892,649 (August 2015), while the population of the urban area is estimated by Eurostat to be 1.7 million inhabitants. The municipality covers an area of 130.17 km^2. The population density is 6,900 inhabitants/km^2. The average elevation is 239 m above sea level (minimum 204 m – maximum 715 m).

Turin is located in the humid subtropical climate zone. This contrasts with the Mediterranean climate characteristic of the coast of Italy. Winters are moderately cold but dry, summers are mild in the hills and quite hot in the plains. Rain falls mostly during spring and autumn; during the hottest months, otherwise, rains are less frequent but heavier (thunderstorms are frequent). During winter and autumn banks of fog, which are sometimes very thick, may form in the plains but rarely in the city, because of its location at the end of the Susa Valley. Its position on the east side of the Alps makes the weather drier than on the west side, because of the föhn wind effect. The average temperature recorded by Torino Consolata weather station is 12.3°C (minimum average 8.5°C – maximum average 16.1°C). The highest temperature ever recorded was 39.7 °C, while the lowest was −21.8 °C. The average rainfall is 803 mm, with an average number of rainy days equal to 79.

3.1 Energy production and management

Regarding the energy sector, the Metropolitan city of Turin is one of most virtuous areas in Italy for the high number of renewable energy sources and with one of the largest remote heating district, and the city of Turin as a candidate to be one of the Smart Cities in the EU Initiative to foster the dissemination of the most efficient models and strategies.

The total amount of energy supply in the Metropolitan city of Turin in 2011 was 5 Mtoe. The supply grew by 15% from 2000 to 2009 but after 2010 started to decrease. The energy supply depends mainly on natural gas, which was 54% in 2000 and 68% in 2011. This dependency is thus increasing since natural gas is being used more and more for feeding CHP plants. As natural gas increased a lot its contribution to energy supply (from 2.4 Mtoe in 2000 to 3.3 Mtoe in 2011), on the other hand oil products decreased their supply in a very relevant way. Their share turned to be 24% in 2011, against the 38% recorded in 2000.

There are no direct fossil sources or productions on its territory. For this reason, the Metropolitan City of Turin is strongly dependent on foreign supplies (about 93%), especially natural gas. Because of the lack of fossil energy reserves, the only way to limit the external supply and consumption of fossil sources is to resort to a more consistent use of renewable energy and increased efficiency in the final use of energy.

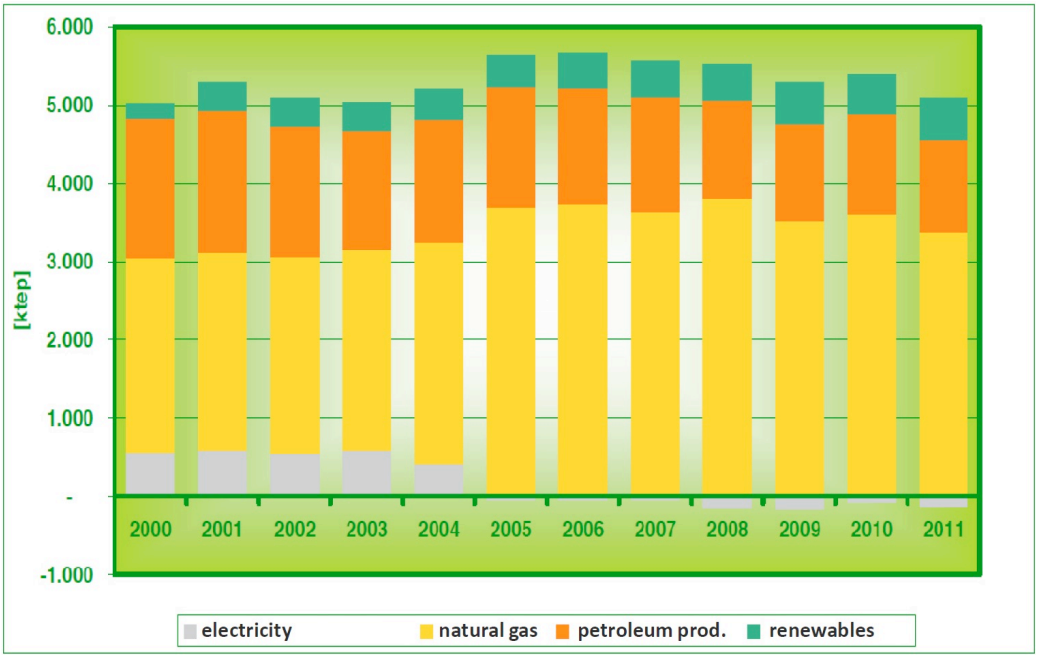

Figure 1.11. Energy consumption in the Metropolitan city of Turin (source: Turin Province, 2012).

Renewable energy sources increased a little bit their share (from 8% in 2000 to 10.4% in 2011) even though in terms of absolute values they had a growth by nearly 50%. Biomass and hydropower are the most relevant renewable source (more than 95% of the total supply in 2011) even though it is probable that solar energy will increase its contribution in the next years. In 2011, the consumption of energy from renewable sources was about 520 ktoe, by which 370 ktoe from domestic production and about 150 ktoe imported from other regions. The average annual rate of growth of renewables is about 4.5%. Renewable sources of energy allocated directly to end-users constitute 86% of the total consumption, the remainder is the energy loss due to energy transformations. Considering only the portion destined to end-uses, it is important to note that 48% is represented by thermal energy, while 52% by electricity.

Biomass is the largest renewable source in the area with an energy contribution of almost 58% on the total of renewables. The annual supply of biomass in the metropolitan city is about 301 ktoe. This use of such supply consists of 2/3 of energy used directly by end-users (log wood, pellets and wood

chips used in boilers) and 1/3 from the processes of production of electricity and heat (from wood chips, biogas and oils power plants).

Heating is becoming more and more important in the overall energy balance of the Metropolitan City of Turin. A total amount of 3,000 GWh of heating was generated and distributed in 2010 mainly to private household customers. Heating represents more than 5% of total final energy consumptions. The total useful energy produced by the thermoelectric sector is, therefore, equal to slightly less than 1.4 Mtoe (16.1 TWh), with a primary energy consumption of nearly 1.9 Mtoe and with a return of about 62%. The total energy consumed is made up of 94.4% for natural gas and 5.3% from biomass (including biogas). The remainder is attributable to petroleum products (fuel oil and diesel fuel). As mentioned before, the thermoelectric sector is largely also cogeneration. In fact, the heat generated is more than two-thirds distributed or sold to end-users through district heating networks and the remainder self-consumed by industrial users. Finally, a residual amount of heat (203 GWh in 2013) comes from thermal power stations, mainly integration systems of the existing district heating networks (Table 1.7).

Table 1.7. Heat production in the Metropolitan city of Turin (source: adapted from De Nigris and Fraire, 2013)

Heat produced (GWh)	**2000**	**2005**	**2010**	**2011**	**2013**
Industrial CHP	1,946	2,002	1,611	1,243	870
CHP for district heating	909	1,197	2,222	2,194	2,888
Thermal production for DH	243	396	469	291	203
Total production	3,148	3,595	4,302	3,728	3,961

The Metropolitan city of Turin turned to be a self-sufficient region for electricity from 2005 on. In the past, the electric deficit was around 60% of its needs. The gap was reduced thanks to few CHP groups that started operating

between 2004 and 2005. All those plants are fed by natural gas with energy efficiency standards in line with best available technologies. The energy generation system of the Metropolitan city of Turin is composed of several plants (about 300, PV excluded), most of which are small-sized. Hydropower plants are 193, Thermoelectric power plants are 100, whereas wind power plants are only 4. Few CHP plants nearby the City of Torino give the main contribution to the overall production of electricity and are also feeding the large district heating system of the city of Turin and surrounding municipalities.

Up to now, Turin district heating system is the largest in Italy, and the extension planned will bring Turin as one of the leaders in Europe in this field. In the whole Metropolitan city of Turin, as shown in the picture below, there are many different district heating grids, the oldest of them was built more than 30 years ago, whereas many of them are currently being developed, some others are still in a planning phase. A complete overview of the situation of district heating in the area is reported in Figure 1.12.

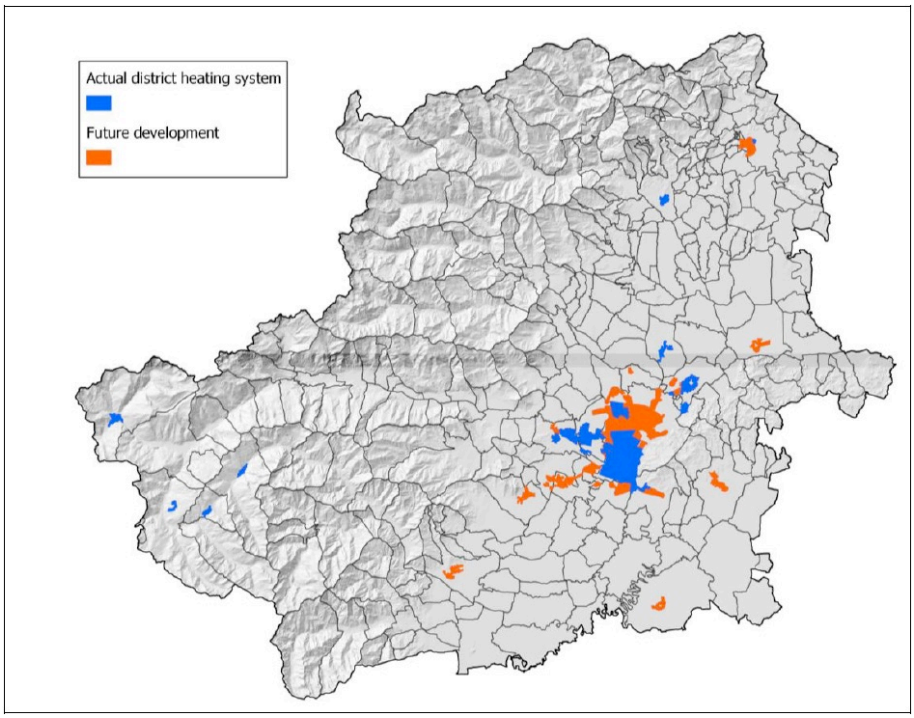

Figure 1.12. District Heating system in the Metropolitan city of Turin. The actual coverage is reported in blue, while the future development (short-medium period) is reported in orange.

3.2 Local pollutants emissions

The air quality monitoring network, which operates in the territory of the Metropolitan City of Turin and is managed by Piedmont Region's Agency for the Environmental Protection (Arpa Piemonte), consists of 20 fixed stations of public ownership, 3 private fixed stations and a mobile vehicle for the realization of measurement campaigns of air quality chemical parameters. All fixed stations are connected to the data acquisition center and transmit the results of the measurements with an hourly frequency, allowing a constant control of the main factors that affect air quality. The location of the monitoring stations is shown in Figure 1.13. The main features of the monitoring stations around the Turin metropolitan area are reported in Table 1.8.

The year 2014 (the latest year for which a comprehensive evaluation is available) in Piedmont was the second warmest after 2011 and the third wettest (preceded by 1977 and by 1960) in the yearly time series since 1958. The annual precipitation observed in the Piedmont area was 1418 mm, greater than about 420 mm (40%) compared to the climatic average 1971-2005.

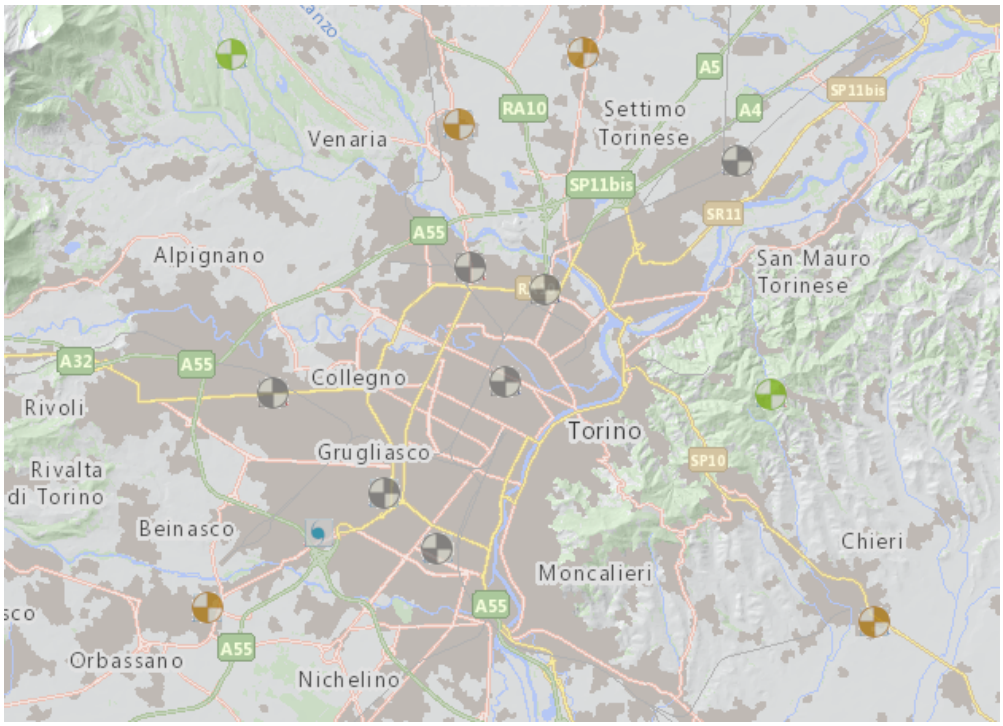

Figure 1.13. Location of ARPA monitoring stations over the metropolitan area of Turin (source: http://webgis.arpa.piemonte.it/)

Table 1.8. Main pollution monitoring stations around the metropolitan area of Turin (source: ARPA)

Station	Active since	Type of station	UTM X coordinate	UTM Y coordinate	Elevation (m a.s.l.)
TO-Consolata	1996	Traffic	1395961	4992226	243
TO-Grassi	1996	Traffic	1394836	4996153	245
TO-Lingotto	1996	Background	1393571	4986609	243
TO-Rebaudengo	1996	Traffic	1397361	4995339	233
TO-Rubino	2007	Background	1391781	4988521	257

3.2.1 NO_x emission

The air quality reports issued by Piedmont's regional protection agency (ARPA) show that NO_x pollution represents a critical factor for air quality in the municipality of Turin. The Italian Legislative Decree 155/2010 establishes an annual average limit of 40 $\mu g/m^3$ for NO_2 (Table 1.4). The trend of recent years, from 1991 to 2014, is shown in Figure 1.14. The annual average concentrations of two urban stations are reported, TO-Lingotto (background station with the lowest values), and TO-Rebaudengo (characterized by intense traffic), as well as a global annual average of all stations. These data show that annual exposure limits are systematically overstepped.

On the other hand, from the curve of the annual average over all stations, a general downward trend in the NO_2 concentration over the years is observed. NO_2 concentration, in fact, decreases from more than 80 $\mu g/m^3$ in 1991 to the value of 52 $\mu g/m^3$ recorded in 2014, a value representing the lowest of the time series. The gradual decrease of the concentrations of NO_2 over the last years is also confirmed in the two reference stations, TO-Rebaudengo (from values greater than 100 $\mu g/m^3$ before 1995, to values lower than 80 $\mu g/m^3$ from 2007 onwards), and TO-Lingotto (from values above 60 $\mu g/m^3$ to values generally ranging within 55 $\mu g/m^3$, and in the last three years around 40 $\mu g/m^3$).

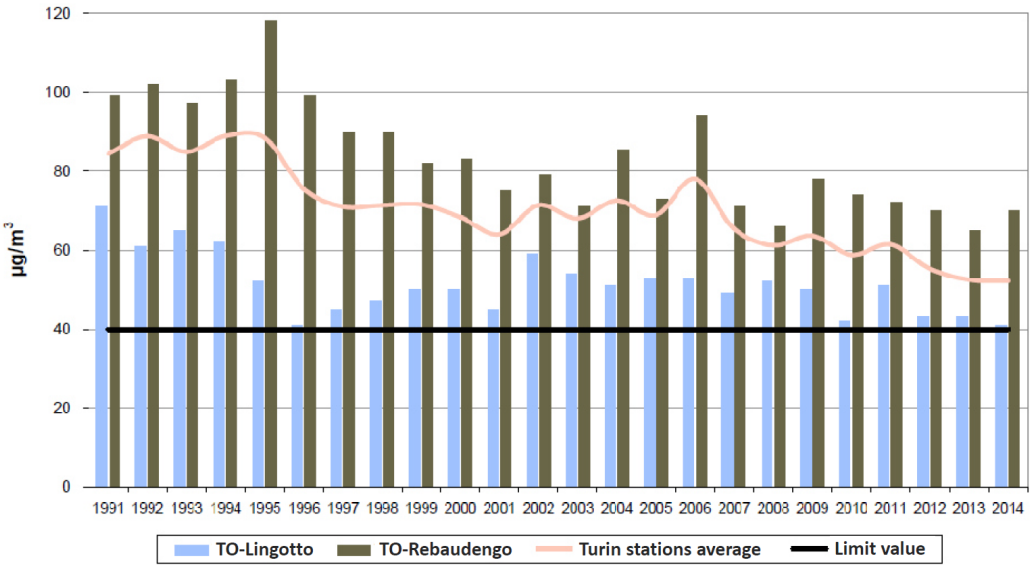

Figure 1.14. Average NO_2 concentration (of the annual averages) of all the monitoring stations working in Turin municipality, detail related to TO-Lingotto and TO-Rebaudengo stations.

A general reduction in the average annual values is found also for the years 2013-2014, as reported in Figure 1.15. For most of the stations, the yearly average concentration of nitrogen dioxide is reduced or in the worst case remains substantially unchanged compared to the previous year, except for two stations.

The situation in the TO-Consolata station, located in the center of Turin, remained stable, shifting from an average of 60 µg/m^3 to 59 µg/m^3; the annual average is still lower than the mean value of nitrogen dioxide detected from 2003 to 2011, that is between 65 and 73 µg/m^3. Almost half of the stations have an average annual value that does not change substantially compared to 2013, and only two of the 21 stations recorded a decline compared to 2013.

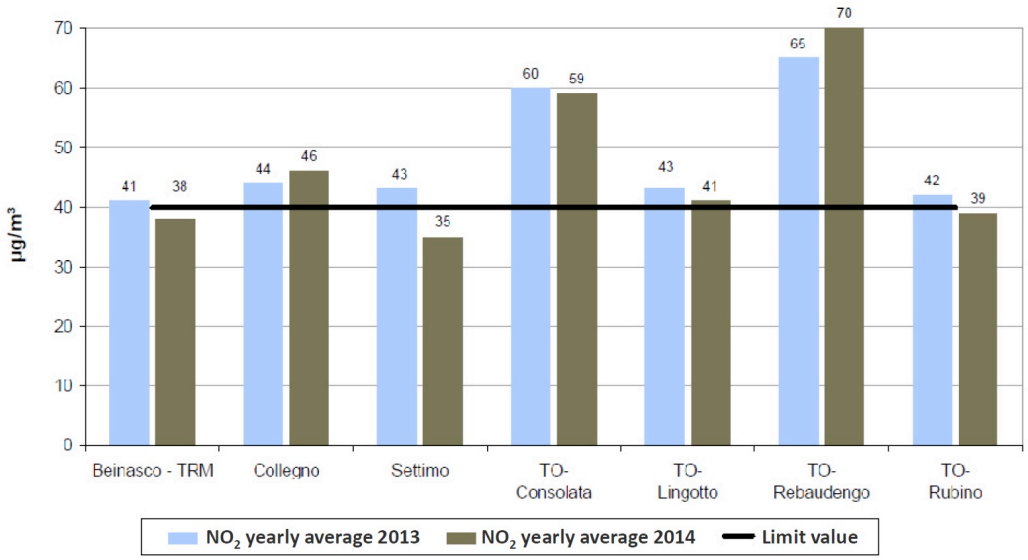

Figure 1.15. Number of exceedances of the annual limit of 40 µg/m^3 for the pollutant NO_2 for the years 2013- 2014 in some of the Turin monitoring stations.

Considering the hourly limit value for the protection of human health (200 µg/m^3, Table 1.4), during 2014 only three exceedances were registered. All exceedances were recorded during the month of January, which was marked by a long phase of atmospheric stability. Usually, in fact, the totality of the overcoming takes place in the winter time because of the meteorological conditions that characterize the cold season, i.e. with thermal inversion phenomena and consequent atmospheric stability that does not allow the mixing of the pollutants. In general, in conditions of atmospheric instability, the temperature decreases with increasing elevation, allowing the mixing of air masses and consequently helping the dispersion of pollutants in the soil; vice versa in the presence of stability, thermal inversion conditions take place on the ground or at a higher altitude. This thermal inversion fosters the accumulation of pollutants in the lower layers of the atmosphere, causing a general worsening of air quality.

Generally, annual averages are less affected by critically isolated episodes: in recent years, sometimes the observed decrease of annual averages did not correspond to a similar improvement in the number of exceedances of the hourly limit. This is because the number of exceedances of the hourly limit value is much more sensitive to weather variations if compared to the annual average, even if these variations are limited to a few critical episodes. This aspect has an important role in the planning of interventions for the reduction of atmospheric pollution

since (in the case of a pollutant subject to hourly limit values like NO_x), few days of meteorological stability can be sufficient to limit the atmospheric diffusion of pollutants and consequently worsen the indicator for the whole year.

In summary, NO_x concentration in Turin has been reduced during the last years, even if much has still to be done to achieve an acceptable level of air quality. As a final consideration, data from the Regional Emission Inventory for the year 2010 (IREA, 2010) are reported in Table 1.9. In this table, a comparison between the overall NO_x emitted in the municipality of Turin, and the partial contribution of different voices of the energy sector is reported. The data show that the energy production sector contributes only in part to the total NO_x emissions. In fact, the partial contribution of different voices is as follows:

- residential installations about 5%;
- electricity production about 8%;
- district heating about 0.4%;
- combustion in boilers, turbines and endothermic engines about 21%, where this latter term considers the totality of the industry sector.

Table 1.9. Total NO_x emission in the municipality of Turin in the year 2010, and comparison with different voices of the energy sector (source: IREA, 2010).

Sector	Fuel	NO_x emission (t/y)
Total emission	**-**	**6,779**
Residential installations	Natural gas	400
	LPG	-
	Diesel oil	4.2
	Wood and similar	11.4
Electricity Production	Natural gas	251.5
	Diesel oil	
	Heavy oil	2.0
District heating	Natural gas	26.5
	Diesel oil	0.00013
Combustion in boilers, turbines and endothermic engines	Natural gas	1,474
	Diesel oil	0.02
	Heavy oil	1.7

3.2.2 Particulate matter emission

The analysis of average annual values of particulate matter concentration in the municipality of Turin also reveals a critical situation. The Italian Legislative Decree 155/2010 establishes an annual average limit of 40 $\mu g/m^3$ for PM_{10} and of 25 $\mu g/m^3$ for $PM_{2.5}$. The air quality reports issued by Piedmont's ARPA show that this limit is currently not respected in most of the monitoring stations located in the area (Figure 1.16). On the other hand, a decreasing trend has been detected over the last years. For the year 2014, data of PM_{10} concentration showed an average annual decrease of about 2 $\mu g/m^3$; currently, the annual averages are around 40 $\mu g/m^3$ in the Turin stations and 30 $\mu g/m^3$ in the stations outside Turin. The highest concentrations are measured in winter, when the contribution of the

heating systems is greater, and at the same time, the most unfavorable weather conditions occur.

If 24-hour exposure limits are considered (50 μg/m^3 and a maximum of 35 exceedances per year, Table 1.5), the situation is even worse, as this limit is not observed in most stations (Figure 1.17). The highest number of exceedances of the daily limit for the year 2014 occurred in TO-Rebaudengo station, located in the north of Turin, and was equal to 94. Also in urban background stations TO-Lingotto and TO-Rubino, the situation is critical, with 59 and 58 exceedances respectively.

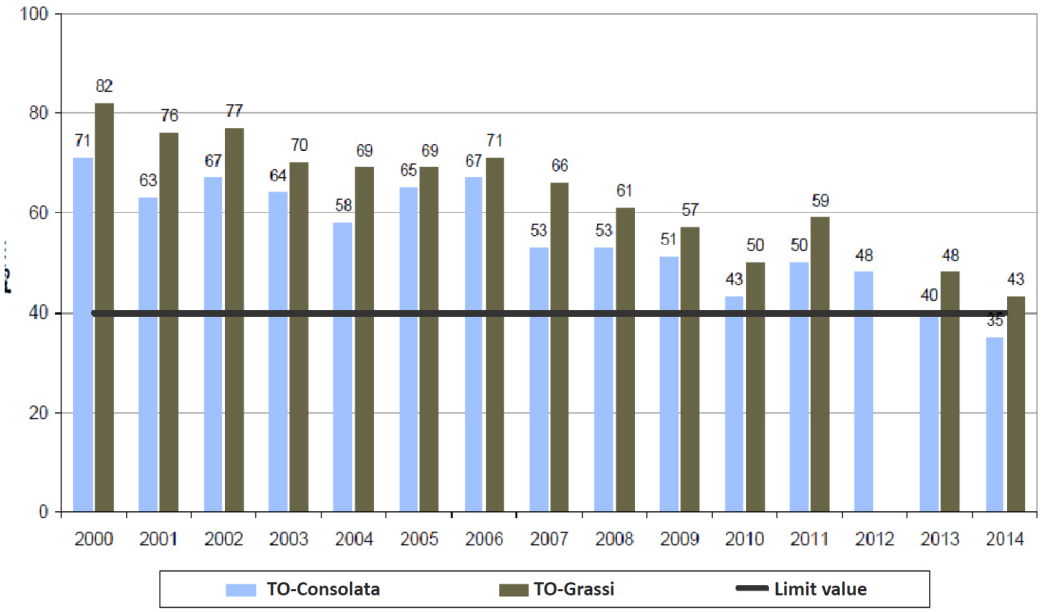

Figure 1.16. Average PM_{10} concentration measured in the city of Turin over the period 2000-2014.

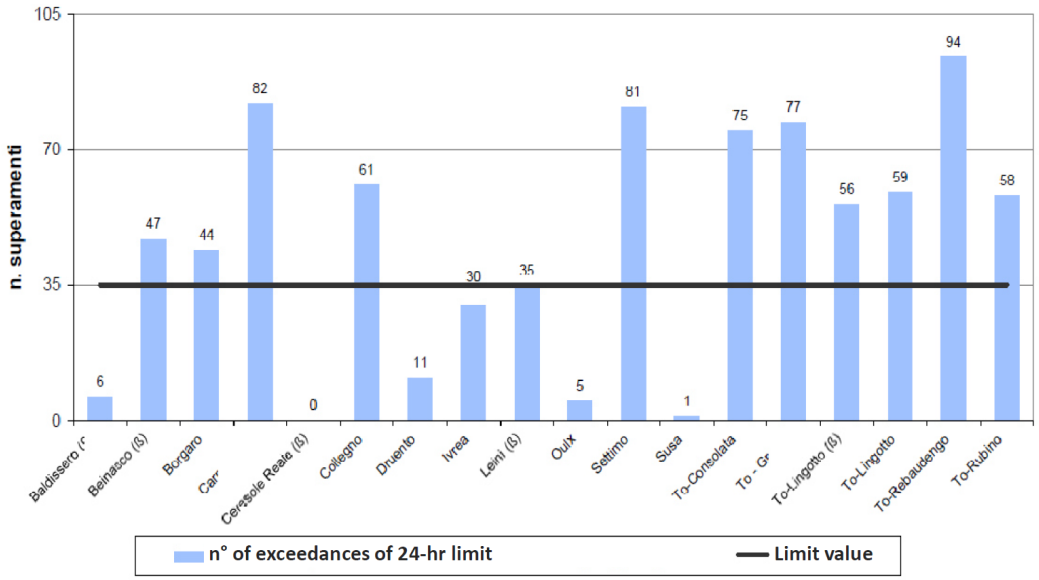

Figure 1.17. Number of exceedances for the parameter PM_{10} of the 24-hour exposure limit (50 µg/m^3).

In 2014, in TO-Lingotto station, $PM_{2.5}$ is on average about 77% of PM_{10} in the cold semester of the year and 65% in the hot semester. This phenomenon, confirmed by the analysis of time series, can be attributed to the fact that the secondary component of the particulate is more concentrated in the $PM_{2.5}$ fraction.

Total suspended particles (TSP) are measured at the TO-Consolata station, located in the center of the city. The analysis of the TSP concentration, given the long-time series of data, is useful to obtain an indication of the relative PM_{10} trend, even in periods in which this parameter was not measured. In fact, as shown in Figure 1.18, (reporting the annual averages of TSP and PM_{10} at the TO-Consolata station), PM_{10} represents about 70% of TSP. In Figure 1.18, the average annual TSP concentrations measured over more than 30 years are reported. The values that are measured today are strictly lower compared to the 80s; from 1999 to 2006 they have stabilized at around 100 µg/m^3, while, in the last four years, the lowest values ever measured were observed (around 60 µg/m^3). Even if an improving trend over a longer term is detectable, the concentration values are still far from the exposure limits.

The decrease observed with respect to the first years of measurement was obtained by:

- transferring outside the metropolitan area (or even closing) some industrial plants of considerable environmental impact;
- the gradual replacement by natural gas of highly polluting fuels such as fuel oil and coal;
- the reduction of sulfur dioxide emission, a precursor of secondary particulate matter;
- the technological improvements in vehicle emissions.

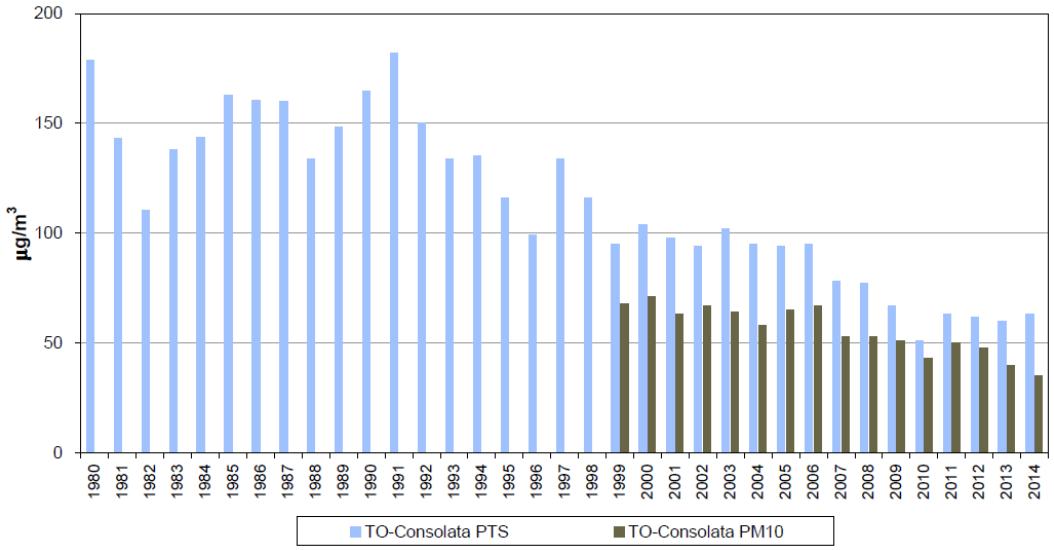

Figure 1.18. TSP and PM_{10} average annual concentration measured at the TO-Consolata monitoring station, over the period 1980-2014.

In conclusion, the statistical analysis of PM_{10} and $PM_{2.5}$ time series in the regional and municipal area of Turin confirms the criticality compared to the European and Italian situation. The objective of lowering particulate matter emission is challenging if it is considered that even in a year with a relatively favorable meteorological dispersion of pollutants (as 2014), the 24-hour limit value was exceeded many times. The typical weather and climate conditions of the Po Valley necessarily require strong reductions in atmospheric emissions to comply the regulation requirements.

As a final consideration, data from the Regional Emission Inventory for the year 2010 (IREA, 2010) are reported in Table 1.10. In this table, a comparison between the overall PM_{10} and $PM_{2.5}$ emitted in the municipality of Turin, and the partial contribution of different voices of the energy sector is reported. The data

show that the energy production sector contributes only in part to the total PM emissions. In fact, the partial contribution of different voices is as follows:

- residential installations about 4% (PM_{10}) and 7% ($PM_{2.5}$);
- electricity production about 0.1% (PM_{10}) and 0.2% ($PM_{2.5}$);
- district heating about 0.03% (PM_{10}) and 0.06% ($PM_{2.5}$);
- combustion in boilers, turbines and endothermic engines about 0.5% (PM_{10}) and 0.9% ($PM_{2.5}$).

The same data also show that almost the entire fraction emitted by the energy-related activities is composed of ultrafine particles (below 2.5 μm).

Table 1.10. Total PM_{10} and $PM_{2.5}$ emission in the municipality of Turin in the year 2010, and comparison with different voices of the energy sector (source: IREA, 2010).

Sector	Fuel	PM_{10} emission (t/y)	$PM_{2.5}$ emission (t/y)
Total emission	**-**	**657.7**	**371.7**
Residential installations	Natural gas	2.30	2.30
	LPG		
	Diesel oil	0.017	0.017
	Wood and similar	1.14	1.14
Electricity Production	Natural gas	0.71	0.71
	Diesel oil		
	Heavy oil	0.066	0.063
District heating	Natural gas	0.090	0.080
	Diesel oil	0.218	0.218
Combustion in boilers, turbines and endothermic engines	Natural gas	0.00001	0.00001
	Diesel oil	3.19	3.19
	Heavy oil	0.0013	0.0013

3.3 Greenhouse gas emissions

The Italian objective for the Kyoto protocol for the period 2008-2012 was a reduction of greenhouse gas emission of 6.5% compared to 1990. In 2011, carbon dioxide emissions in the Metropolitan City of Turin associated with energy use fell, for the first time, below 12 million tons (Mton), almost 20% less than in 1990 (Figure 1.19).

Compared with the trend at the national level, this region presents a dynamic contraction of emissions much more relevant: in 2010 in Italy, a reduction of 3.5% of the CO_{2eq} emissions and a reduction of 2.1% of CO_2 was registered; in the same year in the Metropolitan City of Turin, the figure of CO_2, although referred to the only energy use, was 13.1%. CO_2 emissions in the Metropolitan City of Turin decreased over the last years. After the peak in 2000 when a data of 16 Mton was reached, emissions have started to shrink, and the decrease was more evident from 2007. In particular, during the period 2007-2013 emissions were reduced by more than 2 million metric tons per year (Figure 1.19).

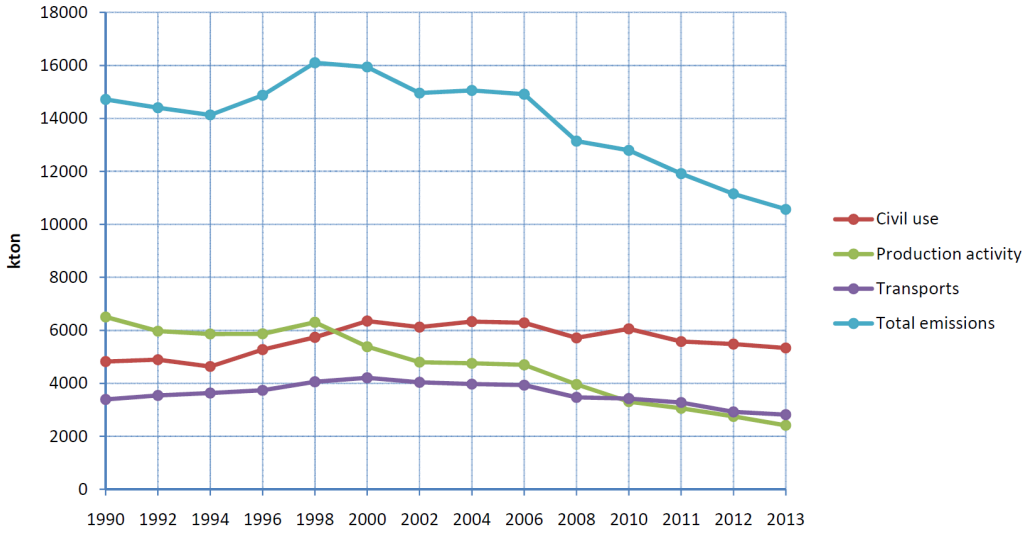

Figure 1.19. CO_2 emissions for the energy sector in the Metropolitan City of Turin.

The specific indicators reported in Figure 1.20 show that emissions fall both with respect to the resident population (from 7 t/inhab. in 2000 to 5.1 t/inhab. in 2011) and if compared to the climatic conditions. The regional data of this indicator are lower than the national ones. Particularly significant is the decrease

of the specific emission if compared to the energy consumed in the end use, which for the period 2009-2011 amounts to about 2.75 t/toe. This indicator, next to 3.5 t/toe in 1990 and 3.05 t/toe in 2005, describes the carbon intensity of energy use and its reduction may be the result both of improved efficiency in the processes of conversion and use of energy (e.g. more efficient conversion units), and of processes of fuels substitution, from high carbon intensive energy carriers (e.g. petroleum products) to those that involve lower emissions (e.g. renewable sources). Over the last years both changes have happened: there has been a substantial reduction of specific emissions to produce electricity (a value of the national mix of about 440 g/kWh in 2011, as compared to values well above 500 g/kWh in the year 2000s) and a continuous decline in the importance of oil products, substituted by natural gas and renewable sources.

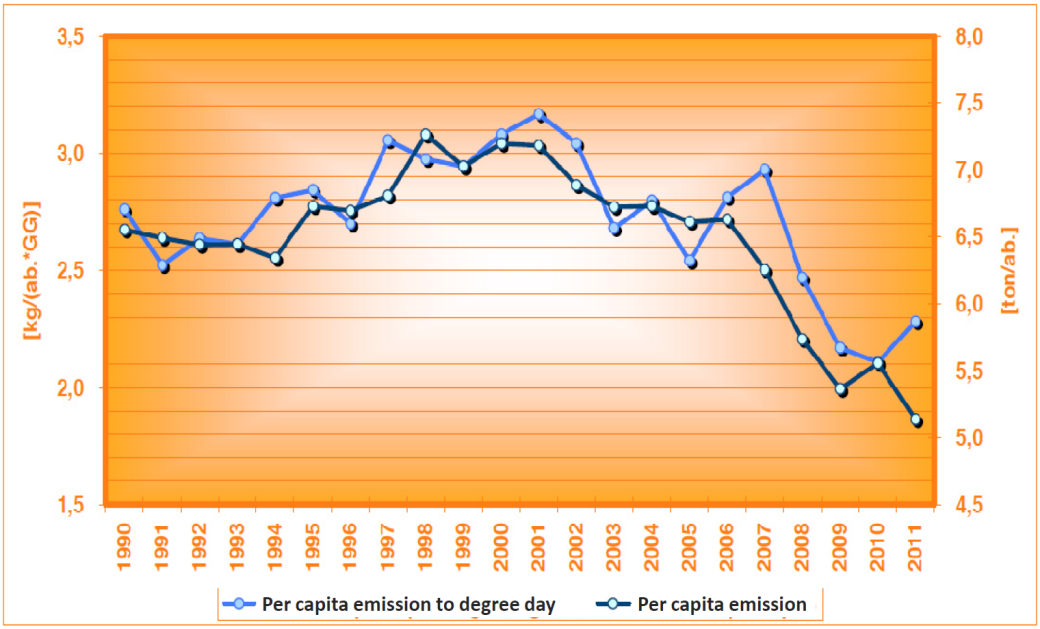

Figure 1.20. Per capita CO_2 emissions in the Metropolitan City of Turin, in absolute values (t/inhab., right axis) and referred to the climate conditions (t/inhab/DD, left axis).

As previously mentioned, the relative decrease of importance of the industrial and transport sectors on the overall energy balance caused that the impact on CO_2 emissions was more pronounced compared to what happened on the end-uses. Both sectors have, in fact, a greater carbon intensity for the consumed energy than the civil sector. In this latter, the use of natural gas prevails over other energy carriers (for the industry the prevalence is on electricity, while transports depend

on petroleum products) and the use of distributed heat through district heating networks and renewable sources is prevailing with respect to other macro sectors.

In 2011, the CO_2 emissions depend on 38.2% by electricity (production and consumption) and on 31.5% by natural gas. The contribution of petroleum products went down to 30.4%. Data from the Regional Emission Inventory for the year 2010 (IREA, 2010) concerning the power sector are reported in Table 1.11. In this table, a comparison between the overall CO_2 and CO_{2eq} emitted in the municipality of Turin, and the partial contribution of different voices of the power sector is reported. The data show contribution of different voices of the energy production sector is as follows:

- residential installations about 21%
- electricity production (excluding cogeneration plants) about 2.4%
- district heating about 1.9%
- combustion in boilers, turbines and endothermic engines about 28%.

Table 1.11. Total CO_2 and CO_{2eq} emission in the municipality of Turin in the year 2010, and comparison with different voices of the power sector (source: IREA, 2010).

Sector	Fuel	CO_2 emission (kt/y)	CO_{2eq} emission (kt/y)
Total emission	**-**	**2,897**	**3,120**
Residential installations	Natural gas	631.8	635.9
	LPG	5.24	5.30
	Diesel oil	16.82	16.99
	Wood and similar	-	0.699
Electricity Production	Natural gas	40.00	41.36
	Diesel oil	0.243	0.244
	Heavy oil	32.32	32.32
District heating	Natural gas	60.63	60.72
	Diesel oil	0.03	0.03
Combustion in boilers, turbines and endothermic engines	Natural gas	860.1	866.6
	Diesel oil	0.028	0.029
	Heavy oil	1.26	1.27

The reduction targets for greenhouse gas emissions for the Metropolitan City of Turin are contained in the Action Plan for Sustainable Energy (PAES in Italian), issued in 2014. The reduction strategy includes three key elements: sustainability, security of supply and competitiveness, and is consistent with the

long-term EU decarbonisation scenarios, that point to a substantial increase in the share of renewable sources. There is also the need to ensure a profitable development of the renewable energy potential, in line with the stability requirements of the system, and consistent with other EU policies, namely: mitigation of the effects of climate change, promotion of the internal market, international cooperation, development of research and protection of the environment, including biodiversity. The actions are grouped in activity lines, as shown in the following Table 1.12.

Table 1.12. Planned actions for the reduction of greenhouse gas emissions in the Metropolitan City of Turin (source: Turin Province, 2013)

Activity	Mode of intervention
Monitoring of energy consumption and energy production at a municipal and regional level	• Observatory on energy • Buildings energetic cadastre
Assistance to local administrators in the definition of energy projects and policies	• Sustainable local energetic planning of smart cities and smart territory • Sustainable mobility • Energy management • Training and technical updating
Rational use of energy infrastructures	• Natural gas • District heating
Promotion to final users of energy saving and renewable sources	• Promotion of a correct maintenance of thermal plants • Information, training, education • Support to interventions in private construction and industrial sectors
Energy production	• Licenses
Heritage property	• Energy management systems • Energetic improvement of buildings and installations

Chapter 4

Introduction to the two case studies

As already anticipated in Chapter 2, the development of the study consists of the analysis of two significant real cases located in the Metropolitan City of Turin. The two case studies are characterized by different application contexts and different scales of operation, and for this reason, they are expected to provide important information with respect of the pursuit of goals. The first case study is represented by a system for the production and conversion of biogas and biomethane, located in the immediate suburbs of the metropolitan area of Turin. The second case study is represented by an operation of extension of the district heating network in the urban area of the city, connecting new households to the existing network. These cases are presented in continuation.

4.1 Case study 1 – Biogas production and conversion facility

The first case study is represented by a system for the production and conversion of biogas and biomethane, located in the immediate suburbs of the metropolitan area of Turin. This facility is sited in an agricultural area, not far from housing settlements and industrial applications. Biogas is produced by anaerobic digestion of maize silage and cattle slurry, in similar proportions. Biogas is cleaned and then sent to a cogenerative endothermic engine that produces about 1 MW of thermal energy and 1 MW of electricity. Electricity is injected to the national transmission grid, while heat may either be used or not to satisfy a nearby demand (depending on the existence of such a demand). In

alternative to being directly burned, biogas may be upgraded to biomethane. This is made by separating CO_2 and CH_4 fractions in an absorption column with pressurized water. A pure methane fraction is obtained (named biomethane) that can either be injected into the national gas grid or used as a fuel for transport media.

The features of the biogas and biomethane installation analyzed correspond to the most frequently observed configuration in Northern Italy. Biogas installations in Italy had a strong spread in 2007, when new subsidy schemes and regulations were introduced. As of March 2016, the Metropolitan City of Turin accounts for around 30 biogas plants in operation fed by agricultural or zootechnical wastes, having an electric nominal power between 100 kW and 1000 kW. The total electric power installed is estimated to be 24 MW, with a total energy content of the biogas of around 60 MW. In addition, around 10 installations producing biogas from urban solid waste are present. These latter account for a total electric power of 32 MW, and a total energy content of the biogas of around 80 MW (Cuccatto, 2016).

The main features of the agricultural and/or zootechnical biogas plants in operation in the Metropolitan City of Turin are:

- plant sized between 500 and 1000 kW of electric power are the most frequent, account to around 50% of the total; the remainder is between 100 kW and 500 kW.
- around 60% of the plants is fed by energy crops and cattle manure; 30% by cattle manure only; the remainder by energy crops only or municipal solid waste.
- the biogas reactor is by majority a Continuous Stirred Tank Reactor (CSTR);
- the systems are by majority mesophilic (digester temperature of 40-42°C);
- only a small proportion (less than 10%) of the installations work in full cogeneration mode, i.e. recovering the thermal energy from the exhaust gases.

This latter point represents a critical aspect of the situation of biogas production in Italy, since frequently, if combustion takes place in endothermic engines, the energy potential of the biomass is not entirely exploited. In fact, after the lowering of the subsidies introduced in 2007, a decrease in the diffusion of

this type of installations was observed. As an alternative solution, in 2013 a new regulation (Italian Minister of Economic Development, 2013) introduced the possibility of producing biomethane to be injected into the national gas grid or used as transports fuel. The production of biomethane allows the achievement of an energy vector that can be moved away from the converting facility, eliminating the need for an energy use in the surrounding. In the last three years, a small number of facilities around the Metropolitan City of Turin have started converting biogas and producing biomethane. Unfortunately, at today, a series of bureaucratic criticisms hinders the operation of these plants, impeding the final use of this energy vector.

The environmental analysis of the biogas/biomethane installation is entirely reported in Part 2. Part of this study has been previously published in a research article (Ravina and Genon, 2015).

4.2 Case study 2 – Extension of the district heating network in Turin

The second case study is represented by an intervention of extension of the district heating network in the urban area of Turin, connecting new households to the existing network. The extension considers part of the northern and eastern districts of Turin. In these areas, part of the centralized residential heaters is removed and substituted by district heating. This portion of the system is powered by the Torino Nord cogeneration unit, consisting of a combined cycle (gas turbine and steam turbine) fueled by natural gas. The environmental consequence of this change in energy management is calculated as the difference between present and future operation. The difference in NO_x and particulate matter impacts are quantified locally in terms of increased (or decreased) values of concentration. Global impact on greenhouse effect is quantified by calculating the change in CO_2 emissions associated with the different operative configurations of the power units involved.

The city of Turin is developing the largest district heating grid in Italy, inter-connecting different power stations and integration and reserve systems. District heating in Turin started in Le Vallette district in 1982, when the formerly Municipal Electric Society AEM (currently IREN) placed a combined heat and power plant with diesel engines to increase the already existing small network (a

group of popular houses heated by a central boiler) which reached in the following years the volume of 3 million m^3 of served buildings (about 30,000 inhabitants). Another combined heat and power plant was installed in 1988 in the southern part of the city (Mirafiori Nord) and the connected grid reached up to 2.25 million m^3 of buildings. Later this grid was included in the large grid named Torino Sud, also owned by IREN, which was developed gradually since 1994 reaching all the southern part of the city (27 million m^3, 270,000 inhabitants), fed by the Moncalieri combined heat and power plant and by the backup boilers in Centrale BIT. Further development of the network in southern Turin was implemented in 2001 with the increase of power of the Moncalieri plant, which reached the actual configuration, and the installation of backup boilers and heat storage at Politecnico site. In 2011, the old Vallette plant was replaced by the new and more powerful plant named Torino Nord, constituted by combined heat and power unit, backup boilers and heat storage. The new plant allows to increase the grid in the northern area of the city and to connect it with the rest of the network. The features of the main generation units that power the district heating network of Turin are resumed in Table 1.13. Two storage systems (at Politecnico and Torino Nord plants) allow storing night heat production, contributing up to 5% of global heat demand and shaving heat peak demand on early morning hours.

In the last three years, around 2050 GWh of heat have been distributed, covering the demand of 550,000 inhabitants, as 57 million m^3 of building connected by a 515 km distribution grid (double pipe system).

The complete environmental analysis of a potential extension of the district heating network in Turin is reported in Part 3.

Table 1.13. Main generation units powering the Turin district heating network (source: modified from De Nigris and Fraire, 2013)

Generation Unit	Electric nominal power (MW)	Thermal nominal power (MW)
Moncalieri 3 CHP	390	260
Moncalieri 2 CHP	390	260
Moncalieri boilers	-	140
BIT boilers	-	255
Politecnico boiler	-	255
Politecnico storage	-	2500 m^3
Torino Nord	390	220
Torino Nord boilers	-	340
Torino Nord storage	-	5000 m^3
Martinetto storage	-	5000 m^3

Chapter 5

Methodological approach

As already stated previously, the methodology applied in the study of environmental effects of energy interventions aims to characterize and quantify the impacts with respect to both local and global scale. For each of the considered studies and configurations, the intent is initially to characterize the processes in terms of mass and energy balance, and then quantify the related environmental aspects. The environmental impact of the interventions is quantified in terms of changes in emissions, i.e. by comparing the present situation with one (or more) future scenarios, and calculating the possible improvement (or deterioration) brought by new energy configurations. This comparison is achieved using a series of modeling tools.

The comprehensive methodological approach must therefore provide a set of tools and procedures for the analysis of both NO_x and particulate local dispersion and the contribution to global warming. The operation envisages, for each case study, a common first step that defines the characteristic matter and energy balance. Then, a second phase consists in the application of tools and specific procedures for the different scales of analysis. The instruments used in the analysis must be apt to ensure a degree of objectivity and comparability of results. At the same time, a certain degree of flexibility in their use is also required, to make them adaptable to the various scenarios or configurations considered.

The modeling tools and the application procedures used in the study are generally described and motivated in the following paragraphs. More information on the specific use will then be given during the discussion of each case study.

5.1 Dispersion modeling of local pollutants

Local environmental impact is defined by estimating the dispersion of pollutants using a mathematical dispersion model.

Air pollution models are frequently used in environmental impact assessments, risk analysis and emergency planning, and source apportionment studies. They provide for computational procedures for predicting concentrations downwind of a pollutant source, based on knowledge of the emissions characteristics (stack exit velocity, plume temperature, stack diameter, etc.), terrain (surface roughness, local topography, nearby buildings) and state of the atmosphere (wind speed, stability, mixing height, etc.). These models must be able to predict rates of diffusion based on measurable meteorological variables such as wind speed, atmospheric turbulence, and thermodynamic effects.

The dispersion models may be classified into three categories based on the theoretical approach to the pollutants plume:

- Eulerian models;
- Lagrangian models;
- Statistical Particle models.

The Eulerian model treats a plume as containing coupled boxes or grid cells with the assumption that particles are uniformly mixed in a box or cell. The distribution of particles is described by changing the concentrations at discrete points in a cell. Concentrations and flux of particles passing through a cell are usually presented as a function of space. The Lagrangian model approaches a plume as a dispersion story of individual particles transporting along a trajectory. The change of concentration is described as a probability of particles that diffuse at a certain time. The Lagrangian model can be classified into steady state Lagrangian model and Lagrangian segmented of PUFF model. The Steady State Lagrangian model executes a story of particle dispersion in a certain time at a steady state condition. The concentration and flux are calculated by integrating a dispersion equation over a certain range of time. For PUFF Lagrangian models, the story of the emission dispersion is approached in small periods of time. In other words, a plume is segmented into small pieces. The concentration and flux are calculated by summing the concentration and flux of segmented plume. The Statistical Particle model considers a plume as a series of particles in which individual particles move randomly along a trajectory or a grid cell. The

concentration and flow are calculated by summing the probability of emission concentrations along a trajectory or in a cell.

In the present study, the PUFF Lagrangian model CALPUFF is used. The dispersion model CALPUFF (US EPA, 2011) is a lagrangian non-stationary puff model containing modules for the simulation of complex orography, deposition and chemical transformations. The CALPUFF Modeling System includes three main components: CALMET, CALPUFF, and CALPOST and a large set of preprocessing programs designed to interface the model to standard, routinely-available meteorological and geophysical datasets. CALMET is a meteorological model that develops wind and temperature fields on a three-dimensional gridded modeling domain. Associated two-dimensional fields such as mixing height, surface characteristics, and dispersion properties are also included in the file produced by CALMET. CALPUFF is a transport and dispersion model that advects “puffs” of material emitted from modeled sources, simulating dispersion and transformation processes along the way. In doing so it typically uses the fields generated by CALMET, or as an option, it may use simpler non-gridded meteorological data much like existing plume models. Temporal and spatial variations in the meteorological fields selected are explicitly incorporated in the resulting distribution of puffs throughout a simulation period. The primary output files from CALPUFF contain either concentrations or deposition fluxes evaluated at selected receptor locations. CALPOST is used to process these files, producing tabulations that summarize the results of the simulation, identifying the highest and second highest 3-hour average concentrations at each receptor, for example. A general scheme of the modeling system is reported in Figure 1.21.

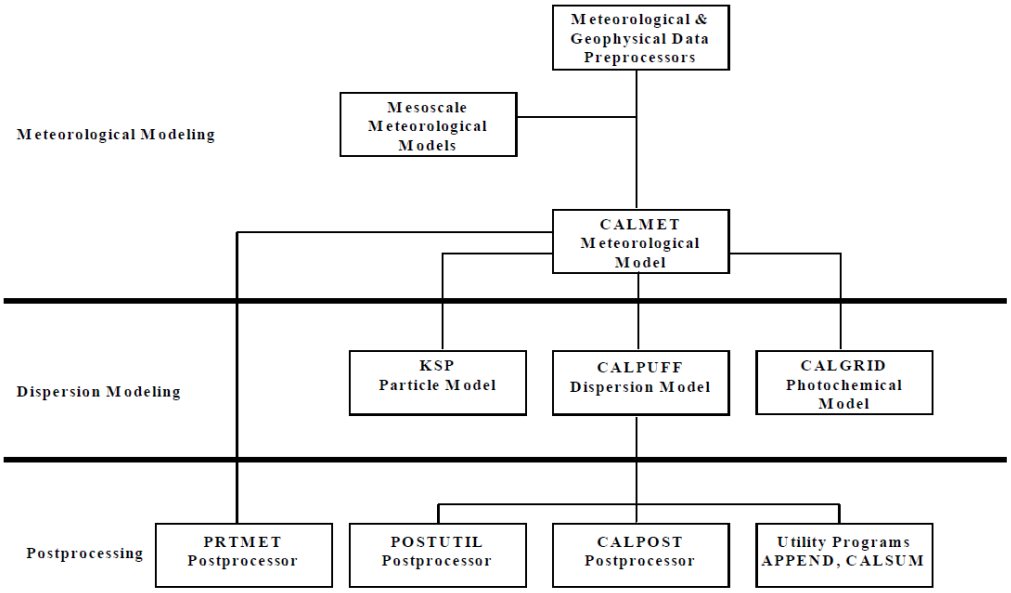

Figure 1.21. Overview of the program elements in the CALMET/CALPUFF modeling system (source US EPA, 2011).

CALPUFF can simulate the effects of time- and space-varying meteorological conditions on pollutant transport, transformation, and removal. It contains algorithms for near-source effects such as building downwash, transitional plume rise, partial plume penetration, subgrid scale terrain interactions as well as longer range effects such as pollutant removal (wet scavenging and dry deposition), chemical transformation, vertical wind shear, overwater transport and coastal interaction effects. It can accommodate arbitrarily-varying point source and gridded area source emissions. Most of the algorithms contain options to treat the physical processes at different levels of detail depending on the model application.

The major features and options for the CALPUFF model are summarized in Table 1.14.

Table 1.14. Major features of the CALPUFF model (source US EPA, 2011).

Source types
Point sources (constant or variable emissions)
Volume sources (constant or variable emissions)
Area sources (constant or variable emissions)
Line sources (constant or variable emissions)

Table 1.14 (continued). Major features of the CALPUFF model (source US EPA, 2011).

Non-steady-state emissions and meteorological conditions Gridded 3-D fields of meteorological variables (winds, temperature) Spatially-variable fields of mixing height, friction velocity, convective velocity scale, Monin-Obukhov length, precipitation rate Vertically and horizontally-varying turbulence and dispersion rates Time-dependent source and emissions data
Efficient sampling functions Integrated puff formulation Elongated puff (slug) formulation
Dispersion coefficient (σ_y, σ_z) options Direct measurements of σ_v and σ_w Estimated values of σ_v and σ_w based on similarity theory PDF treatment of dispersion in convective boundary layers Pasquill-Gifford (PG) dispersion coefficients (rural areas) McElroy-Pooler (MP) dispersion coefficients (urban areas) CTDM dispersion coefficients (neutral/stable)
Vertical wind shear Puff splitting Differential advection and dispersion
Plume rise Partial penetration Buoyant and momentum rise Stack tip effects Vertical wind shear Building downwash effects
Building downwash Huber-Snyder method Schulman-Scire method PRIME method
Subgrid scale complex terrain Dividing streamline, H_d: - Above H_d, puff flows over the hill and experiences altered diffusion rates - Below H_d, puff deflects around the hill, splits, and wraps around the hill
Interface to the Emissions Production Model (EPM) Time-varying heat flux and emissions from controlled burns and wildfires

Table 1.14 (continued). Major features of the CALPUFF model (source US EPA, 2011).

Dry Deposition Gases and particulate matter Three options: - Full treatment of space and time variations of deposition with a resistance model - User-specified diurnal cycles for each pollutant - No dry deposition
Chemical transformation options Pseudo-first-order chemical mechanism for SO_2, $SO^{=}_4$, NO_x, HNO_3, and NO^{-}_3(MESOPUFF II method) Pseudo-first-order chemical mechanism for SO_2, $SO^{=}_4$, NO, NO_2, HNO_3, and NO^{-}_3(RIVAD method User-specified diurnal cycles of transformation rates No chemical conversion
Wet Removal Scavenging coefficient approach Removal rate a function of precipitation intensity and precipitation type

Some of the technical algorithms are briefly in the following:

Dry Deposition: A full resistance model is provided in CALPUFF for the computation of dry deposition rates of gases and particulate matter as a function of geophysical parameters, meteorological conditions, and pollutant species. Options are provided to allow user-specified, diurnally varying deposition velocities to be used for one or more pollutants instead of the resistance model (e.g., for sensitivity testing) or to by-pass the dry deposition model completely.

Wet Deposition: An empirical scavenging coefficient approach is used in CALPUFF to compute the depletion and wet deposition fluxes due to precipitation scavenging. The scavenging coefficients are specified as a function of the pollutant and precipitation type (i.e., frozen vs. liquid precipitation).

Chemical Transformation: CALPUFF includes options for parameterizing chemical transformation effects using the five-species scheme (SO_2, $SO^{=}_4$, NO_x, HNO_3, and NO^{-}_3) employed in the MESOPUFF II model or a set of user-specified, diurnally-varying transformation rates.

Subgrid Scale Complex Terrain: The complex terrain module in CALPUFF is based on the approach used in the Complex Terrain Dispersion Model (CTDMPLUS) (Perry et al., 1989). Plume impingement on subgrid scale hills is evaluated using a dividing streamline (H_d) to determine which pollutant material is deflected around the sides of a hill (below H_d) and which material is advected over the hill (above H_d). Individual puffs are split into up to three sections for these calculations.

Puff Sampling Functions: A set of accurate and computationally efficient puff sampling routines are included in CALPUFF which solve many of the computational difficulties with applying a puff model to near-field releases. For near-field applications during rapidly-varying meteorological conditions, an elongated puff (slug) sampling function is used. An integrated puff approached is used during less demanding conditions. Both techniques reproduce continuous plume results exactly under the appropriate steady state conditions.

Wind Shear Effects: CALPUFF contains an optional puff splitting algorithm that allows vertical wind shear effects across individual puffs to be simulated. Differential rates of dispersion and transport occur on the puffs generated from the original puff, which under some conditions can substantially increase the effective rate of horizontal growth of the plume.

Building Downwash: The Huber-Snyder and Schulman-Scire downwash models are both incorporated into CALPUFF. An option is provided to use either model for all stacks, or make the choice on a stack-by-stack and wind sector-by-wind sector basis. Both algorithms have been implemented in such a way as to allow the use of wind direction specific building dimensions. The more advanced treatment of the PRIME downwash model is also incorporated as an option. This includes treating representative streamline patterns and diffusion rates in both the near and far wakes and recirculation effects in the cavity zone.

Dispersion Coefficients: Several options are provided in CALPUFF for the computation of dispersion coefficients, including the use of turbulence measurements (σ_v and σ_w), the use of similarity theory to estimate σ_v and σ_w from modeled surface heat and momentum fluxes, or the use of Pasquill-Gifford (PG) or McElroy-Pooler (MP) dispersion coefficients, or dispersion equations based on the Complex Terrain Dispersion Model (CDTM). Options are provided to apply an averaging time correction or surface roughness length adjustments to the PG coefficients. When similarity theory is used to compute turbulence-based

dispersion coefficients, an option is also provided for a PDF treatment of dispersion in the convective boundary layer.

5.2 Quantification of global carbon footprint

The environmental balance on a global scale is calculated as total carbon footprint associated with the steady state operation of the plants. The carbon footprint is defined as the total set of greenhouse gas emissions caused by a process, expressed as CO_2 equivalent (CO_{2eq}).

The most efficient procedure, as well as that most commonly used for the calculation of the carbon footprint, is Life Cycle Assessment (LCA). Life-cycle assessment is a technique to assess environmental impacts associated with all the stages of a process or product life, from cradle to the grave (i.e., from raw material extraction through materials processing, manufacture, distribution, use, repair and maintenance, and disposal or recycling). LCAs can help avoid a narrow outlook on environmental concerns by:

- compiling an inventory of relevant energy and material inputs and environmental releases;
- evaluating the potential impacts associated with identified inputs and releases;
- interpreting the results to help make a more informed decision.

LCA is a structured procedure, regulated by specific norms (UNI EN ISO 14040-14044), providing for clear evaluation phases, in terms of the definition of the system boundaries and the functional unit, and choice of the emission factors by a set of default databases. Moreover, the quantification of the environmental impacts can consist in the calculation of numerous environmental indicators associated with the process under study. The calculation of the contribution to global warming is just one of these indicators.

According to the objectives of the present study, the interest is not to conduct a comprehensive LCA on the considered energy interventions. The intention is thus not to apply step by step the analysis process, but rather use its methodological approach, which consists in assigning emission factors to the characteristic mass and energy flows. For each case study, the boundaries of the system will then be adapted, limiting them to the only phases that are relevant in

view of the global CO_{2eq} balance. As it will be showed in continuation, the carbon footprint of the biogas/biomethane case study will in fact be calculated on the basis of a "cradle to end use" approach, as the production of substrates (both in terms of credit and emissions of CO_{2eq}) has a significant impact on the final result. By contrast, for the case study on district heating, the overall balance will depend solely on the operating phase of the considered power units, having the other phases of the life cycle a negligible influence. More detailed information on the calculation methodology of GHG emission balance is reported in the description of each case study.

Part 2

Global and local emissions of a biogas plant considering the production of biomethane as an alternative end-use solution

Chapter 6

Introduction

Biofuel applications are acquiring an increasing importance as a component of low-carbon and renewable energy source. The European Union pushed member states toward the development of these technologies, by the emission of energy policies, as the Directive 2009/28/EC (2009), that promote the reduction of the greenhouse gas (GHG) emission and the use of energy from renewable resources. EU countries adopted these policies by introducing local regulations and feed-in schemes, further increasing the interest in bioenergy production.

Nonetheless, there is concern about the sustainability of bioenergy chains (Cherubini, 2008; Blengini et al., 2011). The conversion of biomass to energy is a complex process that involves physical and biological transformations, with relevant mass and energy exchanges connected both to agri-forestry subsystems and to industrial processes. The environmental compatibility of biofuel chains must be assessed, in order to guarantee an efficient performance in terms of GHG saving and production of renewable energy resources.

Anaerobic digestion of agricultural products (maize silage, triticale, sorghum etc.) and organic wastes from industry and agriculture is the most frequently employed bioenergy technology to this day. A survey study made by Fraunhofer Institute (2012) indicated around 10,000 biogas installations in Europe in 2012, expecting a raise to 13,500 units by 2016.

Until today, the predominant final use of biogas has been its on-site combustion in endothermic engines for the cogeneration of electricity and heat (Combined Heat and Power, CHP). Combustion represents an efficient destination for biogas, mostly if there is a need of thermal energy next to the production site (Patterson et al., 2011). On the other hand, biogas combustion holds back some environmental issues, that concern both global and local aspects. Local impacts are mainly represented by the formation of thermal NO_x due to the Zeldovich mechanism (Hill and Douglas, 2000), or by the generation of primary and secondary particulate matter (PM) (Tree and Svensson, 2007). Both pollutants represent a hazard to human health and ecosystems.

Research is addressing efforts to look for sustainable alternatives to biogas combustion. A possible future competition for conventional anaerobic degradation might be represented by biohydrogen, which has received significant attention from both the scientific community and stakeholders (Bakonyi et al., 2014). Anyway, to this day the most common alternative to biogas combustion consists in the production of biomethane, that is, separating methane fraction from other gaseous components by mean of a treatment process commonly referred as biogas upgrading.

Currently, the market of upgrading technologies is at the stage of development. Most these applications derive from the other gas separation know-how. The most frequently used technologies are pressurized water scrubbing (PWS), pressure swing absorption (PSA), chemical absorption with amine solutions (MEA), membrane permeation (MB) and cryogenic separation (CRY) (Makaruk et al., 2010). Other emerging technologies are those based on carbon mineralization. These latter may be distinguished between alkaline with regeneration (AwR) or bottom ash for biogas upgrading (BABIU) (Starr et al., 2011).

The mentioned processes allow the achievement of a methane rich fraction whose energy yield is potentially nearly equal to the one of biogas, thanks to limited conversion losses. In addition, the quantity of residual contaminants present in the methane fraction (H_2S, CO_2, oxygen, nitrogen, and other organic components) may be also limited, that makes biomethane adapt to be injected into the national gas transmission grid, or be employed as fuel in transports.

Although it represents a good opportunity, biomethane must be justified by an environmental perspective, since it involves additional energy consumption and

emissions with respect to biogas, seen that part of the methane is lost during the upgrading process. This environmental assessment represents the object of the present study. Part of the dissertation reported in the present Chapter has been previously published in a research article (Ravina and Genon, 2015).

Environmental sustainability of biogas has been treated widely in literature, in particular employing Life Cycle Assessment (LCA) tools, and there is a growing interest addressed to biomethane. Nonetheless, since biomethane is a quite novel application, there is a substantial lack of knowledge on the environmental aspects connected to the upgrading technologies. Poeschl et al. (2010b) included the analysis of different biogas utilization pathways in their study, indicating that the most efficient solution for small and large-scale biogas plants in terms of primary energy input to output was CHP generation with heat utilization at a relatively short transmission distance. Pertl et al. (2010) tried to identify an upgrading scenario featuring minimum overall GHG emissions. The study considered four different upgrading technologies (PWS, MB PSA and BABIU). BABIU-scenarios showed the lowest impact of GHG emissions thanks to the CO_2 sequestrated by the bottom ash. However, the authors put in evidence that the data obtained from this method are based solely on laboratory experiments. Considering the methods in practice, PWS was identified as the more ‘‘climate-friendly”. Starr et al. (2011) evaluated the LCA of four different biogas upgrading technologies (PWS, MEA, PSA, CRY) comparing them with AwR and BABIU on the basis of 1 ton of CO_2 removed (functional unit). The results still highlight that BABIU process shows the least environmental impact. Anyway, the authors put in evidence that these performances go beyond any economical evaluation.

This study, rather than give an insight on the different upgrading technologies, aimed to evaluate the environmental aspects of a biogas plant in terms of global (greenhouse gases) and local (NO_x and particulate matter) emissions, by comparing two alternative end-uses: the “traditional” combustion in a CHP unit and the “novel” upgrading to biomethane. The GHG contribution was calculated by using the carbon footprint methodology. A Gaussian model and a Lagrangian model were employed to calculate the local dispersion and concentration of gaseous pollutants NO_x and PM. The work was organized into three separate sections, described as follows:

- Task 1: Carbon footprint of biomethane production process was compared to that generated by the direct on-site combustion of biogas in a CHP unit.

- Task 2: Carbon footprint of biomethane production process was calculated for different levels of methane losses from the upgrading process.
- Task 3: Local dispersion of NO_x and PM was calculated for the combustion of the biogas and for its alternative solutions.

Chapter 7

Materials and methods

In the present chapter, the biogas producing process, the upgrading installation and the methodology employed for the environmental evaluation are described.

7.1 Biogas plant

The present study considers a biogas production through anaerobic digestion of cattle slurry and energy crops (maize silage). At today, the facility is not yet in operation, thus its exact location and technical configuration are only hypothesized. The location of the plant is supposed to be in the municipality of Borgaro Torinese, close to the urban center of Turin. The area of location is currently used for agricultural purposes. The selected location is strategic, as the following elements are present in the surroundings (Figure 2.1):

- Industrial activities, at a distance of around 500 meters, which represent a potential use of the thermal energy produced by the plant;
- Residential areas, at a distance of around 600 m, which also represent a possible use of the thermal energy produced, also through the construction of a small heating network;
- Two farms, at a distance of around 800-1000 m, which represent both a possible use of heat and a possible provider of substrates for the digester;

- A fuel station, which represents a possible reference site for the final use of biomethane.

The technical features of the plant were defined according to the most frequent configuration observed in the region, following the information collected and reported in the previous Part 1, Chapter 4.1. The plant works with a mesophilic process (42°C) and a hydraulic retention time of around 60 days. The anaerobic digester is fed by 47.5 t/d of maize and 48.5 t/d of cattle slurry. Biogas production is around 14,051 m^3/d and it is assumed to be composed of 53% of CH_4 and 47% of CO_2, percentages in volume. The feedstock-to-biogas mass balance of the plant is reported in Table 2.1. The data presented in Table 2.1 were taken from the average of the commercial plants in operation in Italy, reported by Saracco and Antonini (2014) and Brizio (2012). Biogas produced corresponds to about 2.5 MW of thermal energy available. It is desulfurized and then conveyed to an Otto engine, generating around 1 MW of electrical energy and 1 MW of thermal energy. The combustion takes place with an excess air ratio value of 40%.

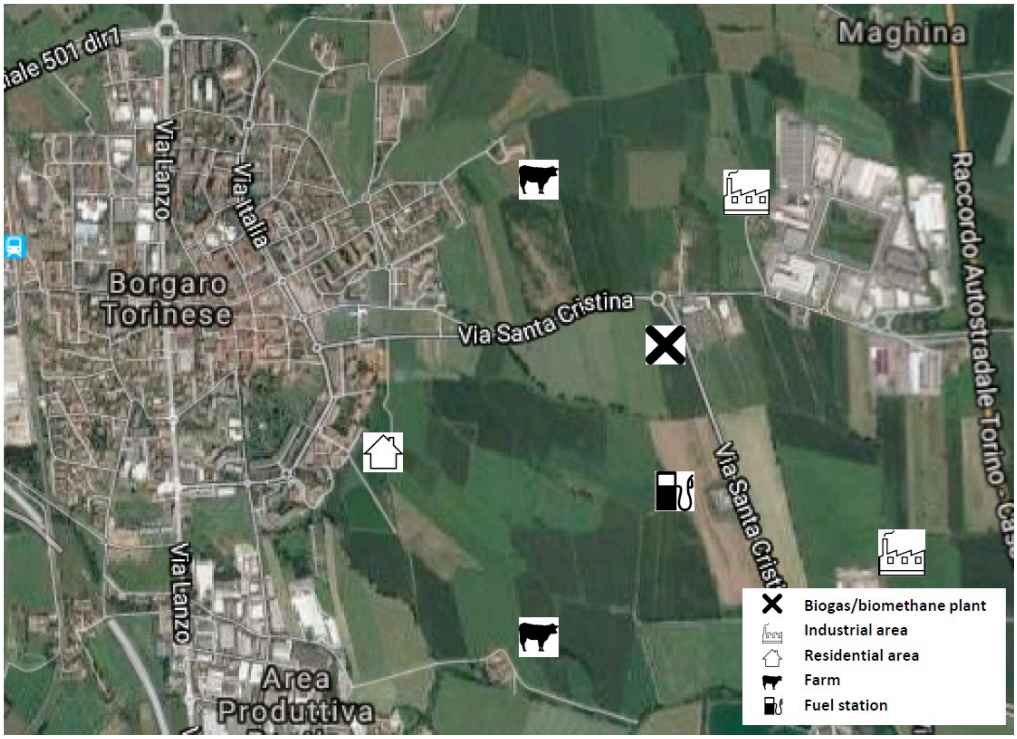

Figure 2.1. Location of the biogas plant and the potentially related activities in its surroundings.

Table 2.1. Estimation of biogas production of the reference plant

	Input (t/d)	Dry matter mass fraction	Volatile solids/ Dry Matter mass fraction	Volatile solids (VS) (t VS/d)	Biogas yield / Volatile solids (m^3/t VS) [1]	Biogas production (m^3/d)	Biogas production (t/d)
Cattle manure	48.5	0.22	0.75	8.0	400	3,200.3	
Maize silage	47.5	0.35	0.95	15.5	700	10,850.5	
Total	96	0.56		23.5		14,050.9	15.46

The functional scheme of the process together with the relevant flows for biogas combustion is reported in Figures 2.2 and 2.3. Biogas losses from digester were assumed to be 0.3% of total biogas produced, according to Dumont et al. (2013). Emission of unburnt methane from the engine was assumed to be 1.78% of the total methane contained in the biogas, according to Dumont et al. (2013)

[1] all volume magnitudes refer to normal conditions

and van Dijk (2011). The operating time of the plant was estimated to be 8,000 h/y. The amount of electricity auto-consumed by the plant was estimated to be 400 MWh/y. This value comes from field measurements made by Buratti et al. (2013) on a 1 MW biogas plant with similar working conditions of the present. Other studies show a variability in parasitic electricity demand, depending on requirements for stirring to maintain slurry homogeneity, pumping and conveying liquid feedstock and other auxiliary equipment (Poeschl et al., 2010b). The amount of thermal energy auto-consumed by the plant was calculated as the sum of the power needed to heat up the incoming fresh matter (0.23 MW) and the power needed to compensate thermal dispersion of the digester (0.05 MW).

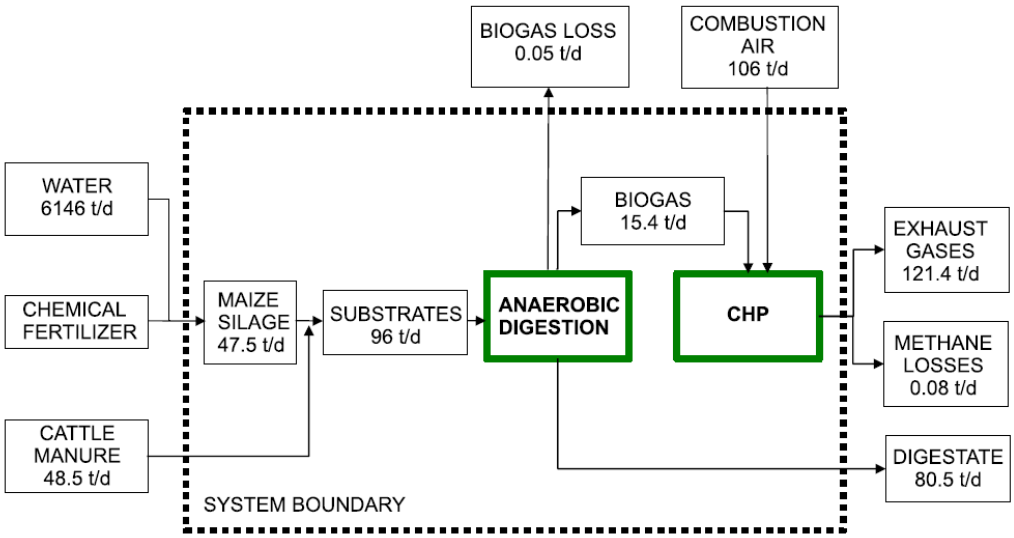

Figure 2.2. Mass balance of biogas production and combustion in a CHP unit (daily values referred to one year of exercise)

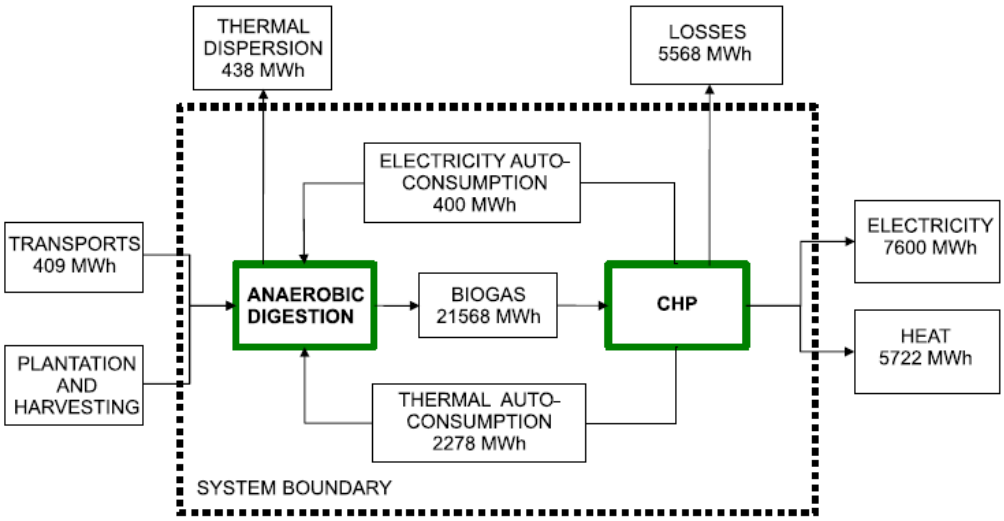

Figure 2.3. Energy balance of biogas production and combustion in a CHP unit (values referred to one year of exercise)

7.2 Biogas refining plant

Biomethane is obtained by physical absorption of CO_2 with pressurized water (6-12 atm). Physical absorption is the most commonly used technique for biogas refining to this day, thanks to its high recovery efficiency and limited cost and environmental aspects (Ryckebosch et al., 2011). A reference scheme of the process is reported in Figure 2.4. Biogas is first desulfurized and dried, then it is introduced from the bottom of a tall vertical tower and the water is fed in counterflow at the top of the tower. Due to its relatively high solubility in water, CO_2 is absorbed while most part of the CH_4 remains in the gaseous phase. Unfortunately, a part of the methane is also absorbed by the water, so the system must better be equipped with a flash tank and a recirculation system, where a methane-rich gas mixture is recovered and recirculated at the biogas input. The water is then depressurized to 2-5 atm and separated from CO_2 in the desorption column. A detailed description of the process design is reported in Appendix 1.

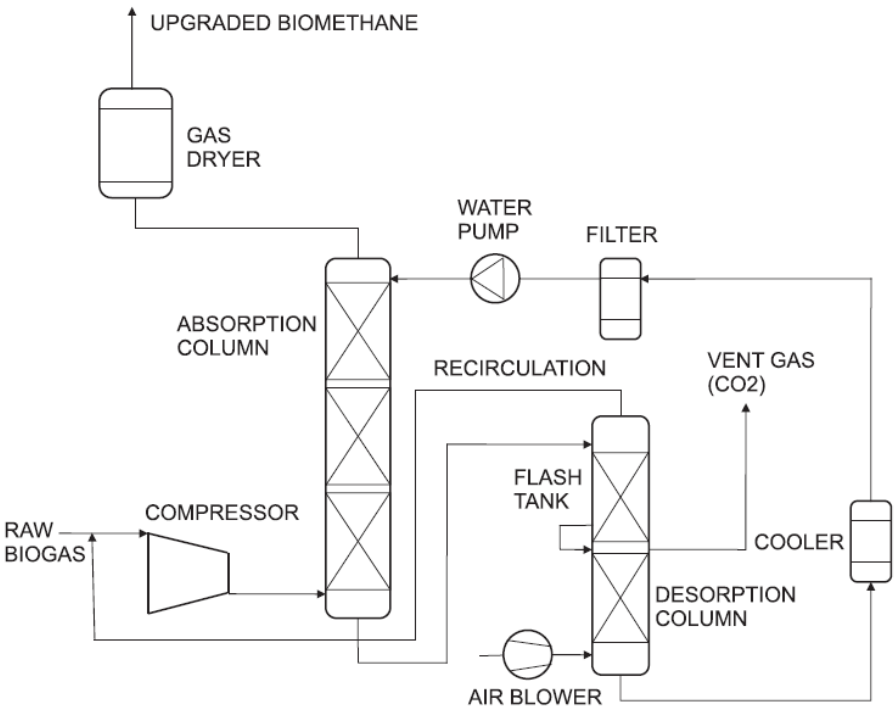

Figure 2.4. Biogas upgrading process with pressurized water

Three system configurations were selected for the study, depending on the fraction of methane still absorbed in the water at the end of the process (i.e. the methane slip), that is thought to affect the environmental balance of the plant. The dimensioning of each of the three configurations was carried out by solving a system of equations representing the simultaneous absorption of CO_2 and CH_4 and the overall material balance of the system (see Appendix 1). The calculation was solved numerically by using GNU Octave software (GNU, 2014). The results are resumed in Table 2.2. These data were taken as reference for the calculation of GHG balance reported in the following sections. They are referred as low, middle and high methane slip scenario (LO-SLIP, MID-SLIP, HI-SLIP) and correspond to a methane loss of 0.05%, 1.4% and 4% of the original methane content respectively.

Table 2.2. Simulation results for upgrading process balance depending on methane losses. L is the flow of absorbing water; y refers to molar fraction in the gas; x refers to the molar fraction in the liquid; subscript b refers to the exit of the column; superscript refers to methane, otherwise to CO_2; subscript FT refers to the exit of the flash tank; F is the recirculated flow; Z is the height of the absorption column

Scenario Methane slip	Flash tank	L (m^3/h)	P (atm)	y_b	x_b	x'_b	x_{FT}	x'_{FT}	y_{FT}	y'_{FT}	F (mol/h)	Z (m)
HI-SLIP 4%	no flash tank	59.2	12	0.470	$3.07\cdot10^{-3}$	$1.47\cdot10^{-4}$	-	-	-	-	-	11.50
MID-SLIP 1.4%	flash tank @ 5 atm	90.0	10	0.486	$2.20\cdot10^{-3}$	$1.12\cdot10^{-5}$	$2.00\cdot10^{-3}$	$3.22\cdot10^{-5}$	0.721	0.279	1,438	10
LO-SLIP 0.05%	flash tank @ 2 atm	150.0	12	0.771	$4.92\cdot10^{-3}$	$6.30\cdot10^{-5}$	$1.09\cdot10^{-3}$	$7.4\cdot10^{-7}$	0.984	0.016	32,392	18.50

The functional scheme of the process together with the relevant flows for biomethane production for the MID-SLIP scenario is reported in Figures 2.5 and 2.6. In the case of biomethane production, no engine is present, so it was assumed that the electricity needed for auto-consumption was taken from the Italian national distribution grid, with an efficiency of conversion of 92% (net kWh per delivered kWh). Thermal energy demand was satisfied by a boiler fueled by natural gas, also considering an efficiency of conversion of 92% (Buratti et al., 2013). The only components of the refining plant causing relevant electricity consumption were intended to be the compressor for the biogas input to the absorption column and the pump for the circulation of the absorbing water along the column. A partial recovery of the thermal energy generated by biogas compression was considered.

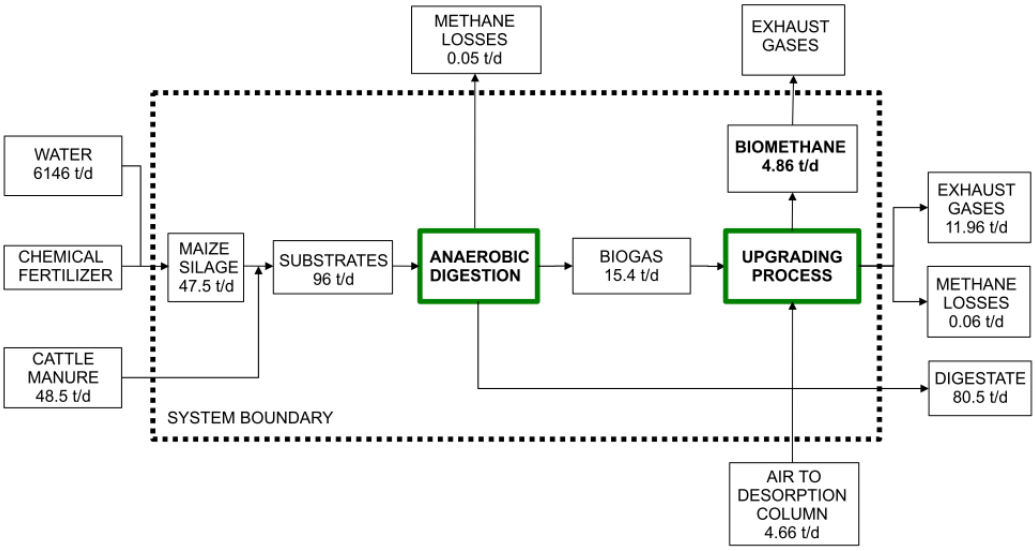

Figure 2.5. Mass balance of biogas production and upgrading to biomethane (MID-SLIP scenario, daily values referred to one year of exercise)

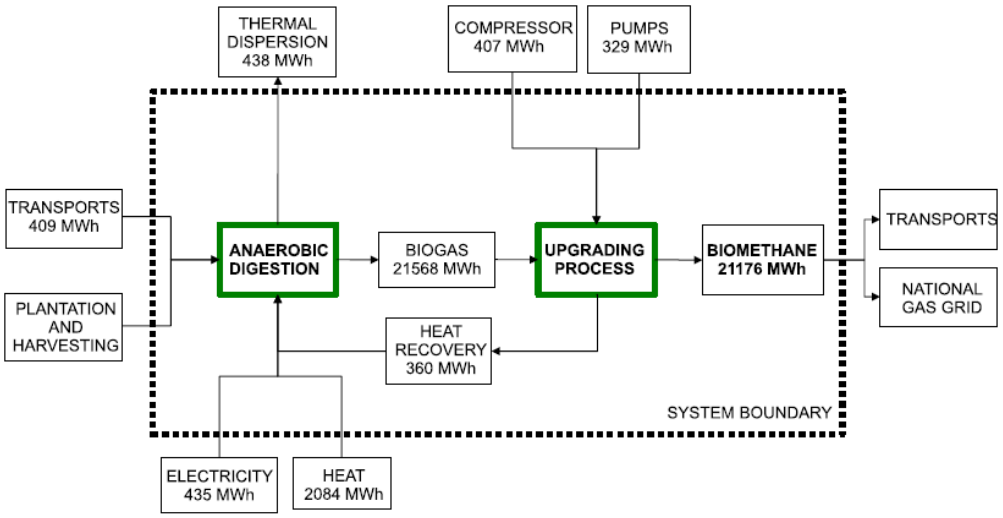

Figure 2.6. Energy balance of biogas production and upgrading to biomethane (MID-SLIP scenario, values referred to one year of exercise)

7.3 Methodology for carbon footprint

Carbon footprint is part of the Life Cycle Assessment (LCA) of a material or process and calculates the burden of greenhouse gases in terms of equivalent CO_2 emitted. Carbon footprint was employed in the calculation of CO_{2eq} emissions of biogas and biomethane production process according to ISO/TS 14067 standards

(2013). In Task 1, the CO_{2eq} emissions of biomethane production process (MID-SLIP scenario) were compared to those generated by the direct on-site combustion of biogas in a cogenerating engine. Biomethane emissions were evaluated depending on two different utilizations, i.e. injection to the national grid or use as fuel for transports. For biogas, both the utilization or not of the thermal energy produced was considered. Thus, Task 1 consisted of four different scenarios:

- biogas combustion with cogeneration of electrical and thermal energy (scenario B-H);
- biogas combustion with the generation of electricity only (scenario B-NH);
- biomethane to be injected into the national grid at an absolute pressure of 5 atm (scenario M-G);
- biomethane to be used in transports, considering a compression and storage system working at 247 atm and consuming an electrical power of around 120kW (CRPA, 2009) (scenario M-T).

In Task 2 a comparison of the CO_{2eq} emissions for three different scenarios of methane slip for biomethane production plant was calculated, considering injection to the national grid as the final use. In all cases, the system boundaries were defined following a "cradle to end-use" approach. The "cradle" boundary was identified with the production process of the feedstock entering the digester. The "end-use" boundary for biogas combustion was the engine exhaust stack, while for biomethane production was its combustion in means of transport or for generic residential use. The functional unit selected was the ton of biogas produced. Biogas is assumed to be composed of 53% of CH_4 and 47% of CO_2 in volume.

The calculation started by the characterization of the relevant mass and energy flows for the cases considered. Mass and energy flows were then coupled with relative CO_{2eq} emission factors, selected among those reported in the bibliography. The emission factors are reported in Table 2.3, together with their references. The other main assumptions taken for the study are:

- emissions from digestate management were not considered, nor as an output during the post-production storage (assuming a completely sealed storage) nor as a credit for its re-use in agriculture.
- direct (dLUC) and indirect (iLUC) land use change contribution to emissions were not considered;

- CO_2 emissions from biogas and biomethane combustion were not considered, as they were generated from a biogenic source;
- for biogas combustion scenarios, temporary storage and distribution of cogenerated heat and electricity were not accounted, which meant considering the user or the transmission grid at a close distance from the plant;
- for biomethane scenarios, no processes between the final gas storage and the combustion were accounted, which meant neglecting infrastructure for gas injection and possible losses due to leaky pipelines or shut-off devices.

Table 2.3. Emission factors for equivalent CO_2 emissions

Emission flow	Value of emission factor	Reference	Note
Maize silage plantation (direct emissions)	606.79 gCO_{2eq}/ha	IPCC	Considering a specific production of 42.5 t biogas/ha, single crop (Brizio, 2012)
Maize silage plantation (indirect emissions)	490.24 gCO_{2eq}/ha	IPCC	
Temporary storage of substrates	1.74 gCO_{2eq}/MJ biogas	Buratti et al. (2013)	Comprehensive value estimated for a biogas plant with same conditions and size
Substrates transportation to digester	266.76 gCO_{2eq}/kWh of carriage	IPCC	Assuming a covering distance of 50 km for both the transportation of maize silage and manure, using tank trucks with 27 tons of capacity
Methane losses	GWP=25	IPCC	Methane global warming potential
Electrical energy	440 gCO_{2eq}/kWh	PAEE (2011)	Italian national energy mix for grid electricity.

Table 2.3 (continued). Emission factors for equivalent CO_2 emissions

Emission flow	Value of emission factor	Reference	Note
Thermal energy	202 gCO_{2eq}/kWh	IPCC	Italian national energy mix for thermal energy
Emission credit for substitution of fossil fuel with biomethane in transport	256 gCO_{2eq}/kWh	IPCC; ANFIA (2014)	Average value of diesel, gasoline and LPG emission factors, weighted for the percentage of diffusion in Italian transports

7.4 Methodology for NO_x and particulate matter local emission and dispersion

The objective of Task 3 is the evaluation of NO_x and particulate matter (PM) emission and dispersion to estimate local impacts of the biogas plant and its alternative solution. The environmental impacts were quantified by calculating the concentration difference at ground level between present and future energy configurations. The results were then reported in form of a map indicating an increase or decrease in NO_x and PM average concentrations with respect to the present situation. Two operating scenarios were considered:

- **Scenario 3-B.** Biogas is conveyed to a gas engine for its direct on-site combustion and cogeneration. This scenario contemplates that a demand of thermal energy (from industrial or residential activities) is effectively present in the surrounding of the plant. Thus, the present energetic configuration is represented by a conventional industrial (or residential) heater fueled by natural gas, while the future configuration is represented by the cogeneration unit fueled by biogas.
- **Scenario 3-M.** Biogas combustion is substituted by the production of biomethane. This scenario contemplates that a demand of thermal energy is not actually present in the surrounding of the plant. In this case, the present energetic configuration generates no emissions next to the production site. Biomethane is in fact considered as an energy

vector going to either be injected to the national gas grid or used as a fuel for transports. Emissions generated by its combustion are thus not eliminated but transferred to an unspecified location outside the system boundaries. The future configuration is represented by the emissions generated by the auxiliary system connected to the biogas facility. The auxiliary system considered in the future configuration is assumed to be a conventional heater fueled by natural gas, technically equal to that considered in scenario 3-B.

An alternative to 3-M scenario could consist in directly burning part of the produced biogas to satisfy the demand of auxiliary systems. This is a quite common operative option in the reality, as it does not contemplate an external source of thermal energy (C.R.P.A., 2009). Nevertheless, this opportunity was not considered in the present study, because the intent was to evaluate the environmental performance of biomethane considering its maximum potential use. In addition, a secondary reason for which 3-M scenario is in some case preferable is that subtracting part of the biomethane to the final use may result in a worse economic balance (lower income from subsidies schemes).

7.4.1 Source characterization

For the characterization of the emission sources, a literary review was conducted on existing studies on biogas combustion in endothermic engines, keeping into account that NO_x formation is strongly affected by the excess air-to-fuel ratio (λ) (Hill and Douglas, 2000). Blengini et al. (2011) report an NO_x concentration at the stack of 112.5 to 450 mg/m^3, depending if a selective catalytic removal system (SCR) is installed or not. A study from Thomas and Wyndorps (2011) reports measurements of NO_x emitted by a 192 kW engine fed by biogas with λ ranging from 1.5 to 1.65. Values of concentration range initially between 300 and 1,000 mg/m^3, firmly approaching to 350-400 mg/m^3 once air-to-fuel ratio is forced to the upper limit (λ=1.65). A measurement campaign reported by van Dijk (2011) revealed an average NO_x concentration value of 670 mg/m^3 for a 360 kW power engine working with an excess air of 43%. A third study, from Huang and Crookes (1998) reports an NO_x concentration ranging between 614 and 3,926 mg/m^3 depending on the excess air reaching the combustion chamber, the higher values corresponding to the lower ratio (λ=1.05). The Italian environmental regulation imposes a limit concentration for NO_x of 500 mg/m^3,

meaning that an abatement system should be installed if the emissions approach this order of magnitude. Given these considerations, the value of NO_x concentration at the stack for this plant is assumed to be 400 mg/m^3, corresponding to an NO_x mass flow of 178 mg/s.

The emission of PM leaving the biogas engine was calculated as total suspended particulate (TSP), considering the contribution of both primary and secondary particulate. The composition of the exhaust gases from biogas combustion in a gas engine reported by Blengini et al. (2011) was taken as a reference. The concentration of primary particulate was estimated to be 1 mg/m^3, corresponding to a mass flow of 1.3 mg/s. The concentration of secondary particulate was calculated starting by other gaseous pollutants and applying the following aerosol formation factors, to be considered by weight: NO_x 0.88; SO_2 0.54; NH_3 0.64; volatile organic compounds (VOC) 0.02 (de Leeuw, 2002). The calculation of the emission mass flow of primary and secondary PM is reported in Table 2.4. The value of total particulate matter emitted from the stack is 168.8 mg/s.

Table 2.4. Mass flow of primary and secondary particulate matter emitted from the biogas engine stack.

Component	Concentration (mg/m^3) (Blengini et al., 2011)	Emission factor for secondary PM (de Leeuw, 2002)	PM flow (mg/s)
Primary PM	1	-	1.3
NO_x	400	0.88	157.0
VOC	100	0.02	0.9
SO_2	40	0.54	9.6
NH_3	-	0.64	-
Sum of Secondary PM			167.5
Total PM			**168.8**

NO_x and PM emitted from the conventional NG heater were estimated starting by EPA emission factors (US EPA), as reported in Table 2.5, considering the same aerosol formation factors provided by de Leeuw (2002). This table also

differentiates the emission flows between 3-B and 3-M scenarios. The emission flow in 3-M scenario is clearly lower than 3-B scenario since the thermal energy demand is produced just for the plant auto-consumption.

Table 2.5. Emission factors and emission flows for NG industrial boiler. Data were taken from US EPA.

Component	Emission factor (lb/ft^3 fuel)	Emission factor (g/m^3 fuel)	Emission flow Scenario 3-B (mg/s)	Emission flow Scenario 3-M (mg/s)
Primary PM ($PM_{2.5}$+PM_{10})	$7.6 \cdot 10^{-6}$	1.87	3.54	0.92
NO_x	$1.9 \cdot 10^{-4}$	46.88	88.54	23.07
VOC	$5.5 \cdot 10^{-6}$	1.36	2.56	0.67
SO_2	$6 \cdot 10^{-7}$	0.15	0.28	0.07
Secondary PM			78.12	20.35
Total PM			**81.66**	**21.28**

7.4.2 Dispersion models

The dispersion of NO_x and PM was estimated using two different models, estimating the concentration at ground level (Hill and Douglas, 2000):

- A stationary plume Gaussian model;
- The CALPUFF Lagrangian model.

Stationary Gaussian model

The stationary gaussian model was developed with the GNU Octave software (GNU, 2014). Mean wind speed (3 m/s) and mean temperature (12.5°C) at source location were estimated according to the meteorological data available (ARPA). The dispersion coefficients were calculated using Pasquill-Gifford formulations (Mohan and Siddiqui, 1998). For the calculation of particulate matter concentration, a deposition speed of particles was considered according to Stokes law, considering a mean particle radius of 10 μm. A detailed description of the

model formulation and parameters is reported in Appendix 2. The relevant parameters of the two sources are reported in Table 2.6.

Simulations were run with assuming A and F atmospheric stability class, i.e. unstable and stable conditions respectively. Concentrations of NO_x and PM were calculated generating ground level maps for the immediate evaluation of the impacts.

Table 2.6. Parameters for the Gaussian dispersion model

Parameter	Biogas CHP unit	NG conventional boiler
Mean wind speed at source location (m/s)	3.0	3.0
Mean ambient temperature (°C)	12.5	12.5
Exit speed of exhaust gases (m/s)	17.9	15.9
Chimney internal radius (m)	0.15	0.1
Exhaust gas temperature (°C)	500.0	200.0
Height of emission source (m)	10.0	10.0

CALPUFF Lagrangian model

In alternative to the gaussian model, the scenarios were reproduced using the CALPUFF model. The general description of this model is reported in Part 1, Chapter 5.1. The simulations of the present case studies were run with the same general settings of the model reported in Part 3, Chapter 12.4. The definition of the modeling domain, as well as weather and orographic data, are the same. They are not reported here to avoid repetitions.

The biogas plant and the conventional NG boiler were treated as point sources. Not having a real position, the conventional boiler was placed in the same location of the stack of the biogas engine (UTM coordinates: X=1,395,769 m; Y=5,000,276 m). The source parameters used in the simulations were the same as those used with the Gaussian model, reported in Table 2.6.

The procedure for generating the source input files, as well as that used for data post-processing is the same as described in Part 3 of the present study.

Chapter 8

Results of global emissions

The results of the analysis on global emissions are reported in the present chapter, followed by a brief comprehensive discussion. It must be pointed out that the main sources of emission are characterized by a high degree of uncertainty, in particular for what concerning biogas production. The energy consumption and GHG emission of the whole process of farming, temporary storage and transport of the substrates, as well as the losses from the digester may vary up to one order of magnitude from the values considered in the present study (Tufvesson et al., 2013; Flesch et al., 2011). The calculation of the energy auto-consumption of the system is also affected by a high level of uncertainty. Electricity consumption of auxiliary installations was calculated as a fraction of the output electrical power; the thermal power requirement was determined on the basis of average meteorological conditions and average configuration (dimensions, materials) of the system. In the part of the process concerning biomethane production, the uncertainty was restrained by defining a more detailed dimensioning of the system, as reported in Chapter 7.2.

8.1 Global balance of biomethane vs. biogas combustion (Task 1)

Global emissions for the four scenarios included in Task 1 were calculated in terms of tons of CO_{2eq} emitted on a yearly basis and tons of CO_{2eq} per ton of biogas leaving the anaerobic digester. The relevant mass and energy flow influencing the GHG balance are reported in Table 2.7. The complete results in

terms of CO_{2eq} emissions are reported in Table 2.8. Negative values refer to emission savings.

Table 2.7. Mass and energy flow influencing GHG emissions for one year of exercise (Task 1).

	Scenario			
	B-H	**B-NH**	**M-G**	**M-T**
Plantation surface (ha)	1.12	1.12	1.12	1.12
Energy consumption for transports of substrates (kWh)	409,337	409,337	409,337	409,337
Methane losses from digester (t)	8.2	8.2	8.2	8.2
Methane losses from combustor (t)	27.02	27.02	-	-
Net electrical energy injected to the grid (MWh)	7,600	7,600	-	-
Electrical energy extracted from the grid for biogas plant auxiliary systems (MWh)	-	-	434.78	434.78
Thermal energy produced and capitalized (MWh)	5,722	-	-	-
Thermal energy for auto-consumption of biogas plant, taken from external source (MWh)	-	-	2,084.3	2,084.3
Methane losses from biomethane production process (t)	-	-	21.2	21.2
Electrical energy extracted from the grid for biomethane production (MWh)	-	-	737	1,697
Biogas energy content (MWh)	21,568	21,568	21,568	21,568
Biomethane energy content (MWh)	-	-	21,176	21,176

Table 2.8. GHG balance for one year of exercise (Task 1)

	Tons of CO_{2eq} emitted				**Specific emission (tCO_{2eq}/t biogas)**			
	Scenario				**Scenario**			
	B-H	**B-NH**	**M-G**	**M-T**	**B-H**	**B-NH**	**M-G**	**M-T**
Temporary storage of substrates	135.1	135.1	135.1	135.1	0.026	0.026	0.026	0.026
Transport of substrates to digester	109.2	109.2	109.2	109.2	0.021	0.021	0.021	0.021
Maize silage plantation	408.6	408.6	408.6	408.6	0.079	0.079	0.079	0.079
Methane losses from digester	563.2	563.2	563.2	563.2	0.109	0.109	0.109	0.109
Methane losses from combustor	1858.0	1858.0	-	-	0.361	0.361	-	-
Electrical energy produced	-3,344.0	-3,344	-	-	-0.649	-0.649	-	-
Electrical energy consumed for auxiliary systems (biogas plant)	-	-	191.3	191.3	-	-	0.037	0.037
Thermal energy produced	-1,156.0	-	-	-	-0.224	-	-	-
Thermal energy for auto-consumption (biogas plant)	-	-	421.0	421.0	-	-	0.082	0.082
Methane losses from biomethane production process	-	-	1,457.3	1,457.3	-	-	0.283	0.283
Electrical energy consumed for biomethane production	-	-	324.3	746.7	-	-	0.063	0.145
Substitution of natural gas into the grid	-	-	- 4,277.9	-	-	-	0.830	-
Substitution of transport fuels	-	-	-	-5,411.2	-	-	-	-1.050
Produced emissions	3,074.1	3,074.1	3,610.0	4,032.4	0.596	0.596	0.700	0.782
Avoided emissions	-4,500.0	-3,344	-4,278	-5,411.2	-0.873	-0.649	-0.830	-1.050
Balance	**-1,425.9**	**-269.9**	**-667.9**	**-1,378.8**	**-0.277**	**-0.053**	**-0.130**	**-0.268**

All scenarios show a negative balance of GHG gases, meaning that avoided emissions are higher than produced emissions. CHP combustion of biogas with thermal energy utilization (scenario B-H) shows the most favorable result in terms of CO_{2eq}, while the balance worsens if the thermal energy is not used and entirely released to the atmosphere, approaching to a null specific emission (-0.052 tCO_{2eq}/t biogas of scenario B-NH).

The upgrading process of biogas to biomethane causes higher CO_{2eq} emissions, due to the electricity consumption for compressing, pumping and storage systems. The specific emission rises from 0.596 tCO_{2eq}/t biogas (scenarios B-H and B-NH) to 0.701 and 0.783 tCO_{2eq}/t biogas (scenarios M-G and M-T respectively). Reduction of specific emission in scenario M-G is on the same range of scenario B-H, as both cases concern the substitution of natural gas. The contribution of methane losses from the process on the emission is similar for both B and M scenarios. In fact, in B scenarios, a fraction of methane equal to 27 t/y is not burnt and escapes from the engine, while in M scenarios a quantity of 21 t/y of methane is lost during the upgrading process. Emission savings increase if biomethane for transports is considered. The specific CO_{2eq} reduction rises from -0.873 tCO_{2eq}/t biogas of scenario B-H to -1.050 tCO_{2eq}/t biogas of scenario M-T, due to the substitution of a fossil fuel mix (diesel, gasoline, LPG) causing higher environmental impacts than natural gas.

The results show that direct combustion of biogas in a CHP unit represents the most favorable solution in terms of GHG emission only in the case that there is a real external need of thermal energy (heating, cooling, process water or vapor). Sustainability comes less if the cogenerated thermal energy is not capitalized. This aspect is confirmed by studies reported in the literature (Patterson et al., 2011; Poeschl et al., 2012b). On the other hand, biomethane production represents a viable alternative, especially for the substitution of fossil fuel for transports. A study by Poeschl et al. (2010a) reports a GHG saving for biomethane for transports of 1.15 $kgCO_{2eq}$/kg biomethane, corresponding to -1,721.8 t/y of CO_{2eq}. The work of Buratti et al. (2013) reports a specific emission produced of 0.947 tCO_{2eq}/t biogas for a plant configuration comparable to scenario M-T. Another study from Power and Murphy (2009) reports a net GHG saving for biomethane in transports ranging between 0.017 kg/MJ and 0.02 kg/MJ depending on the feedstock, corresponding to -1,295 to -1,524 t/y of CO_{2eq}. Pertl et al. report a specific emission for biomethane production ranging from 0,235 tCO_{2eq}/t biogas (BABIU process) to 2,355 tCO_{2eq}/t biogas (MB process).

For the evaluation of these results, it is also important to recall the considerations made on the uncertainty related to the data. To give an example, if methane loss from the digester was increased from 0.3% to 1% (value that was measured by Flesch et al. during their field campaign), the CO_{2eq} balance for scenario B-H would shift from -0.277 tCO_{2eq}/t biogas to -0.02 tCO_{2eq}/t biogas, corresponding to almost no environmental benefit for the process. With the aim of better characterize the variability on biogas process, some authors reported sensitivity analysis with respect to the main variables affecting GHG emissions in biomethane and biogas systems, in particular: the feedstock employed as substrate (Blengini et al., 2011; Poeschl et al., 2012b; Tufvesson et al., 2013), methane losses from the digester (Flesch et al., 2011), the distance of transportation of the substrates (Poeschl et al., 2012b) and the digestate management (Poeschl et al., 2012a, 2012b; Tufvesson et al., 2013).

8.2 Contribution of methane emissions (Task 2)

Task 2 consisted of the evaluation of three different upgrading configurations (LO-SLIP, MID-SLIP and HI-SLIP). MID-SLIP scenario represents the same configuration of M-G scenario. Mass and energy balance for the portion of the process concerning biogas production does not differ from those reported for scenario M-G, except for the amount of thermal energy needed for the auto-consumption of the biogas plant, which also depends on the thermal energy recovered from the compressors. The relevant mass and energy flow related to the upgrading process are reported in Table 2.9. The complete results in terms of CO_{2eq} emissions are reported in Table 2.10. Negative values refer to GHG emission savings.

Table 2.9. Mass and energy flow influencing GHG emissions for one year of exercise (Task 2).

	Scenario		
	LO-SLIP (0.05%)	**MID-SLIP (1.4%)**	**HI-SLIP (4%)**
Biomethane production (t)	1,513.4	1,492.9	1,451.0
Biomethane loss (t)	0.75	21.2	60.6
Energy content of biomethane (MWh)	21,616	21,176	20,608
Upgrading process consumption			
Compressors (MWh)	1,037.6	407.5	423.3
Pumping system (MWh)	665.5	329.4	262.9
Heat recovery from compressors (MWh)	398.2	360.4	398.2
Thermal energy for auto-consumption of biogas plant, taken from external source (MWh)	2,043.2	2,084.3	2,043.2

Table 2.10. GHG balance for one year of exercise (Task 2)

	Tons of CO_{2eq} emitted			**Specific emission (tCO_{2eq}/t biogas)**			**Contribution to total emission (%)**		
	Scenario			**Scenario**			**Scenario**		
	LO-SLIP (0.05%)	**MID-SLIP (1.4%)**	**HI-SLIP (4%)**	**LO-SLIP (0.05%)**	**MID-SLIP (1.4%)**	**HI-SLIP (4%)**	**LO-SLIP (0.05%)**	**MID-SLIP (1.4%)**	**HI-SLIP (4%)**
Biogas production process (see Table 2.8)	1,820.1	1,828.4	1,820.1	0.353	0.355	0.353	69.4	50.6	29.0
Biogas upgrading process electrical consumption	749.4	324.3	301.9	0.145	0.063	0.059	28.6	9.0	4.8
Methane losses from upgrading process	51.9	1,457.3	4,164.2	0.010	0.283	0.808	2.0	40.4	66.2
Produced emissions	2,621.4	3,610.0	6,286.2	0.509	0.701	1.220	100	100	100
Substitution of natural gas into the grid	-4,366.8	-4,277.9	-4,163.2	-0.848	-0.830	-0.808	-	-	-
Avoided emissions	-4,366.8	-4,277.9	-4,163.2	-0.848	-0.830	-0.808	-	-	-
Balance	**-1,745.4**	**-667.9**	**2,123.0**	**-0.339**	**-0.130**	**0.412**	**-**	**-**	**-**

The LO-SLIP scenario shows a favorable emission balance, accounting for a specific emission of -0.339 tCO_{2eq}/t biogas. The electricity consumption reaches 1,703 MWh/y, due to the high circulation flow and high pressure in the absorption column, but the relative emissions are counterbalanced by the low amount of methane released during the upgrading process (around 0.8 t/y).

GHG emission balance of HI-SLIP scenario results positive, indicating that 0.412 tons of CO_{2eq} are emitted for each ton of biogas produced. The process results no longer environmentally sustainable. It is important to note that, in this case, the avoided emissions obtained by the injection of biomethane into the grid are completely canceled by those generated by methane losses (0.808 t/y).

The results are still more evident if the contribution of the processes is evaluated in terms of percentage of the total process emissions, as reported in Table 2.10 and Figure 2.7. A methane loss of 1.4% corresponds to the 40% of the total CO_{2eq} released to the atmosphere. The contribution in percentage still rises to 66% if methane slip increases to 4%, while it decreases to 2% when losses are contained within 0.05%.

Other authors reported on the importance of limiting methane losses from biomethane production process. Patterson et al. (2011) evaluated the impact of increasing methane losses to 5% and reducing methane losses to 0.5%. In the first case, GHG emission was increased by 16% for a scenario similar to M-T and by 6% for a scenario similar to M-G. Decreasing methane losses to 0.5% had the effect of reducing GHG emission by 30% for a scenario similar to M-T and by 8.5% for a scenario similar to M-G. These results highlight the requirement to reduce technical and operational methane losses during the upgrading process as far as is practicable.

The contribution to GHG emissions of the electricity consumption of biogas upgrading process results less significant than methane slip, although it gains weight for the LO-SLIP scenario. In this perspective, the choice of the upgrading technology results essential. Some authors reported on the specific energy consumption of different upgrading technologies. Bekkering et al. (2009) calculated the electricity need of four different upgrading processes, indicating the following average values per cubic meter (normal conditions) of clean gas: PWS, 0.4 kWh; PSA with vacuum, 0.25 kWh; MB, 0.14 kWh; Chemical absorption, 0.12 kWh. Another study by Brizio (2012) considered four different systems

(PWS, absorption with glycol ethers, MEA and PSA) indicating a specific energy consumption between 0.1 and 1.03 kWh per m^3 of biomethane.

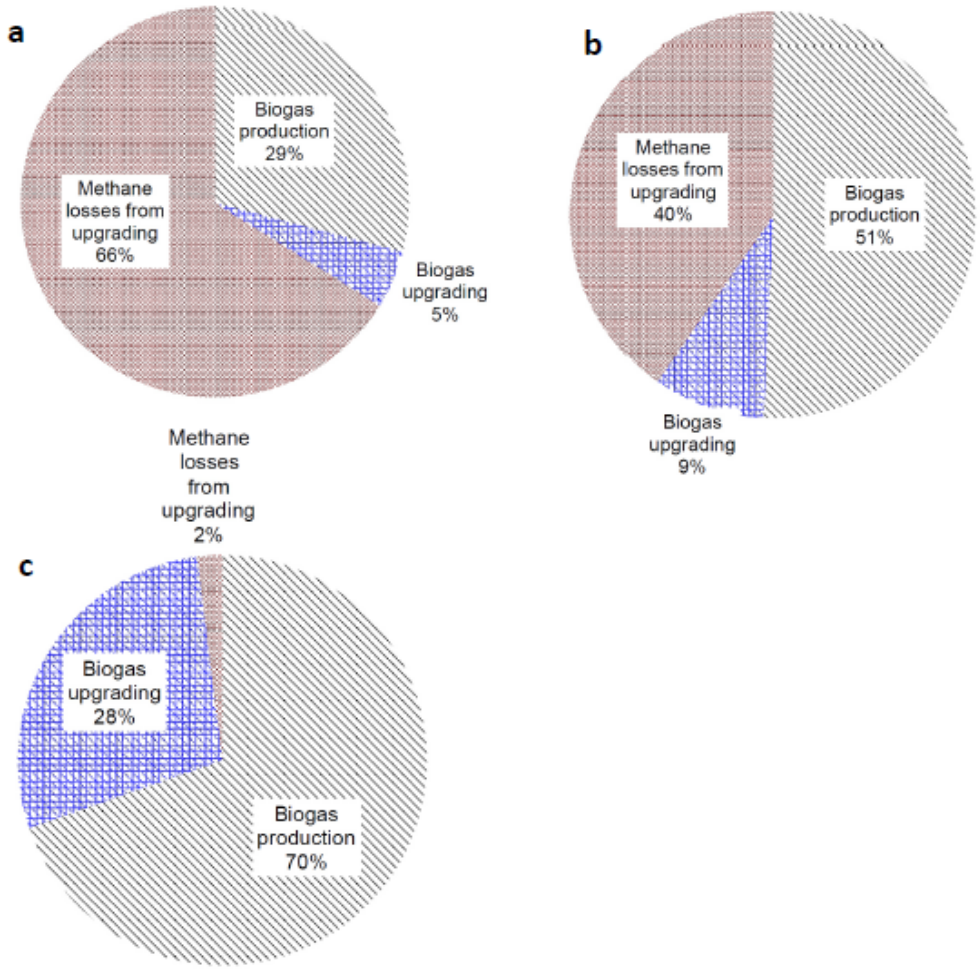

Figure 2.7. Contribution of different sub-processes to the total GHG emissions, in the case of HI-SLIP scenario (a), MID-SLIP scenario (b), LO-SLIP scenario (c).

Chapter 9

Results of local emissions (Task 3)

The dispersion of NO_x and particulate matter was calculated using the Gaussian model and the CALPUFF Lagrangian model described in Chapter 7.4. The environmental impacts were quantified through the calculation of a concentration difference, i.e. by comparing the effects of present and future energy configurations. Two operating scenarios were considered: scenario 3-B, assuming direct on-site combustion of the biogas, and scenario 3-M, assuming the refining of biogas to biomethane. The results are reported in continuation These outcomes are first presented separately, then jointly discussed.

9.1 Biogas on-site combustion (scenario 3-B)

Scenario 3-B assumes that biogas is conveyed to a gas engine for its direct on site combustion and cogeneration. This case implies that a demand of thermal energy (from industrial or residential activities) is effectively present in the surrounding of the plant. Thus, the present energetic configuration is represented by a conventional industrial heater fueled by natural gas, while the future configuration is represented by the cogeneration unit fueled by biogas.

9.1.1 Gaussian model

By simulating pollutant dispersion with the Octave-based Gaussian model, the concentration at ground level was determined at discrete distances x and y from the emission source, where x is the main wind direction and y is the cross direction. The calculation was made for stable and unstable conditions,

represented by F and A stability class respectively (Pasquill classification). It is reminded that the dispersion parameters depend strongly on atmospheric stability class through k_1 to k_5 coefficients of the Pasquill-Gifford formulation (Mohan and Siddiqui, 1998).

The maps of NO_x and TSP concentration difference resulting from the simulations are reported in Figures 2.8 - 2.9 and 2.10 - 2.11 respectively. Positive values indicate an increase of the contaminants with respect to the present situation, while negative values indicate a reduction of the contaminants. The result of NO_x indicates two different effects:

- a general increase in the average concentration, interesting a distance up to 3000 m from the source. For stability class F, a maximum increase of around 4 $\mu g/m^3$ is detected, at a distance from the source of around 800 m. For stability class A, the maximum is closer to the source (around 200 m) and reaches around 3 $\mu g/m^3$.
- a limited area where a decrease of concentration is found. For stability class F, this area is located at a distance between 200 m and 500 m from the source, showing a maximum decrease of around 1 $\mu g/m^3$ is detected. The extension of this reduction is almost no detectable for stability class A.

The result of TSP dispersion also indicates a general increase in the concentration. The maximum level of increase is comprised between 2.5 $\mu g/m^3$ and 6 $\mu g/m^3$ for stability class A and F respectively. This maximum is found at a distance of around 200 m and 500 m (for stability class A and F respectively).

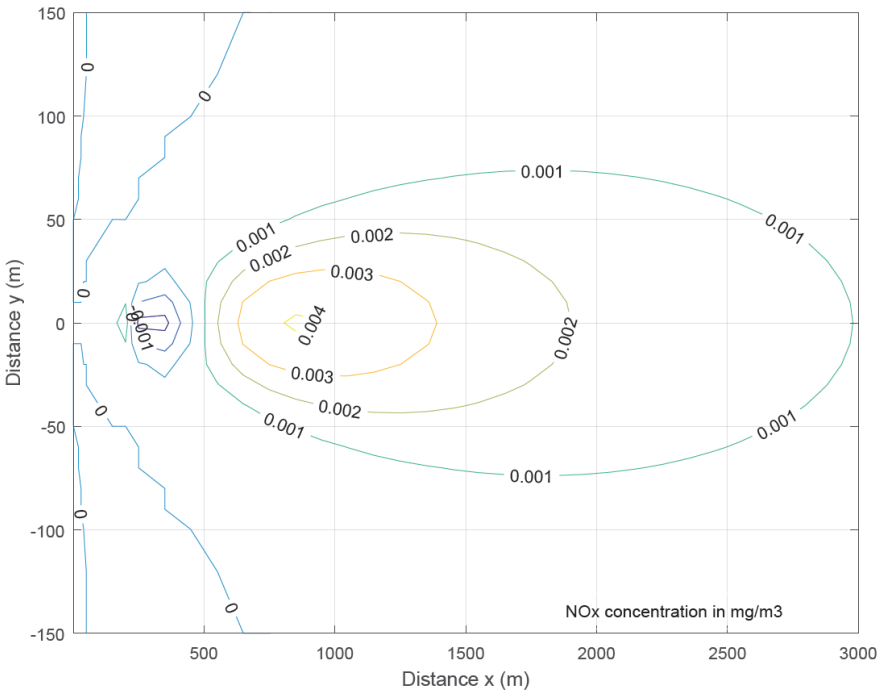

Figure 2.8. Map of NO_x concentration difference at ground level resulting from the Gaussian model simulations (Scenario 3-B, F stability class).

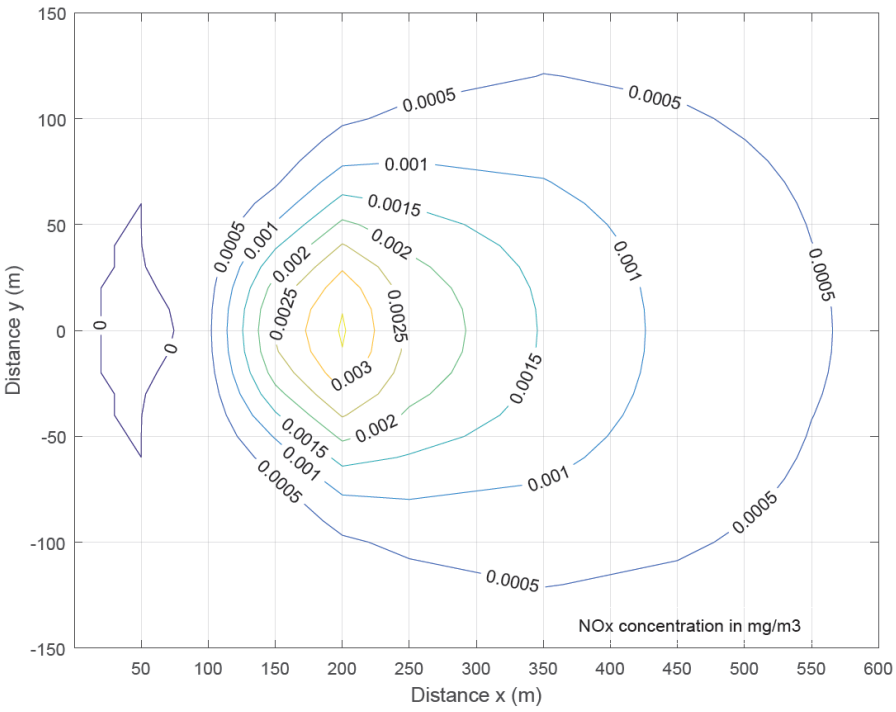

Figure 2.9. Map of NO_x concentration difference at ground level resulting from the Gaussian model simulations (Scenario 3-B, A stability class).

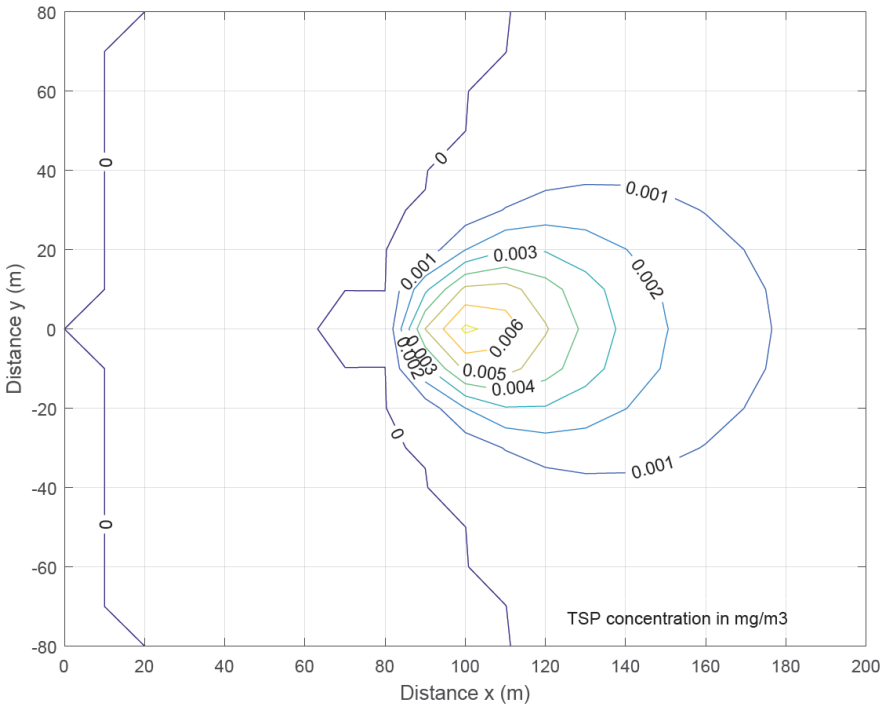

Figure 2.10. Map of TSP concentration difference at ground level resulting from the Gaussian model simulations (Scenario 3-B, F stability class).

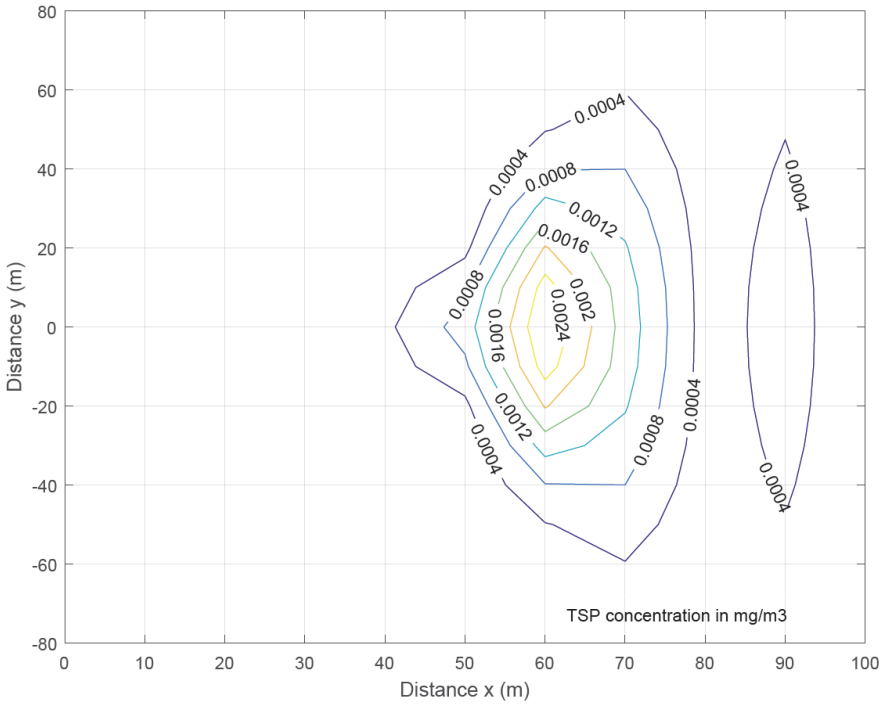

Figure 2.11. Map of TSP concentration difference at ground level resulting from the Gaussian model simulations (Scenario 3-B, A stability class).

The results of the calculations of the separate contribution of the single sources are then reported on the concentration maps of Figures 2.12 and 2.13 for NO_x and Figures 2.14 and 2.15 for TSP. Considering NO_x and stable conditions (Figure 2.12), the concentration generated by the biogas plant (Figure 2.12a) reaches its maximum of 14 $\mu g/m^3$ at a distance of around 600 m from the source. The dispersion decays slowly, falling to 3 $\mu g/m^3$ when $x > 3{,}000$ m. The plume results stretched, meaning that the transversal dispersion in direction y is limited. The results for the conventional NG boiler (Figure 2.12b) shows a similar higher peak of concentration. Due to the lower emission temperature and lower speed of exhaust gases, the plume impacts the ground at a lower distance from the source (around 400 m). The concentration is lower than 2 $\mu g/m^3$ for $x > 2{,}000$ m. Unstable atmospheric conditions (class A) lead to a higher dispersion of the pollutant. For the biogas plant (Figure 2.13a) the maximum ground level concentration approaches 8 $\mu g/m^3$ at distance x of 150-200 m. The concentration decays faster, reaching 1 $\mu g/m^3$ when $x > 600$ m. The transverse dispersion of the plume is slightly higher than the one for stability class F. For the conventional NG boiler (Figure 2.13b), the maximum concentration value is around 6 $\mu g/m^3$ at a distance of 100-150 m.

The results for ground-level concentrations of particulate matter, reported in Figures 2.14 and 2.15, are comparable to those of NO_x, with the only difference that the impact of PM involves lower extensions and lower peak values with respect to NO_x, due to the lower emission rate and the gravitational deposition of particles. In fact, the maximum concentration for TSP detected is around 10 $\mu g/m^3$ (biogas plant, stability class A). The maximum distance at which concentration remains below 1 $\mu g/m^3$ does not exceed 500 m.

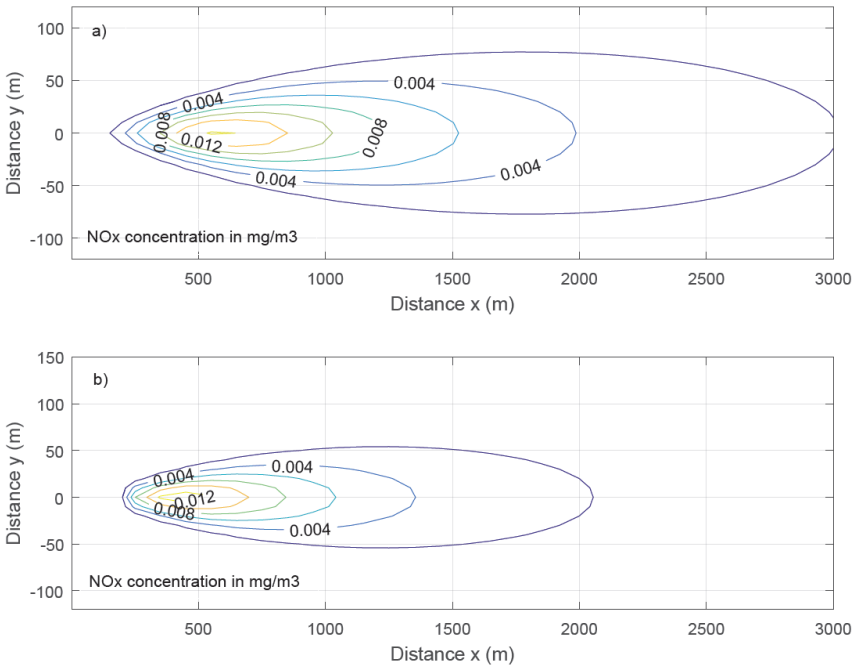

Figure 2.12. Maps of NO_x ground level concentration resulting from the simulation with the Gaussian model, F stability class, for biogas plant (a) and natural gas industrial boiler (b)

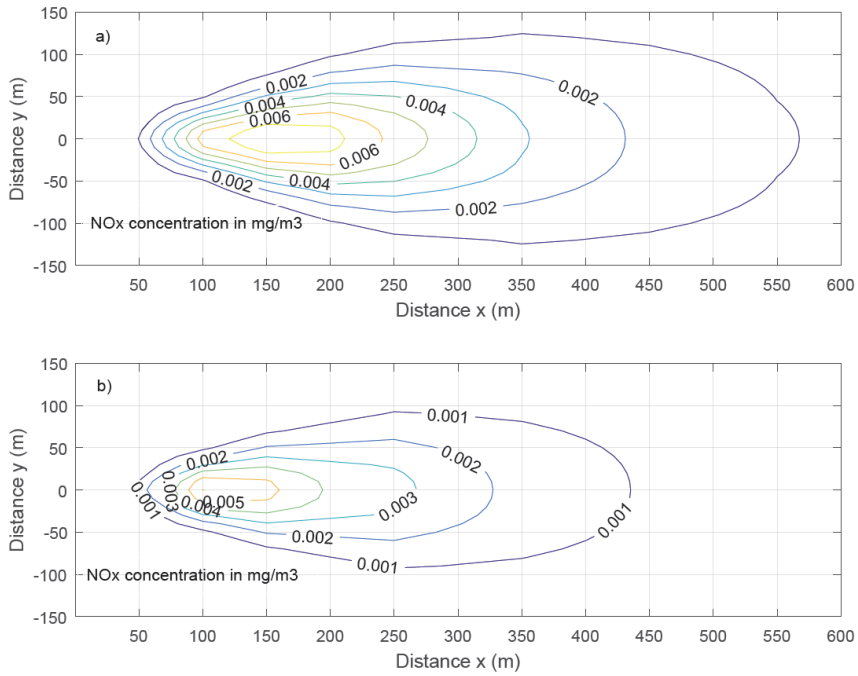

Figure 2.13. Maps of NO_x ground level concentration resulting from the simulation with the Gaussian model, A stability class, for biogas plant (a) and natural gas industrial boiler (b)

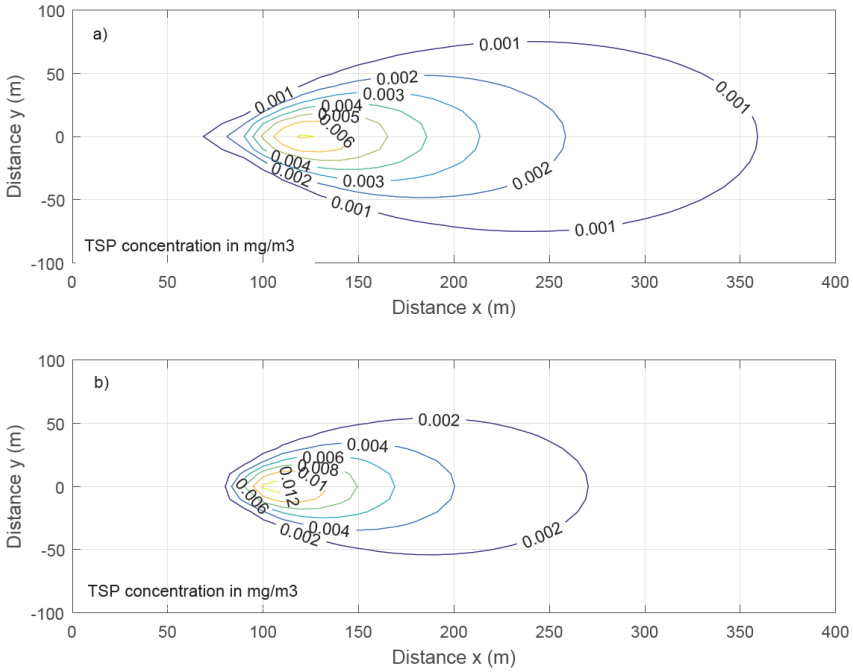

Figure 2.14. Maps of TSP ground level concentration resulting from the simulation with the Gaussian model, F stability class, for biogas plant (a) and natural gas industrial boiler (b)

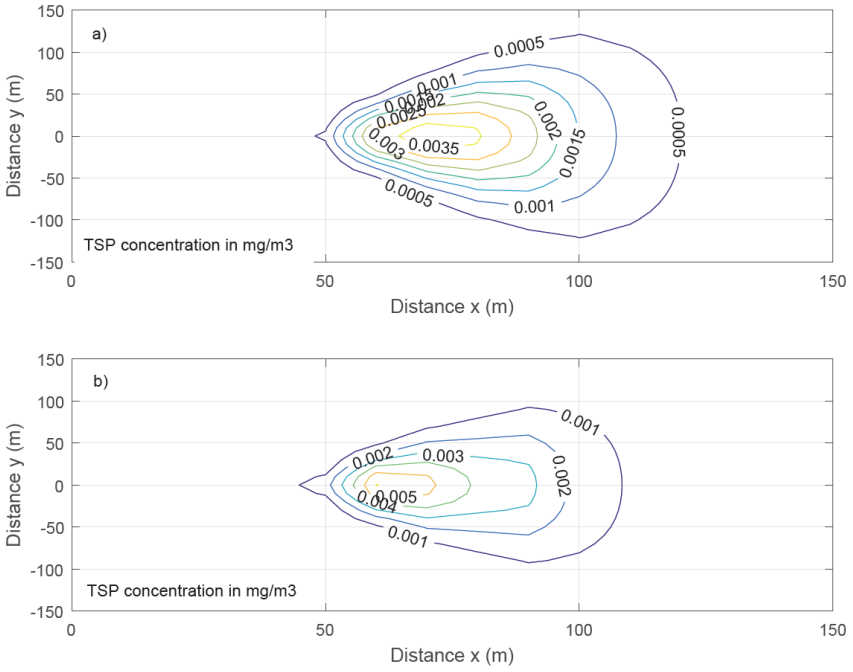

Figure 2.15. Maps of TSP ground level concentration resulting from the simulation with the Gaussian model, F stability class, for biogas plant (a) and natural gas industrial boiler (b)

9.1.2 CALPUFF model

The results of the local emission impacts, calculated with CALPUFF model, is reported in Figures 2.16 and 2.17 for NO_x and TSP respectively. The concentration values reported in those figures are the hourly average of the 6 coldest months of the year (October to January). Positive values indicate an increase of the contaminants with respect to the present situation, while negative values indicate a reduction of the contaminants. The result of both NO_x and TSP indicate an improvement in air quality. In fact, the minimum values of concentration difference approach -0.08 µg/m^3 for NO_x and -0.07 µg/m^3 for TSP, meaning a reduction of the contaminant with respect to the present situation. However, this reduction is of the order of 10^{-2} µg/m^3, thus not significant. The figures indicate that local effects are limited to the area around the source (around 1000 meters maximum), and the difference fast approaches zero in the surroundings.

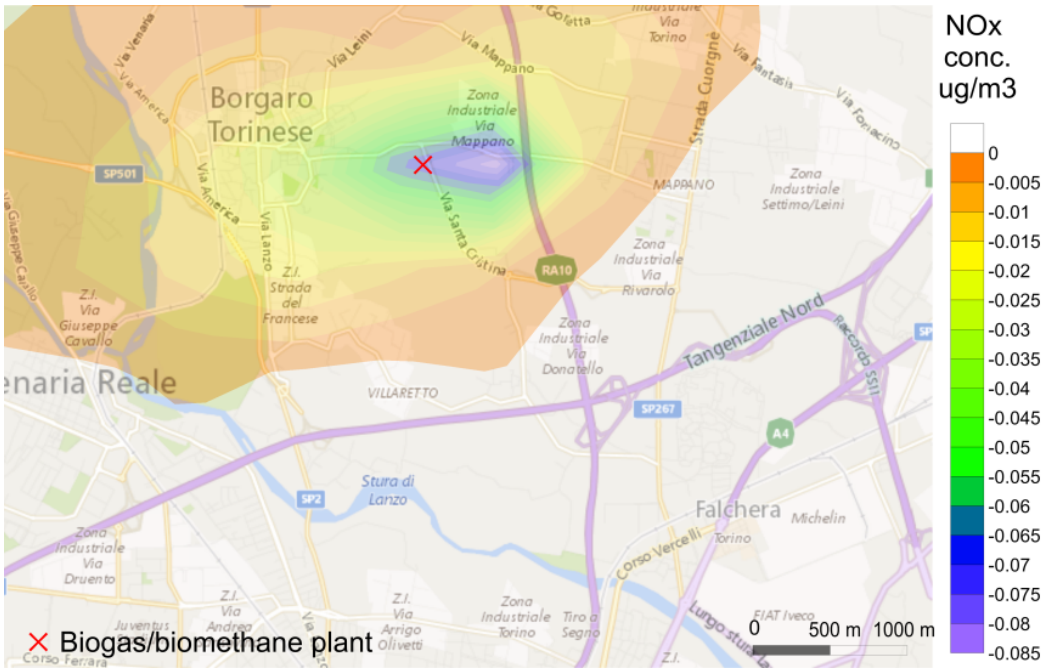

Figure 2.16. Map of NO_x concentration difference at ground level resulting from CALPUFF simulations (Scenario 3-B).

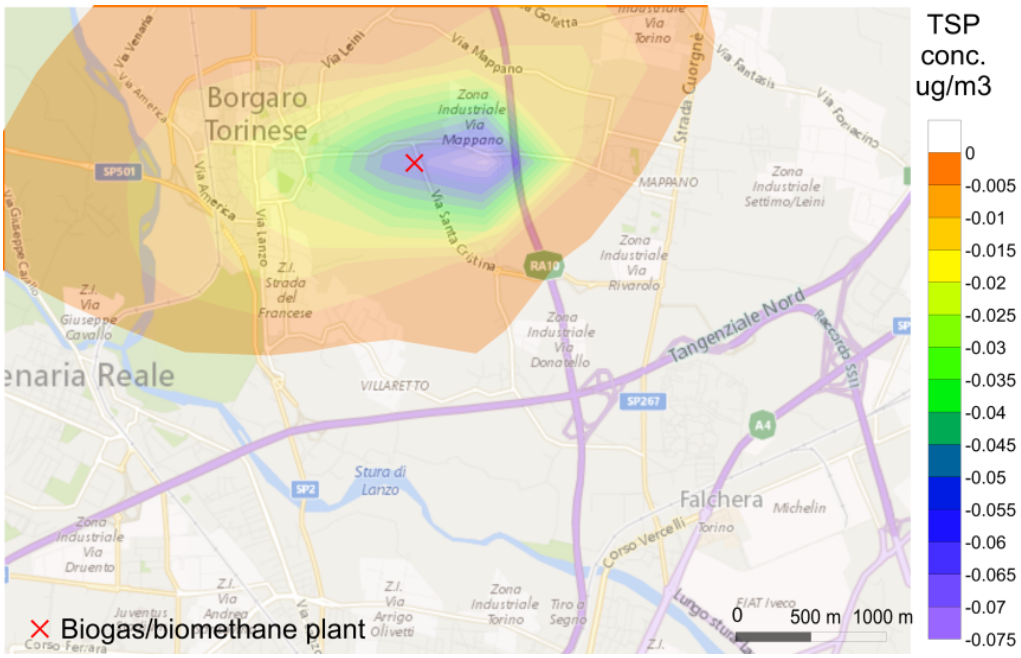

Figure 2.17. Map of TSP concentration difference at ground level resulting from CALPUFF simulations (Scenario 3-B).

The results of the calculations of separate contribution of the single sources are then reported on the concentration maps of Figures 2.18 to 2.21. These figures confirm that both sources (biogas plant and conventional heater) generate similar impacts at ground. In fact, NO_x maximum concentration resulting by the biogas plant reaches around 0.13 and 0.2 µg/m^3 for biogas plant and conventional heater respectively. The emission of TSP generates concentration levels of the same order of magnitude compared to NO_x. The maximum concentration reaches 0.12 and 0.17 µg/m^3 for biogas plant and conventional heater respectively. The figures also show that the effects of the biogas plant emissions interest a greater area than the conventional heater. This is probably due to the higher emission temperature and a higher gas exit speed of the biogas system.

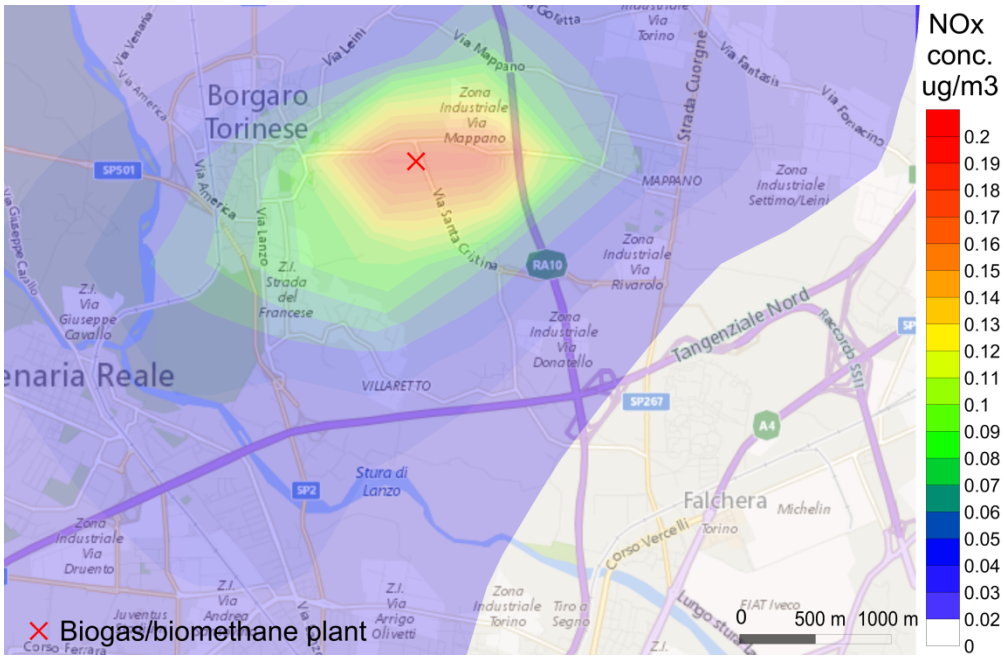

Figure 2.18. NO_x concentration map at ground level (modeled with CALPUFF) generated by the conventional NG heater (Scenario 3-B, present situation).

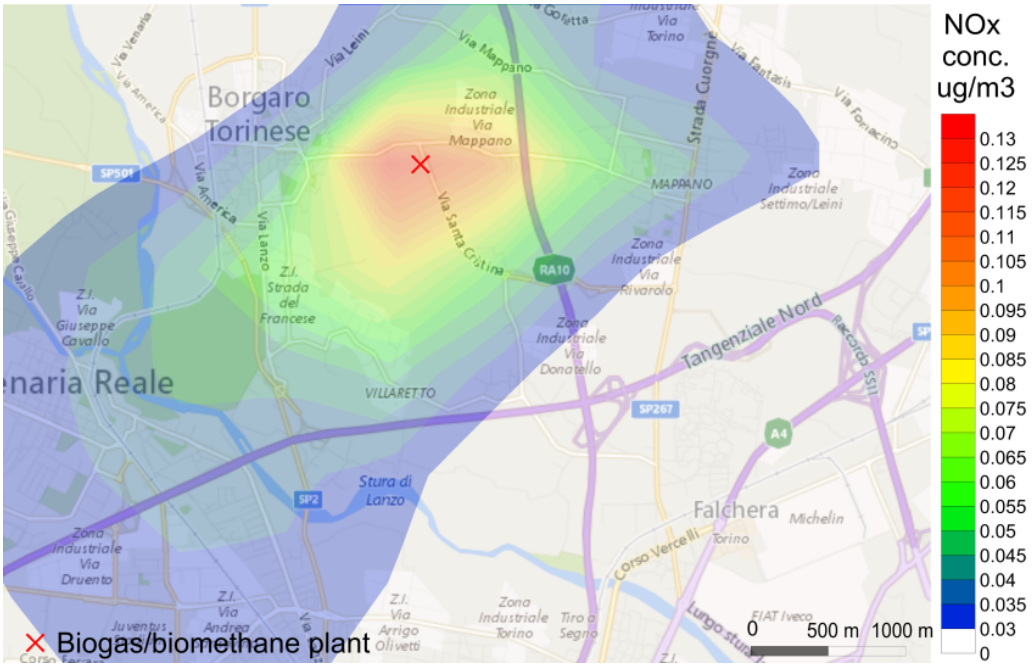

Figure 2.19. NO_x concentration map at ground level (modeled with CALPUFF) generated by the biogas combustion plant (Scenario 3-B, future situation).

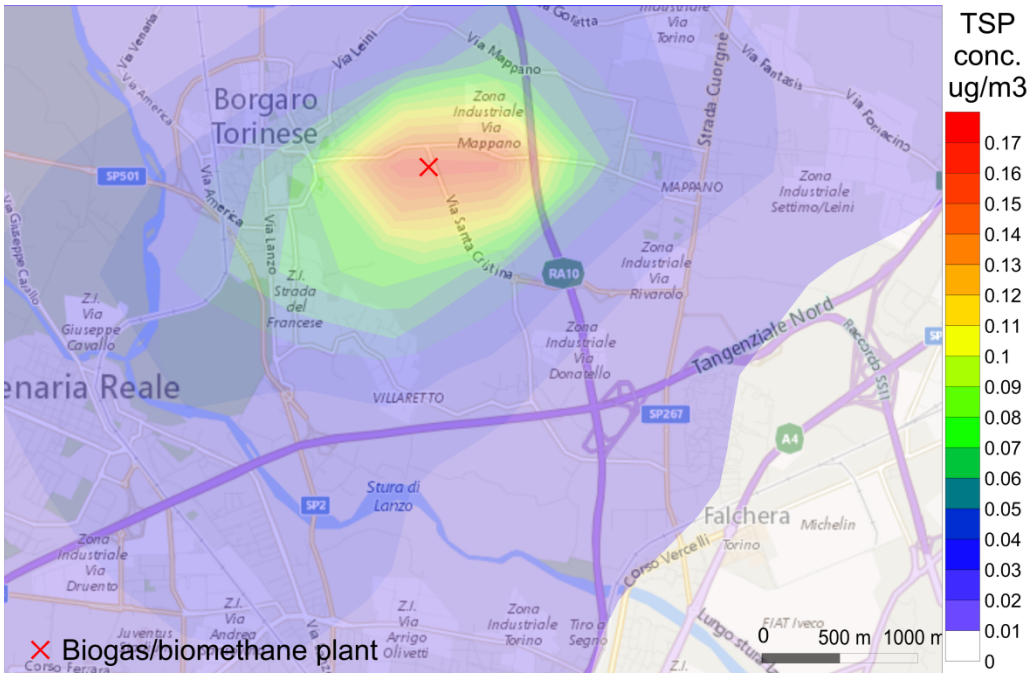

Figure 2.20. TSP concentration map at ground level (modeled with CALPUFF) generated by the conventional NG heater (Scenario 3-B, present situation).

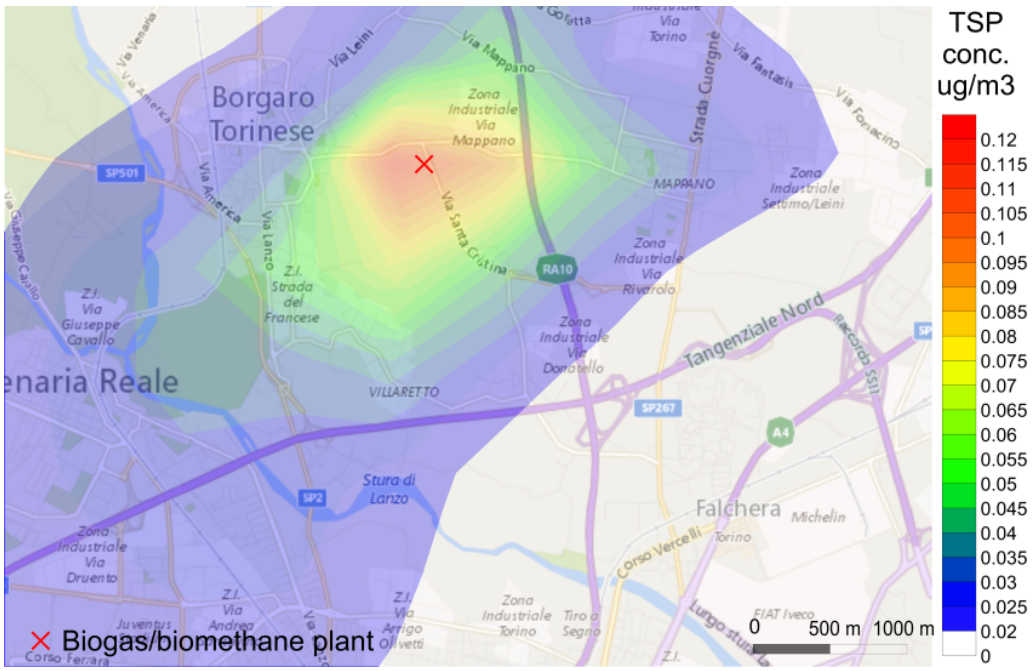

Figure 2.21. TSP concentration map at ground level (modeled with CALPUFF) generated by the biogas combustion plant (Scenario 3-B, future situation).

9.2 Biomethane production (scenario 3-M)

Scenario 3-M assumes that biogas combustion is substituted by the production of biomethane. This scenario implies that a demand of thermal energy is not actually present in the surrounding of the plant. Thus, the present energetic configuration consists in no emissions, while the future configuration is represented by the emissions generated by the auxiliary system connected to the biogas facility (in Table 2.5 the emission flow is reported). The auxiliary system considered in the future configuration is assumed to be a conventional heater fueled by natural gas, technically equal to that considered in scenario 3-B.

9.2.1 Gaussian model

The maps of NO_x and TSP concentration difference resulting from the simulation emission with the Gaussian model (scenario 3-M) are reported in Figures 2.22 and 2.23 respectively. Considering NO_x and stable conditions (Figure 2.22), the concentration generated by the conventional heater reaches its maximum of 3 $\mu g/m^3$ at a distance of around 500 m from the source. The dispersion decays slowly, falling below to 0.5 $\mu g/m^3$ when $x > 2{,}000$ m. The plume results stretched, meaning that the transversal dispersion in direction y is limited. Unstable atmospheric conditions (class A) lead to a higher dispersion of the pollutant. The maximum ground level concentration approaches 1.5 $\mu g/m^3$ at distance x of 100-150 m. The concentration decays faster, reaching 1 $\mu g/m^3$ when $x > 200$ m. The transverse dispersion of the plume is slightly higher than the one for stability class F.

The results for ground level concentrations of particulate matter, reported on the concentration map of Figure 2.23, are comparable to those of NO_x, with the only difference that the impact of PM involves lower extensions and lower peak values with respect to NO_x, due to the lower emission rate and the gravitational deposition of particles. In fact, the maximum concentration for TSP detected is around 1.5 $\mu g/m^3$ (stability class F). The maximum distance at which concentration remains below 0.2 $\mu g/m^3$ does not exceed 300 m.

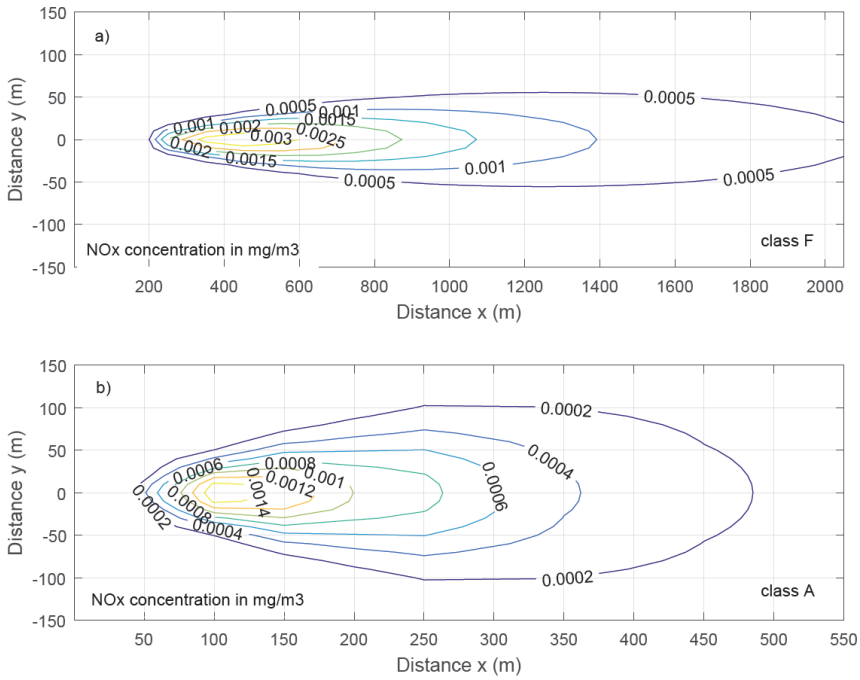

Figure 2.22. Map of NO_x concentration difference at ground level resulting from the Gaussian model simulations (Scenario 3-M), for stable (a) and unstable (b) atmospheric conditions.

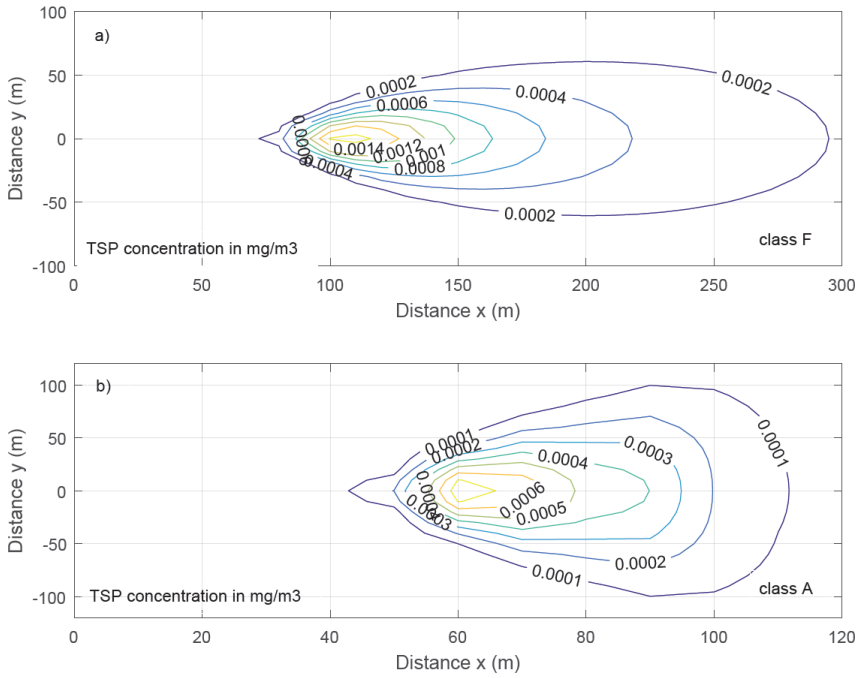

Figure 2.23. Map of TSP concentration difference at ground level resulting from the Gaussian model simulations (Scenario 3-M), for stable (a) and unstable (b) atmospheric conditions.

9.2.2 CALPUFF model

The results of the local NO_x and TSP dispersion modelling of scenario 3-M, calculated with CALPUFF, is reported in Figures 2.24 and 2.25. According to the definition of this scenario, the final concentration difference corresponds to the future configuration, i.e. only to the additional increase of concentration given by the conventional heater satisfying the auto-consumption of the biogas/biomethane system. The concentration values reported in those figures are the hourly average over the entire heating season (October to January). The result of both NO_x and TSP obviously indicate an increase of pollutants concentration. Such an increase is of the order of 0.05 µg/m^3 for NO_x and 0.04 µg/m^3 for TSP. The worsening of air quality is not therefore expected to be significant.

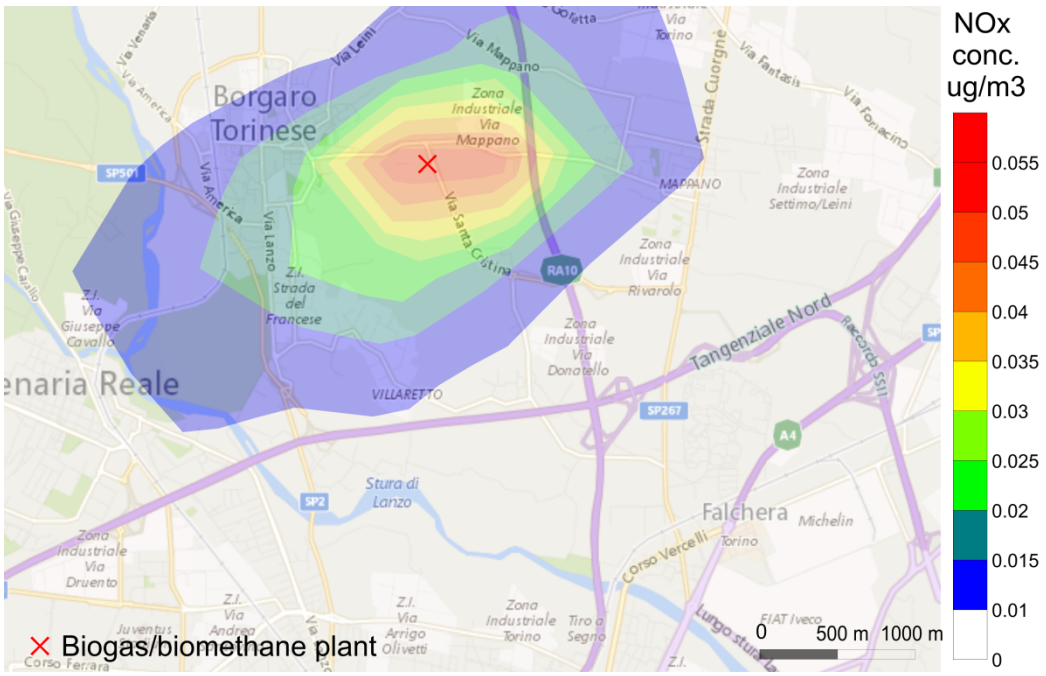

Figure 2.24. NO_x concentration map at ground level (modeled with CALPUFF) generated by the conventional NG heater (Scenario 3-M, future situation).

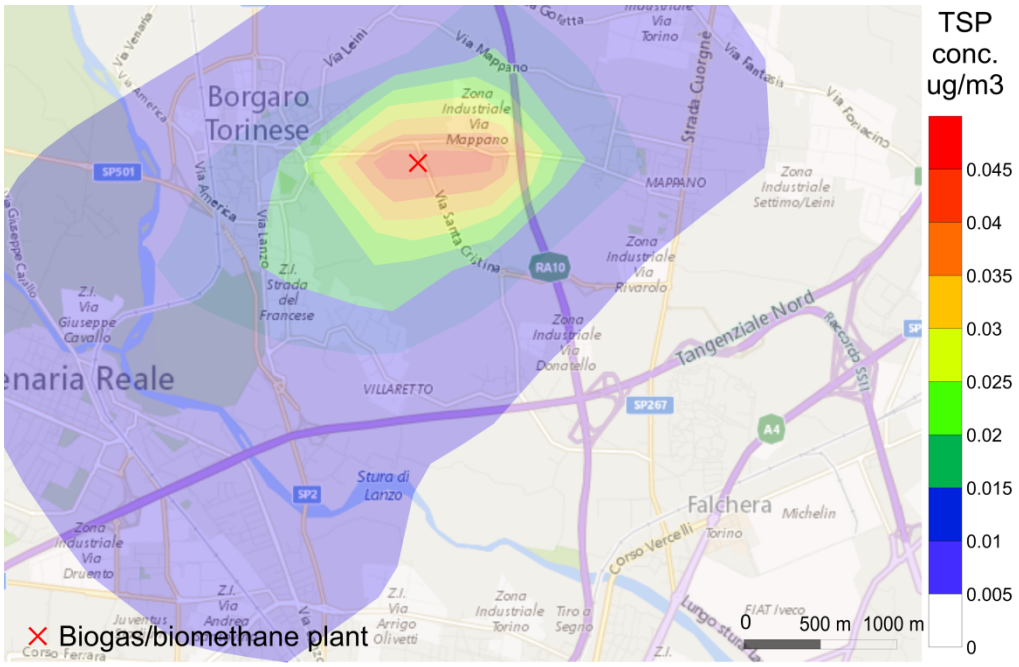

Figure 2.25. TSP concentration map at ground level (modeled with CALPUFF) generated by the conventional NG heater (Scenario 3-M, future situation).

9.3 Comparison of the simulations

The simulations of local NO_x and TSP dispersion generate different results depending on the modeling tool employed. The results given by the Gaussian model show an average positive (unfavorable) concentration difference in the order of units of μg/m^3. On the other hand, CALPUFF model provides a slightly favorable result, with a reduction in concentration of around 0.1 μg/m^3. The reasons for such a difference in the results might be several.

First, it must be said that the two modeling tools employed are very different from each other. CALPUFF is a highly-developed model capable of simulating complex dispersive scenarios, with sophisticated weather data and complex orography. For the setup of the simulations (as will be described in the next Part), the dispersion parameters were estimated and pre-processed from real measurements of meteorological and climatic variables. The Gaussian model was instead created by simulating only a constant wind speed in one main direction, and two levels of atmospheric stability, without considering additional weather or land factors obtained from field measurements. It is therefore believed that the

real dispersion of pollutants can be greater than that calculated by this model, and thus closer to what was represented by CALPUFF.

As for the difference between the results of the two models (unfavorable for the Gaussian model and favorable for CALPUFF), the differences between the emission parameters emissivity of the two sources must be considered. The greater emission flow of the biogas plant (178.4 mg/s for NO_x) compared to the conventional NG heater (88.5 mg/s for NO_x) would lead to expect a greater concentration at ground level of the former case, as calculated by the Gaussian model. Nevertheless, there are two other differences that may significantly affect the dispersion: the first is the exhaust gas temperature from the chimney, which is much greater for the biogas plant (773 K, against the 473 K assumed for the conventional heater); the second is the output velocity of gases, that also, in this case, is greater for the biogas system (17.9 m/s, against 15.9 m/s of the conventional heater). A possible reason for the difference in the concentration values could then be related to these two parameters. Higher temperature and velocity values may, in fact, affect the buoyancy and transport phases of the polluting plume, increasing the dispersion and the impact distance from the source.

The Italian regulation (2010) imposes an annual limit concentration for NO_x of 40 $\mu g/m^3$, for PM_{10} of 40 $\mu g/m^3$ and for $PM_{2.5}$ of 25 $\mu g/m^3$. The scenarios considered in the present study are not expected to generate an emission overstepping those limits. Nonetheless, the contribution given by these installations should be considered when considering the aggregated emissions.

Chapter 10

Discussion and conclusion

The obtained results present a methodological approach for the evaluation of the alternatives about biogas utilization: besides the specific interest for the operators of a single plant, a general approach strategy seems to be interesting.

The results require some further discussion, from one side with respect to the sensitivity of the results in relation to the considered operating hypothesis; from the other side as concerns the organization of the different results (Task 1 and Task 3 chiefly) in a general decision path.

New research studies may be addressed on local and global impacts of biomethane production. Regarding global impacts, the objective is minimizing the losses of methane with a limited energy consumption. For example, an analysis of the climate balance of the different upgrading techniques, like done by Pertl et al. (2010), represents a point of interest. For what concerns local impacts, there is need of more detailed field measurements of exhaust gas emission from combustion systems fueled by biogas, especially for the characterization of primary and secondary particulate. In addition, several in-depth analyses could be conducted on the problem, such as sensitivity analysis on emission parameters, comparative analysis with different dispersion models or simulation of cumulative impacts for multiple emission. Finally, the framework followed in the present study could represent a solid approach to extend the evaluation of the environmental burden to other biofuels.

It must also be considered that the technology concerning biogas upgrading is not completely at a maturity stage and important improvements probably could be forecast: the performances, costs and operating conditions of different upgrading systems should be considered (as in part is anticipated in Task 2), and the results of this optimal assessment could influence the results obtained as concerns the energy balance and GHG emissions (Task 1) and local atmospheric impact (Task 3).

As concerns the general integration of different, local and global aspects, of environmental sustainability, it is important to note that the specific interest of the local population, that is chiefly interested in the local impact from macro and micro-pollutants, is addressed to the considerations that are introduced within the analysis at the local scale (Task 3), while for the general benefit of a considered territorial area, or of a nation, the aspects of sustainability in direction of limitation of climate change, as they are introduced by the global analysis (Task 1), are of paramount interest. It is a specific task of policy makers to combine these two aspects in a comprehensive evaluation scheme, considering environmental, economic and planning considerations, in order to define the best scheme for the biogas utilization. In fact, also if in many cases the decision oriented by considerations deriving from Task 1 move in opposite direction in comparison with Task 3, only a coordinated approach can be justified from a general point of view.

10.1 Conclusion

The present study reported an evaluation on the global and local emission of biogas production process, considering different end-use solutions. A coordinated discussion of the different economic, environmental and planning aspects connected with different schemes of biogas utilization seems to be necessary for the public authorities, to arrive at the final, optimal solution. In fact, both the strategy concerning the best satisfaction of the different aspects of energetic needs must be considered (electricity, fuels, local district heating), together with considerations concerning the limitation in local impact, chiefly regarding atmospheric pollution.

In the specific case, in conclusion, the present study points out that the biogas upgrading to biomethane may represent an environmentally sustainable alternative to the on-site combustion of biogas in CHP units, especially in those cases in

which the energy content of the gas is not fully cogenerated, and all or part of the thermal energy produced is not capitalized.

This consideration could be modified in the hypothesis of an optimal localization of biogas energetic plants, with a strong attention to the possibility to integrally use the produced thermal energy.

Part 3

Environmental analysis of the potential district heating network powered by large scale cogeneration plants.

Chapter 11

Introduction

District heating (DH) through combined heat and power (CHP) systems is an increasingly popular solution to meet the needs of thermal energy in urban areas (Lund and Van Mathiesen, 2015). Among the most frequent plant configurations, the combined cycle (CC) units fueled by natural gas are identified. These systems allow the achievement of high conversion efficiency, thanks to the simultaneous production of heat and electrical energy (Lund et al., 2014). The environmental analysis of generation plants connected to DH networks is crucial, as these are usually located in heavily populated urban areas, thus characterized by the combined contributions of different emission sources such as traffic, industrial and residential activities.

The Turin metropolitan area is currently in a leading position in the DH sector, having one of the largest networks in Europe. For more information about the actual network structure and operating mode, refer to Jarre et al. (2016). Due to the persistence of critical concentrations values of pollutants in the air of Turin, the administrations are by some years exploring the possibility to achieve an environmental benefit by extending the DH network, removing part of the centralized residential heaters. The evaluation of the emissions should be conducted both at the global level, namely by assessing the overall contribution to the greenhouse effect, both at the local level, identifying the potentially harmful pollutants and studying their dispersion in the territory (Ravina and Genon, 2015). Among the most important pollutants present at the local level, nitrous oxides

(NO_x) and particulate matter (PM) are of paramount interest, as these substances are harmful to human health and ecosystems (Singh et al., 2016; Liora et al., 2016).

11.1 State of the art

District heating is a technology used for supplying a town district or a complete town with the heat generated in large production plants. By concentrating and scaling up the heat production instead of using single house boilers, a lower specific heat production cost can be obtained as well as a higher boiler efficiency and the possibility to co-generate electricity. District heating networks are commonly proposed in the literature as an environmentally friendly solution for providing heating services for the built environment due to their multiple benefits, such as centralized heat, production located outside of urban centers, possible utilization or renewable heat sources and increased comfort for the consumers. Currently, there is about 6,000 district heating networks operating in Europe with an overall length of 200,000 km (Connolly et al., 2014). A further expansion of such systems, in particular in Europe, is suggested in the literature (Colmenar-Santos et al., 2016).

By analyzing the scientific literature, many works concerning different aspects of DH are showed. Vesterlund et al. (2016) applied a simulation tool developed in MATLAB/Simulink to analyze the flow distribution in the district heating network of the town of Kiruna (Sweden). Andrić et al. (2016) developed a work to make use of emergy approach to infer the environmental performance of the heat provided by district heating networks, considering two types of district heating systems: ESPEX (four – pipe network) and traditional two-pipe district heating network.

Lake et al. (2016) show the implementation of district heating and cooling systems across a broad set of case studies reported in the literature. Topics addressed include their history, system identification, energy sources, design considerations, environmental impact, economic feasibility, performance analysis and the role of energy policy. Bach et al. (2016) analyze the integration of large – scale heat pumps in DH systems in Copenaghen.

From the environmental point of view, the literature provides numerous local studies on NO_x and PM local emissions associated with the operation of cogeneration plants for DH. Such studies often use dispersion models for the

calculation of the concentration of pollutants at ground level. The results reported can differ, depending on the size of the plant, the type of fuel and the operating conditions. Among the publications, a study by Brattebo and Reenaas (2012), conducted on a waste to energy cogeneration plant, underlines the increased NO_x emissions compared to an alternative scenario for waste management and the need for advanced abatement technologies. Genon et al. (2009) analyzed the local impact of a future small DH system fueled by natural gas engines. Their study considered two cases where 22 and 105 residential heaters were replaced with a CHP and DH system. The results indicated that the NO_x emissions may in some cases exceed the existing emissions, although this aspect is strongly related to the type of conversion facility considered. A second study by Torchio et al. (2009) developed the study by Genon et al. (2009), showing a reduction of PM concentration for the DH system connected to the 105 buildings. Recently, Torchio (2015) proposed an environmental and economic comparison of three different options: the district heating option, the distributed generation option and the separate production of heat and power. The results for the district heating option showed that the systems driven by micro turbines and fuel cell technologies lead to a reduction of the NO_x emissions, while internal combustion engines did not show a local NO_x saving. Similar results are confirmed by a study by Haichao et al. (2013).

11.2 Objective of the study

The aim of the present study is to evaluate the environmental compatibility of a potential intervention of expansion of the DH network in the urban area of Turin, Italy. The environmental compatibility is assessed considering both global scale emissions (contribution to the greenhouse effect) and local scale dispersions of nitrous oxides and particulate. The effects on air quality are evaluated by calculating the changes of emissions, corresponding to the difference between the present and future situation. The target results are thus represented by:

- NO_x and PM values of increased (or decreased) concentration on the area of study if local emissions are considered;
- CO_2 amount emitted (or avoided) by the energy system if global emissions are considered.

To achieve the calculation of the final local and global emission balance, the methodology described in continuation is applied. In principle, the general objective of this case study is thus achieved through the following steps:

- analysis of the present configuration of DH network and characterization of the areas next to be connected;
- analysis of the present energy production and operating conditions of the generation and integration unit powering the DH system;
- calculation of the thermal energy demand of the buildings next to be connected to the DH network;
- calculation of the future operating conditions of the existing generation and integration power units to satisfy the total heat demand;
- elaboration of assumptions on the possible entry into service of new power units;
- estimation of pollutant dispersion corresponding to a new potential energy configuration in the area of study and comparison with the present situation (local scale assessment);
- estimation of CO_2 flows from the system, by comparing present and future scenarios (global scale assessment).

11.3 Present and future scenarios

The study of local and global environmental impacts was conducted over a period of one year (2014), comparing the analysis of the present scenario with a possible future configuration.

The present and future areas of extension of the Turin DH network are reported in Figure 3.1. The planned extension includes four districts of the northern and eastern parts of the city (Barriera di Milano - Regio Parco, Aurora – Vanchiglia, Borgata Vittoria – Madonna di Campagna, Falchera, Figure 3.2 and Table 3.1). The residential volume currently served by the DH network amounts about 57 million m^3, corresponding to approximately 570,000 inhabitants. The total extension of the network amounts 527 km. The development project considered involves approximately further 20 million m^3.

The areas are characterized by aligned buildings with a height of around 15-20 meters (Figure 3.3). The urbanized density is quite high and green spaces are not abundant. The building stock is part of those areas that were constructed around the city center especially in the post-war period and in the 60s and 70s, thanks to Italian Law n° 167/1962. The buildings were mostly built before the laws on the reduction of energy consumption (Fracastoro et al., 2013).

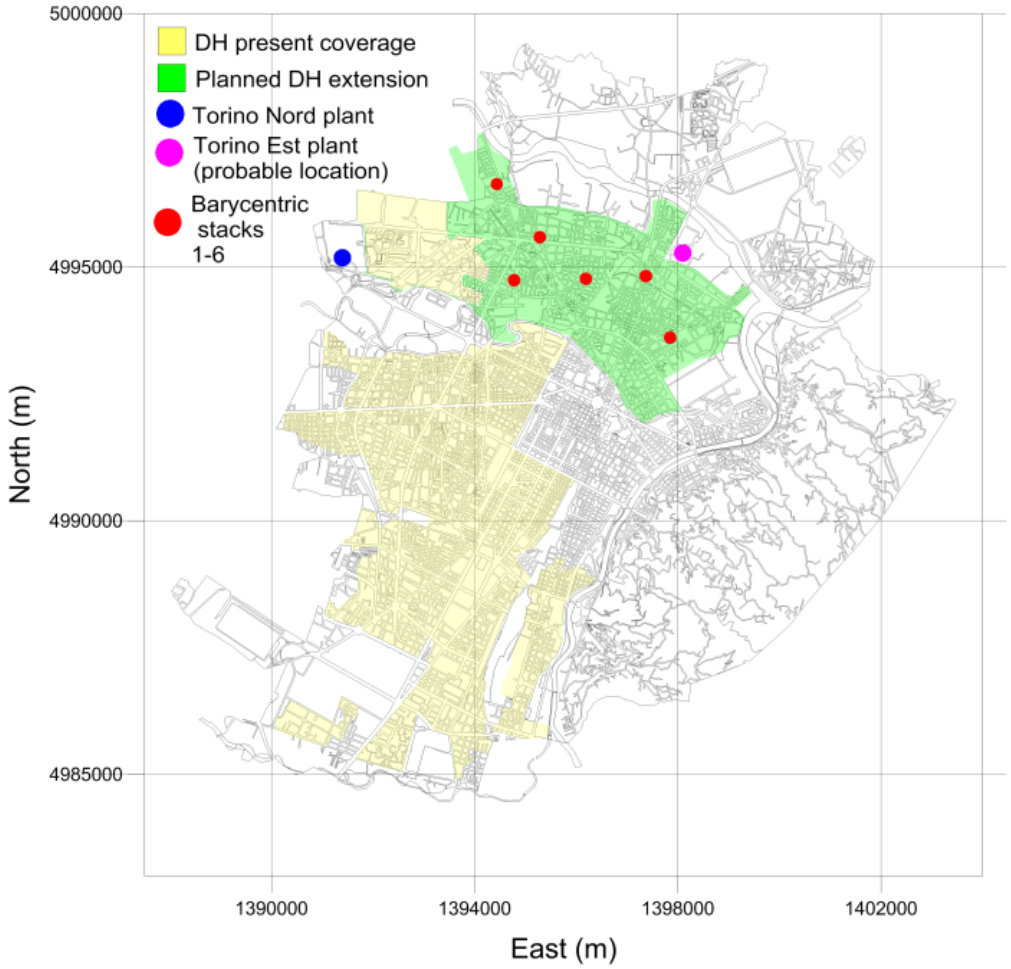

Figure 3.1. Current and planned extension of the DH network in the urban area of Turin. Location of the emission sources considered in the study. Coordinates system is UTM ED50 32T.

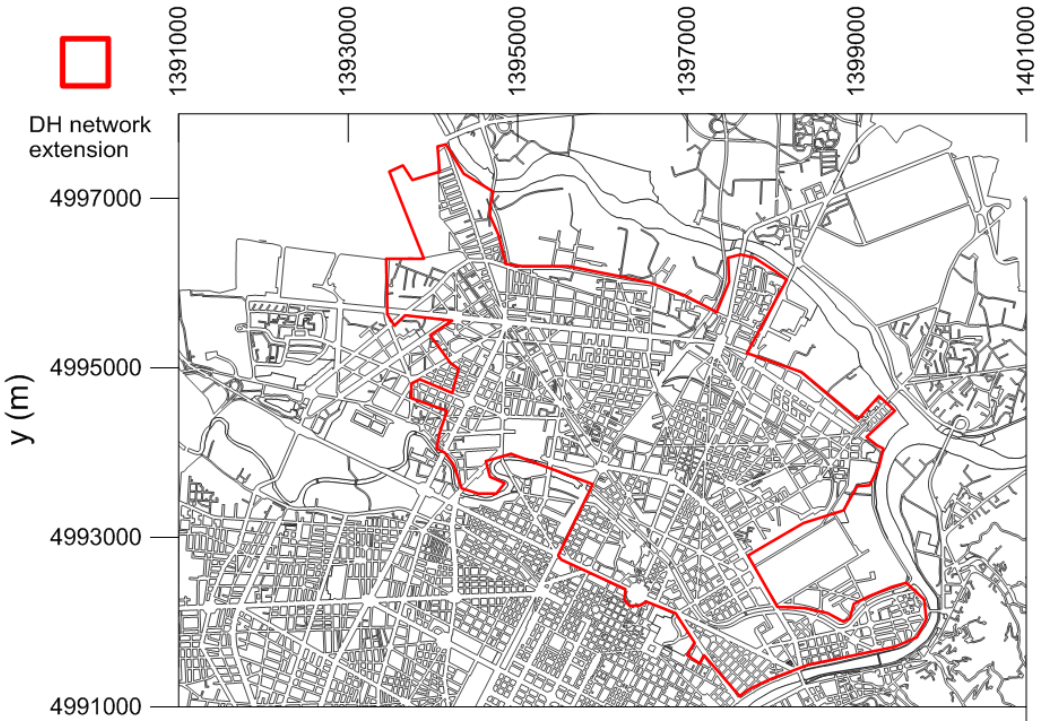

Figure 3.2. Planned extension of the DH network in the urban area of Turin (detail).

Figure 3.3. Representative picture of the buildings interested by the potential DH network extension (source: www.google.it/maps).

Table 3.1. List of the six sub-areas and related residential volume.

Area ID	District	Estimated residential volume (10^6 m^3)
TO-A1	Madonna di Campagna	1.1
TO-A2	Borgo Vittoria 1	3.9
TO-A3	Borgo Vittoria 2	1.6
TO-A4	Aurora - Vanchiglia	3.0
TO-A5	Barriera di Milano	6.5
TO-A6	Regio Parco	3.3
	Total	19.4

11.3.1 Present scenario (year 2014)

At present, the main power unit feeding the northern portion of the DH network is the Torino Nord cogeneration plant (the TO-N plant), which description is reported in Paragraph 11.4. The buildings in the area of study are currently served by centralized heaters, that will be removed following the DH network extension. The annual thermal energy produced by the TO-N plant is reported in Table 3.2. This datum was obtained by the continuous emissions monitoring system (CEMS) installed on the plant.

Table 3.2. Energy balance of present and future scenario.

Source	Present thermal energy production / demand (MWh/y)	Future thermal energy production / demand (MWh/y)	Difference (MWh/y)
TO-N plant (combined cycle)	336,720	586,050	+ 279,330
TO-N plant (auxiliary boilers)	10,075	40,214	+30,139
TO-E plant	-	347,480	+ 347,480
Buildings not connected to DH network	943,299	316,351	- 626,948
Buildings connected to DH network	-	626,948	+ 626,948

11.3.2 Future scenario

The future scenario involves the connection to the DH network of the residential units equipped with a centralized heater, considering an average commercial penetration factor of 0.8 (Province of Turin, 2009). For the characterization of the energy demand of the buildings, 6 homogeneous sub-areas were defined, considering the different type of building (period of construction) and population density (Figure 3.4). The heat demand was calculated using the model proposed by Fracastoro et al. (2013), starting from data of surface, number of floors, type of fuel (natural gas, diesel oil, LPG or heavy oil), type of system (centralized or autonomous) and period of construction. Production of hot water for sanitary purposes is included in the calculation. Data of surface and volume of the buildings that occupy the area of study were taken from the 2001 Italian Census (Istat, 2001). The average distribution of the heating systems in terms of fuel was considered as:

- natural gas: 92.7%
- diesel oil: 6.4%
- heavy fuel oil: 0.8%
- LPG: 0.1%

The data were extracted and processed using the Quantum GIS application (QGIS). The application of the model returned an annual value of thermal energy need, reported in Table 3.2.

In principle, the increase of heat demand due to the DH network extension could be satisfied by the TO-N plant. However, considering hourly distribution of thermal demand, TO-N plant would not be able to cover the peaks of request at morning and evening hours. For this reason, the entry in operation of a new integration and reserve system was assumed for the future scenario. This system was identified in the Torino Est (TO-E) plant, described at Paragraph 11.5. The hourly distribution of thermal demand is analyzed in detail in the following Chapter. The future total energy production of TO-N and TO-E plants is reported in Table 3.2.

Figure 3.4. Indicative delimitation of the six sub-areas elaborated with the QGIS software.

11.4 Torino Nord cogeneration plant

The thermal energy for the northern portion of the DH network is supplied by the Torino Nord plant, consisting of:

- a combined cycle (CC) cogeneration unit plant fueled by natural gas;
- 4 auxiliary boilers for integration and reserve, 85 MW each, fueled by natural gas;
- a heat storage system consisting of 6 batteries with a total capacity of about 5,000 m^3;
- a system for pumping, pressurization, expansion and replenishing of the water in the DH network.

The combined cycle process employs the high temperature heat of the fuel to the gas turbine and transfers the remaining heat to the environment at a lower temperature, corresponding to the condenser of the steam turbine, thus determining the optimal conditions for gross yields of the order of 56%.

The main technical data of the generation units are shown in Table 3.3.

Table 3.3. Technical data of the main components of the Torino Nord generation plant (modified from Jarre et al. 2016).

Component	Value	Torino Nord plant
Gas turbine	Gross nominal electrical power (MW)	270
	Fuel	Natural gas
Steam generator for the thermal recovery (high / medium / low pressure stages)	Pressure (bar)	125/30/4.5
	Temperature (°C)	550/550/237
Steam turbine	Gross nominal electrical power (MW)	119
District heating heat exchangers	Nominal thermal power	220
	Inlet temperature (°C)	70
	Outlet temperature (°C)	120
Condenser	Cooling fluid	Air
Combined cycle operation (ISO conditions on site)	Net electric power (MW)	390
	Global efficiency (-)	56%
Combined cycle + cogeneration operation (ISO conditions on site)	Thermal power (MW)	220
	Global efficiency (-)	87%

Figure 3.5. Location of Torino Nord power plant (source: Iren Energia 2014b).

Figure 3.6. Image of Torino Nord plant. (source: Iren Energia, 2014b)

The thermoelectric unit combined-cycle cogeneration is equipped with a catalytic system for emission reduction of NO_x in the atmosphere (Figure 3.7). The catalyst is installed in the recovery steam generator. To reduce NO_x, ammonia in aqueous solution is used as the reducing agent (NH_4OH) at a concentration lower than 25% by weight. The system's operation temperature range is 320–420 °C.

The catalyst system is composed of the following parts:

- selective catalytic removal (SCR) catalyst;
- injection and distributing grid for the ammonia in the steam generator;
- system for the evaporation, mixing and dosing of the ammonia;
- system for the storage and flow of the aqueous ammonia solution;
- loading / unloading system of aqueous ammonia solution;
- regulation system of the ammonia flow and control of NO_x emissions and ammonia slip;
- support structures and support of the catalyst.

The grid for ammonia injection is placed at a suitable distance from the surface of the catalyst to make the flow completely homogeneous and well distributed. The ammonia injection is provided on both sides of the steam generator. The storage of the aqueous ammonia solution is realized by means of two horizontal tanks of 50 m^3 each, with relative containment basins and vapors trap. The flow system for the aqueous ammonia solution consists of 2 pumps, with a vertical axis and the electric motor completely above the ground, including filters and relief valves.

The automation, control and regulation of the catalytic system for the reduction of NO_x emissions in the atmosphere is implemented through an integrated PLC equipped with the appropriate redundancies. The instrumentation for the measurement of the pollutant concentrations and the temperature of the exhaust gas is installed upstream and downstream of the catalyst. With the use of this catalytic system described, the emission of NO_x in the atmosphere is reduced by 30 to 10 mg/Nm^3. The ammonia slip is estimated to be less than 5 ppmv.

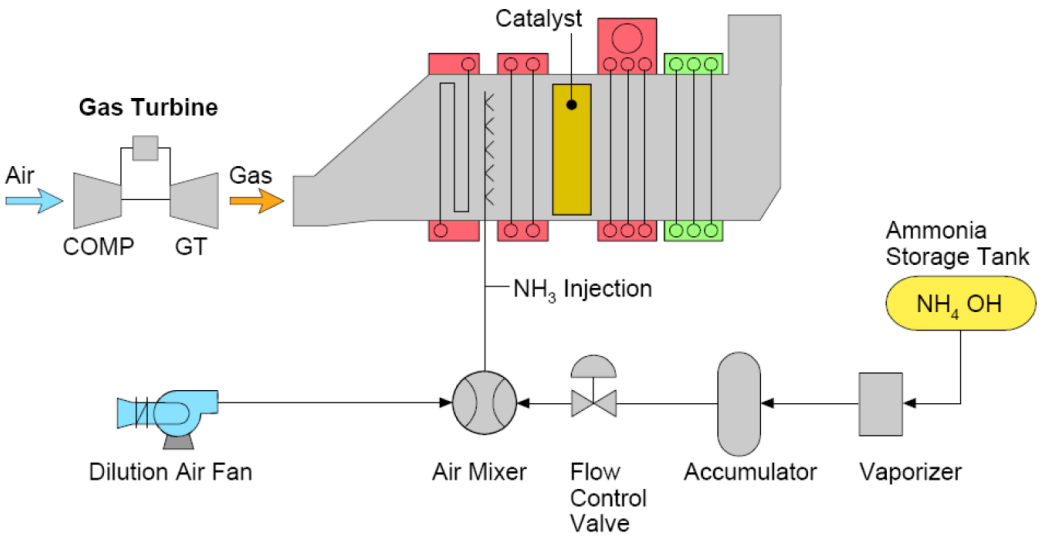

Figure 3.7. Scheme of the Torino Nord plant NO_x abatement system (source Iren Energia, 2008)

The thermoelectric unit combined-cycle cogeneration powers the district heating network through the steam bleed of the low-pressure turbine. In relation to the thermal power required by the district heating network, the system regulates the low-pressure steam extraction, that is sent to an appropriate heat exchanger that transfers the heat to the district heating network water. The condensate produced by said heat exchanger is cycled back by a pumping system. The production system of superheated water at 120 °C for the district heating network is designed for a nominal thermal power of about 220 MW.

A more detailed description of the Torino Nord plant is reported in Appendix 3.

11.5 Torino Est integration and reserve plant

The Torino Est integration and reserve plant is simulated with the aim of ensuring the continuity of operation of the DH network during the peak hours of request. Previous feasibility studies (Turin Province, 2009) located these facilities in the portion of territory between Via Reiss Romoli and Via Botticelli (Figure

3.8), as such area is an industrial area, central with respect to the two large portions of territory separated from the railway.

Previous studies evaluated different potential sites with respect to some common characteristics: size, accessibility, hydrogeology, type and distance of the surrounding buildings. The detailed analysis led to identifying the site reported in Figure 3.8, which is an area occupied by a dismissed industrial complex. This site is large enough and barycentric compared to the network, it is favorable from the point view of accessibility and the construction of the plant will not constitute a source of nuisance to residential areas.

Figure 3.8. Potential location of Torino Est integration and reserve power plant (source google maps).

The Torino Est integration and reserve plant is assumed to be composed by 4 boilers, each with a nominal thermal power of MW, for a total of 340 MW. The fuel used is natural gas. The steam produced by the boilers will be sent to a heat exchanger to produce superheated water at 120 °C for the DH network.

The boilers have the double function of:

- Integration, to cover the peak loads of the DH network;

- Reserve, in case of out of service of the Torino Nord combined cycle thermoelectric unit.

The boilers are water tube type with natural circulation. The steam produced by the boilers will be used in an overheated water production system, including heat exchangers in which circulates the water of the DH network. The key features and technical specifications of boilers will be:

- boiling pressure: 16 bar;
- design temperature: 250 °C;
- working pressure: 12 bar.
- emissions into the atmosphere (ref. 3% O_2 on dry gases): NO_x (as equivalent NO_2): 120 mg/Nm^3; CO: 30 mg/Nm^3;
- starting time: around 3 hours (from 10°C); 30 minutes (from 110°C).

The boilers' chimneys will have a circular cross-section of 8 m in diameter, which will contain 4 stacks of about 1.8 m of diameter each.

The heat exchangers are shell and tube type and their main characteristics will be:

- primary and secondary design pressure: 18 bar;
- primary and secondary design temperature: 210 °C;
- primary operating pressure: 12 bar;
- nominal flow: 3,000 m^3/h;
- DH water flow temperature: 120 °C;
- DH water return temperature: 70 °C.

Chapter 12

Methodology for the local emission analysis

The study of local environmental impacts consisted in the analysis of NO_x (as equivalent NO_2) and PM (as total suspended particulate, TSP) in terms of overall emission flow and concentration differences at ground level. Once defined the energy balance, the flow of pollutants emitted by the sources was calculated, and the dispersion was simulated using CALPUFF dispersion model (US EPA, 2011). The analysis procedure is described in the following.

12.1 Calculation of local environmental impacts

The local environmental impacts generated by NO_x and TSP emission were defined by calculating the average concentration differences at ground level using CALPUFF dispersion model. The concentration difference was calculated between present and future scenario. It represents the avoided emissions obtained by removing the centralized heaters from the buildings connected to the DH network.

12.1.1 Present scenario (year 2014)

For the characterization of the TO-N plant, two point sources of emission were considered, one for the main stack of the CC unit and one for the four auxiliary boilers. This corresponds to the real plant configuration since the four

stacks of the boilers are in fact joined into a single stack. The hourly thermal energy produced by the main generation unit and the auxiliary boilers was calculated starting by the thermal power transferred to the DH network (E_{tlr}), that is directly measured by the continuous emissions monitoring system (CEMS) installed on the plant (Iren Energia, Figure 3.9). Thus, the thermal energy produced by the boilers E_{cald} was calculated by difference as:

$$E_{cald} = E_{tlr} - E_{tonmax} \quad \text{if } E_{tlr} > E_{tonmax} \quad \text{Eq. 3.1}$$

$$E_{cald} = 0 \quad \text{if } E_{tlr} < E_{tonmax} \quad \text{Eq. 3.2}$$

where E_{tonmax} is the maximum thermal energy that can be transferred to the DH exchanger, namely 220 MWh.

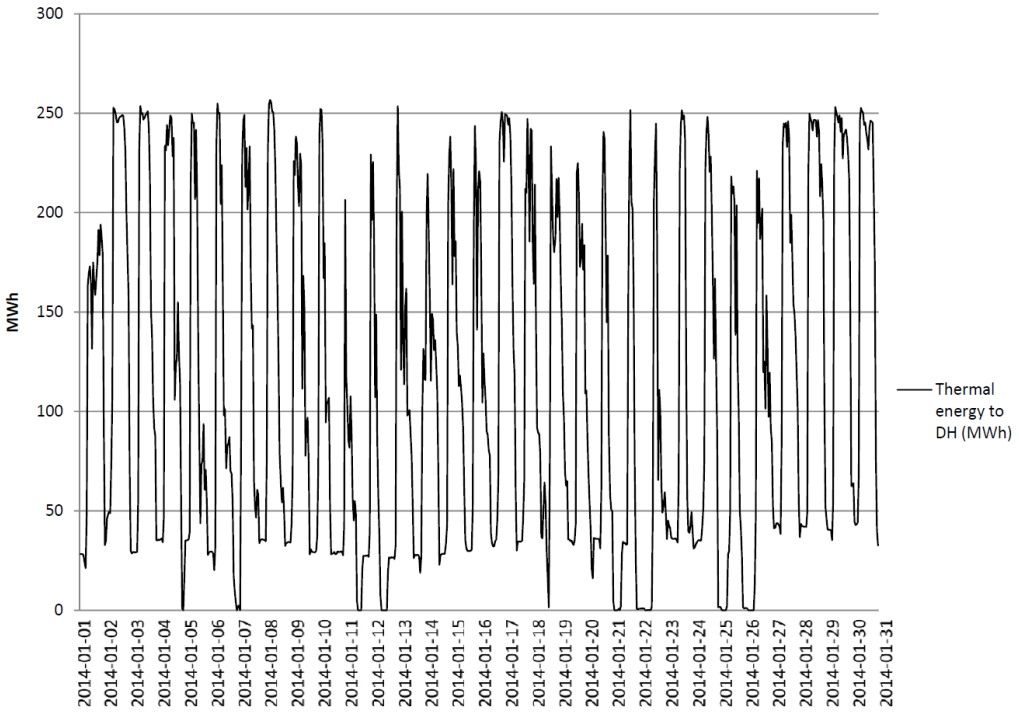

Figure 3.9. Actual thermal energy demand of the DH network, January 2014 (source CEMS).

The flow of NO_x emitted by the CC unit was also directly extracted by the CEMS. The emission flow for the month of January is reported in Figure 3.10. This diagram shows that NO_x emission is constant around 10 kg/h when the plant

is not running in cogeneration mode (i.e. producing only electricity), then some peak is registered in correspondence of the DH network demand.

The NO_x emission of the auxiliary boilers was calculated by multiplying E_{cald} for the average emission factor declared by the plant operator for the year 2014 (Table 3.4). The flows of TSP were instead calculated by applying the EMEP/EEA emission factors (Table 3.4).

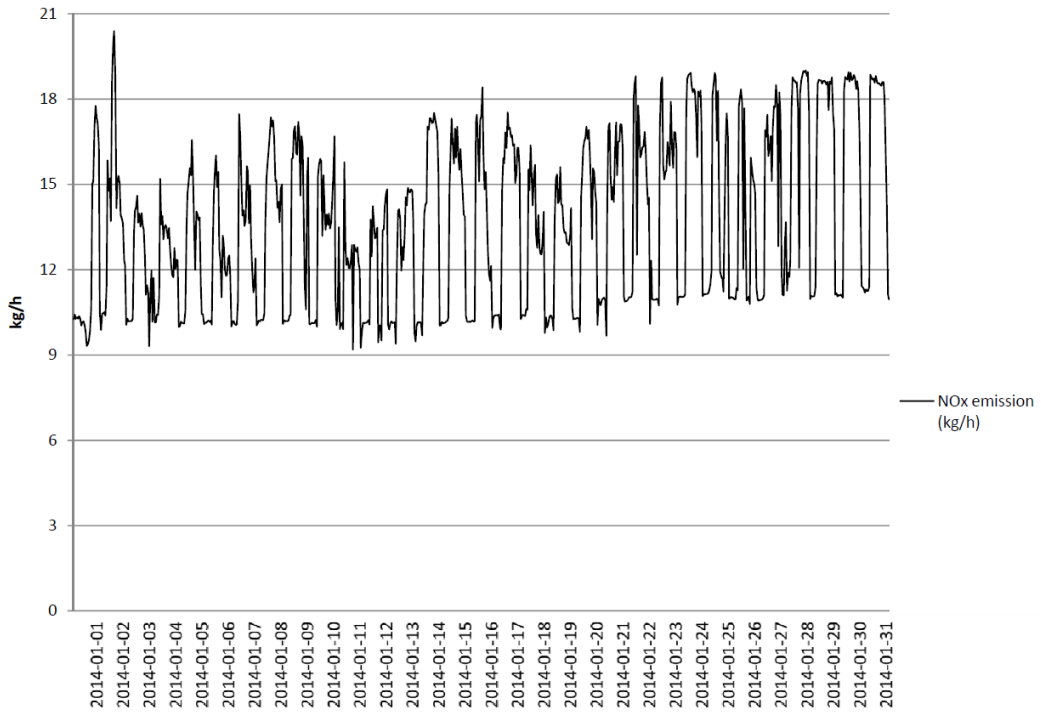

Figure 3.10. Actual NOx emissions from Torino Nord plant (source CEMS).

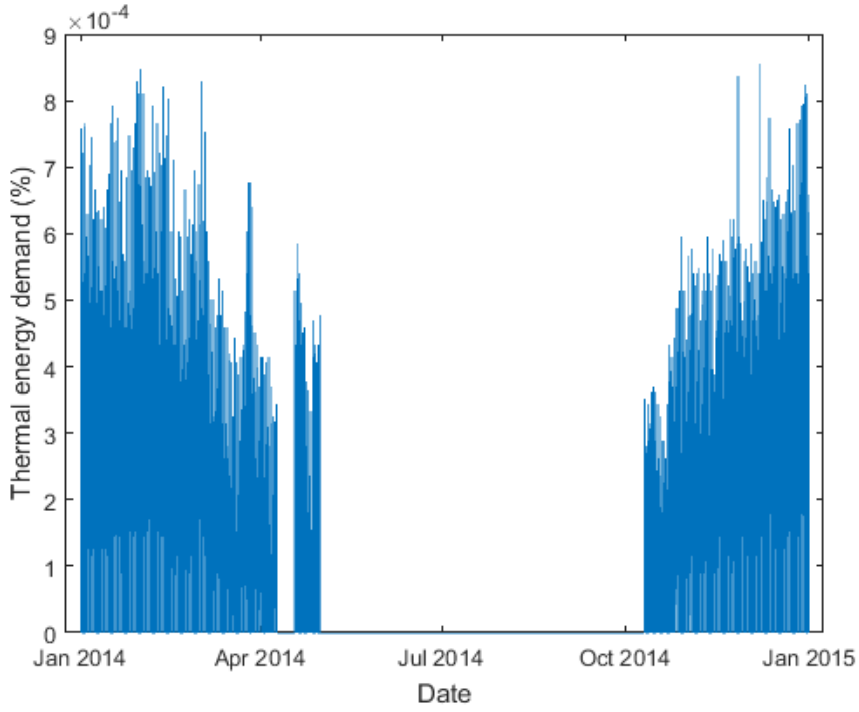

Figure 3.11. Hourly breakdown of the benchmark building in terms of percentage of the total yearly thermal energy demand.

As described previously, the residential areas were divided into 6 sub-areas. A barycentric stack was assigned to each area (Figure 3.4). The total heat demand of the buildings was multiplied by the hourly distribution of a benchmark building, i.e. using the real-time demand curve of a representative building, located in Turin and subject to continuous measurement. The hourly thermal energy request was then multiplied by the corresponding emission factor (Table 3.4).

Table 3.4. Emission factors of NO_x and TSP.

Emission source	**NO_x emission factor (kg/MWh)**	**TSP emission factor (kg/MWh)**	**Ref.**
Torino Nord –combined cycle	0.167 [1]	$5.55 \cdot 10^{-5}$ [2]	[1] Iren Energia [2] EMEP/EEA
Torino Nord – auxiliary boilers	0.063 [3]	$2.47 \cdot 10^{-4}$ [4]	[3] Iren Energia, 2014 [4] EMEP/EEA
Torino Est	0.063	$2.47 \cdot 10^{-4}$	-
Residential stacks (natural gas)	0.180	$1.62 \cdot 10^{-3}$	EMEP/EEA
Residential stacks (diesel oil)	0.180	$5.4 \cdot 10^{-3}$	EMEP/EEA
Residential stacks (LPG)	0.180	$5.4 \cdot 10^{-3}$	EMEP/EEA
Residential stacks (heavy oil)	0.540	$1 \cdot 10^{-1}$	EMEP/EEA

Figure 3.12. Photo of the benchmark building sited in Turin and subject to continuous measurement of thermal energy consumption (source google maps).

12.1.2 Future scenario

The future scenario was constructed considering the connection to the DH network of the only buildings with centralized heating, considering an average commercial penetration factor. The annual thermal energy consumption of the 6 sub-areas was then divided into a portion connected to DH (E_{fut_tlr}) and a portion not connected to DH, that continues to be heated independently (E_{fut_notlr}):

$$E_{fut\_tlr} = E_{cen} \cdot F_p \quad \text{Eq. 3.3}$$

$$E_{fut\_notrl} = E_{cen} \cdot \left(1 - F_p\right) + E_{aut} \quad \text{Eq. 3.4}$$

where E_{cen} is the thermal energy requirement of buildings with a centralized heating system, F_p is the average commercial penetration factor of 0.8 (Province of Turin, 2009), and E_{aut} it is the thermal energy requirement of the buildings with an autonomous heating system. The annual amounts E_{fut_tlr} and E_{fut_notlr} were then

distributed on an hourly basis using the same methodology described above. The term E_{fut_tlr} was subsequently added to the current term E_{trl}, to obtain the required total hourly thermal energy to meet in the future operational mode E_{fut_tot}:

$$E_{fut\_tot} = E_{fut\_tlr} + E_{tlr} \qquad \text{Eq. 3.5}$$

The performance of E_{fut_tot} term in the month of January is shown in Figure 3.13. As can be seen, the peak values reach around 900 MWh, going beyond the operational joint capacity of the TO-N plant and the related auxiliary boilers (220 MWh + 340 MWh). This is the reason for assuming the entry in operation of the Torino Est (TO-E) plant, anticipated previously. Assuming the operation of TO-E plant, it was possible to calculate the future operational structure of the power plants needed to meet the thermal energy requirements. To this end, the following heat dispatching priority was assumed:

- TO-N combined cycle;
- TO-E auxiliary boilers;
- TO-N auxiliary boilers.

The hourly curves of production of the three generation units were multiplied by the corresponding emission factors, obtaining the hourly emission flow of NO_x and TSP. The Turin emission factors for TO-E plant were assumed equal to those of the TO-N auxiliary boilers (Table 3.4). The calculation of the hourly energy distribution in the future scenario was implemented in a GNU Octave script, that is reported in Appendix 4.

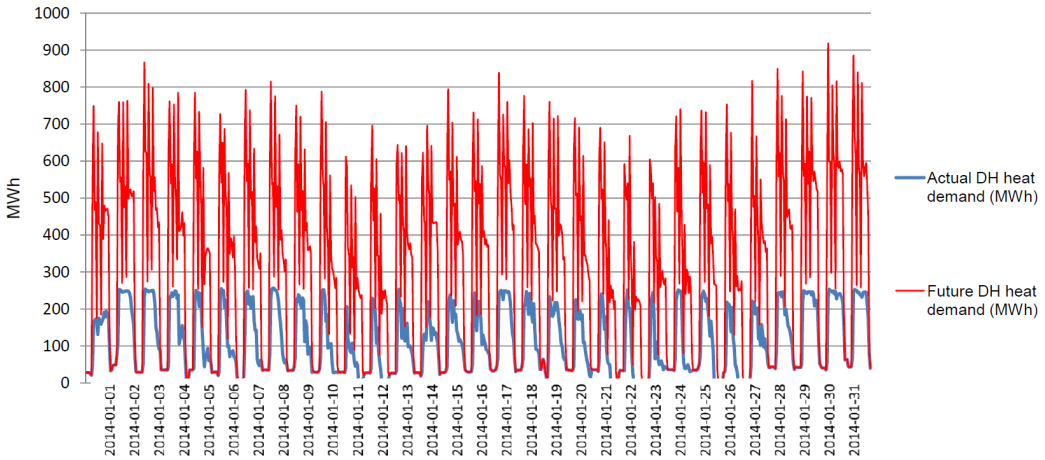

Figure 3.13. Hourly thermal power demand of the DH network in northern and eastern areas of Turin, present and future scenario, month of January.

12.2 Simulation of pollutants dispersion

The local environmental impacts of NO_x and TSP emissions were evaluated by calculating the average concentration difference at ground level by using CALPUFF dispersion model. The result was obtained overlapping the concentration maps of produced and avoided emissions in the future scenario. Produced emissions are those generated by the power units (in their modified operating mode) and by the buildings remained unconnected to the DH network. Avoided emissions result from the residential units connected to the DH network.

As described in Part 1, Chapter 5.1, the dispersion model CALPUFF (US EPA, 2011) is a lagrangian non-stationary puff model containing modules for the simulation of complex orography, deposition and chemical transformations. The CALPUFF Modeling System includes three main components: CALMET, CALPUFF, and CALPOST and a large set of preprocessing programs designed to interface the model to standard, routinely-available meteorological and geophysical datasets. CALMET is a meteorological model that develops wind and temperature fields on a three-dimensional gridded modeling domain. Associated two-dimensional fields such as mixing height, surface characteristics, and dispersion properties are also included in the file produced by CALMET. CALPUFF is a transport and dispersion model that advects "puffs" of material emitted from modeled sources, simulating dispersion and transformation processes along the way. In doing so it typically uses the fields generated by CALMET. Temporal and spatial variations in the meteorological fields selected are explicitly incorporated in the resulting distribution of puffs throughout a simulation period. The primary output files from CALPUFF contain either concentrations or deposition fluxes evaluated at selected receptor locations. CALPOST is used to process these files, producing tabulations that summarize the results of the simulation, identifying the highest and second highest 1-hour and 3-hour average concentrations at each receptor, for example.

A brief overview of CALPUFF technical configuration is already been provided in Part 1, Chapter 5.1. The following paragraph reports information on the modeling structure, aiming to describe the practical operations conducted to set up the dispersion simulations. A focus is maintained on the elements of the model employed in the present study.

The input data sets used by CALPUFF are summarized in Table 3.5.

CALPUFF reads user inputs from a control file with a default name of CALPUFF.INP. This file contains the user's selections for the various model options, technical input variables, output options, and other user-controllable options.

Table 3.5 Summary of CALPUFF input files (source: US EPA, 2011).

Default file name	Contents	Format type
CALPUFF.INP	Control file inputs	Formatted
CALMET.DAT	Geophysical and time-varying meteorological data, created by the CALMET meteorological model	Unformatted
BCON.DAT	Boundary condition concentration file (optional)	Formatted
PTEMARB.DAT	Source and emissions data for point sources with arbitrarily-varying emission parameters (optional)	Formatted
BAEMARB.DAT	Emissions data for area sources with arbitrarily-varying emission parameters. Can be derived from EPM model files (optional)	Formatted
VOLEMARB.DAT	Emissions data for volume sources with arbitrarily-varying emission parameters (optional)	Formatted
LNEMARB.DAT	Emission data for line sources with arbitrarily-varying line source emissions (optional)	Formatted
OZONE.DAT	Ozone measurements at one or more ozone stations (optional)	Formatted

A meteorological data file (CALMET.DAT) contains hourly or sub-hourly gridded fields of micro-meteorological parameters and three-dimensional wind and temperature fields. The meteorological data file also contains geophysical data such as terrain heights and land use which are required by both the meteorological model (e.g., for terrain adjustment of the wind fields) and by the CALPUFF model.

Arbitrarily-varying source data may be provided in files for point sources (default name PTEMARB.DAT), area sources (default name BAEMARB.DAT),

line sources (default name LNEMARB.DAT), and volume sources (default name VOLEMARB.DAT). The present study included the use of point and area sources.

Hourly or sub-hourly observations of ozone data are used in the calculation of SO_2 and NO_x transformation rates if the MESOPUFF II chemical transformation scheme is selected. Ozone data for one or more ozone stations are read from a data file called OZONE.DAT.

The CALPUFF output files considered in the present study are summarized in Table 3.6. The list file contains a copy of the inputs used in the run, optional output fields of gridded and discrete receptor concentrations, wet deposition fluxes, and dry deposition fluxes and other run data.

Table 3.6. Summary of CALPUFF output files used in the study (source: US EPA, 2011).

Default file name	Contents	Format type
CALPUFF.LST	List file produced by CALPUFF	Formatted
CONC.DAT	Time-averaged concentrations (g/m^3) at the gridded and discrete receptors for species selected by the user in the control file (optional)	Formatted
QATERR.GRD	gridded terrain elevations (m a.s.l.) in SURFER GRD format, created when CALMET.DAT is used with variable topography	Formatted
QALUSE.GRD	gridded land use in SURFER GRD format, created when CALMET.DAT is used	Formatted

The choice of CALPUFF model dictated by the need to develop a simulation on a largely dispersed domain, characterized by a complex topography and a variable meteorology. In this perspective, CALPUFF has the advantage of allowing the plume trajectory to vary from hour-to-hour in a systematic manner.

Compared to other gaussian models like ISC3, even though gaussian models and CALPUFF can be made to produce the same concentrations in a steady state

environment, a variable state environment can produce higher ground level concentrations with CALPUFF with respect to ISC3. Climatological characteristics of a region appear to be a factor, but the accumulation of hour by hour meteorological conditions on the transport of CALPUFF puffs is the key to understanding the differences that are produced by this two kind of model (US EPA, 1998).

12.2.1 Weather and orographic data

The meteorological data file (CALMET.DAT) contains hourly or sub-hourly gridded fields of micro-meteorological parameters and three-dimensional wind and temperature fields. The meteorological data file also contains geophysical data such as terrain heights and land use. The requirements of the CALMET.DAT input file are summarized in Table 3.7.

Table 3.7. Geophysical and meteorological parameters required by the CALMET pre-processing model for the reconstruction of CALPUFF meteorological input (source: US EPA, 2011).

Geophysical data
Gridded fields of:
surface roughness lengths (z_0)
land use categories
terrain elevations
leaf area indices
Meteorological data
Gridded fields of:
u, v, w wind components (3-D)
air temperature (3-D)
surface friction velocity (u*)
convective velocity scale (w*)
mixing height (z_i)
Monin-Obukhov length (L)
PGT stability class
precipitation rate
air density (ρ_a)
air temperature
short-wave solar radiation
relative humidity
precipitation type

To simulate the dispersion of NO_x and PM in the scenarios considered, geophysical and meteorological input data were obtained from the Regional Agency for Environmental Protection of the Piedmont Region (ARPA Piemonte, 2012; Calori et al., 2006). The steps performed in the elaboration included the following:

- Meteorological data included wind and temperature analyzed fields from the European Centre for Medium Range Weather Forecast (ECMWF), two radiosoundings (located outside the computational domain) and 14 surface stations.
- These data were employed to reconstruct 3D wind and temperature fields on an hourly basis, using MINERVE diagnostic model. MINERVE (Aria Technologies, 2001) is a diagnostic-type model which reconstructs 3D wind fields starting from vertical profiles and near-ground wind measurements.
- An interpolated temperature field was also reconstructed with MINERVE, keeping into account the variation of temperature with terrain height.

Turbulence fields needed by the dispersion model were estimated by SURFPRO meteorological pre-processor (Arianet, 2002). Starting from topography and land-use data managed by the modeling system and gridded fields of average meteorological variables (e.g. wind, temperature and humidity) given by MINERVE, SURFPRO computes 2D gridded fields of turbulence scaling parameters (i.e. roughness length, sensible heat flux, friction velocity, Monin–Obukhov length, mixing height and convective velocity scale).

Weather and orographic data covered a domain of 100 x 100 km^2 with a horizontal resolution of 1000 meters. The same grid represented also the modeling domain. The domain extension was wider than the expected extension of dispersion impacts. This was done to consider the meteorological features of the area, because the surrounding orographic reliefs may indirectly affect the dispersion.

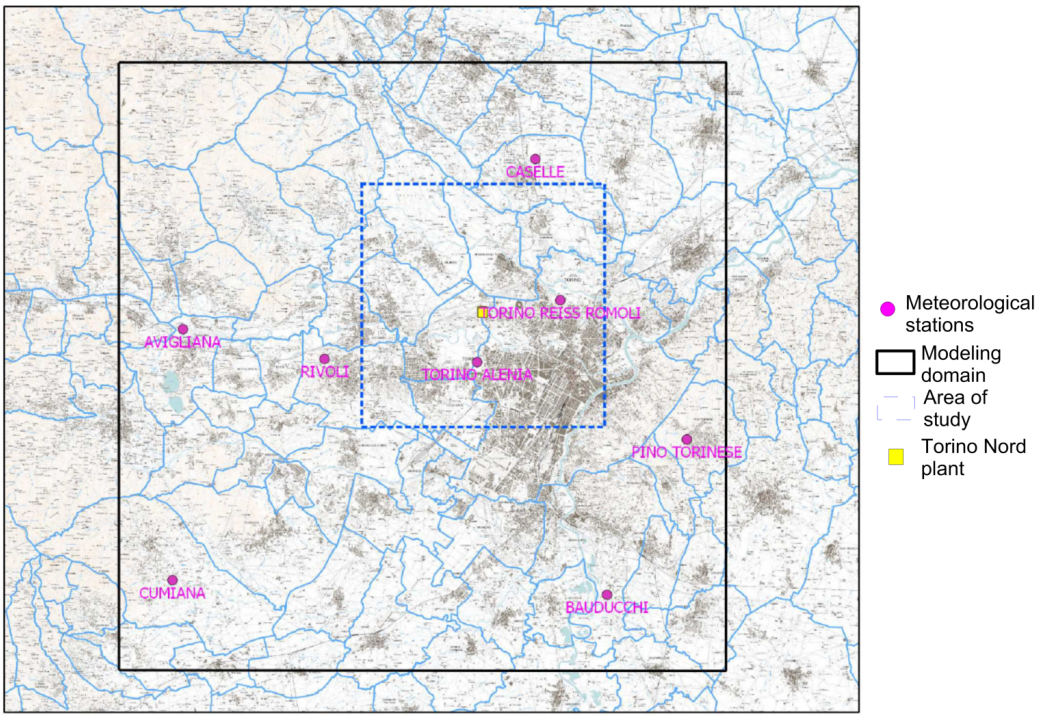

Figure 3.14. Modeling domain with an indication of the meteorological stations used in the calculation of the CALPUFF input variables. (source: modified from Arpa Piemonte, 2012).

The complete list of variables imported from MINERVE and SURFPRO is reported in Table 3.8. The data were collected in NetCDF format. NetCDF is a set of software libraries and self-describing, machine-independent data formats that support the creation, access, and sharing of array-oriented scientific data. Assessed the completeness and availability of the data, the reference year used was 2010.

Table 3.8. Meteorological and geophysical variable imported from Arpa Piemonte datasets in netCDF format.

Variable name	Content
TIME	time
Z0	surface roughness lengths
U,V,W	u, v, w wind components (3-D)
REL	terrain elevations

Table 3.8 (continued). Meteorological and geophysical variable imported from Arpa Piemonte datasets in netCDF format.

Variable name	Content
LAI	leaf area indices
TEMPK	air temperature (3-D)
USTAR	surface friction velocity
WSTAR	convective velocity scale
HMIX	mixing height
L	Monin-Obukhov length
PGT	PGT stability class
PREC	precipitation rate
TOTRAD	total solar radiation
NETRAD	net solar radiation

12.2.2 Integration of missing meteorological data

Two of the variables required by CALPUFF (Table 3.7), namely relative humidity and air density, where not included in the series provided by Arpa Piemonte, so they were calculated starting by the available data.

Relative humidity (H_r) was calculated as:

$$H_r = \frac{H_S}{MR} \cdot 100 \qquad \text{Eq. 3.6}$$

where H_s is the specific humidity and MR is the mixing ratio, calculated as:

$$MR = \frac{0.622 \cdot P_v}{P_{atm} - P_v} \qquad \text{Eq. 3.7}$$

where P_{atm} is the atmospheric pressure and P_v is the vapor pressure of water at equilibrium, calculated as:

$$P_v = 6.11 \cdot 10^{\left(\frac{7.5 \cdot T}{237.7 \cdot T}\right)} \qquad \text{Eq. 3.8}$$

where T is temperature.

Air density (ρ) was calculated as:

$$\rho = \frac{P_{atm}}{RT} \qquad \text{Eq. 3.9}$$

were R is the gas constant (287.05 J/kgK).

The values of H_s, P_{atm} and T were taken from Arpa Piemonte data series.

12.2.3 Format conversion of climate input files

The files containing meteorological variables required a conversion from netCDF format to the format readable by CALPUFF model. The procedure followed to convert the format was the following:

- Needed variables (Table 3.8) were extracted from the original files using NCKS package (netCDF kitchen sink, https://linux.die.net/man/1/ncks) installed in Linux MSYS interface program (http://www.mingw.org/wiki/msys);
- The files containing the series of each variable were imported and reformatted with GNU Octave software;

The creation of an algorithm in Fortran allowed then to reproduce the correct sequence of the information request from CALPUFF to read meteorological and geophysical data. A file having the same format as the output format from the pre-processor CALMET was created. The full text of this algorithm is reported in Appendix 5.

The format conversion algorithm from netCDF to CALPUFF is of interest because, with appropriate modifications and insights, it may be a useful and fast device in the setting up of the simulations with CALPUFF.

12.2.4 Characterization of emission sources

The key parameters of the emission sources used in the simulations are reported in Table 3.9. The geometric parameters of the stacks of the Torino Nord plant (main unit and integration boilers) were taken from the project

documentation. The exit speed of TO-N CC exhaust gases was calculated from the flow rate, which was directly read from the CEMS. The exit speed of exhaust gases emitted by the integration boilers was assumed to be 11.8 m/s (average value declared by the operator) when in operation, and zero when not in operation. The temperature values of the exhaust gases, not being directly read from the CEMS, were supposed equal to those of the Moncalieri plant (Iren Energia, 2014c), characterized by a size and a configuration similar to Torino Nord.

For what concerning the residential sources, the height of the stacks was fixed at 15 meters. Although in some areas the buildings are higher, this value is precautionary in simulating pollutant dispersions. The values of the diameter, the flue gas exit temperature and speed comply with the average data found in the literature for the type of housing considered.

Table 3.9. Parameters of the emission sources at the input of CALPUFF model.

Source ID	Description	East coord. (km) [6]	North coord. (km) [6]	Height (m)	Diameter (m)	Average temperature (°C)	Average speed (m/s)
TO-N1	Torino Nord – combined cycle	1390.95	4995.64	60 [1]	6.0 [1]	274 [4]	Variable [5]
TO-N2	Torino Nord – auxiliary boilers	1390.98	4995.56	60 [1]	8.0 [1]	274 [4]	11.8 [1]
TO-E1	Torino Est	1398.36	4995.21	60 [2]	8.0 [2]	274 [2]	11.8 [2]
TO-A1	Bar. stack area 1	1394.42	4996.94	15 [3]	0.8 [7]	270 [7]	5.0 [7]
TO-A2	Bar. stack area 2	1394.09	4995.44	15	0.8	270	5.0
TO-A3	Bar. stack area 3	1395.20	4995.07	15	0.8	270	5.0
TO-A4	Bar. stack area 4	1396.31	4995.21	15	0.8	270	5.0
TO-A5	Bar. stack area 5	1397.34	4994.29	15	0.8	270	5.0
TO-A6	Bar. stack area 6	1397.36	4993.00	15	0.8	270	5.0

NOTES: 1 Project datum; 2 Assumed to be equal to Torino Nord auxiliary boilers; 3 Average building height extracted from Census data (Istat, 2001); 4 assumed to be equal to the Moncalieri plant, for which the data of the CEMS is available; 5 Calculated on an hourly basis from the datum of flow of exhaust gases from the stack; 6 reference system ED50 UTM 32N; 7. Average data found in the literature.

After collecting the emission sources data, files containing sources input data to (PTEMARB.DAT or BAEMARB.DAT, Table 3.6) were created, according to the format required by CALPUFF. This was done by editing a Fortran algorithm, which text is reported in Appendix 6.

12.2.5 CALPUFF model settings

The simulation was run on the entire heating period of the year, i.e. from October to March. The model settings for the base case simulation were the following:

- chemical transformation scheme: MESOPUFF II (Scire, 1984);
- building downwash method: ISC method (Huber and Snyder, 1976);
- building profile for downwash calculation: buildings 15 m high and 15 m wide, spaced every 10°. This profile simulates a very dense urban structure and was initially chosen to evaluate the worst conditions from the emissive aspect.
- plume rise calculation method: Briggs (1975);
- stack tip downwash calculation method: Briggs (1973);
- method for the calculation of horizontal and vertical dispersion: from internally calculated coefficients using micrometeorological variables. (US EPA, 2011);
- vertical wind shear: not modeled;
- type of terrain adjustment: simple;
- elongated slugs: not simulated;
- transitional plume rise: modeled;
- puff splitting: not allowed;

12.2.6 Background ozone concentration

The transformation processes included in the MESOPUFF II mechanism are the conversion of sulphur dioxide to sulphate and of nitrogen oxides to nitrate aerosol. These processes include photochemical reactions which transformation rates are expressed as a function of ozone concentration in air. For this reason, hourly measurements of ozone concentration taken by the monitoring station located in Via della Consolata, Turin, had to be introduced to the model.

12.3 Data post-processing

The output data from CALPUFF were sent to CALPOST post-processor, obtaining the hourly concentration grids. Subsequently, the creation of an algorithm in GNU Octave allowed the extraction and localization of the maximum

values, the calculation of the average monthly concentration grid, and the reformatting of the data in the form of concentration maps of NO_x and TSP at ground level.

12.3.1 Calculation of the concentration difference

For the future scenario, the generated emissions were simulated separately from the avoided emissions. The CALPOST post-processor provided then a series of grids, one per hour, of pollutants concentration on the entire dispersive domain. To achieve the visualization of the results, a GNU Octave script was created. This script performed the following tasks in sequence:

- imports hourly concentration grids from CALPOST;
- overlays, adding algebraically, generated emission grids to avoided emission grids, obtaining the emission balance;
- calculates the hourly average concentrations over the period;
- reformats the average concentration values to be readable by SURFER software.

In parallel with the calculation of the average concentration over the period considered, the script was also set to calculate the average concentration only in daytime hours.

The full text of the algorithm mentioned above is reported in Appendix 7.

12.3.2 Analysis of maximum and minimum concentration

The same script described in the previous paragraph included the calculation of the absolute maximum and minimum values of the results. The maximum and minimum values were calculated on the average hourly concentration differences. The maximum values thus indicate the worst conditions, in which the generated emissions overtake reduced emissions (positive concentration differences). On the other hand, the minimum values indicate the moments of greater advantage from the environmental point of view (negative values of concentration difference). The algorithm was set up to:

- locate the 5 maximum and minimum values on the entire space and time domain of the calculation;

- returning values to an external file, indicating also the corresponding time and location;
- taking the hourly grid corresponding to the maximum (or minimum) value and reformat it to be readable with SURFER software.

12.3.3 Elaboration of concentration maps

The grids of concentration difference (see previous paragraph) were imported in SURFER software to generate concentration maps at ground level. Two types of representation were chosen, depending on the scale of detail. In the first type, the only urban area of Turin was reported, overlaying concentrations values to a geo-referenced map of the city. In the second type, a three-dimensional rendering of the entire computational domain was created, to highlight the orographic features that characterize the surroundings of the city. The three-dimensional representation of the computational domain is reported in Figure 3.15.

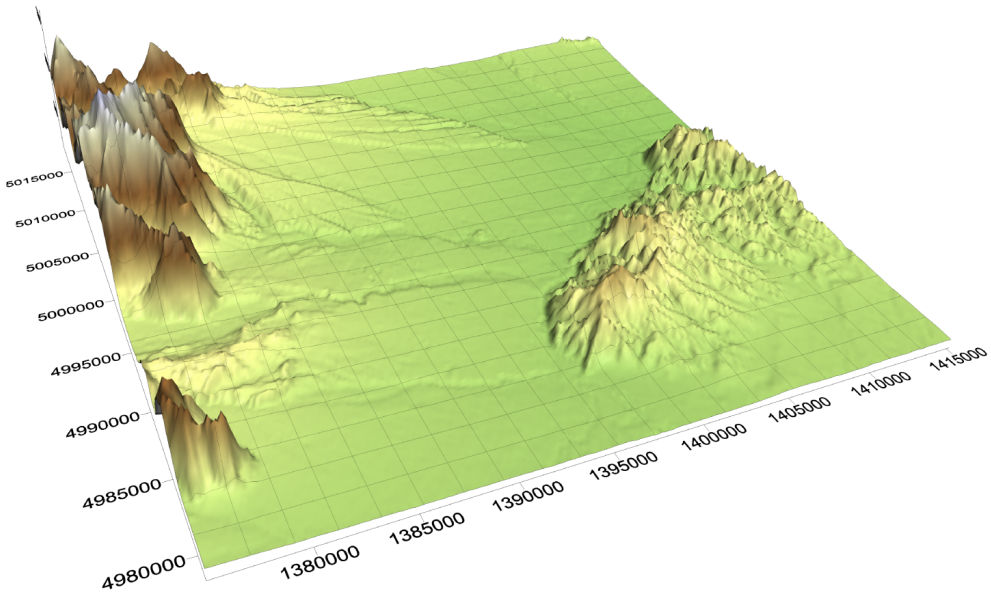

Figure 3.15. Tridimensional representation of the modeling domain with SURFER software.

12.4 Analysis of uncertainties

Once completed the base case simulation, an analysis of uncertainty was made on two model settings that showed to have a strong contribution to the

results. First, the building downwash configuration was modified with respect to the base case, by assuming two different profiles of the buildings around the residential emission sources:

- the “higher and less dense” profile, characterized by buildings 30 m high and 15 m wide, spaced every 20°;
- the “less dense” profile, characterized by buildings 15 m high and 15 m wide, spaced every 20°.

The simulation of these two different profiles had the objective of evaluating the contribution of the downwash phenomenon on the pollutants dispersion. The downwash effect is more evident for sources of limited height.

Secondly, the simulations were repeated by changing the height of the residential sources. The height of the stack was thus first set to 20 meters, then to 30 meters. The increase of the emission height was also expected to influence the resulting concentrations.

As a final step, the base case simulation was repeated assigning an area source type to the residential emissions, instead of a point source type. An input source file BAEMARB.DAT for each scenario was created with a procedure similar to that reported at the previous paragraphs.

Chapter 13

Methodology for the global emission analysis

For the present case study, the balance of the emissions at a global scale was calculated in terms of carbon footprint, representing the burden of greenhouse gases in terms of CO_2 emitted.

It has long been demonstrated that for natural gas combustion, as for the other fossil fuel electricity or heating systems, the dominant contributor to GHG emissions is CO_2 from the power plant (Dones et al., 2003; Spath and Mann, 2000). For this reason, the selected approach for this case study was not of LCA-type, i.e. considering the entire process "from the cradle to the end-use". The only operational phase of energy production was thus considered in the calculation of the GHG emission balance.

Based on these considerations, the comparison of CO_2 emissions is only focused on the difference between the exercise of the power plants and the aggregate of the residential sources, considering one year as a time base.

The definition of emission flows is based on the overall energy balance of the system reported at Chapter 11.3, Table 3.2. The same table is recalled in continuation.

Table 3.10. Energy balance of present and future scenario.

Source	Present thermal energy production / demand (MWh/y)	Future thermal energy production / demand (MWh/y)	Difference (MWh/y)
TO-N plant (combined cycle)	336,720	586,050	+ 279,330
TO-N plant (auxiliary boilers)	10,075	40,214	+30,139
TO-E plant	-	347,480	+ 347,480
Buildings not connected to DH network	943,299	316,351	- 626,948
Buildings connected to DH network	-	626,948	+ 626,948

13.1 CO_2 allocation method

The allocation method is the methodology which can provide information how to share benefits and drawbacks from cogeneration. A meaningful allocation method allows the sources of CO_2 and other emissions to be better understood and, where appropriate, reduced (Rosen, 2006).

The three most common methods to allocate emissions from a CHP plant are (CCAR, 2008):

- Efficiency method: GHG emissions are allocated based on the energy inputs used to produce the separate steam and electricity products.
- Energy content method: GHG emissions are allocated based on the energy content of the output heat and electricity products.
- Work potential method: GHG emissions are allocated based on the exergy content of the heat and electricity products.

The advantages and limitations of these methods have been widely studied in the literature, evidencing the best conditions for their application. The main organization working on greenhouse effect published recommendations about this topic (see for example IEA 2016b, CCAR 2008, ICFPA 2005).

The allocation method used in this case study is the Energy Content Method. The energy content method allocates emissions based on the amount of energy in each energy output. The energy content of electrical power is simply the amount of electricity produced by the system. The energy content of heat is equivalent to the energy content transferred to the DH network in form of hot water. Losses due to inefficient use of either the electricity or heat are not considered. This allocation method is particularly well suited for situations in which thermal energy is used for process heat.

The reasons for selecting this method may be resumed in the following:

- GHG emissions are allocated according to the useful energy contained in each CHP output stream;
- It is the recommended method when heat can be characterized as useful energy, e.g., for process or district heating.

In addition, the other two methods may not be recommendable for the present case study, because:

- The Efficiency method allocates GHG emissions according to the amount of fuel energy used to produce each final energy stream. For the present case study, a single value of fuel consumption is available for the combined cycle, thus no sufficient information is available to assign an amount of fuel energy to each energy stream.
- The Work Potential method may not be appropriate in this case, because the energy streams are not associated with a production of mechanical work.

The methodology for the calculation of the greenhouse gas emission balance is described in detail in the next chapters.

13.2 Calculation of CO_2 balance

The overall global CO_2 balance was calculated as the algebraic sum of the present and future situation:

$$\Delta CO_2 = F_{CO2,fut} - F_{CO2,pres} \quad \text{Eq. 3.10}$$

where $F_{CO2,fut}$ and $F_{CO2,pres}$ are the mass flow of the CO_2 emitted by the system in the future and present situation respectively.

Both terms include the contribution of the following emission sources:

$$F_{CO2,pres} = F_{th,pres} + F_{el,pres} + F_{boi,pres} + F_{res,pres} \quad \text{Eq. 3.11}$$

$$F_{CO2,fut} = F_{th,fut} + F_{el,fut} + F_{boi,fut} + F_{res,fut} \quad \text{Eq. 3.12}$$

where $F_{th,pres}$ and $F_{th,fut}$ are the present and future CO_2 emission respectively, corresponding to the thermal energy produced by the Torino Nord CC cogeneration unit; $F_{el,pres}$ and $F_{el,fut}$ are the CO_2 emission respectively, corresponding to the electrical energy produced by the Torino Nord CC cogeneration unit; $F_{boi,pres}$ is the CO_2 emission corresponding to the thermal energy produced by Torino Nord integration and reserve heaters; $F_{boi,fut}$ is the is the CO_2 emission corresponding to the thermal energy produced by Torino Nord and Torino Est integration and reserve heaters; $F_{res,pres}$ and $F_{res,fut}$ are the present and future CO_2 emission respectively, corresponding to the thermal energy produced by the centralized heaters installed in the area of intervention.

Each value of emission flow was obtained by multiplying the energy flow for the corresponding emission factor. The methodology of calculation of the individual emission contributions is given in continuation.

13.2.1 Torino Nord combined cycle emission ($F_{th,pres}$, $F_{el,pres}$, $F_{th,fut}$, $F_{el,fut}$)

The annual CO_2 flow emitted from Torino Nord plant was calculated as the sum of hourly values of thermal and electrical energy produced, multiplied by the corresponding emission factor.

The available starting data were elaborated by the measures of the continuous emission monitoring system (CEMS) for the year 2014, namely:

- hourly CO_2 flow emitted by the chimney (CO_{2tot}): this parameter was provided by the plant's operator on the basis of the measured fuel consumption;
- hourly thermal power transferred to the DH network ($P_{th,\ pres}$);
- hourly electric power produced ($P_{el,\ pres}$).

The proportion of thermal energy over the total energy produced ($\%_{th,pres}$) was thus calculated for each hour, as:

$$\%_{th,pres} = \frac{P_{th,pres}}{(P_{th,pres}+P_{el,pres})} \quad \text{Eq. 3.13}$$

The CO_2 flow referring to the sole thermal power was thus calculated as:

$$CO_{2th} = CO_{2tot} \cdot \%_{th,pres} \quad \text{Eq. 3.14}$$

Consequently, the average emission factor for thermal energy was calculated as the ratio of the sum of all the i-th hourly values of CO_{2th} and the sum of all the i-th hourly values of $P_{th,pres}$:

$$EF_{TON,th} = \frac{\sum_{i=1}^{8760} CO_{2th,i}}{\sum_{1=1}^{8760} P_{thpres,i}} \quad \text{Eq. 3.15}$$

In the same way, the proportion of electrical energy over the total energy produced ($\%_{el,pres}$) was calculated for each hour, as:

$$\%_{el,pres} = \frac{P_{el,pres}}{(P_{th,pres}+P_{el,pres})} \quad \text{Eq. 3.16}$$

The CO_2 flow referring to the sole electrical power was thus calculated as:

$$CO_{2el} = CO_{2tot} \cdot \%_{el,pres} \quad \text{Eq. 3.17}$$

Consequently, the average emission factor for thermal energy was calculated as the ratio of the sum of all the i-th hourly values of CO_{2el} and the sum of all the i-th hourly values of $P_{el,\ pres}$:

$$EF_{TON,el} = \frac{\sum_{i=1}^{8760} CO_{2el,i}}{\sum_{1=1}^{8760} P_{elpres,i}} \quad \text{Eq. 3.18}$$

Based on the calculations reported so far, the annual emission flows for the present scenario referring to Torino Nord plant turn out to be:

$$F_{th,pres} = \sum_{i=1}^{8760} CO_{2th,i} \quad \text{Eq. 3.19}$$

$$F_{el,pres} = \sum_{i=1}^{8760} CO_{2el,i} \quad \text{Eq. 3.20}$$

Considering the future scenario, the thermal energy production of TO-N plant was that defined according to the hourly energy balance, previously reported in Chapter 12.1.2.

Electricity production

For the estimation of electricity production, the operation of the combined cycle was deeper investigated, to achieve information on the allocation between electricity and heat produced. The present operating mode of the system is represented in Figure 3.16, where the hourly values of net electrical power were reported against the heat provided to the DH network. Figure 3.16 shows that all the operational points of the system are comprised within a given area. This "power to heat" graph results from the necessity to find an equilibrium between electricity and heat production; it was also evidenced and studied in an article of Jarre et al. (2016), conducted on the same TO-N plant. Figure 3.16 shows that there it is no clear direct relationship between the two variables. In general, five different schemes of operation may be found, corresponding to different areas of the graph:

- an area with no thermal production and variable electricity production;
- an area with constant electricity production corresponding to around 190MWe or 50% of the total nominal power of the turbines, and variable heat production;
- an area with constant electricity production corresponding to around 330MWe or 85% of the total nominal power of the turbines, and variable heat production;
- an area, delimited by two horizontal lines (190MWe and 330MWe), of variable operation of both electricity and heat;
- an area of maximum production of both electricity and heat, corresponding to the upper right corner of the graph.

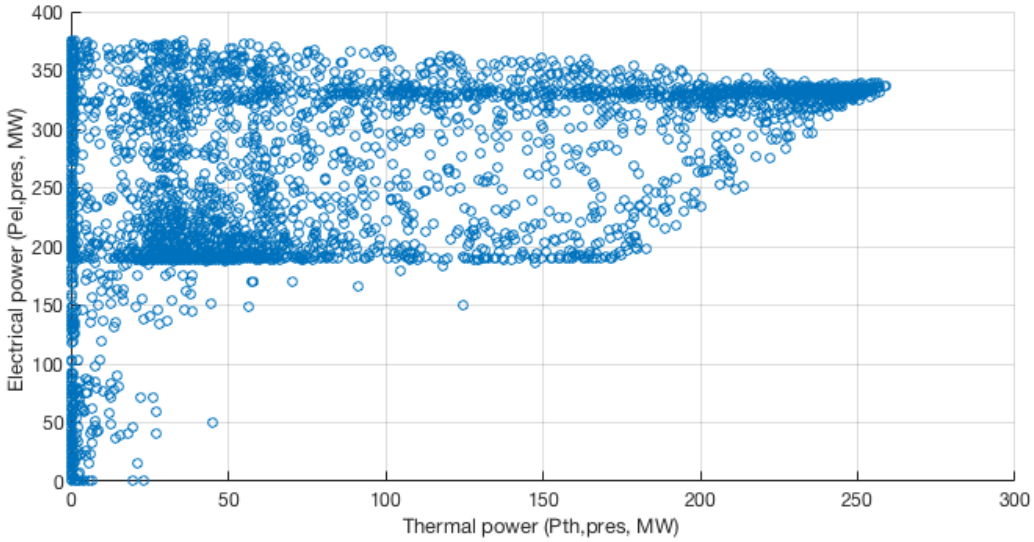

Figure 3.16. Present operational graph of TO-N plant, represented as electrical power versus thermal power.

Production of electricity and thermal energy depends on different factors. In fact, if the first is mainly regulated by the market, the heat production chiefly depends on the demand of the DH network. Both market and DH network demand show hourly and seasonal fluctuations. For this reason, the relationship between the two variables was hypothesized based on hourly production ratios, differentiating between heating (cold) and non-heating (hot) season. The two ratios were defined as:

$$\%_{pres,win,i} = \frac{P_{av,th,pres,i}}{P_{av,el,pres,i}} \text{ with i=1,2...24.} \qquad \text{Eq. 3.21}$$

$$\%_{pres,sum,j} = \frac{P_{av,th,pres,j}}{P_{av,el,pres,j}} \text{ with j=1,2...24.} \qquad \text{Eq. 3.22}$$

where $\%_{pres,win,i}$ is the ratio between the produced thermal and energy power during the heating season, for the i-th hour of the day; $P_{av,th,pres,i}$ and $P_{av,el,pres,i}$ are the average of thermal and electrical power produced in the i-th hour of the day, calculated over the heating period; $\%_{pres,sum,j}$ is the the ratio between the produced thermal and energy power during the non-heating season, for the j-th hour of the day; $P_{av,th,pres,j}$ and $P_{av,el,pres,j}$ are the average of thermal and electrical power produced in the j-th hour of the day, calculated over the non-heating period;

The calculated values of the two ratios were used to estimate electricity production in the future scenario, as follows:

$$P_{el,fut,win} = \sum_{i=1}^{24} \left[\sum_{k=1}^{182} \frac{P_{th,pres,i,k}}{\%_{pres,win,i}} \right] \quad \text{Eq. 3.23}$$

$$P_{el,fut,sum} = \sum_{j=1}^{24} \left[\sum_{h=1}^{183} \frac{P_{th,pres,i,h}}{\%_{pres,sum,j}} \right] \quad \text{Eq. 3.24}$$

$$P_{el,fut} = P_{el,fut,win} + P_{el,fut,sum} \quad \text{Eq. 3.25}$$

where k and h are the number of days of the heating and non-heating period respectively; $P_{th,pres,i,k}$ (or $P_{th,pres,i,h}$) is the thermal power produced by the combined cycle at hour i of day k (or day h).

Once the term $P_{el,fut}$ was calculated, an algorithm in GNU Octave was created to check that the single couples of ($P_{th,fut}$, $P_{el,fut}$) values respected the original operational "power to heat" graph of Figure 3.16. The algorithm introduced a correction in case that a couple of values fell outside the given area. The resulting operational graph for the future scenario is reported in Figure 3.17, compared to the present one. In can be seen from Figure 3.17 that almost all the couples of ($P_{th,fut}$, $P_{el,fut}$) values respect the present operational setting of the plant.

In this way, the future values of $F_{th,fut}$ and $F_{el,fut}$ result to be:

$$F_{th,fut} = \sum_{i=1}^{8760} P_{thfut,i} \cdot EF_{TON,th} \quad \text{Eq. 3.26}$$

$$F_{el,fut} = \sum_{i=1}^{8760} P_{elfut,i} \cdot EF_{TON,el} \quad \text{Eq. 3.27}$$

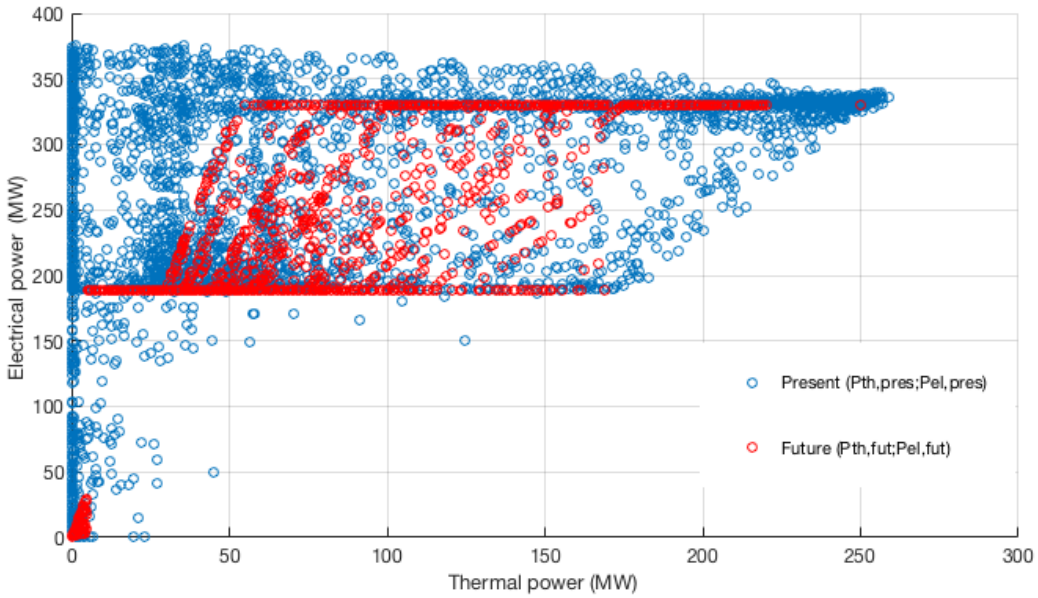

Figure 3.17. Present and future operational graph of TO-N plant, represented as electrical power versus thermal power.

13.2.2 Torino Nord integration and reserve heaters ($F_{boi,pres}$, $F_{boi,fut}$)

The CO_2 emission flow generated by the Torino Nord integration and reserve heaters was calculated by supposing an average emission factor (EF_{boi}) starting by the data measured by the CEMS (Table 3.11):

$$EF_{boi} = \frac{\sum_{i=1}^{8760} CO_{2boi,i}}{\sum_{i=1}^{8760} P_{boipres,i}} \qquad \text{Eq. 3.28}$$

where CO_{2boi} is the CO_2 flow emitted by the Torino Nord integration and reserve system, that is directly measured by the CEMS of the plant.; P_{boi} is the hourly thermal power produced by the same system, calculated by difference based on the thermal power sent to the DH network (see Chapter 13.2).

The present CO_2 flow emitted by the integration and reserve system results thus to be:

$$F_{boi,pres} = \sum_{i=1}^{8760} CO_{2boi,i} \qquad \text{Eq. 3.29}$$

For the future scenario, the CO_2 flow results to be:

$$F_{boi,fut} = \sum_{i=1}^{8760} P_{boifut,i} \cdot EF_{boi} \quad \text{Eq. 3.30}$$

Where $P_{boi,fut}$ turns out to be the summed contribution of Torino Nord ($P_{boiTON,fut}$) and Torino Est ($P_{boiTOE,fut}$) integration and reserve systems:

$$P_{boi,fut} = P_{boiTON,fut} + P_{boiTOE,fut} \quad \text{Eq. 3.31}$$

The emission factor value is supposed to be equal in the two systems due to the preliminary assumptions of the study, where the new integration plant was supposed to be technically identical to the existing one.

13.2.3 Residential centralized heaters ($F_{res,pres}$, $F_{res,fut}$)

For the characterization of the CO_2 emission flows of the residential sources involved in the potential extension of the DH network, the same procedure used in the definition of local emission balance was followed. The heat demand of the buildings, calculated with the method reported in Chapter 13.3, was thus multiplied by the corresponding emission factor, variable with respect to the fuel feeding the centralized heater (Table 3.11).

The emissions contributing to the present scenario ($F_{res,pres}$) were generated by the totality of the buildings covering the areas interested by the potential extension of the DH system. The emission contributing to the future scenario ($F_{res,fut}$) were accounted to be generated by the only buildings remained not connected to the DH network.

Table 3.11. Emission factors of CO_2 emission.

Emission source	Acronym	CO_2 emission factor (kg/MWh)	Ref.
Torino Nord –combined cycle – thermal energy	$EF_{TON,th}$	320.6	Iren Energia
Torino Nord –combined cycle – electrical energy	$EF_{TON,el}$	376.5	Iren Energia
Torino Nord – auxiliary boilers	EF_{boi}	259.3	Iren Energia
Torino Est	EF_{boi}	259.3	Iren Energia
Residential stacks (natural gas)	$EF_{res,ng}$	231.1	EMEP/EEA
Residential stacks (diesel oil)	$EF_{res,do}$	249.5	EMEP/EEA
Residential stacks (LPG)	$EF_{res,lpg}$	227.2	EMEP/EEA
Residential stacks (heavy oil)	$EF_{res,ho}$	278.6	EMEP/EEA

Chapter 14

Results of local emissions

The concentration values reported in the following result from the simulation of the considered emission sources and do not include the background concentrations.

14.1 Overall emission balance

The overall environmental balance of the intervention considered, comparing the present and future annual mass flow of NO_x and TSP, is reported in Table 3.12. Table 3.12 shows that the extension of the DH network would bring a reduction on total NO_x emissions of around 5.4 t/y, corresponding to 2.3% of actual emission. For TSP, the reduction would be around 0.17 t/y, corresponding to 5.5% of actual emission.

Table 3.12. Changes in total NO_x and TSP emission between present (year 2014) and future scenario.

Emission source	NO_x (t/y)		TSP (t/y)	
	Present	Future	Present	Future
TO-N plant	57.68	104.70	0.578	1.078
TO-E plant	-	62.55	-	1.113
Buildings not connected to DH	172.47	57.49	2.497	0.715
Buildings connected to DH (avoided emissions)	-	114.98	-	1.781
Total produced emissions	230.15	224.74	3.075	2.906

14.2 Average concentration difference

The concentration maps resulting from the simulation of pollutants dispersion are reported in Figures 3.18 to 3.23. The result referred to the urban area of Turin, base case simulation, is shown in Figures 3.18 to 3.21. The same result, extended to the entire modeling domain, is reported in Figures 3.22 and 3.23. Positive and negative values indicate increased or reduced impacts respectively, compared to the present situation. The result shows from 0.2 to $\mu g/m^3$ to 4 $\mu g/m^3$ reduction of NO_x concentration with respect to the present situation. Figure 3.22 indicates that local effects are mainly limited to the urban area and the concentration difference approaches zero in the surrounding.

The result of TSP dispersion indicates a negligible reduction of the concentration, limited to around 10^{-2} $\mu g/m^3$. TSP emission flows are relatively low compared to NO_x, both in CC plants fueled by natural gas, and in residential centralized systems (TSP emission factors are 2 to 4 order of magnitudes lower than NO_x emission factors, Table 3.4).

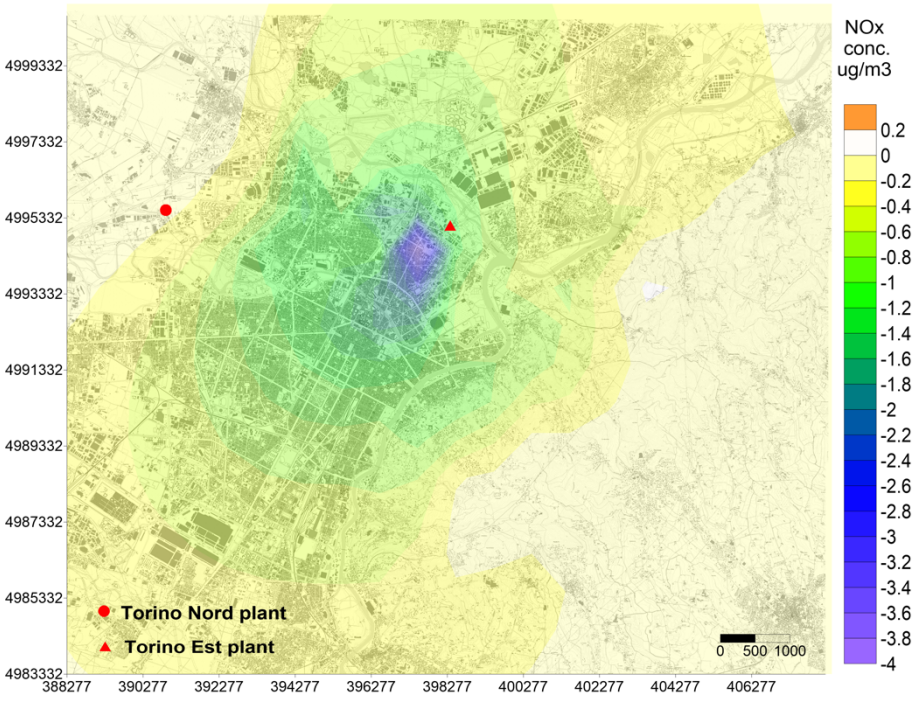

Figure 3.18. Map of NO_x concentration difference at ground level in the urban area of Turin, **base case simulation.**

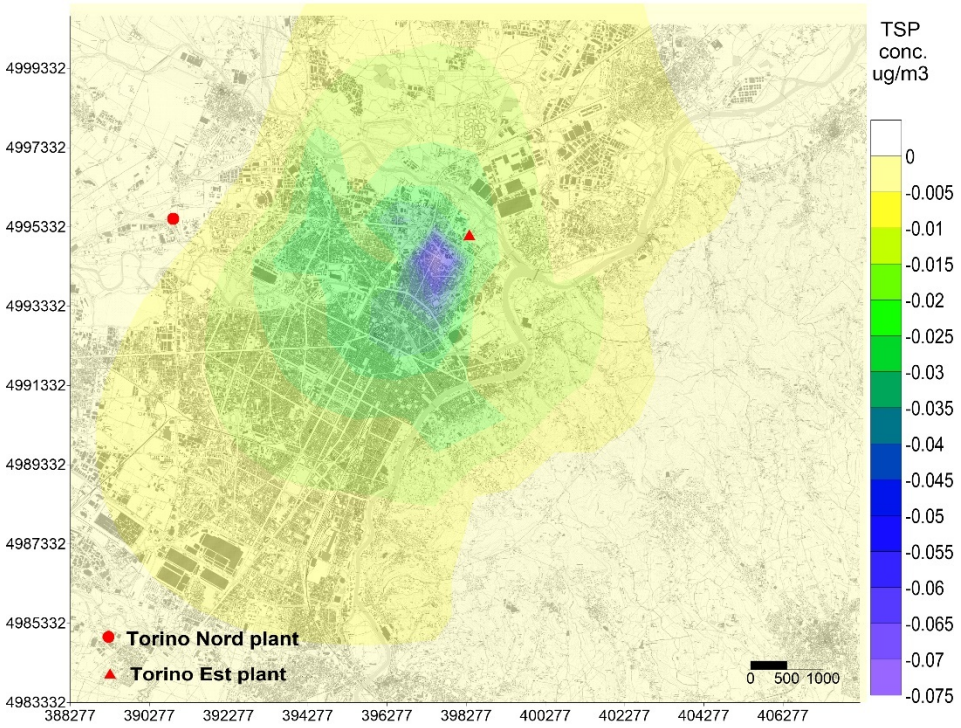

Figure 3.19. Map of TSP concentration difference at ground level in the urban area of Turin, **base case simulation.**

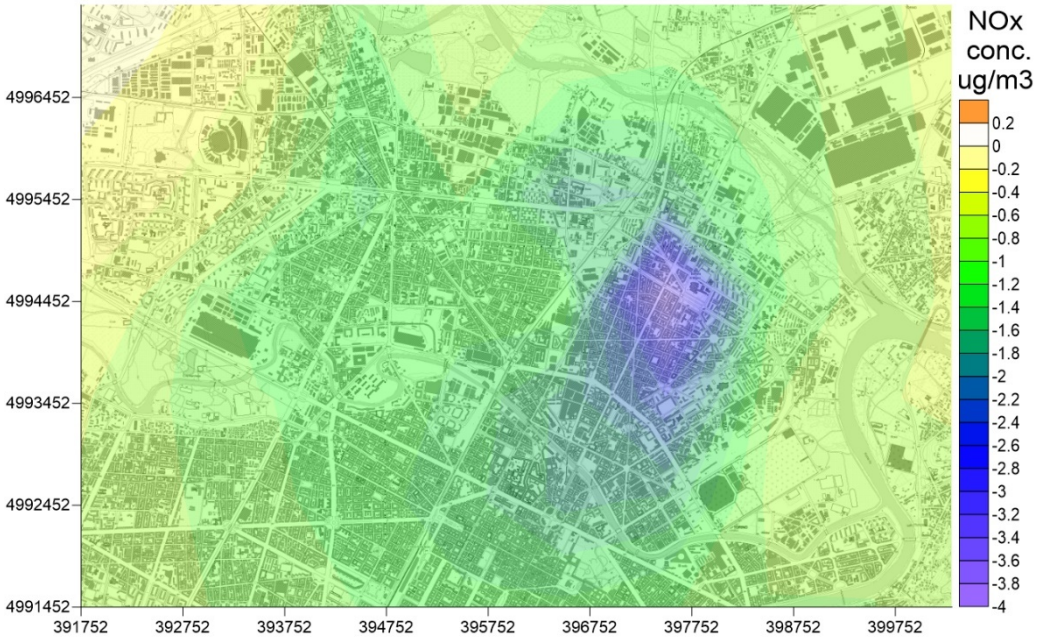

Figure 3.20. Map of NO_x concentration difference at ground level in the urban area of Turin, **base case simulation. Zoom to the areas interested by the DH network extension.**

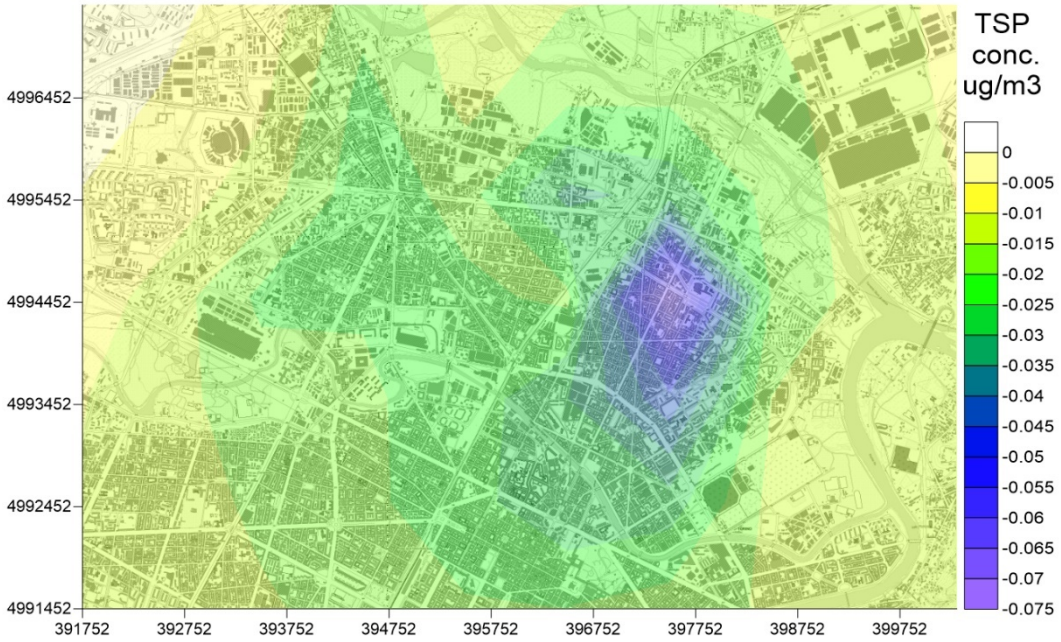

Figure 3.21. Map of TSP concentration difference at ground level in the urban area of Turin, **base case simulation. Zoom to the areas interested by the DH network extension.**

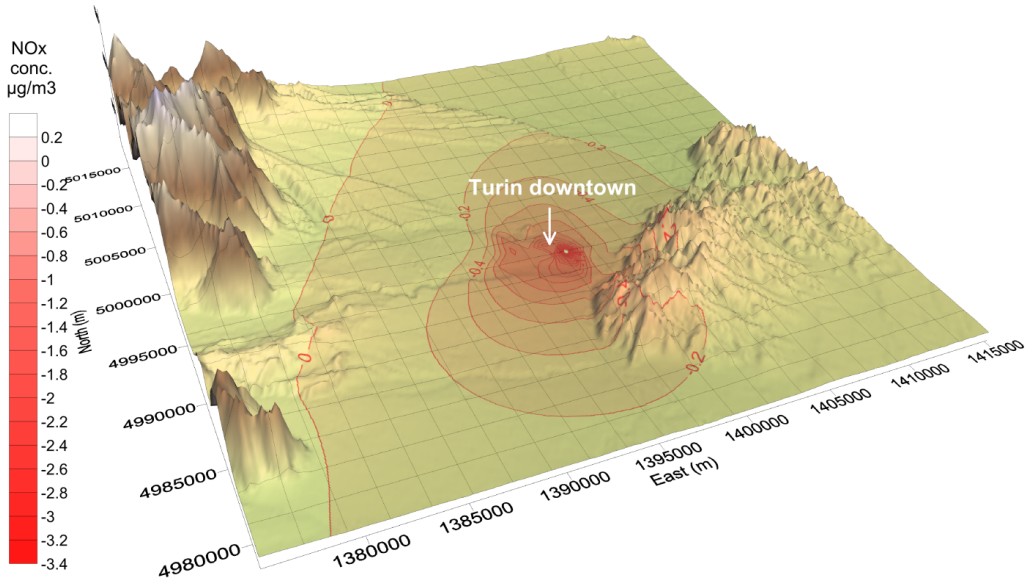

Figure 3.22. Map of NO_x concentration difference at ground level in the urban area of Turin, **base case simulation. Zoom to the entire modeling domain.**

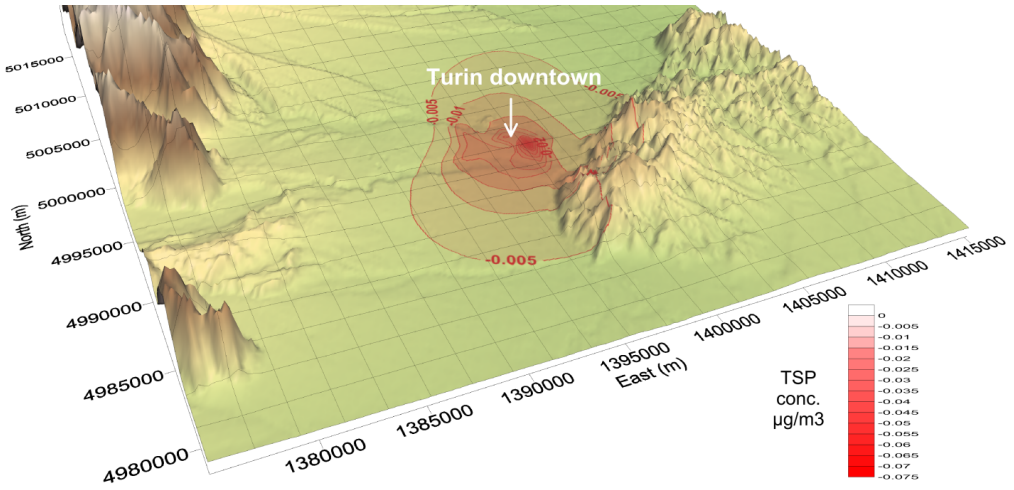

Figure 3.23. Map of TSP concentration difference at ground level in the urban area of Turin, **base case simulation. Zoom to the entire modeling domain.**

14.3 Contribution of single emission sources

To assess the contribution of different sources on the total balance, the same sources were simulated separately, both for the present that for the future scenario. This series of simulations were run considering the only month of January and the only pollutant NO_x. The contribution of TO-N plant for the present scenario is shown in Figure 3.24. The concentration is relatively low in comparison to the one caused by residential systems, reported in continuation.

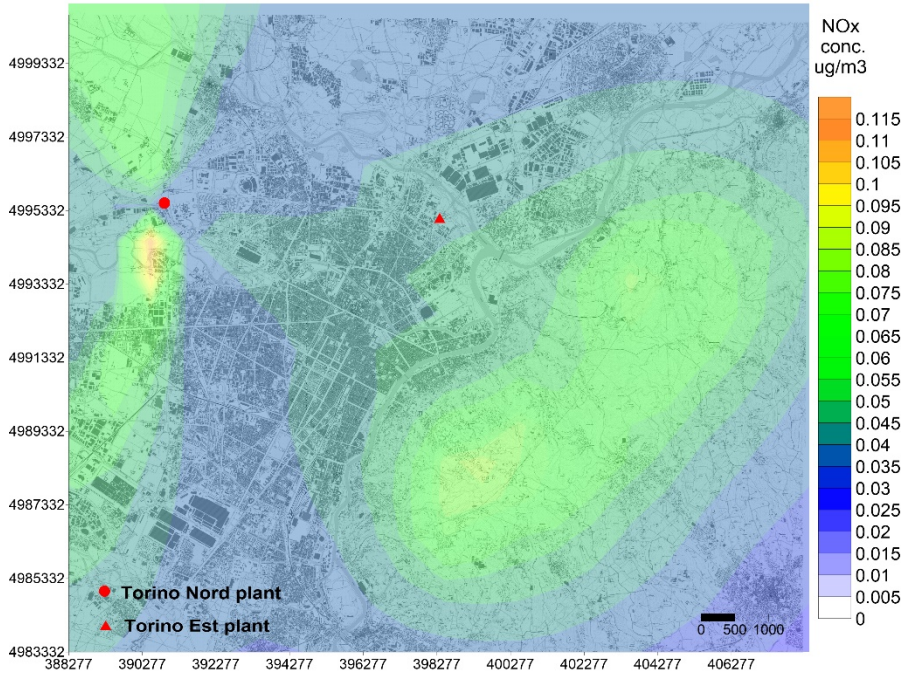

Figure 3.24. NO_x average concentration at ground level in the urban area of Turin for the **present scenario**, month of January, considering the **only contribution of TO-N plant**.

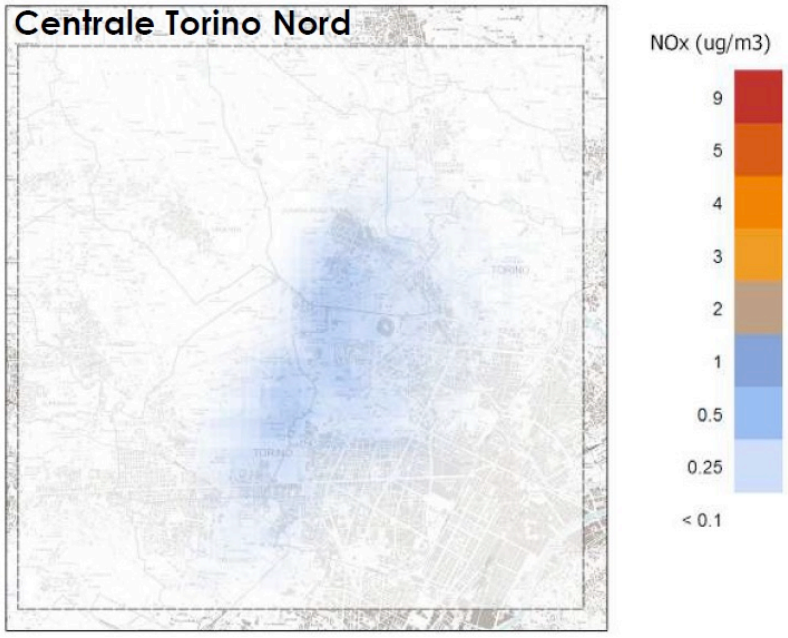

Figure 3.25. NO_x average concentration at ground level in the urban area of Turin, considering the **only contribution of TO-N plant. Result of a study by ARPA Piemonte (2012).**

The result of Figure 3.24 is comparable, in terms of order of magnitude, to a previous study done by Arpa Piemonte on the impacts of TO-N plant (ARPA Piemonte, 2012), whose result is shown in Figure 3.25. The average concentration of NO_x at ground level in the urban area of Turin, referring to the future scenario and only to the generated emissions is shown in Figures 3.26 and 3.27. Figure 3.26 refers only to the contribution of TO-N and TO-E plants. Figure 3.27 includes also the contribution of the emissions from the residential areas remained unconnected to the DH network. These figures reveal that the increase in the operation of TO-N plant and entry into operation of TO-E plant cause a moderate increase of pollution with respect to the present scenario. In addition, TO-E plant causes a moderate impact on the hilly areas located east of the Turin downtown, characterized by a maximum elevation of about 600 m above sea level. The emissions generated by the power stations are, however, still significantly lower than those due to the portion of autonomous buildings still not connected to the DH network (Figure 3.27). The contribution of the removed emissions by the residential areas connected to the DH network in the future scenario is finally shown in Figure 3.28.

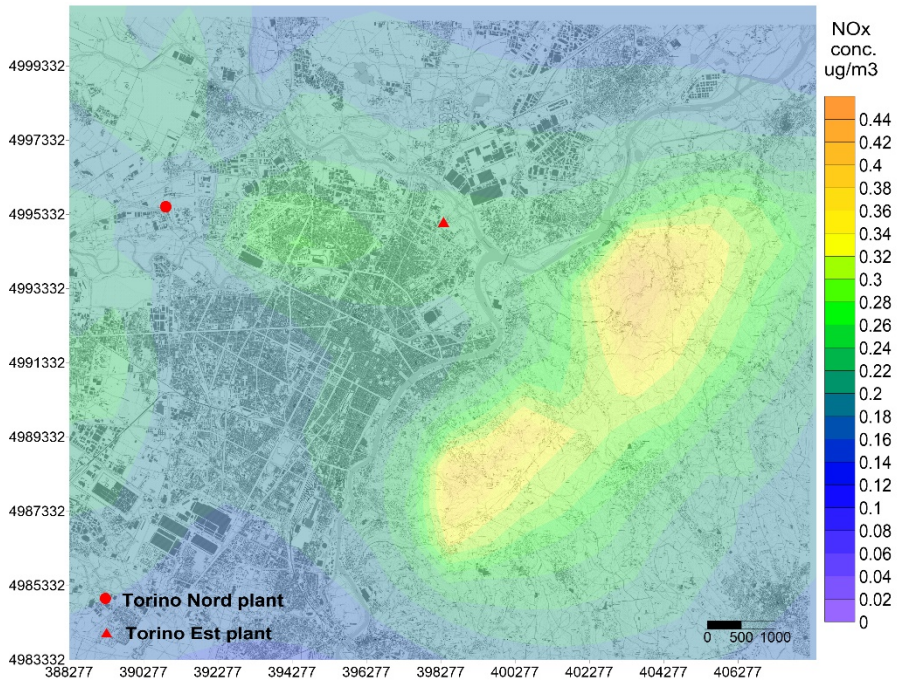

Figure 3.26. NO_x average concentration at ground level in the urban area of Turin for the **future scenario**, month of January, considering the **only contribution of TO-N and TO-E plants**.

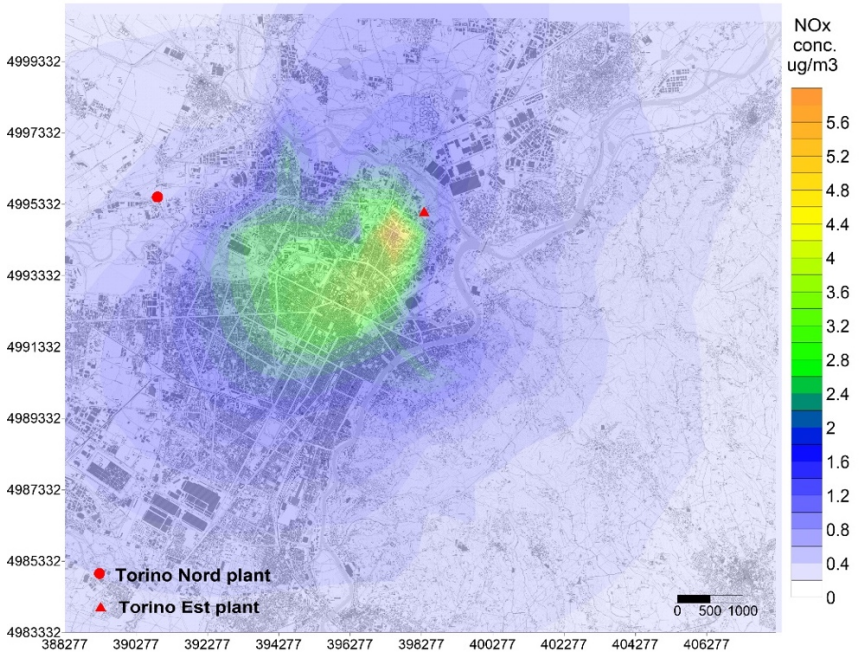

Figure 3.27. NO_x average concentration at ground level in the urban area of Turin for the **future scenario**, month of January, considering the **joined contribution of the generation plants and the residential areas still not connected to the DH network (generated emissions).**

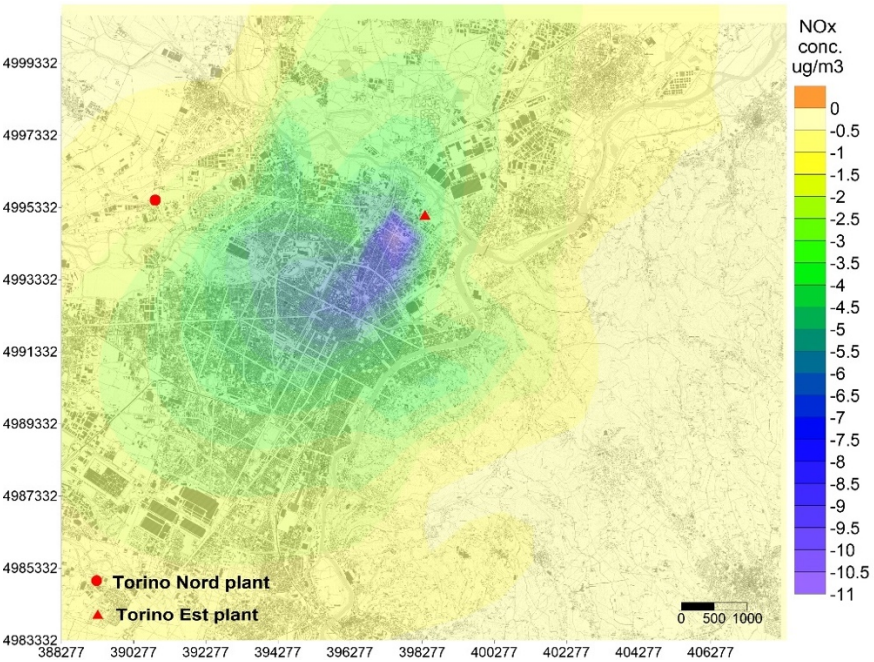

Figure 3.28. NO_x average concentration at ground level in the urban area of Turin for the **future scenario**, month of January, considering the **contribution of the residential areas connected to the DH network (avoided emissions).**

14.4 Maximum and minimum concentrations

The absolute maximum and minimum values extracted by running the GNU Octave algorithm (Appendix 7) are reported in Table 3.13 and Table 3.14. These tables show the occurrence of peak concentrations which shift significantly from the average values. Peak concentrations are influenced by both pollutants emission rate and dispersion conditions. Maximum (positive) values are the effect of the pollutant plume emitted by TO-N and TO-E plants, that impacts on the hilly areas surrounding Turin (Figure 3.30). Minimum (negative) values are recorded in the area interested by the DH network extension and result from the impact at ground of low residential stacks emissions (Figure 3.29).

Table 3.13. Maximum values of ground level concentration with relative date and position extracted from the simulations.

NO_x maximum relative conc. ($\mu g/m^3$)	TSP maximum relative conc. ($\mu g/m^3$)	Month / Day / time	East coord. (km)	North coord. (km)
63	0.07	02/06 07:00	1403.500	4993.500
59	0.07	01/31 07:00	1401.500	4989.500
50	0.06	01/31 07:00	1400.500	4989.500

Table 3.14. Minimum values of ground level concentration with relative date and position extracted from the simulations.

NO_x minimum relative conc. ($\mu g/m^3$)	TSP minimum relative conc. ($\mu g/m^3$)	Month / Day / time	East coord. (km)	North coord. (km)
-270	-5.0	12/04 15:00	1397.500	4994.500
-220	-4.0	12/22 11:00	1397.500	4994.500
-212	-3.9	01/09 12:00	1397.500	4994.500

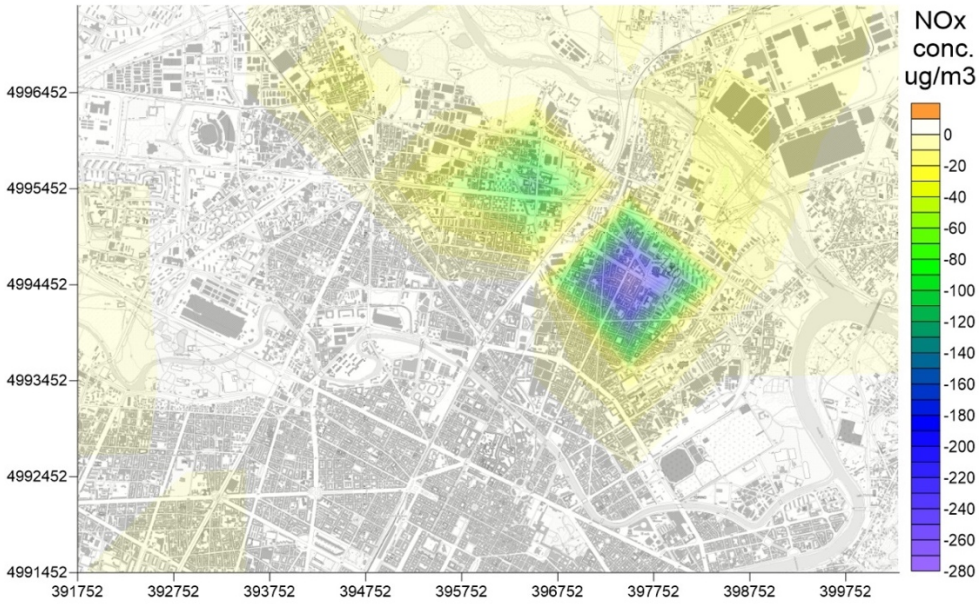

Figure 3.29. NO_x concentration map at ground level in the urban area of Turin corresponding to the **minimum simulated concentration**, recorded at hour 15:00 of day December 4. The minimum value (i.e. maximum pollutant reduction) is located in the area of extension of the DH network.

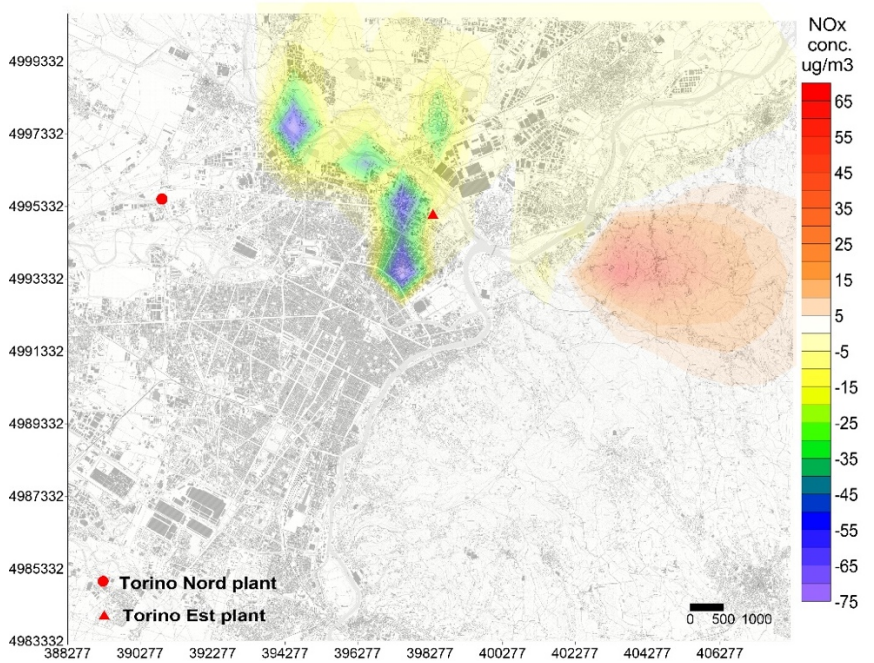

Figure 3.30. NO_x concentration map at ground level in the urban area of Turin corresponding to the **maximum simulated concentration**, recorded at hour 7:00 of day February 6. The maximum value (i.e. maximum increase of pollutant) is located in the hilly areas surrounding Turin.

14.5 Daytime averages

Another set of simulations was run to consider the contribution of only daytime hours (6:00 to 20:00) to the calculation of the average concentration. The results were then compared to the complete base case simulation, to evaluate the pollutant dispersion in the hours of maximum activity of the power units. The maps of concentration difference resulting from the calculation of the daytime averages are reported in Figures 3.31 and 3.32. As expected, the result of local NO_x and TSP dispersion is more significant if referred to the only daytime hours. In fact, the minimum NO_x concentration decreases from around -5.4 μg/m^3 to -5.8 μg/m^3; similarly, the minimum TSP concentration decreases from -0.075 μg/m^3 to -0.105 μg/m^3. Nevertheless, these results do not differ significantly from the reported base case.

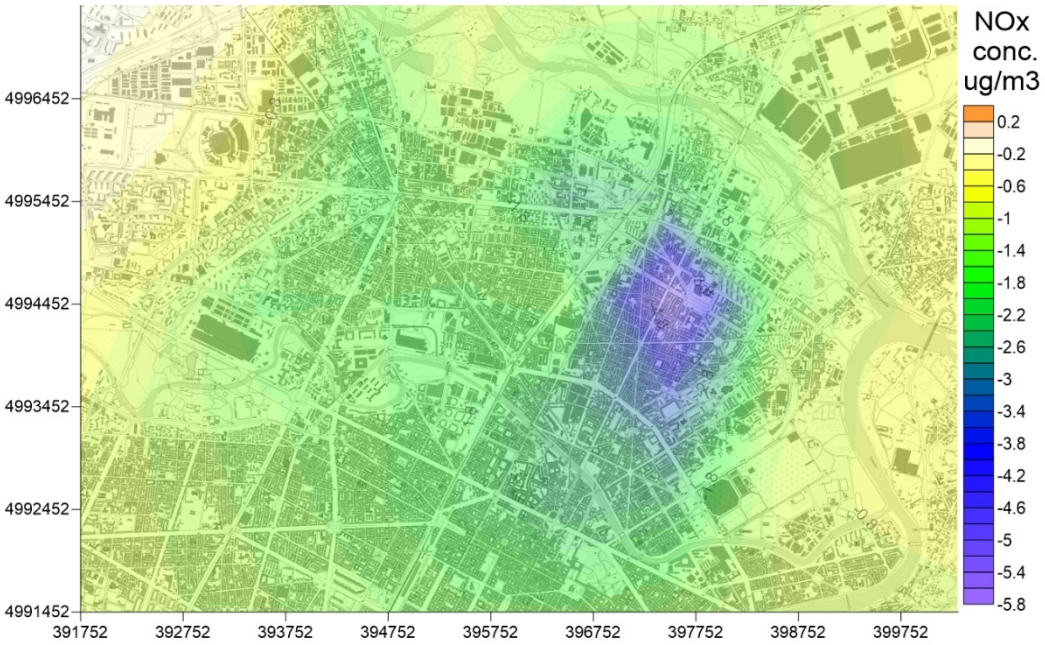

Figure 3.31. Map of NO_x concentration difference at ground level in the urban area of Turin, **average hourly concentration referring to daytime hours (6:00 to 20:00).**

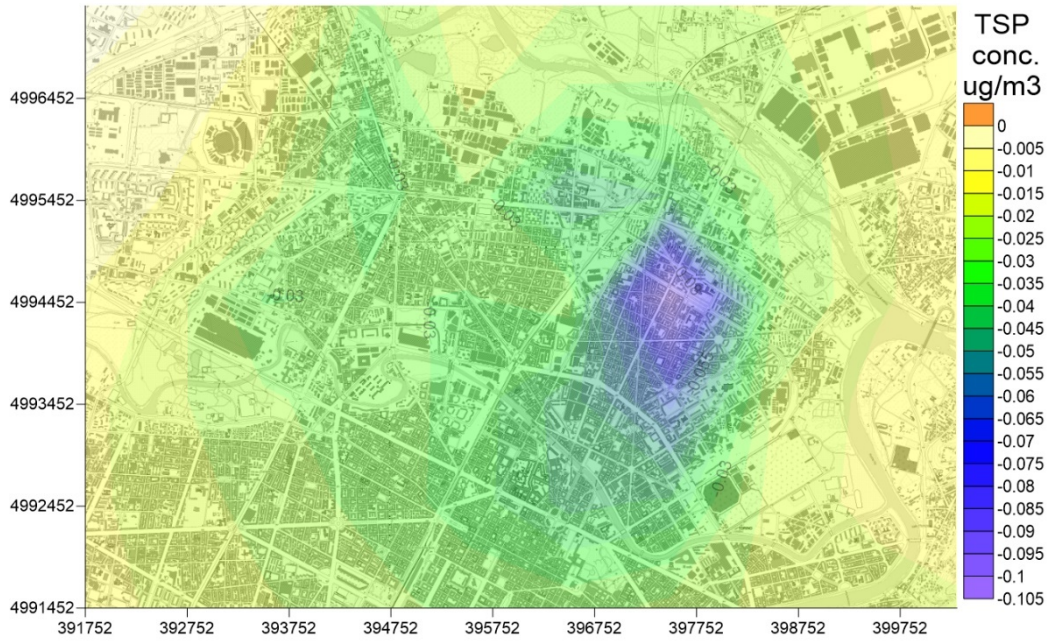

Figure 3.32. Map of TSP concentration difference at ground level in the urban area of Turin, **average hourly concentration referring to daytime hours (6:00 to 20:00).**

14.6 Modified building downwash configuration

With the aim of reducing the uncertainties on the simulated scenarios, the simulation was repeated for the only month of January and for the only contaminant NO_x by changing different settings of the model.

First, the building downwash configuration was modified to figure out possible different building profiles around the emission sources. The reason of this is that the presence of buildings of different height and shape around the emission sources has a significant importance in the modeling of pollutant dispersion in urban areas, as it influences the plume downwash phenomena (Hanna et al., 1982). Two different settings in comparison to the base case were tested: the "higher and less dense" profile, characterized by buildings 30 m high and 15 m wide, spaced every 20°, and the "less dense" profile, characterized by buildings 15 m high and 15 m wide, spaced every 20°. The result related to the "higher and less dense" profile, is reported in Figure 3.33. This figure highlights lower concentration values with respect to the base case (Figures 3.18 and 3.20), indicating that the higher and denser is the urban structure, the more pronounced

is the downwash effect, thus the more important is the fallout of the pollutants to the ground. By simulating a "less dense" profile, the result does not differ significantly from the base case simulation.

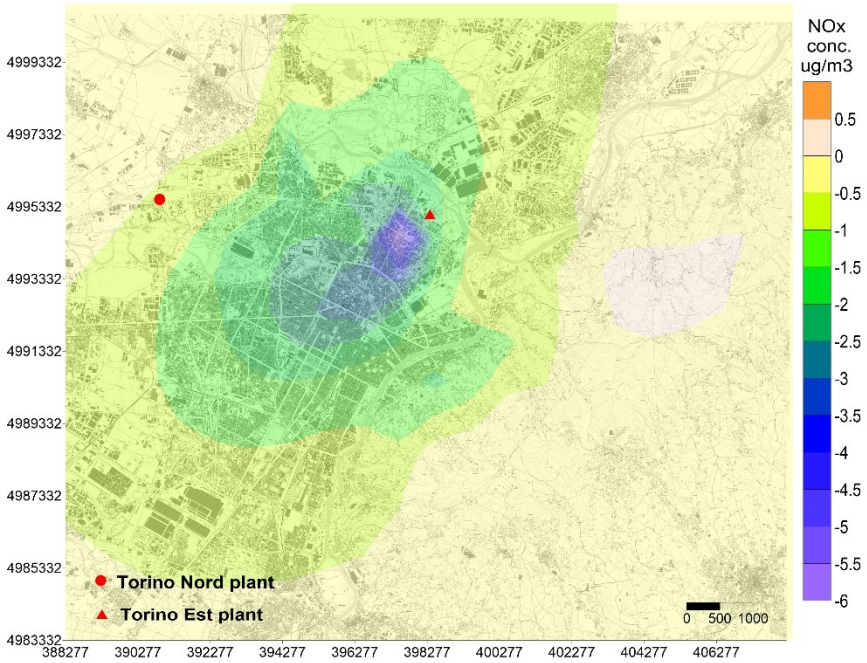

Figure 3.33. Map of NO_x concentration difference at ground level in the urban area of Turin, month of January, **with modified settings of the building profile around the emission sources (buildings 30 m high and 15 m wide, spaced every 20°).**

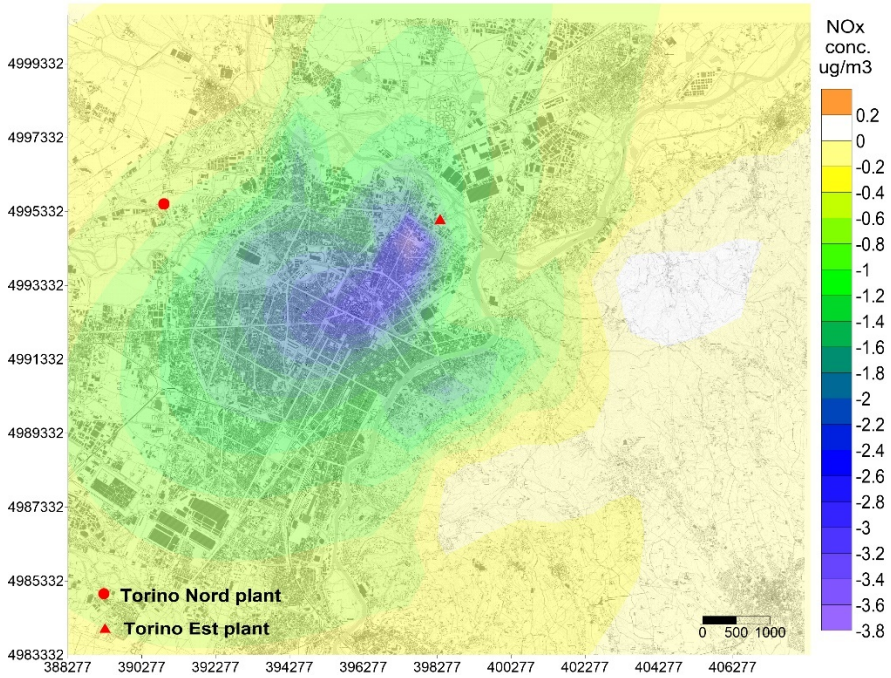

Figure 3.34. Map of NO_x concentration difference at ground level in the urban area of Turin, month of January, with **modified settings of the building profile around the emission sources (buildings 15 m high and 15 m wide, spaced every 20°).**

14.7 Modified height of emission sources

Another set of simulations was run by modifying the height of the barycentric stacks with respect to the base case scenario, in which the sources were located at a height of 15 m. The height of the barycentric stacks covering the extension area was increased to 20 and 30 meters. These values were determined through the analysis of the Census data used in the energy modeling phase. An on-site inspection, evidencing buildings characterized by 5 to 10 floors of different construction periods, confirmed these range of values.

The result of concentration difference with a barycentric stack height of 30 m is reported in Figure 3.35. As expected, the NO_x removal results more disperse and less pronounced in comparison with the base case, but the effect on air quality remains beneficial for most of the investigated area.

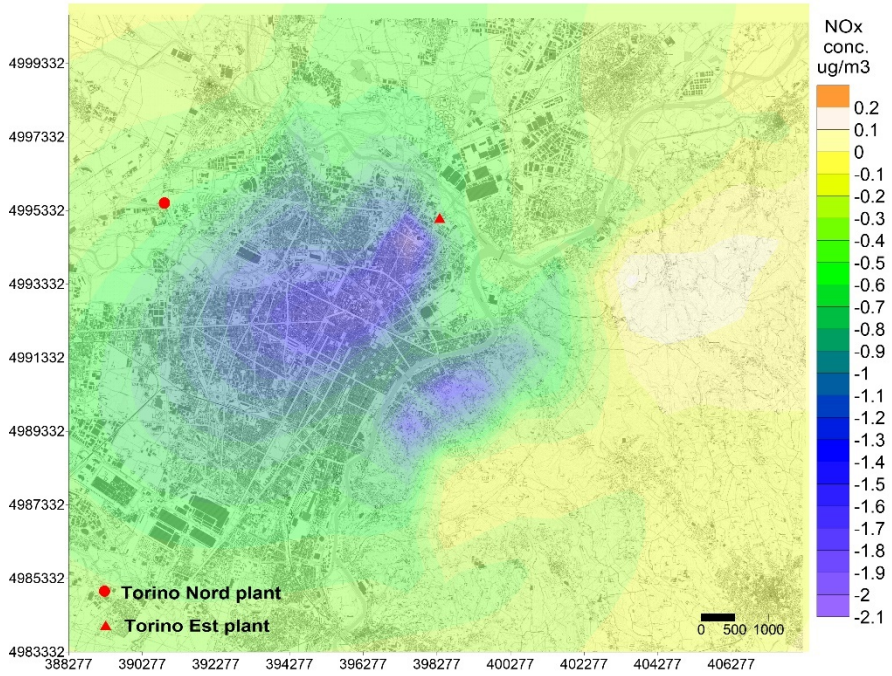

Figure 3.35. Map of NO_x concentration difference at ground level in the urban area of Turin, month of January, with **modified height of the emission sources of the residential areas (30 m).**

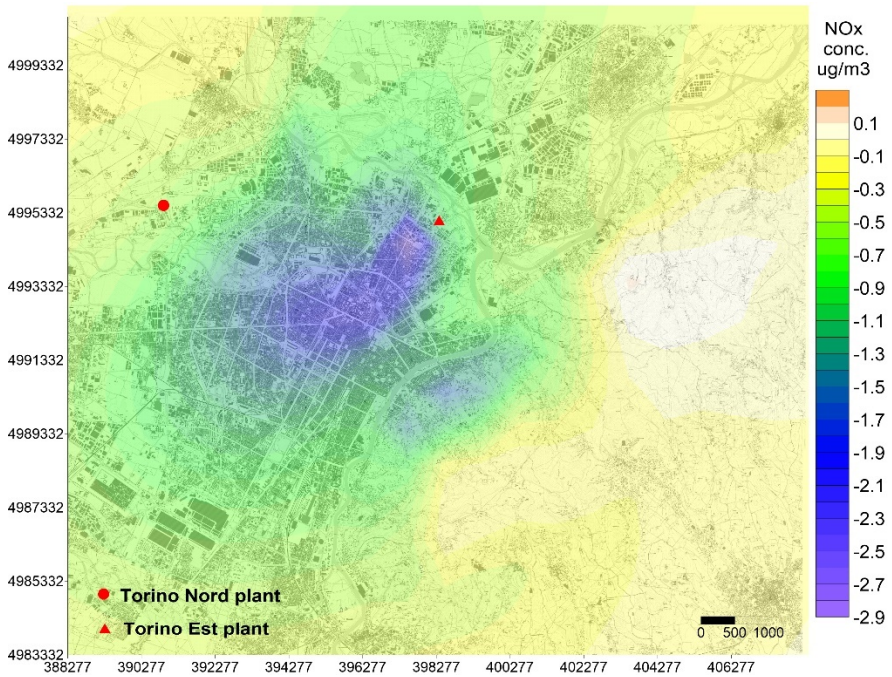

Figure 3.36. Map of NO_x concentration difference at ground level in the urban area of Turin, month of January, with **modified height of the emission sources of the residential areas (20 m).**

14.8 Modified source type

As a final investigating step, the evaluation of the base case was reproduced simulating the emissions of the 6 residential areas using an area source type instead of a point source type. The results are shown in Figures 3.37 to 3.40. The concentration difference values reported in continuation represent the hourly average of the entire heating season (October to January). It can be concluded from Figures 3.37 to 3.40 that the contaminant removal is more dispersed over the area in comparison with point source simulations.

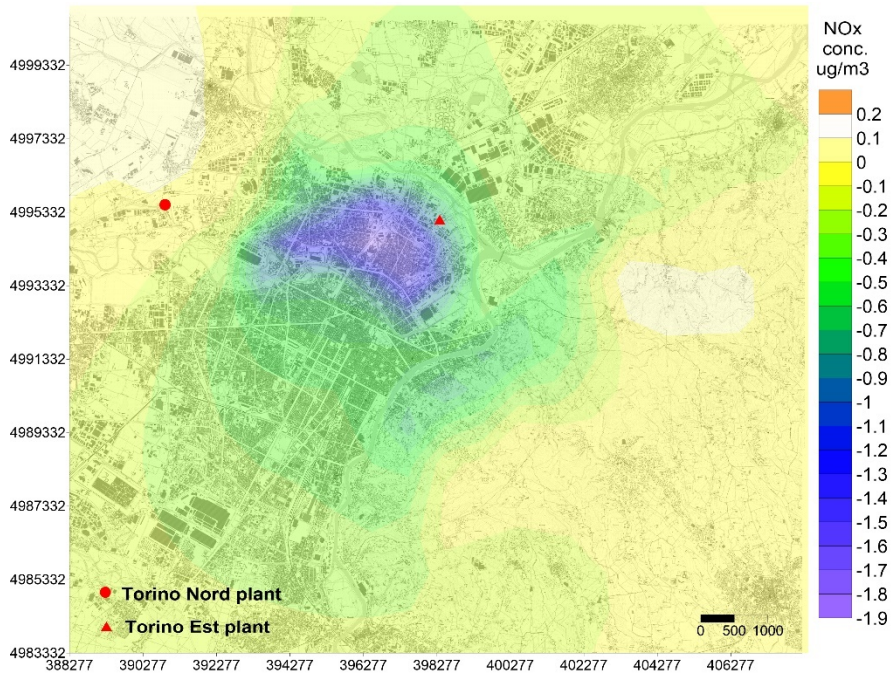

Figure 3.37. Map of NO_x concentration difference at ground level in the urban area of Turin, month of January, **simulating residential emissions as areas sources.**

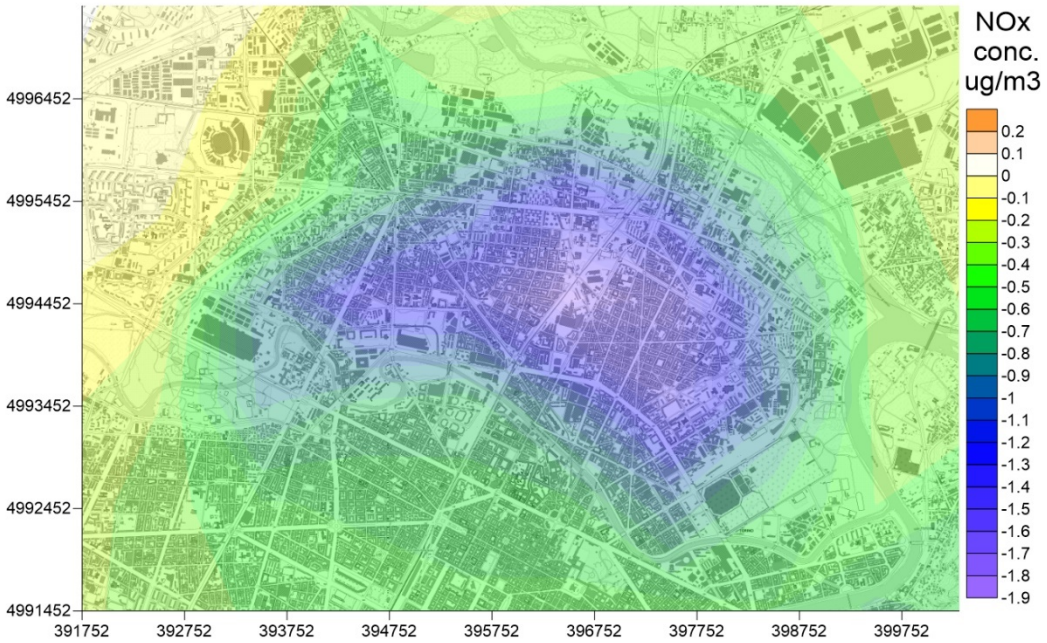

Figure 3.38. Map of NO_x concentration difference at ground level in the urban area of Turin, month of January, **simulating residential emissions as areas sources (zoom to the areas interested by the DH network extension).**

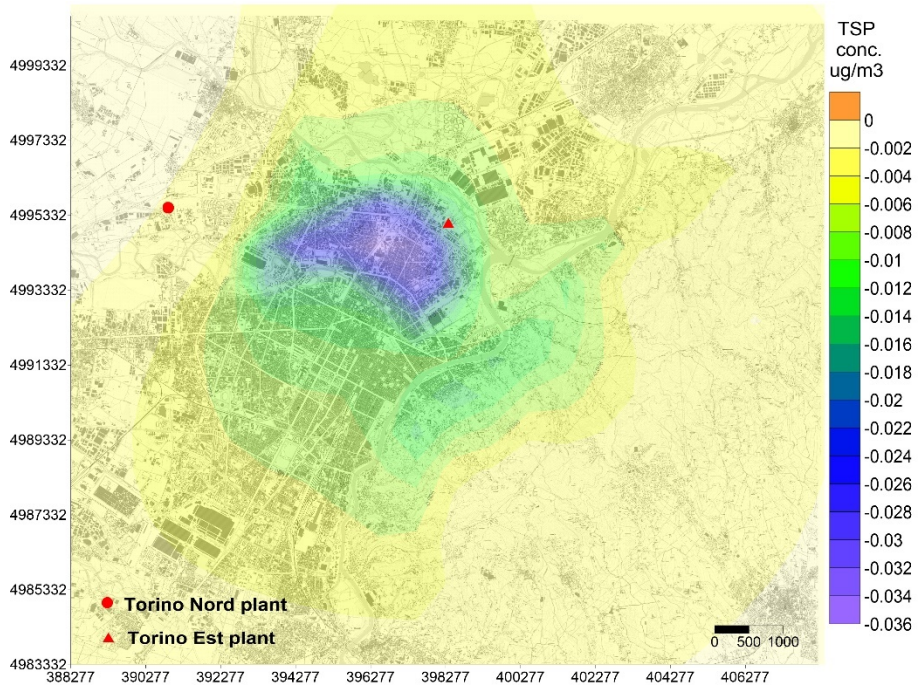

Figure 3.39. Map of TSP concentration difference at ground level in the urban area of Turin, month of January, **simulating residential emissions as areas sources.**

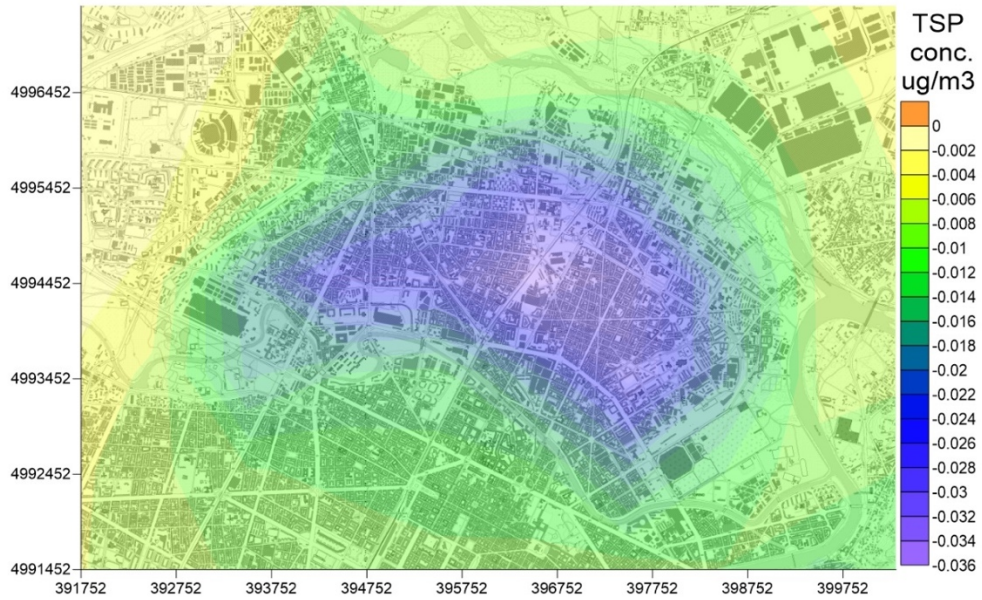

Figure 3.40. Map of TSP concentration difference at ground level in the urban area of Turin, month of January, **simulating residential emissions as areas sources (zoom to the areas interested by the DH network extension).**

14.9 Comparison of the results with a monitoring station

With the aim of achieving information about the correct calibration of the model, as well as validate the results obtained, the simulation results were compared with the measurements of a reference monitoring station, located in the area interested by the possible extension of the DH network. The selected monitoring station is called Torino-Rebaudengo and it is managed by the regional agency for environmental protection (ARPA). The location of the unit is reported in Figure 3.41, and the main technical features are reported in Table 3.15.

Such a comparison represents a controversial task, as the concentration measured by the monitoring station is the aggregate contribution of different sources, such as traffic and industrial activities. Emissions from residential heating represent only a small portion of the overall NO_x concentration. The comparison may thus be made in mainly two terms:

- By comparing the overall emission flows over the reference period;
- By comparing the trend and variability of the simulated concentration with respect to the trend of the total measured concentration.

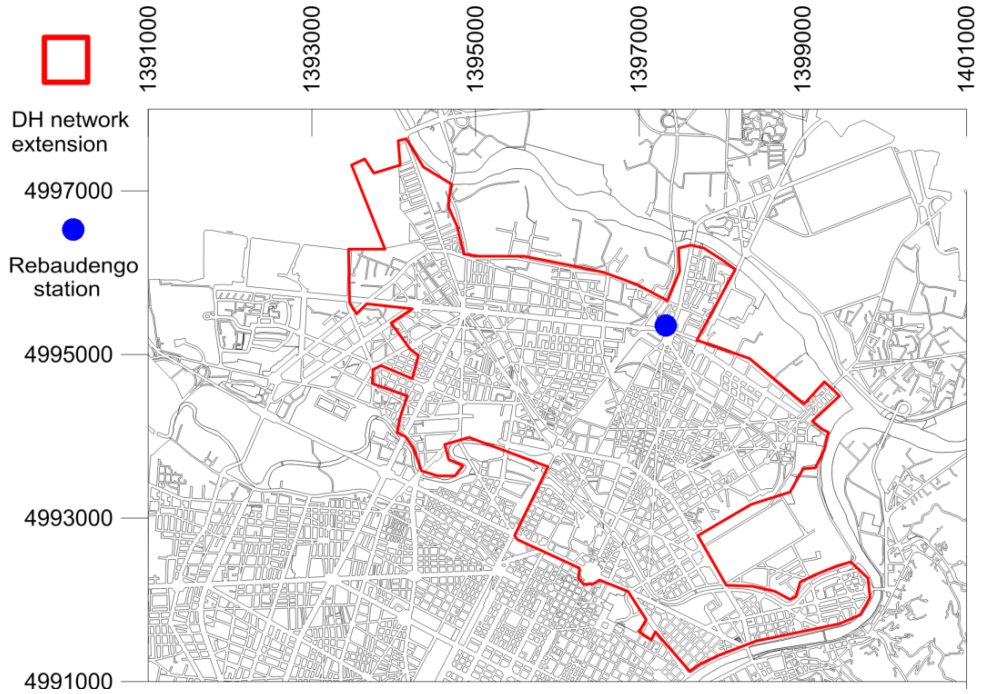

Figure 3.41. Location of the Torino Rebaudengo monitoring station managed by ARPA.

Table 3.15. Features of Torino Rebaudengo monitoring station (Ariaweb).

Location	Piazza Rebaudengo 23, Turin
Active since	1996-01-01
Type of location	Urban area
UTM X coordinate	1397361
UTM Y coordinate	4995339
Elevation	233 m a.s.l.
NO_x monitoring instrument	TELEDYNE API 200

14.9.1 Comparison of total emission flows

The first comparison of results obtained from the simulations was made by mean of the following procedure:

- On the one side, the only contribution of residential emissions produced in the present scenario (Figure 3.1) was considered. The result of the single

cell corresponding to the location of the Torino Rebaudengo station was extracted from the grid domain, resulting in a string of 8760 hourly concentration values (C_{cal}).

- On the other side, the total values of NO_x concentration measured by Torino Rebaudengo station were extracted by the ARPA database, obtaining a second string of 8760 hourly values (C_{reb}). To be congruent with the simulations, the reference year selected was 2010.

The two series of values were then plotted as a function of time, and the integral over time was calculated by means of the GNU Octave software, using the trapezoidal numerical integration function (*trapz*). The result obtained indicates the amount of total pollutant during the reference period, referred to a cubic meter of air. The two values obtained are Q_{reb}, i.e. the quantity measured from Torino Rebaudengo station, and Q_{cal}, i.e. the amount corresponding to the simulation with CALPUFF model:

$$Q_{reb} = trapz(C_{reb}) = 1{,}091{,}791\ \mu g \qquad \text{Eq. 3.31}$$

$$Q_{cal} = trapz(C_{cal}) = 21{,}990\ \mu g \qquad \text{Eq. 3.33}$$

The results show that the amount Q_{cal} is equal to approximately 2% of the amount Q_{reb}. This indicates that, relatively to the cell considered, belonging to CALPUFF simulations, the emissive contribution of residential heating systems on the total NO_x emissions is equal to 2%. To have a real feedback of the validity of this figure, reference must be made to the data reported on the regional atmosphere emissions inventory (IREA in Italian) for the year 2010 (IREA), summarized in Figure 3.42. This figure indicates that the estimated contribution of residential heating installations to the total emission of NO_x in the municipality of Turin is around 5%. It could, therefore, be concluded that the simulation result is in line with the real order of magnitude.

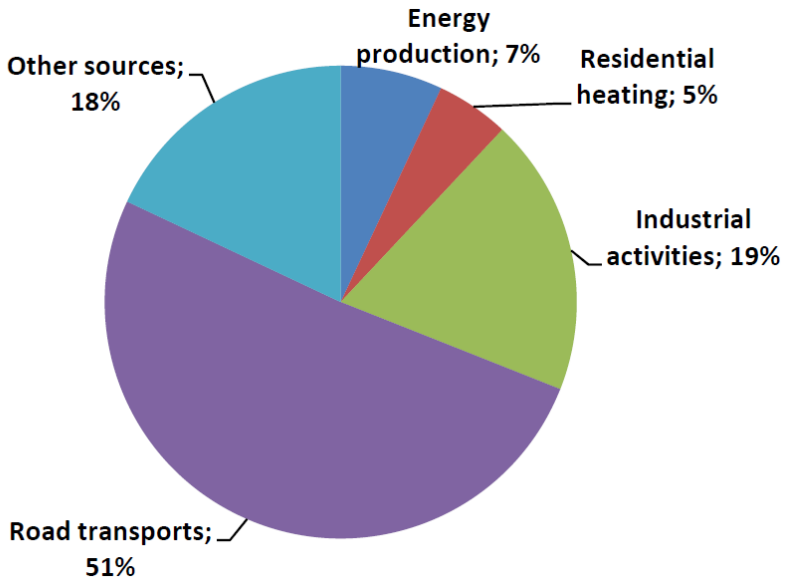

Figure 3.42. Contribution to NO_x emission by sector, city of Turin, year 2010 (IREA)

14.9.2 Comparison of concentration trends

A second evaluation of the achieved results consisted in analyzing the trends of hourly concentration values measured from Torino Rebaudengo Station and compare them with the simulation of only residential heating systems in the current scenario.

As a first operation, the diagram of the NO_x measured concentration values was overlapped to that of the simulated concentrations. The result, considering the heating season (October to March), is shown in Figure 3.43. No useful information may be obtained from Figure 3.43, as the simulated values are characterized by substantial fluctuations. The correlation between the two variables is equal to 0.20, that is, very low.

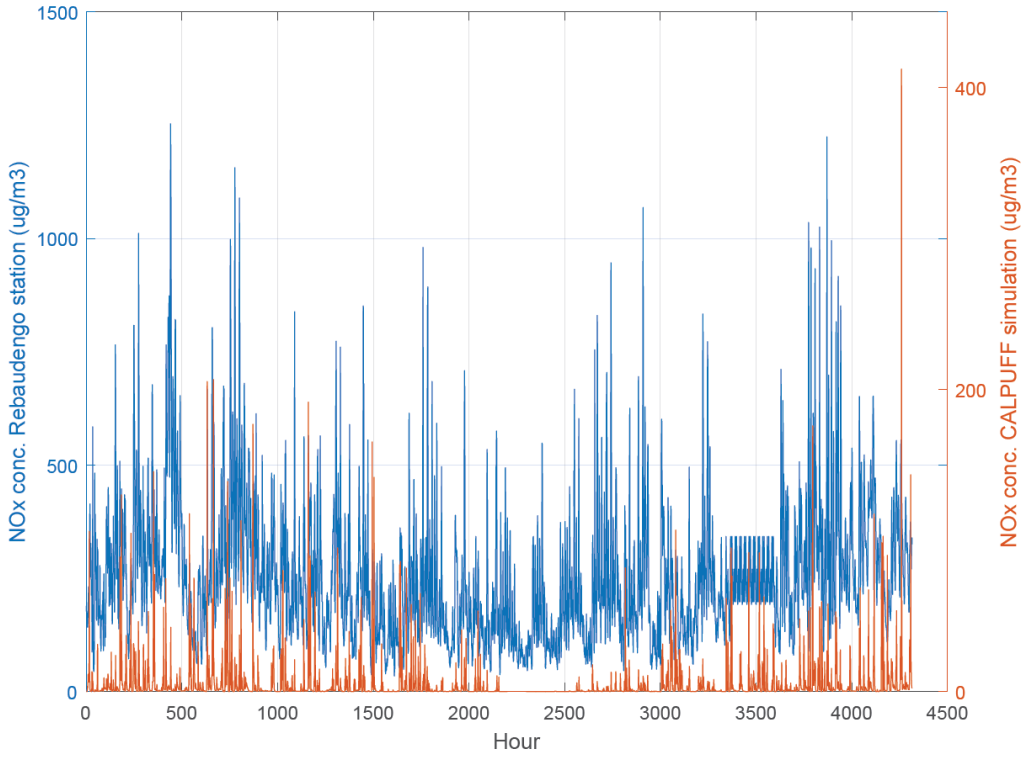

Figure 3.43. Comparison between hourly NO_x concentration measured by Torino Rebaudengo monitoring station and the concentration obtained with CALPUFF simulation of actual residential sources.

The results change if the moving averages of the two series are considered. The results of the comparison between the moving averages of the two variables, calculated over a period of 7 and 14 days respectively, are shown in Figures 3.44 and 3.45. The two figures show how, if fluctuations are reduced, a clear similarity in the trends of the two variables may be found. The corresponding correlation values confirm this trend, shifting to 0.63 for the 7 day moving averages and to 0.8 for the 14 days moving averages. This comparison provides thus important information on the validity of the simulations performed.

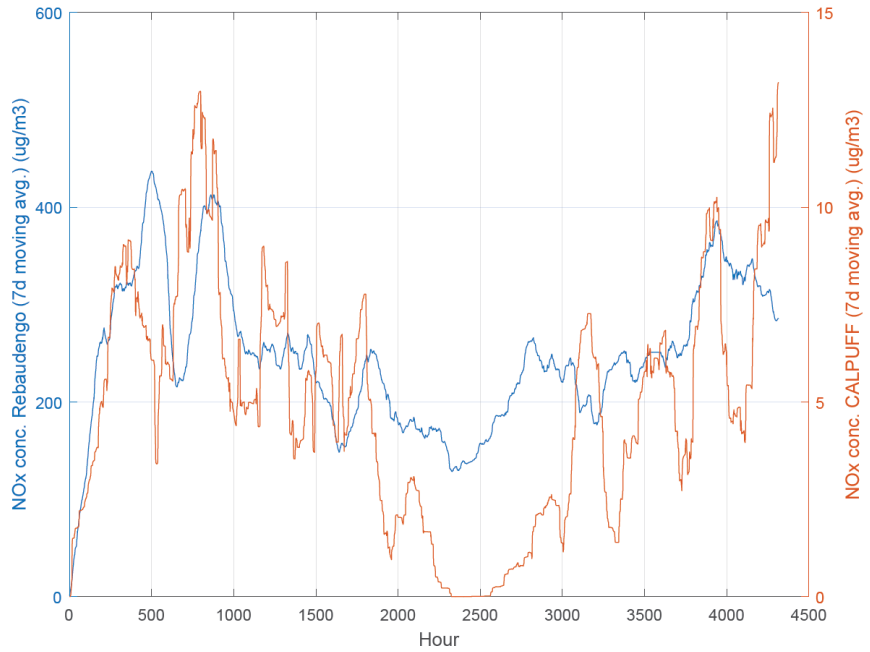

Figure 3.44. Comparison between NO_x concentration measured by Torino Rebaudengo monitoring station and the concentration obtained with CALPUFF simulation of actual residential sources. Moving averages on a 7-day period.

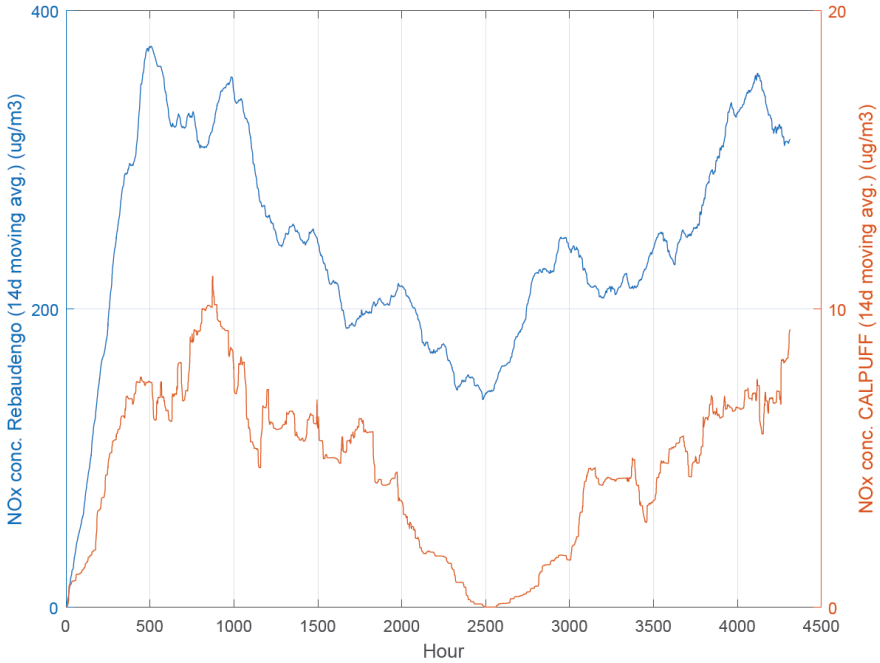

Figure 3.45. Comparison between NO_x concentration measured by Torino Rebaudengo monitoring station and the concentration obtained with CALPUFF simulation of actual residential sources. Moving averages on a 14-day period.

14.10 Discussion

The results show a general reduction in the presence of NO_x and TSP in the urban area of Turin following the extension of the DH network. This reduction is driven by a connection of the following factors:

- Lower overall emissions;
- Higher elevation of the emission sources, corresponding to a greater dispersion of the pollutants' plume;
- Greater distance between emission sources (power units) and the receptor sites (residential areas).

To evaluate the order magnitude of the concentration decrease, the reference monitoring stations in the study area (Torino Rebaudengo and Torino Consolata) were considered. The annual average concentration measured by these stations in 2014 was 70 $\mu g/m^3$ for NO_x and 63 $\mu g/m^3$ for TSP. This means that the interventions considered would bring to a maximum NO_x reduction of 5.7% and a maximum TSP reduction of 0.1% of the total concentration (considering base case). These numbers demonstrate a significant result for NO_x, while the reduction of TSP is almost negligible. Of the literature studies already mentioned, the one by Genon et al. (2009) considered two cases where respectively 22 and 105 residential systems were replaced with a CHP and DH system. In the first case, the average NO_x concentration in the calculation domain worsened of 0.2 $\mu g/m^3$, while in the second case an average improvement of 1.7 $\mu g/m^3$ was found. A second study (Torchio et al., 2009) connected to the previous one indicated a reduction of PM concentration, with peaks reaching 0.6 $\mu g/m^3$.

Useful information is provided by the additional simulations conducted to provide a first estimation of the uncertainty, which is inevitably high given the size of the system and the number of factors involved. These simulations show that the characterization of the emission sources (height of the sources and reproduction of the building profiles in their surroundings) has an importance and a high influence on the result. A point for the improvement of this study could, therefore, consist in a more detailed reconstruction of the residential areas and their sources.

The simulation of the separate contributions confirms that the centralization of the energy production has some advantages, namely:

- a primary energy saving thanks to the improved efficiency of the system as reported by Finney et al., (2012);
- more control and reduction of the emissions: the modern CC plants as TO-N are equipped with advanced abatement systems and CEMS supervised by both the operator and the public environmental control agencies (Rezaie and Rosen, 2012).

It must be put in evidence that the exercise of these type of large-scale plants is also in connection to the economic issues (Åberg et al., 2012; Jarre et al. 2016) that are not considered in this study, that could influence the configuration of the energy production (mainly in terms of electrical/thermal energy balance) and consequently the emission scenario.

On the use of the mathematical dispersion model, a largely consolidated model as CALPUFF was used. The model resulted adequate to the magnitudes and to the scale of study. The result of the dispersion modeling using area type sources provided a more uniform concentration compared to the use of barycentric stacks, that is what it could be expected in the reality. On the other hand, the disadvantage in using area type sources with CALPUFF is that the simulation of building downwash phenomena is not implemented.

Finally, the analysis of maximum and minimum values reveals a high variability of the average results due to the weather conditions that may occur in the area of study. Turin is a scarcely ventilated city. The average wind speed obtained from the time series (1990-2005) is 0.9 m/s, while the average annual number of wind calm days is equal to 75 (Arpa Piemonte, 2007). These conditions foster situations of poor mixing and the formation of a stable urban boundary layer (Hanna et al., 1982). To obtain more information on the variables leading to peak concentrations, weather records in correspondence of maximum and minimum values were investigated. The coexistence of the following factors was observed:

- limited height of the mixed layer (below 100 m);
- positive values of the Monin-Obukhov length;
- low horizontal wind speed (below 2 m/s);
- low air temperature (between -2°C and 3°C);
- low total radiation (below 60 W/m^2).

Chapter 15

Results of global emissions

The results of the calculation of global CO_2 balance are reported in continuation. The main findings are first reported separately by source, comparing present and future trends. Subsequently, results are joined into a single final balance calculation.

15.1 Torino Nord combined cycle emission ($F_{th,pres}$, $F_{el,pres}$, $F_{th,fut}$, $F_{el,fut}$)

The total CO_2 flow emitted by the Torino Nord combined cycle plant for the present and future scenario is reported in Figure 3.46. Based on the equations 3.13 to 3.20 of Chapter 13.2.1, as well as the emission factors reported in Table 3.11, the calculation of the annual flows of CO_2 is reported in continuation.

$$F_{th,pres} = \sum_{i=1}^{8760} CO_{2th,i} = 1.084 \cdot 10^5 \text{ t/y}$$

$$F_{el,pres} = \sum_{i=1}^{8760} CO_{2el,i} = 4.09 \cdot 10^5 \text{ t/y}$$

In the future operating mode, the energy balance reported in Table 3.10, Chapter 13, indicates an increase in the thermal energy produced yearly from

$3.367 \cdot 10^5$ MWh (present scenario) to $5.860 \cdot 10^5$ MWh (future scenario). Consequently, the CO_2 flow emitted is expected to grow as reported in continuation.

$$\mathrm{F_{th,fut}} = \sum_{i=1}^{8760} P_{thfut,i} \cdot \mathrm{EF_{TON,th}} = 1.890 \cdot 10^5 \ \mathrm{t/y}$$

$$\mathrm{F_{el,fut}} = \sum_{i=1}^{8760} P_{elfut,i} \cdot \mathrm{EF_{TON,el}} = 4.312 \cdot 10^5 \ \mathrm{t/y}$$

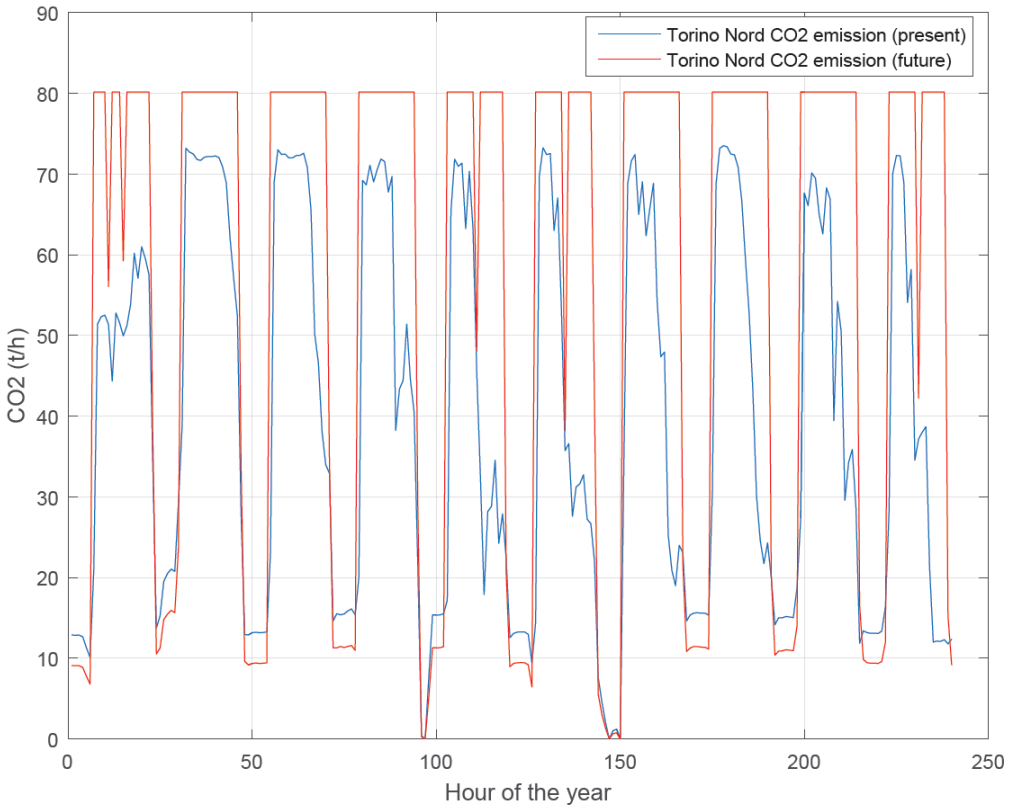

Figure 3.46. CO_2 flow emitted by the Torino Nord combined cycle, present and future scenario (comparison done on the first 10 days of the year).

15.2 Torino Nord integration and reserve heaters ($F_{boi,pres}$,$F_{boi,fut}$)

The total CO_2 flow emitted by the Torino Nord and Torino Est integration and reserve heaters, for the present and future scenario, is reported in Figure 3.47. Based on the equations 3.21 to 3.27 reported in chapter 13.2.1, as well as the emission factors reported in Table 3.11, the calculation of the annual flows of CO_2 is reported in continuation.

$$F_{boi,pres} = \sum_{i=1}^{8760} CO_{2boi,i} = 2.822 \cdot 10^3 \text{ t/y}$$

In the future operating mode, the energy balance described in in Table 3.10, Chapter 13, indicates an increase in the thermal energy demand for the auxiliary heaters, corresponding to an increased use of Torino Nord heaters and the start of operation of Torino Est plant. Consequently, the annual thermal energy production of integration systems rises from $1.007 \cdot 10^4$ MWh (present scenario) to $3.877 \cdot 10^5$ MWh (future scenario). The corresponding CO_2 flow emitted is expected to grow as reported in continuation.

$$F_{boi,fut} = \sum_{i=1}^{8760} P_{boifut,i} \cdot EF_{boi} = 1.005 \cdot 10^5 \text{ t/y}$$

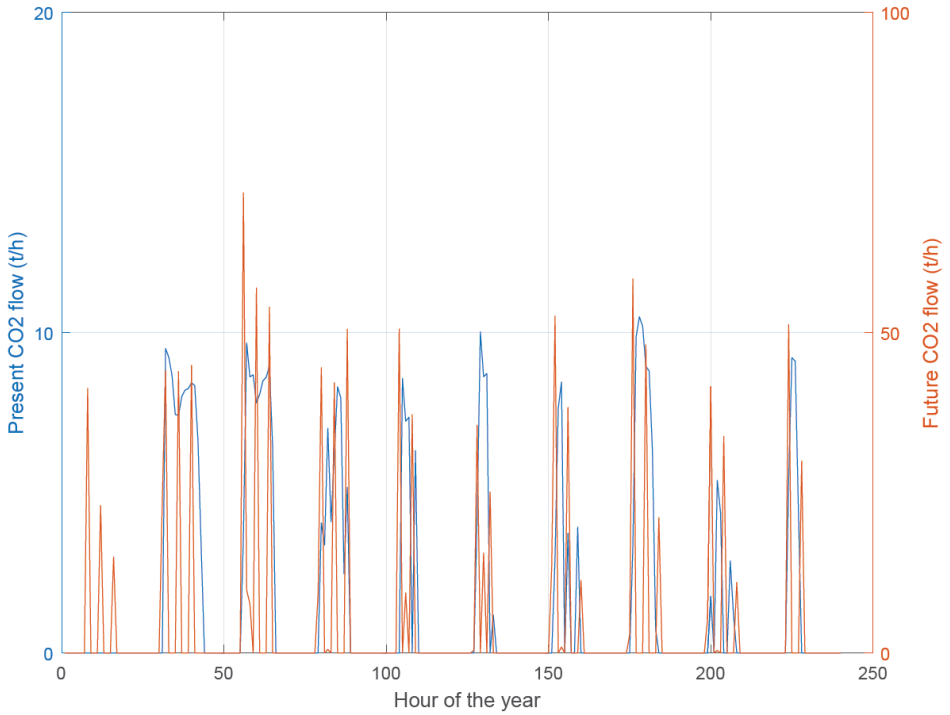

Figure 3.47. CO_2 flow emitted by the Torino Nord and Torino Est integration and reserve heaters, present and future scenario (comparison done on the first 10 days of the year).

15.3 Residential centralized heaters ($F_{res,pres}$, $F_{res,fut}$)

The annual CO_2 flow emitted by the residential heaters covering the area of the DH network extension was calculated by multiplying the heat demand for the corresponding emission factor, variable with respect to the fuel feeding the centralized heater (Table 3.11). The emission contributing to the future scenario were accounted to be generated by the only buildings remained not connected to the DH network.

The overall present and future annual thermal energy demand of the 6 sub-areas, divided by fuel type is reported in Table 3.16. The corresponding CO_2 flow is reported in Table 3.17.

Table 3.16. Thermal energy produced by the centralized residential heaters, divided by sub-area and fuel type, present and future scenario.

	Thermal energy produced by centralized heaters (kWh/y)									
Sub-area	**Natural gas**		**Diesel oil**		**Heavy oil**		**LPG**		**TOTAL**	
	Pres.	**Fut.**	**Pres.**	**Fut.**	**Pres.**	**Fut.**	**Pres.**	**Fut.**	**Pres.**	**Fut.**
1	$5.19 \cdot 10^{7}$	$1.78 \cdot 10^{7}$	$3.59 \cdot 10^{6}$	$8.02 \cdot 10^{5}$	$4.41 \cdot 10^{5}$	$9.00 \cdot 10^{4}$	$6.98 \cdot 10^{4}$	$2.99 \cdot 10^{4}$		
2	$1.75 \cdot 10^{8}$	$6.02 \cdot 10^{7}$	$1.21 \cdot 10^{7}$	$2.70 \cdot 10^{6}$	$1.48 \cdot 10^{6}$	$3.03 \cdot 10^{5}$	$2.35 \cdot 10^{5}$	$1.00 \cdot 10^{5}$		
3	$6.98 \cdot 10^{7}$	$2.40 \cdot 10^{7}$	$4.83 \cdot 10^{6}$	$1.07 \cdot 10^{6}$	$5.92 \cdot 10^{4}$	$1.21 \cdot 10^{5}$	$9.38 \cdot 10^{4}$	$4.02 \cdot 10^{4}$		
4	$1.34 \cdot 10^{8}$	$4.64 \cdot 10^{7}$	$9.33 \cdot 10^{6}$	$2.08 \cdot 10^{6}$	$1.14 \cdot 10^{6}$	$2.33 \cdot 10^{5}$	$1.81 \cdot 10^{5}$	$7.78 \cdot 10^{4}$		
5	$2.94 \cdot 10^{8}$	$1.01 \cdot 10^{8}$	$2.03 \cdot 10^{7}$	$4.54 \cdot 10^{6}$	$2.50 \cdot 10^{6}$	$5.10 \cdot 10^{5}$	$3.95 \cdot 10^{5}$	$1.69 \cdot 10^{5}$		
6	$1.47 \cdot 10^{8}$	$5.08 \cdot 10^{7}$	$1.02 \cdot 10^{7}$	$2.28 \cdot 10^{6}$	$1.25 \cdot 10^{6}$	$2.56 \cdot 10^{5}$	$1.98 \cdot 10^{5}$	$8.51 \cdot 10^{4}$		
TOT	$\mathbf{8.74 \cdot 10^{8}}$	$\mathbf{3.00 \cdot 10^{8}}$	$\mathbf{6.04 \cdot 10^{7}}$	$\mathbf{1.35 \cdot 10^{7}}$	$\mathbf{7.42 \cdot 10^{6}}$	$\mathbf{1.51 \cdot 10^{6}}$	$\mathbf{1.17 \cdot 10^{6}}$	$\mathbf{5.03 \cdot 10^{5}}$	$\mathbf{9.43 \cdot 10^{8}}$	$\mathbf{3.16 \cdot 10^{8}}$

Table 3.17. CO_2 emitted by the centralized residential heaters, divided by sub-area and fuel type, present and future scenario.

	CO_2 emission (kg/y)									
Sub-area	**Natural gas**		**Diesel oil**		**Heavy oil**		**LPG**		**TOTAL**	
	Pres.	**Fut.**	**Pres.**	**Fut.**	**Pres.**	**Fut.**	**Pres.**	**Fut.**	**Pres.**	**Fut.**
1	$1.20 \cdot 10^{7}$	$4.13 \cdot 10^{6}$	$8.96 \cdot 10^{5}$	$2.00 \cdot 10^{5}$	$1.22 \cdot 10^{5}$	$2.50 \cdot 10^{4}$	$1.58 \cdot 10^{4}$	$6.80 \cdot 10^{3}$	$1.30 \cdot 10^{7}$	$4.36 \cdot 10^{6}$
2	$4.04 \cdot 10^{7}$	$1.39 \cdot 10^{7}$	$3.02 \cdot 10^{6}$	$6.74 \cdot 10^{5}$	$4.14 \cdot 10^{5}$	$8.45 \cdot 10^{4}$	$5.34 \cdot 10^{4}$	$2.29 \cdot 10^{4}$	$4.39 \cdot 10^{7}$	$1.47 \cdot 10^{7}$
3	$1.61 \cdot 10^{7}$	$5.55 \cdot 10^{6}$	$1.20 \cdot 10^{6}$	$2.69 \cdot 10^{5}$	$1.65 \cdot 10^{5}$	$3.37 \cdot 10^{4}$	$2.13 \cdot 10^{4}$	$9.14 \cdot 10^{3}$	$1.75 \cdot 10^{7}$	$5.86 \cdot 10^{6}$
4	$3.11 \cdot 10^{7}$	$1.07 \cdot 10^{7}$	$2.32 \cdot 10^{6}$	$5.20 \cdot 10^{5}$	$3.19 \cdot 10^{5}$	$6.51 \cdot 10^{4}$	$4.12 \cdot 10^{4}$	$1.76 \cdot 10^{4}$	$3.38 \cdot 10^{7}$	$1.13 \cdot 10^{7}$
5	$6.80 \cdot 10^{7}$	$2.34 \cdot 10^{7}$	$5.08 \cdot 10^{6}$	$1.13 \cdot 10^{6}$	$6.96 \cdot 10^{5}$	$1.42 \cdot 10^{5}$	$8.99 \cdot 10^{4}$	$3.85 \cdot 10^{4}$	$7.39 \cdot 10^{7}$	$2.47 \cdot 10^{7}$
6	$3.41 \cdot 10^{7}$	$1.17 \cdot 10^{7}$	$2.54 \cdot 10^{6}$	$5.69 \cdot 10^{5}$	$3.49 \cdot 10^{5}$	$7.13 \cdot 10^{4}$	$4.51 \cdot 10^{4}$	$1.93 \cdot 10^{4}$	$3.70 \cdot 10^{7}$	$1.24 \cdot 10^{7}$
TOT	$\mathbf{2.02 \cdot 10^{8}}$	$\mathbf{6.95 \cdot 10^{7}}$	$\mathbf{1.50 \cdot 10^{7}}$	$\mathbf{3.36 \cdot 10^{6}}$	$\mathbf{2.06 \cdot 10^{6}}$	$\mathbf{4.22 \cdot 10^{5}}$	$\mathbf{2.66 \cdot 10^{5}}$	$\mathbf{1.14 \cdot 10^{5}}$	$\mathbf{2.19 \cdot 10^{8}}$	$\mathbf{7.34 \cdot 10^{7}}$

The value of present ($F_{res,pres}$) and future ($F_{res,fut}$) CO_2 flow emitted by the residential heaters is thus equal to:

$$F_{res,pres} = 2.19 \cdot 10^5 \; t/y$$

$$F_{res,fut} = 7.34 \cdot 10^4 \; t/y$$

15.4 CO_2 balance

The comprehensive CO_2 global balance for the entire system, base case formulation is reported in Table 3.18. The results show an increase of CO_2 emissions corresponding to the intervention of extension of the DH network. A detailed discussion of the results is reported in continuation.

Table 3.18. CO_2 emission balance for the DH system for one year of exercise, base case formulation.

Emission source	**CO_2 emission ACTUAL SCENARIO (t/y)**	**CO_2 emission FUTURE SCENARIO (t/y)**	**ΔCO_2 Difference (t/y)**
Torino Nord plant (thermal energy)	$1.12 \cdot 10^5$	$1.89 \cdot 10^5$	**$7.75 \cdot 10^4$**
Torino Nord plant (electrical energy)	$4.09 \cdot 10^5$	$4.31 \cdot 10^5$	**$2.21 \cdot 10^4$**
Torino Nord + Torino Est auxiliary boilers	$2.82 \cdot 10^3$	$1.00 \cdot 10^5$	**$9.77 \cdot 10^4$**
Residential areas	$2.19 \cdot 10^5$	$7.34 \cdot 10^4$	**$- 1.46 \cdot 10^5$**
TOTAL	**$7.43 \cdot 10^5$**	**$7.94 \cdot 10^5$**	**$5.09 \cdot 10^4$**

15.5 Discussion

The result referring to the base case, reported in Table 3.18, shows that the potential intervention of the DH network extension causes an unfavorable global emission balance. CO_2 emissions are in fact estimated to increase by a considerable amount, equal to $5.09 \cdot 10^4$ t/y. The table shows that the increased emissions from the greater use of Torino Nord plant and related integration systems is not counterbalanced by the reduction of greenhouse gas emissions resulting from the removal of centralized residential heaters. This latter value represents however a significant contribution, equal to $1.46 \cdot 10^5$ t/y.

The result reported is unexpected. In fact, district energy is generally associated to a GHG saving in two ways: facilitating the use of non-carbon energy forms for heating and cooling, and replacing less efficient equipment in individual buildings with a more efficient central heating system (Rezaie and Rosen, 2012). Many studies are provided by the literature in which the potential role of district heating is analyzed at different scales (town, city, or region). For example, Henning and Gebremedhin (2012) analyzed the impact of district heating in the town of Gjøvik in Norway, concluding that district heating can play a substantial role in reducing CO_2 emissions. A study by Lončar and Ridjan (2012) demonstrated that district heating is cheaper than individual heating for a town in Croatia. Soltero et al. (2016) proposed a top-down/bottom-up methodology to evaluate the massive implementation of CHP/DH through standard modules replacing existing heating systems. The case study indicates a potential for 589 new fully viable CHP systems for the region, corresponding to the installation of 3000 MW of high efficiency distributed power. The results show the opportunity for an annual CO_2 emissions reduction above 4 million tons. Connolly et al. (2014) identified the potential for district heating in the EU between now and 2050, based on extensive and detailed mapping of the EU heat demand and various supply options. The results indicate that with district heating, the EU energy system will be able to achieve the same reductions in primary energy supply and carbon dioxide emissions as the existing alternatives proposed.

The main reason for the unfavorable CO_2 balance is related to the assumptions made on the emission factors. Table 3.11 shows that there is a considerable difference between the emission factors associated with the Torino Nord plant ($EF_{TON,th}$ and $EF_{TON,el}$) and the emission factor assigned to the residential centralized heaters fueled by natural gas ($EF_{res,ng}$). In fact, while the value of the first two is 320 and 376 kg/MWh, the third is equal to 231 kg/MWh.

This difference has certainly a significant influence on the result of the balance, and the reasons of such an unevenness should be investigated. In a first instance, these values are not easy to compare, because TO-N emission factors come from real-time measurements, while residential heaters emission factors was extracted from the reference EMEP/EEA database. However, it has observed that CHP plants often operate for prolonged times at off-design conditions, depending on power demand, ambient condition, and other considerations (Tereshchenko and Nord, 2015). This would have a significant impact on the plant performance and, consequently to the resulting emission factors.

In continuation, an alternative scenario is reported, in which the same GHG balance is re-calculated using emission factors coming from the same source of data. An experimental analysis of the CO_2 emissions from one or more reference residential systems, and the consequent definition of a specific emission factor, would undoubtedly represent a strong improvement in the optimization of the global CO_2 balance calculation.

The assumptions made on the operation mode of TO-N plant are also thought to have an influence on the results. As reported previously in Chapter 13, the allocation of the energy produced by the Torino Nord CHP plant in the future operating mode was based on assumptions starting by the actual distribution of thermal and electrical energy. These assumptions are questionable, since there is not enough information to define a clear relationship between the produced thermal and electrical energy.

The future operational reality of the Torino Nord power plant could be different from the assumed one, especially if the current energy situation in Italy and Europe is considered. In fact, in recent times, the consumption of electricity has remained stationary or even declined, so a further increase in electricity production may not be required by the market and/or by network operators. The plant operator may then opt to manage the energy production by keeping the production of electricity unchanged, maximizing the only production of heat to meet the request of the DH network.

Remaining in the discussion of the base case, it still must be pointed out that in the definition of the balance, the calculation of the additional quota of electricity produced in the future scenario was not matched to a calculation of avoided emissions resulting from the replacement of other sources. This is due to two reasons:

- the main reason is because this increase in electricity produced is not substantially required, as it only represents the operating response of the plant to the increased demand for thermal energy. Therefore, it is believed that it should only be counted as a produced emission;
- the secondary reason is because the additional electricity produced would be injected to the national grid. If the emission factors are compared, the specific value of the electricity produced in the Torino Nord plant ($EF_{TON,el}$) amounts to 376.5 kg/MWh, while the average value reported for Italian electricity network is equal to 440 kg/MWh (Table 3.11, Chapter 13.2.3). The difference between the two emission factors is therefore limited, and the eventual CO_2 credit resulting from this difference would not modify the overall emission balance.

15.5.1 Alternative scenario

The development of an alternative energy scenario for the calculation of the CO_2 balance is required to assess the effects the assumptions made on TO-N plant emission factors. The alternative scenario involves the re-calculation of the energy balance using emission factors of both power plants and residential heaters coming from the same kind of source, i.e. the reference database commonly used. The sectoral guidance chapter for the energy industry sector of the EMEP/EEA database resend to the IPCC guidance for the CO_2 emission factors of large CHP plants. This latter provides an emission factor for natural gas combustion of 202 kg/MWh (IPCC database). If this emission factor is assigned to the TO-N combined cycle and to the TO-N and TO-E integration and reserve heaters, the resulting CO_2 balance changes significantly. The result of the alternative scenario, reported in Table 3.19, shows that the extension of the DH network corresponds to a CO_2 reduction equal to $9.75 \cdot 10^3$ t/y. Emission of TO-N combined cycle is reduced of $3.32 \cdot 10^4$ t/y compared to the base case. Emission of TO-N and TO-E boilers is reduced of $2.16 \cdot 10^4$ t/y compared the base case.

Table 3.19. CO_2 emission balance for the DH system for one year of exercise, alternative scenario.

Emission source	**CO_2 emission ACTUAL SCENARIO (t/y)**	**CO_2 emission FUTURE SCENARIO (t/y)**	**ΔCO_2 Difference (t/y)**
Torino Nord plant (thermal energy)	$7.00 \cdot 10^4$	$1.18 \cdot 10^5$	**$4.83 \cdot 10^4$**
Torino Nord plant (electrical energy)	$2.19 \cdot 10^5$	$2.31 \cdot 10^5$	**$1.81 \cdot 10^4$**
Torino Nord + Torino Est auxiliary boilers	$2.20 \cdot 10^3$	$7.83 \cdot 10^4$	**$7.61 \cdot 10^4$**
Residential areas	$2.19 \cdot 10^5$	$7.34 \cdot 10^4$	**$- 1.46 \cdot 10^5$**
TOTAL	**$5.11 \cdot 10^5$**	**$5.01 \cdot 10^5$**	**$- 9.75 \cdot 10^3$**

Chapter 16

Conclusion

This part of the study reports the results of the survey on the environmental local and global effects of the potential extension of the DH network in the urban area of Turin. The results of the study on local pollutants dispersion show that the connection to the network of part of the residential heating systems corresponds to an improvement of air quality in terms of NO_x concentration at ground level. The reduction of the contaminant is highest around the areas of intervention (north and east districts of Turin), with effects also extended towards the city center. The average value of pollutant removal is estimated to be around 1-2 $\mu g/m^3$, with a maximum between 2 and 6 $\mu g/m^3$. The last Emission Inventory published by Piedmont Region in 2010 shows that road traffic represents the main source of NO_x and PM emissions, contributing to around 50% of total emissions. Industrial energy production and residential heating sectors account for around 7% and 5% respectively. Considering these data, together with the analysis of annual emission flows reported in Table 3.12, the intervention object of the present study is not expected to bring a significant change in total emission of pollutants. On the other hand, if average concentrations are considered, a maximum 5.7% reduction for NO_x may be obtained. This value would undoubtedly correspond to an environmental improvement at the local level, in this heavily populated area subject to significant air quality issues.

Furthermore, it is known that the removal of obsolete boilers and the centralization of the energy management results in greater efficiency in the use of the heat, and a punctual and accurate control of air emissions.

The results for global emission balance indicate a future increase in CO_2 emissions of $5.09 \cdot 10^4$ t/y if the emission factors coming from real-time monitoring are applied to TO-N plant. If standard reference emission factors (IPCC and EMEP/EEA) are instead considered, the GHG balance turns to a favorable result, corresponding to a CO_2 reduction of $9.75 \cdot 10^3$ t/y.

The reasons of such a discrepancy between the measured and standard emission factors should be investigated. In principle, the prolonged operation of the plant at off-design conditions, is thought to have an influence on the performance and, consequently to the resulting emission factors. To achieve a complete characterization of the emission factors, an experimental analysis of the CO_2 emissions from one or more reference residential systems should be performed.

Another factor influencing the global balance is the operation mode of Torino Nord cogeneration unit, in terms of allocation between thermal and electrical energy produced. Electricity production is mainly regulated by market constraints. By the analysis of the present power to heat graph of TO-N plant, five different modes of operation were observed, each one corresponding to a different power to heat ratio. The simulation of the future operational asset of the power plant has thus been affected by a certain degree of uncertainty.

In conclusion, this study provides important information on the effects on air quality resulting from the modification of the energetic management of an area or settlement. Under a more general point of view, the methodological approach used in this study included the combined analysis of the energy scenario associated with heat generation and distribution in DH networks, and the calculation of the potential dispersion of pollutants connected to it, with the aim of quantifying and locating the potential environmental impacts. It is, therefore, a consistent and comprehensive methodology, valid to be reproduced and developed for other cases of study or other scopes, providing a valid basis for subsequent technical and economic in-depth analysis.

Part 4

General discussion and conclusion

Chapter 17

General discussion

The comprehensive methodology including the joint analysis of local and global emissions has been applied to two different case studies. At a first instance, a comparison of results obtained might seem difficult (Table 4.1). The two energy systems are characterized by different areas of exercise and application contexts. The district heating system is composed of a complex network having the extension of hundreds of kilometers, developed in an urban environment, characterized by numerous technological and constructive peculiarities. The district heating network is powered by a large size combined-cycle plant having a nominal power of hundreds of MW, fueled by natural gas. The distribution of the produced heat is regulated by a complex system of integration and accumulation equipped with interchanges, characterized by modularity in its exercise. The plant for production and combustion of the biogas is instead characterized by a small-medium size, equal to 1 MW, and is located in an agricultural area not distant from industrial activities and residential areas. Biogas itself is a fuel that, although possesses similar characteristics to natural gas, is subject to an on-site production and refining process, which involves different operations compared to the large-scale extraction and distribution of natural gas.

These aspects confirm the substantial differences between the two case studies considered. Nevertheless, starting from the analysis of these differences and making use of the observable similarities, some points of discussion can be raised on global and local emissions. After all, the study has been focused on a single primary goal, i.e. evaluating the effects on the environment of an energy

management action. In addition, if for local emissions the interest is focused more on urban areas, for global emissions, the principle is that *"1 g of CO_2 emitted next to my house is equivalent to 1 g of CO_2 emitted 1,000 km away"*.

The main similarity between the two cases is that both plants are cogeneration plants. In actual operation, it is well established that cogeneration is recognized as an optimal solution for achieving the maximum energy efficiency. The results of the overall carbon footprint balance confirm the environmental importance of cogeneration and combined production (and use) of electricity and heat. This is valid for both the cases studied. In fact, it has been observed that for the biogas plant, the non-use of the thermal energy leads to a near-zero balance. Similarly, it is expected that the result of the global balance of the DH system lowers if an increase of electricity to heat ratio is considered. On the other hand, a decoupling of electricity and heat generation (in the limits of the operating possibility of TO-N system) would result in a significant improvement of the balance.

Remaining in the theme of global emissions, it should be emphasized that the nature and the origin of the fuel have a significant importance. Biogas is an energy carrier produced from organic materials coming from agricultural and livestock waste. These materials possess their "CO_2 credit" which entered in the calculation of the overall budget and contributes to the count of avoided emissions. By contrast, the natural gas does not possess any CO_2 credit and therefore has no "discount" to that effect.

Some more considerations connect to the previous, concerning the scale and scope, and related economic aspects. For a plant size equal to that of the Turin DH system, an alternative fuel to natural gas, which is already the fossil fuel characterized by the lowest emission factors (IPCC), at today it is not conceivable. From the environmental point of view, the only possible solution to achieve an improvement of the global balance of this system would be the reduction of consumption. To keep the future development scenario, the production of electrical energy should, therefore, be minimized against the increased production of thermal energy. In relation to this aspect, economic factors come into play. As already mentioned previously (Part 3 Chapter 15.5), the exercise of large size power plants as Torino Nord is also regulated by market factors, which in turn depend on the demand for electrical energy of the national network. Therefore, the optimization of the environmental performance of the Torino Nord energy system depends also on economic factors, that are not discussed in the present study.

The biogas plant is not excluded from this kind of considerations. The biogas production and combustion technologies have been widely spread in Italy between 2005 and 2010, thanks to the subsidies scheme introduced. These subsidies were exclusively related to the production of electricity, so that the interests of investors were addressed to maximizing the injection of electricity to the national energy grid, without giving a proper regard to the production of thermal energy. This resulted in a remarkable expansion of systems which technically were CHP systems, but in effect produced only electricity. Seen the absence of a potential use in the vicinity, the greatest portion (or the totality) of the thermal energy produced was dispersed in the atmosphere. It is expected that such systems possess a non-optimal environmental balance of global emissions. Fortunately, recently the law has intervened by adjusting the subsidy schemes and imposing the plants to exercise in full cogeneration mode.

Table 4.1. Comparison of the two case studies analyzed.

Term of comparison	**DH system**	**Biogas/biomethane plant**
Generation plant size	Large (220 MW)	Small-medium (1 MW)
Location	Urban area	Rural area, not far from potential residential areas or industrial activities
Fuel type	Natural gas (not renewable)	Biogas (renewable)
Source of fuel	National transmission grid. Imported from abroad	Waste material coming from agricultural activities. Produced on site.
Combustion unit	Cogenerative combined cycle	Cogenerative endothermic engine
Use of electricity	Immission to the national grid (high voltage, subject to constraints due to grid balancing)	Immission to the national grid (medium voltage, not subject to constraints due to grid balancing)
Use of thermal energy	District heating	Not defined. Potential use in agricultural practices, industrial activities or household heating

Table 4.1 (continued). Comparison of the two case studies analyzed.

Term of comparison	DH system	Biogas/biomethane plant
Thermal energy distribution	Advanced DH network composed of storage, integration and interconnection systems	Direct provision to the user. In alternative, potential creation of a small distributed network for household heating
Emission containment and abatement	Advanced containment and abatement system purposely designed on the basis of BATs.	Standard containment system performing emission levels under the regulation limits
Permissions and control of emission	Generation plants are subject to integrated environmental permission. Controls on emission are performed continuously by the operator and the Regional Environmental Agency.	Plant subject to construction permission. Respect of atmospheric emissions is verified and certified periodically by the operator.

The analysis of the local NO_x and TSP dispersion also rises some conclusion on the analogies and differences between the two case studies. For what concerning the DH system, it is clear that the centralization of energy production is favorable to the improvement of air quality in urban areas. A significant number of centralized boilers is in fact replaced by a few plants of larger size and a flexible network for the distribution and storage of energy.

For the case study of the biogas plant, the considerations may be different. The results of the study on local impacts may be compared in the same way as the previous case, i.e. assuming a real thermal energy demand in the surrounding of the plant. In this case, the change is defined as the difference between present and future emissions. The result indicates an improvement in air quality in the immediate vicinity of the plant. The improvement is given, in this case, mainly to lower emission factors of the biogas plant compared to a "traditional" combustion plant, but also by the different geometric factors for the sources (e.g.: higher exhaust gas speed and temperature of conventional plant with respect to biogas plant). The biogas plant's environmental performance may, however, be evaluated in a different way, namely by considering the production of biomethane instead of the direct biogas on-site combustion. In this second case, there would not be a reduction of emissions inside the system boundaries. The result would, therefore, be (though slightly) unfavorable, because of the emissions generated by an external combustor to maintain the digestion process. The alternative of biomethane production would consequently be slightly unfavorable from the point

of view of local emissions, but still appropriate in the case of absence of thermal energy request near the plant.

For what concerning the emission containment and control, the Torino Nord power plant is a facility equipped with an advanced containment and removal system for NO_x. The control unit is also subject to integrated environmental authorization (A.I.A. in Italian), which provides continuous monitoring (under supervision of the Regional Environmental Agency, ARPA) of the pollutant parameters emitted by the chimneys, as well as periodic operation and emissions reporting. This has an influence on the results of the study at the local level, showing that the emission and dispersion of pollutants in the future scenario (network extension) is reduced compared to the current scenario. The biogas plant is also subject to an authorization procedure (Italian Legislative Decree 387/2003) and periodic checks, although not continuous and not directly connected with ARPA Agency. The plant constructors usually guarantee an abatement level that respects the regulation limits, without specifying any detail of the emission factors. The conventional thermal plants are also subject to authorization and periodic control, and are equipped with standard systems for emissions containment. It is therefore expected that the control and containment of emissions for the case of the biogas plant have not impacted significantly on the result of the local NO_x and TSP dispersion.

The application of the methodology is subject, for both case studies, to some phase characterized by a greater uncertainty. For the DH system, it is believed that the phase of greater uncertainty is the energy modeling of the generation plants. Further analysis should be addressed to two aspects of the future scenario: the heat dispatching priority, and the distribution of electricity and heat. For the biogas case study, the greatest uncertainty lies in the real and viable final use of the heat produced, so that modeling was carried out on an annual instead of hourly basis, without providing a detailed use scenario for thermal energy. In this sense, the possible options (not considering the economic aspects) could be:

- the creation of a distributed heating network to supply heat to a group of households adjacent to the installation;
- the supply of heat to industrial activities;
- the supply of heat for the heating of greenhouses for agricultural practices.

For each of the three possibilities, a more detailed analysis (like what done for the DH system) could be constructed. Consequently, both the local and global environmental balance could vary significantly with respect to the reported result.

Based on the information reported so far, with the purpose of comparing the results of the two case studies, two indicators have been developed. The first reports the results of the local NO_x concentration difference amplified to the level of service (i.e. the supply of thermal energy) received by a specific area. The second is the ratio of the result of NO_x local emissions and the total CO_{2eq} balance, so it is defined as a local-to-global emission ratio.

17.1 The “thermal benefit vs. local emission” indicator

The "thermal benefits vs. local emission" (NO_x^{th}) indicator has the objective of evaluating the local impacts on a specific area in the light of the consumption of thermal energy in the area itself. It is defined in each cell of the computational domain as:

$$NO_x^{th} = C_{NOx} \cdot E_{th} \qquad \text{Eq. 4.1}$$

where: C_{NOx} is the NO_x concentration difference between present and future scenarios resulting from the simulations; E_{th} is the average thermal energy demand of the area provided by the generating plants. The NO_x^{th} indicator is then calculated only on the cells of the computational domain in which there is an actual use of thermal energy. It indicates the local change of impacts, in terms of concentration, amplified to the "beneficial" effect received (hence the term "thermal benefit"), that is the amount of heat required by the uses and supplied by the energy system. The NO_x^{th} indicator is therefore measured in $\mu g \cdot kWh/m^3$. The unit indicates that this quantity has no direct physical meaning. In any case, it is considered that this magnitude provides useful indications for the comparison of the case studies.

The procedure and the result of the calculation of NO_x^{th} indicator are reported in continuation.

17.1.1 Domain cell extraction

The cells subjected to an effective use of thermal energy were extracted from the resulting grids of the local emissions study. For the biogas plant, this corresponds to a single cell (it is recalled that the dimensions of the cells are of 1000 x 1000 meters), as it is assumed that the thermal energy produced by the plant is being used in its surrounding. For the DH system, the area of study is that corresponding to the potential extension of the DH network. The coordinates of these areas have been extracted by mean of QGIS software. These areas cover an extension equal to 7 x 5 cells, corresponding to about 35 km^2 (Figure 4.1).

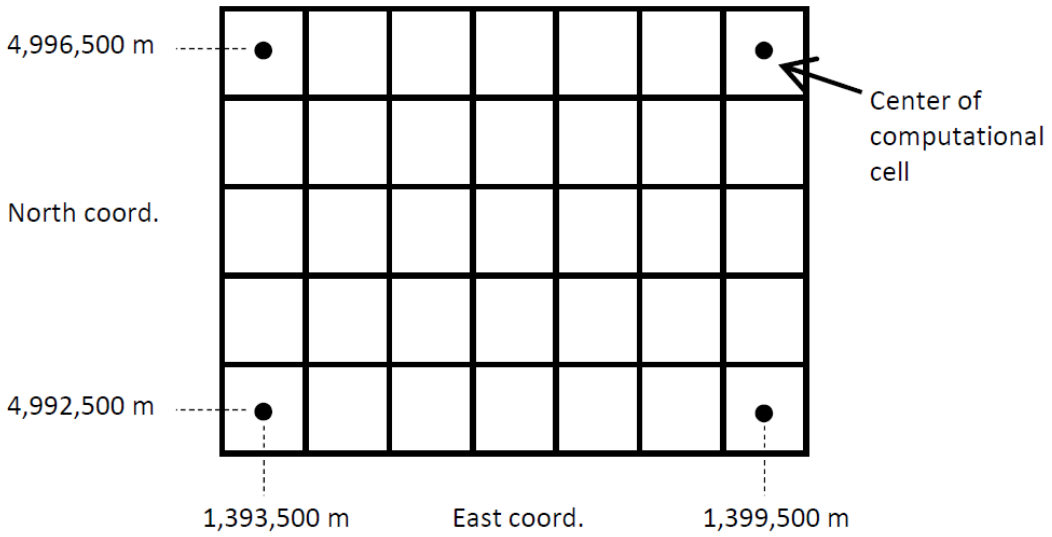

Figure 4.1. Schematic representation of the cells extracted from the computational domain of the DH system simulation for the calculation of the NO_x^{th} indicator.

17.1.2 Indicator calculation– biogas plant

The thermal benefit E_{th} provided by the biogas plant has been calculated by assuming the construction of a small decentralized network of heat distribution connected to a housing settlement next to the plant. To quantify the heat demand of a single housing unit, a new benchmark building like that described in Part 3, Chapter 12.3 was considered. This building is currently subject to continuous measurement of the thermal energy consumption. The living volume of the building is similar to that a construction in the peri-urban area considered may

have. The annual energy consumption of the benchmark building is equal to 119,530 kWh/y, with an hourly recorded maximum equal to 131 kWh/h.

Assuming that the biogas plant is connected to a CHP unit running in full cogeneration mode (B-H scenario, Part 2, Chapter 7.3), the yearly thermal energy produced in steady state equals 5,722,000 kWh/y, and corresponds to 715 kWh/h (based on 8,000 operating hours per year). The number of buildings that the plant is capable of heating, may be defined in two different ways:

1. if it is assumed that the distributed network is equipped with a heat storage system of infinite capacity, so that heat can be stored and redistributed fully satisfying the heat demand of buidlings, then the number of buildings is equal to 5,722,000/119,530 = 47.87 ≈ 47. If it is assumed that all the 47 buildings are constructed next to the plant, the corresponding thermal benefit E_{th} is 47 · 119,530 = 5,617,910 kWh/y, corresponding to about 641 kWh/h.
2. if it is assumed that the distributed network is not equipped with a heat storage system, then the number of buildings depends on the ratio between the maximum hourly value that the facility is able to provide (715 kWh) and the maximum thermal demand value of the benchmark building (131 kWh). In this way, the maximum number of buildings is equal to 715/131 = 5.45 ≈ 5. The corresponding thermal benefit E_{th} is 5 · 119,530 kWh = 597,650 kWh/y, equivalent to about 68 kWh/h.

To define the value of the indicator, the local NO_x concentration in the considered cell (C_{NOx}) must be extracted. This value is equal to -0.083 μg/m^3. The indicator value NO_x^{th} thus becomes:

1. In the case of 47 buildings connected to the system:
   NO_x^{th} = -0.083 · 641 = -53 μg·kWh/m^3
2. In the case of 5 buildings connected to the system:
   NO_x^{th} = -0.083 · 68 = -6 μg·kWh/m^3

This same result may also be shown in form of a map, after the elaboration with SURFER software. The result for biogas plant (case 1) is shown in Figure 4.2.

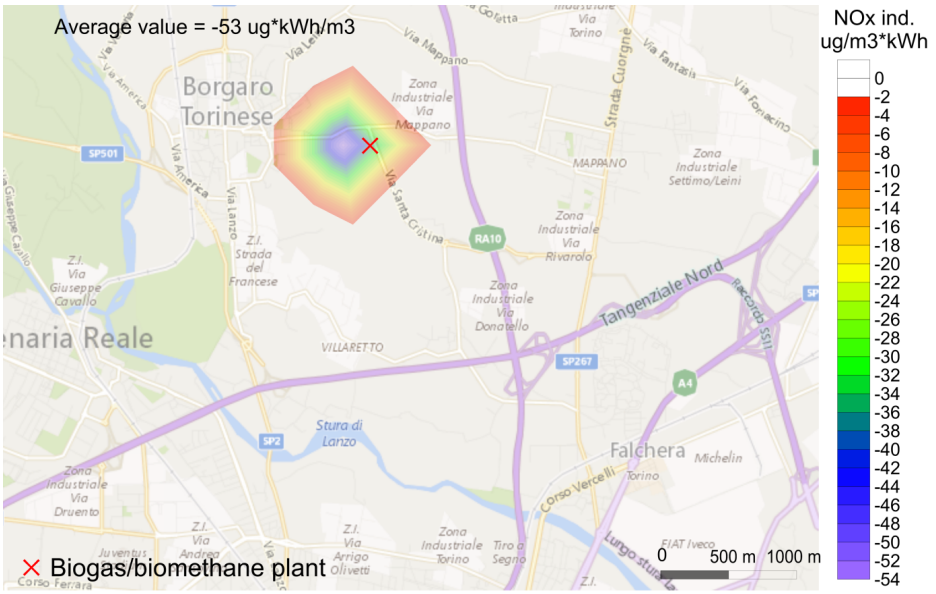

Figure 4.2. Thermal benefit vs. local emission indicator. Calculation referred to 47 buildings potentially served by the biogas plant.

17.1.3 Indicator calculation – DH system

As indicated previously, the potential extension of the DH network covers 35 cells of the computational domain (Figure 4.1). For each cell, the term E_{th} was calculated and the value of NO_x concentration difference (C_{NOx}) was extracted. The thermal benefit E_{th} was calculated by uniformly distributing the annual thermal energy demand over the domain cells. The energy calculation reported in Part 3, Chapter 12.3 indicates a value of annual heat demand of 626,947,872 kWh/y, corresponding to 71,659 kWh/h. If this value is distributed over 35 cells, an E_{th} value of 2,044 kWh/h is obtained.

The concentration values C_{NOx} were extracted from the simulation result using OCTAVE software. A matrix of NO_x^{th} values was then obtained and represented as a map (Figure 4.3).

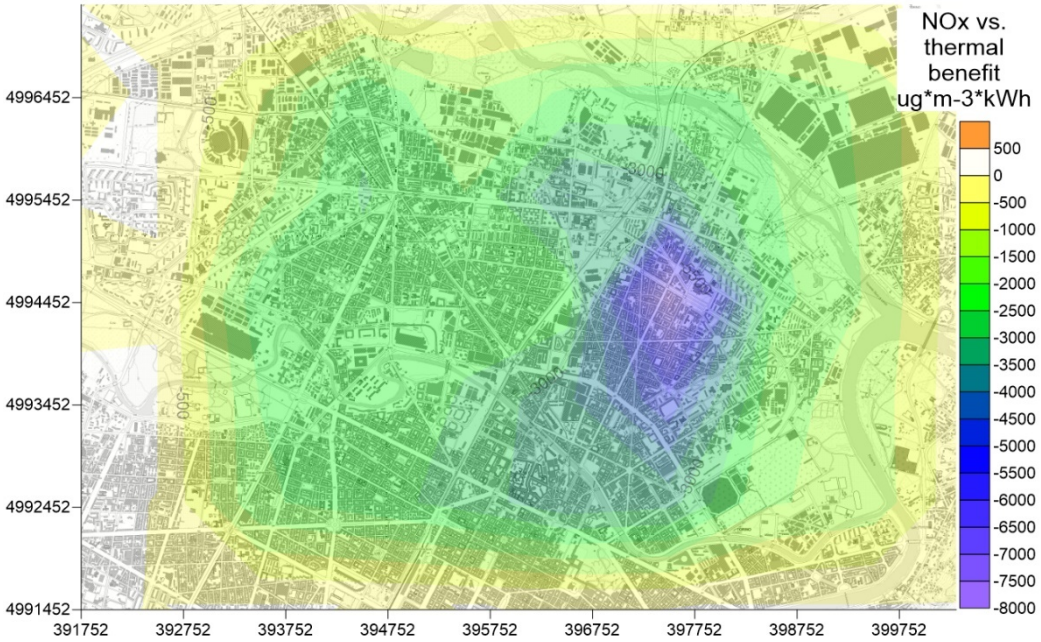

Figure 4.3. Thermal benefit vs. local emission indicator for the potential extension of the DH network. Calculation referred to the base case simulation.

17.1.4 Comparison of the results

Being the value of NO_x concentration difference negative for both the case studies (that indicates a reduction of concentration with respect to the present situation), lower values of the NO_x^{th} indicator correspond to a more favorable result. At equal concentration of pollutant removed, the higher benefit received has, in fact, greater importance.

The result of Figure 4.3, referred to the DH system, indicates an average value of NO_x^{th} equal to -2380 μg·kWh/m^3, with a maximum equal to -927 μg·kWh/m^3 and a minimum equal to -7890 μg·kWh/m^3. These values indicate a better performance of the DH system with respect to the biogas plant (that equals -1154 μg·kWh/m^3).

It is noteworthy that this comparison is not intended to assign an absolute validity to this result, stating that a solution is better than another. In addition, the two comparative scenarios are very different: if the scenario of heat use in DH system is real and well-defined, this cannot be said for the use of the heat generated from biogas combustion, which is based on assumptions, and whose

data come only from the comparison with a sample building. The hypothesis of a small network of distributed heat generation also does not include considerations about the real feasibility from a technical and economic point of view.

Nevertheless, it is believed that this indicator provides useful additional information on the local distribution of the environmental effects linked to the exercise of the power plants.

17.2 The local to global emission ratio

The "local to global emission ratio" (NO_x/CO_2) indicator has the objective of comparing the results of local impacts with the global carbon footprint balance on the same area of the computational domain. It is calculated in each cell as:

$$NO_x/CO_2 = (C_{NOx} / C_{avgNOx}) / (E_{CO2eq} / E_{totCO2eq}) \qquad \text{Eq. 4.2}$$

where: C_{NOx} is the average NO_x concentration difference resulting the simulation of local impacts; C_{avgNOx} is average hourly NO_x concentration for the year 2010 measured by a reference monitoring station, namely the Torino Rebaudengo unit; E_{CO2eq} is the average equivalent CO_2 emitted hourly by the sources covering the area; $E_{totCO2eq}$ is the total emission of equivalent carbon dioxide of the area of Turin municipality that has been estimated for the year 2010 (IREA).

The NO_x/CO_2 indicator is calculated, like the previous indicator NO_x^{th}, only on the cells of the computational domain interested by a modification of the energy configuration. As reported in Equation 4.2, the indicator is composed by a numerator, referring to the local concentration of pollutants, and a denominator, composed of values of CO_{2eq} emission. The C_{NOx} value in each cell is known from the simulation of local impacts. C_{NOx} is then divided by the average concentration recorded by the monitoring station, which is representative of the overall NO_x emissions in the area. Total NO_x concentration includes the contribution of all pollution sources, such as traffic, residential and industrial activities. The numerator is, therefore, the percentage of pollutant removed with respect to its total recorded presence. Similarly, the result of the global balance E_{CO2eq} is scaled to the total CO_{2eq} emissions, in the reference area (Turin municipality). Thus, the ratio reported at the denominator represents the percentage of reduction (or

increase) of carbon emissions compared to a reference amount. In this case, emission flows are used instead of concentration values.

Based its definition, the NO_x/CO_2 indicator represents the level of local improvement (or worsening) of air quality scaled to the relative global improvement (or worsening) of greenhouse gas emissions. Its value is, therefore, dimensionless. A discussion on the interpretation of the results is reported in Chapter 17.2.3.

The procedure and the result of the calculation of NO_x/CO_2 indicator are reported in continuation. The procedure used for the extraction of the domain cells of interest is the same as reported in Chapter 17.1.1. The average concentration value C_{avgNOx} provided by the Torino Rebaudengo monitoring station for the year 2010 is equal to 184.66 $\mu g/m^3$. The value of CO_{2eq} total emission of Turin municipality ($E_{totCO2eq}$) is equal to 3,120,859 t/y, corresponding to 356.262 t/h.

17.2.1 Indicator calculation– biogas plant

To define the indicator, the value of the local NO_x concentration difference in the domain cell (C_{NOx}) must be extracted. Considering the scenario of biogas combustion in a CHP unit (scenario B-H, Part 2, Chapter 7.3), the value of C_{NOx} is equal to -0.08 $\mu g/m^3$. The corresponding global emission balance provides a value of E_{CO2eq} equal to -1425 t/y, or 0.1627 t/h. The value of NO_x/CO_2 indicator is therefore equal to:

NO_x/CO_2, biogas = (-0.08 / 184.66) / (-0.1627 / 356.262) = 0.95

The same result is reported in the form of a map in Figure 4.4.

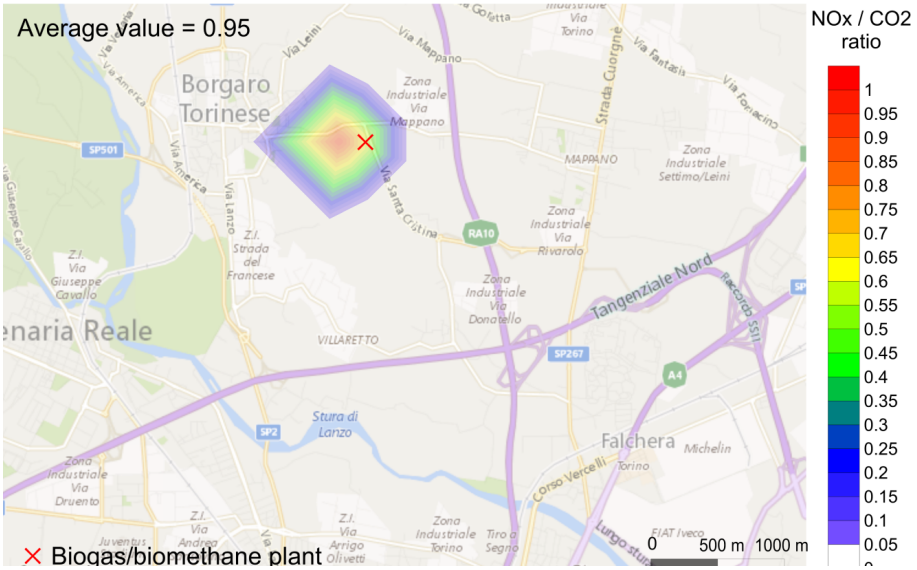

Figure 4.4. Local to global emission ratio for the case of biogas plant combustion in a CHP unit with full recovery of thermal energy.

17.2.2 Indicator calculation– DH system

As indicated previously, the areas affected by the potential extension of the DH network cover 35 cells of the computational domain (Figure 4.1). For each of these, the value of the NO_x concentration difference (C_{NOx}) was extracted using OCTAVE software. The carbon emission flow E_{CO2eq} was calculated by uniformly distributing the result of the carbon footprint balance over the target cells. The corresponding value of E_{CO2eq} for each computational cell is:

E_{CO2eq} = 58,421 t/y / 8,760 h/y = 0.6668 t/h / 35 = 0.19054 t/h

By extending the calculation of NO_x/CO_2 indicator to all the 35 cells, a matrix of NO_x/CO_2 values was obtained and represented as a map (Figure 4.5).

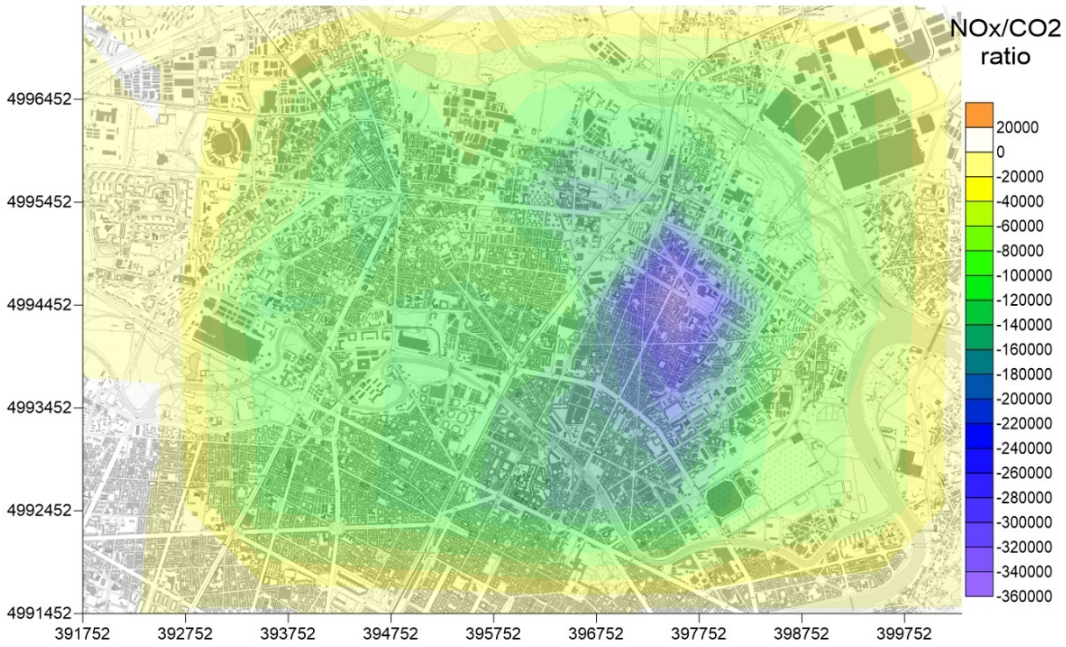

Figure 4.5. Local to global emission ratio for the DH system, base case scenario.

17.2.3 Interpretation and discussion of the results

The results show that the indicator assumes different values depending on the case considered. In fact, the NO_x/CO_2 ratio for the biogas plant is equal to 0.95, while, for the DH system, it varies between -40,222 and -342,376. These results are not easy to evaluate because both local and global magnitudes (C_{NOx} and E_{CO2eq}) can assume positive (increased emissions) or negative (reduced emissions) values. To propose a comparative evaluation of the results, the evaluation grid shown in Figure 4.6 is reported.

According to what is reported in Figure 4.6, it is possible to identify different scenarios depending on the value assumed by the NO_x/CO_2 ratio:

- General improvement: This occurs when both the values of C_{NOx} and E_{CO2eq} are negative (Figure 4.6a, right part). Shifting to the right, the value of numerator increases, a sign that the local benefit will tend to be greater than the global one.
- General worsening: This occurs when both the values of C_{NOx} and E_{CO2eq} are positive (Figure 4.6b, right part). In this case, shifting to the

right, the weight of the worsening at the local level will increase compared to the global level.

- Partial improvement: in case that NO_x/CO_2 assumed negative values, this would indicate that only one of the two results is not favorable, meaning a local worsening and a global improvement, or vice versa. In the case of $C_{NOx}<0$, there would be an improvement at the local level and a worsening at the global level. The lower the value of NO_x/CO_2, the more the global aggravation would be moderate, and/or the local improvement would be evident. In the case of $C_{NOx}>0$, there would be an improvement at the global level and a worsening at the local level. In this case, the lower the ratio of NO_x/CO_2, the more the local aggravation would be moderate, and/or the global improvement would be evident.

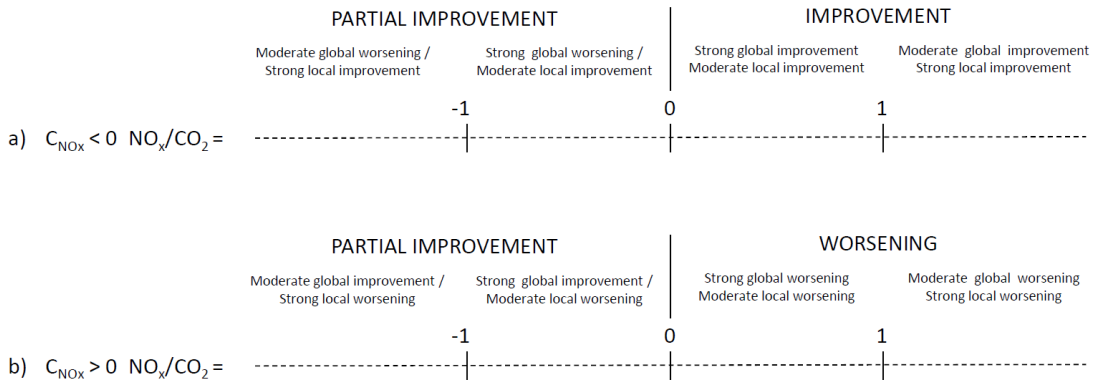

Figure 4.6. Grid for the evaluation of NO_x/CO_2 values, in the case of $C_{NOx}<0$ (a) and $C_{NOx}>0$ (b).

On the basis of this interpretation grid, the NO_x/CO_2 values for the two case studies considered indicate (Figure 4.7.):

- A general improvement for the biogas plant, more pronounced at the global than the local level;
- A strong local improvement and a moderate global worsening for the DH system.

This interpretation is substantially according to the considerations reported in the previous chapters. It is therefore reasonable to think that the calculation of this

indicator can be useful at the time of performing a comparative environmental assessment of different plant solutions, also with different options. Obviously, what reported herein is a preliminary definition, and should be improved. The fact that both local and global impacts are scaled to a reference value is a useful indication of how much a result is important with respect to an aggregate emissive scenario. Nevertheless, it must be verified that the values of C_{avgNOx} and $E_{totCO2eq}$ are representative of the context of study.

At the same time, the interpretation grid presented in Figure 4.6 reports some evaluation thresholds for $NO_x/CO_2=1$ and $NO_x/CO_2=-1$, which assigns a weight to the interpretation of indicator values. This is certainly not obvious, and the threshold values that separate moderated improvement (or worsening) by strong improvement (or worsening), should be redefined in the light of further investigations.

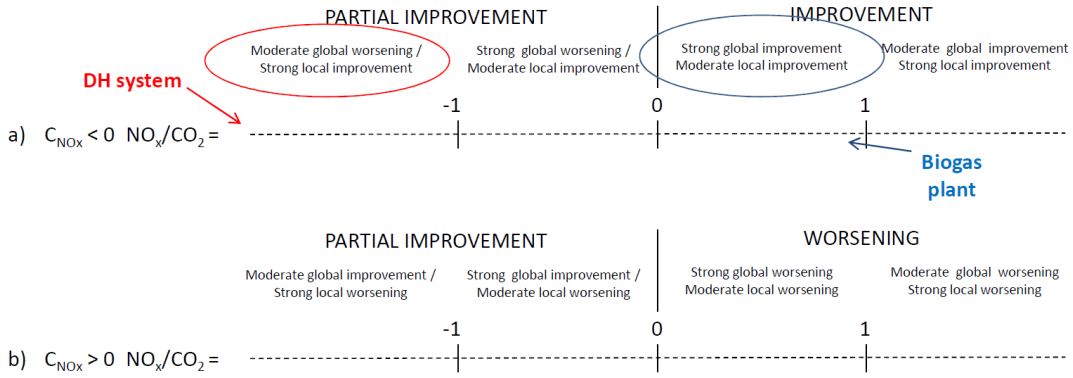

Figure 4.7. Evaluation of the two case studies with respect to the result of the NO_x/CO_2 indicator.

Chapter 18

General conclusion

This study had the objective of developing and discussing a methodology for the assessment of environmental impacts associated with energy management and production interventions. Through the analysis of two case studies characterized by different scales and contexts of application, the environmental impacts on the atmosphere were simulated and quantified. The study was addressed both to the equivalent CO_2 emissions, the effect of which can be found globally, and to the emissions of NO_x and TSP, whose impact typically shows effects at the local level. For each of the case studies, several possible scenarios of use were identified to assess the consequences of a possible change in the energy management of the system.

The first case study reports the analysis of global and local emissions associated with the exercise of a biogas plant located in the surrounding of Turin, with the evaluation of biomethane production as an alternative option. In this case, the global emission balance shows a favorable result, depending on how the produced biogas is used. In the case of biogas is properly employed, the installation of this plant results in a saving of equivalent CO_2 emission with respect to conventional combustion systems. The calculation of the emission impacts at the local scale may result differently depending on the final use selected for the fuel. In particular, the solution to be adopted depends on the potential need of thermal energy, and the corresponding local result may shift from favorable to slightly not favorable.

The second case study analyses the environmental effects associated to the potential extension of the DH network in the urban area of Turin. The results of the analysis of local emissions show that the connection of a part of the residential heating systems to the network corresponds to an improvement of air quality in terms of NO_x concentration at ground level. The reduction of contaminant is highest around the areas of intervention (north and east districts of Turin), with effects also extended towards the city center. The intervention would therefore undoubtedly bring an environmental improvement at the local level, in a heavily populated area subject to significant issues on air quality. The results of global emissions analysis show that the same intervention would not be appropriate from a carbon footprint point of view. However, the discussion of an alternative scenario demonstrates that this result is closely linked to the assumptions made on the emission factors.

Under a more general point of view, the combined analysis of the results and its related uncertainty analysis, as well as the comprehensive discussion of the two case studies reported, rises several concluding remarks.

At a first instance, it is confirmed that a coordinated discussion of the different economic, environmental and planning aspects connected with different schemes of energy utilization seems to be necessary for public authorities, in order to perceive a final, optimal solution. In fact, both the strategy concerning the best satisfaction of the different aspects of energetic needs must be considered (electricity, fuels, local district heating), together with considerations concerning the limitation in local impact, chiefly with reference to atmospheric pollution. Regarding atmospheric pollution, the combined analysis of global and local emissions shows that, in some circumstances, a favorable intervention for the air quality in a specific area (and then for the people living in that area, who obtain the energy demand satisfied), may not be favorable from a global point of view.

The employed methodology is consistent and comprehensive in this sense: through the combined analysis of different scale effects, it was in fact possible to identify the potential optimal solutions for energy production and management, as well as identifying the best "answer" to a given scenario from an environmental point of view. The indicators developed have also provided further discussion tips, to attain an assessment of the possible environmental effects as objective as possible.

The modeling tools used in the application of the methodology resulted consistent for the efficient and complete use of the data available. For the calculation of the emission balance, especially for the biogas plant case study, the use of a LCA-based approach allowed the quantification of mass and energy flows (and their related impacts) over the complete energy production process, including all relevant aspects. Similarly, the local dispersion of NO_x and TSP was calculated by means of an advanced mathematical model able to accurately characterize the evolution in space and time of the pollutant plumes. In addition, several algorithms have been developed to:

- facilitate the management of meteorological input data;
- facilitate the formatting and visualization of output data.

The considerations derived from applying this methodology to two case studies essentially different, but characterized by certain similarities, lead to the conclusion that the combined analysis of the environmental effects must:

- be general enough to be extended to different contexts, identifying the different scenarios in each case;
- be sufficiently adaptable to the case object of study. As seen previously, an LCA approach has been used for a case characterized by a type of renewable fuel produced on site, but not for a large size plant fueled by natural gas. Similarly, the precise local modeling of pollutants mostly suited the case of DH system.
- allow (or at least strive toward) the development of some form of objective comparison between different interventions, characterized by different contexts and scales of application. The indicators developed in the last part of this study are intended as an initial contribution to this end.

In conclusion, this study, through the application of modeling tools applied to processes, methods, and techniques, addressed to apply, analyze and develop a conceptual framework for the joined and comparative analysis of energy management intervention and consequent effects on air pollution.

References

Andrić I., Pina A., Ferrão P., Lacarrière B., Le Corre O. (2016), On the performance of district heating systems in urban environment: an emergy approach, Journal of cleaner production, http://dx.doi.org./10.1016/j.jclepro.2016.05.124;

ANFIA. Italian National Association of the Automotive Industry (2014). Focus on Italian car market January-March. Report. (in Italian)

ARIA Technologies (2001), MINERVE wind field model general design manual, Version 7.0;

Arianet (2002). SURFPRO, surface-atmosphere interface processor user's guide. Arianet Report.

ARPA. Piedmont's Regional Agency for Environmental Protection. Meteorological database of Piedmont Region. (in Italian) http://www.arpa.piemonte.it/banca-dati-meteorologica. [last access 10/08/2014].

ARPA. Piedmont's Regional Agency for Environmental Protection (2012), Study of the pollution sources in the area surrounding the Torino Nord thermal power plant. Synthesis of the results, Report (In Italian);

ARPA. Piedmont's Regional Agency for Environmental Protection (2007), Wind in Piedmont Region. Series on Climate studies in Piedmont, Volume 5 (In Italian);

ARPA. Piedmont's Regional Agency for Environmental Protection (2015). A look to the air 2014. Annual report on air quality in Turin Metropolitan City (in Italian).

Åberg M., Widén J., Henning D. (2012). Sensitivity of district heating system operation to heat demand reductions and electricity price variations: A Swedish example. Energy 41, 525-540. doi:10.1016/j.energy.2012.02.034.

Bach B., Werling J., Ommen T., Münster M., Morales J. M., Elmegaard B. (2016), Integration of large – scale heat pumps in the district heating systems of Greater Copenhagen, Energy, 107, 321 – 334;

Bakonyi P., Nemestóthy N., Simon V., Bélafi-Bakó K. (2014). Review on the start-up experiences of continuous fermentative hydrogen producing bioreactors. Renew. Sustain. Energy Rev. 40 806–813. doi: http://dx.doi.org/10.1016/j.rser.2014.08.014

Balsari P., Dinuccio E. Biogas plants in Piedmont: situation, problems and perspectives. Presentation (in Italian).

Bell R.D., Buckingham F.P. An overview of technologies for reduction of oxides of nitrogen from combustion furnaces. MPR Associates. Report.

Battaglino P., Brighetti M., Marengo P. (2015). Energy saving and emissions in bob applications. Report. (in Italian).

Blengini G.A., Brizio E., Cibrario M., Genon G. (2011). LCA of bioenergy chains in Piedmont (Italy): A case study to support public decision makers towards sustainability. Resour. Conserv. Recycl. 57, 36–47. doi:10.1016/j.resconrec.2011.10.003

Brattebø H., Reenaas M. (2012), Comparing CO_2 and NO_x emissions from a district heating system with mass-burn waste incineration versus likely alternative solutions – City of Trondheim, 1986–2009. Resources, Conservation and Recycling, 60, 147–158;

Briggs G.A. (1973), Diffusion estimates for small emissions (draft). Air Resources Atmospheric Turbulence and Diffusion Laboratory, ATOL No. 79;

Briggs G.A. (1975), Plume rise predictions. In: Lectures on Air Pollution and Environmental Impact Analyses. American Meteorological Society, Boston, MA, 59-111;

Brizio E. (2012). Ecosustainable biomethane and fertilizer production through anaerobic co-digestion of animal manure and energy crops. PHD Thesis. Politecnico di Torino.

Buratti C., Barbanera M., Fantozzi F. (2013). Assessment of GHG emissions of biomethane from energy cereal crops in Umbria, Italy. Appl. Energy 108 128–136. doi: http://dx.doi.org/10.1016/j.apenergy.2013.03.011

Calori G.,Clemente M., De Maria R., Finardi S., Lollobrigida F., Tinarelli G. (2006). Air quality integrated modelling in Turin urban area. Environmental Modelling & Software 21 468–476

CCAR (2008). California Climate Action Registry General Reporting Protocol. Reporting entity-wide greenhouse gas emissions. Version 3.0

Centro Ricerche Produzioni Animali S.p.A. (2009). Feasibility study of the chain of biomethane from cattle manure or landfills for automotive/feed-in (DD n. 717 of 24/11/2008). Piedmont Region Report. (in Italian)

Chang, O.M.C. and England, G.C. (2010). Development of Fine Particulate Emission Factors and Speciation Profiles for Oil and Gas-fired Combustion Systems, Update: Critical Review of Source Sampling and Analysis Methodologies for Characterizing Organic Aerosol and Fine Particulate Source Emission Profiles.

Cherubini F. (2009). GHG balances of bioenergy systems – overview of key steps in the production chain and methodological concerns. Renew. Energy 35 1565–73. doi:10.1016/j.renene.2009.11.035

Colmenares- Santos A., Rosales- Asensio E., Borge- Diez D., Blanes-Peirò J.J. (2016), District heating and cogeneration in the EU – 28: Current situation, potential and proposed energy strategy for its generalization, Renewable and sustainable energy reviews, 62 , 621 – 639;

Connolly D., Lund, H., Mathiesen B.V., Werner S., Möller B., Persson U., Boermans T., Trier D., Østergaard P.A., Nielsen S. (2014), Heat Roadmap Europe: combining district heating with heat savings to decarbonise the EU energy system, Energy Policy ,65, 475-489;

Cuccatto A. (2016). Biogas plants. Administration and environmental aspects. Presentation (in Italian).

de Leeuw F. (2002). A set of emission indicators for long-range transboundary air pollution. Environ. Sci. & Policy 5 135–45.

De Nigris S., Fraire S. (2013). Energy supply analysis in the Province of Torino. CEP-REC Regional Energy Concepts Project Report.

Dones R., Heck T., Hirschberg S. (2013). Greenhouse gas emissions from energy systems: comparison and overview. United Nations Environment Programme, Geneva, Switzerland.

Dumont M., Luning L., Yildiz I., Koop K. (2013). Methane emissions in biogas production, in: Wellinger A., Murphy J., Baxter D., The biogas handbook. Woodhead Publishing Limited 248–266. doi: 10.1533/9780857097415.2.248

EMEP/EEA (2013), Air pollutant emission inventory guidebook. EEA Technical report. ISSN 1725-2237. Technical guidance to prepare national emission inventories;

European Community. Directive 2009/28/EC. On the promotion of the use of energy from renewable sources and amending and subsequently repealing Directives 2001/77/EC and 2003/30/EC.2009.04.23.Off J EU 2009.L 140:16-62.

Finlayson-Pitts B.J., Pitts J.N. (1986). Atmospheric chemistry: fundamentals and experimentals techniques, pp. 63-66, Wiley Interscience, New York.

Finney K.N., Chen Q., Sharifi V.N., Swithenbank J., Nolan A., White S., Ogden S. (2012), Developments to an existing city-wide district energy network: Part II – Analysis of environmental and economic impacts. Energy Conversion and Management, 62, 176–184;

Flesch T.K., Desjardins R.L., Worth D. (2011). Fugitive methane emissions from an agricultural biodigester. Biomass and Bioenergy 35 3927-3935. doi:10.1016/j.biombioe.2011.06.009

Fracastoro G.V., Serraino M. (2011). A methodology for assessing the energy performance of large scale building stocks and possible applications, Energy and Buildings, 43, 844–852;

Fracastoro G.V., Mutani G., Verda V. (2013). Action plan for sustainable energy in the Province of Turin. Anlysis of the energy needs of buildings and the potential energy saving and use of renewables in urban area. Cities on Power porject Report. (In Italian).

Fraunhofer Insitute (2012). Biogas to energy. Cologne / Oberhausen, November 2012, Report.

Genon G., Torchio M.F., Poggio A., Poggio M. (2009), Energy and environmental assessment of small district heating systems: Global and local effects in two case-studies, Energy Conversion and Management, 50, 522–529;

GNU Octave Software, copyright 2014 John W. Eaton and others. http://www.gnu.org/software/octave/ [last access 12/04/2015].

Haichao W., Wenling J., Lahdelma R., Pinghua Z., Shuhui Z. (2013), Atmospheric environmental impact assessment of a combined district heating system, Building and Environment, 64, 200–212;

Hanna S.R., Briggs G.A., Hosker R.P. (1982), Handbook on atmospheric diffusion, Jean S. Smith publication editor;

Henning D., Gebremedhin A. (2012). District Heating and Cooling Enable Efficient Energy Resource Utilisation. In Sustainable Energy - Recent Studies, book edited by Alemayehu Gebremedhin, ISBN 978-953-51-0912-9.

Hill S.C., Douglas Smoot L. (2000). Modeling of nitrogen oxides formation and destruction in combustion systems. Progr. Energy Combust. Sci. 26 417–458.

Huang J., Crookes R. J. (1998). Assessment of simulated biogas as a fuel for the spark ignition engine. Fuel 77, 1793–1801.

Huber A.H., Snyder W.H. (1976), Building wake effects on short stack effluents. Preprint volume for the Third Symposium on Atmospheric Diffusion and Air Quality, American Meteorological Society, Boston, MA;

IAEA – International Agency for Atomic Energy (1999). Health and environmental impacts of electricity generation systems: procedures for comparative assessment. Technical report series n° 394.

ICFPA (2005). International Council of Forest and Paper Associations. Calculation tools for estimating greenhouse gas emissions from pulp and paper mills. Report.

IEA – International Energy Agency (2015). Energy and Climate Change. World Energy Outlook. Special report.

IEA – International Energy Agency (2015). Energy technology perspectives. Report.

IEA – International Energy Agency (2016). Energy and Air Pollution. World Energy Outlook. Special report.

IEA – International Energy Agency (2016b). CO_2 emissions from fuel combustion highlights. Special report.

IPCC - Interngovernmental Panel on Climate Change. Emission Factor Database. http://www.ipcc-nggip.iges.or.jp/EFDB/main.php [last access 03/21/2017].

IPCC (2014). Climate Change 2014: Synthesis Report. Contribution of Working Groups I, II and III to the Fifth Assessment Report of the Intergovernmental Panel on Climate Change [Core Writing Team, R.K. Pachauri and L.A. Meyer (eds.)]. IPCC, Geneva, Switzerland, 151 pp.

Iren Energia (2008). Integrated Environmental Authorization of Torino Nord plant. Report on production processes. (in Italian).

Iren Energia (2014a), Torino Nord plant continuous monitoring system, available at: <http://smetonord.irenenergia.it/tonord/default.asp> (last access 2016-04-20);

Iren Energia (2014b), Torino Nord cogeneration plant. Annual report according to the requirements of the Integrated Environmental Authorization (In Italian);

Iren Energia (2014c). Environmental Declaration of Moncalieri cogeneration power plant. 2nd annual update. (in Italian)

ISO/TS 14067:2013. Greenhouse gases - Carbon footprint of products - Requirements and guidelines for quantification and communication. International Organization for Standardization.

Istat (2001), Italian Population Census, available at: <http://www.istat.it> (last access 2016-05-06);

Italian Minister of Economic Development (2013). Interministerial Decree December 5th. Subsidy scheme for biomethane injected into the natural gas grid.

Italian Government. Law 18 April 1972, n°167. Provisions to facilitate the acquisition of areas for the economic and popular construction.

Italian Government. Legislative Decree of 13 August 2010, 155. Implementation of Directive 2008/50/EC on the ambient air quality and cleaner air for Europe (in Italian).

Jarre M., Noussan M., Poggio A. (2016), Operational analysis of natural gas combined cycle CHP plants: Energy performance and pollutant emissions, Applied Thermal Engineering, 100, 304–314;

Lake A., Rezaie B., Beyerlein S. (2016), Review of district heating and cooling systems for a sustainable future, Renewable and sustainable energy reviews, 67, 417 – 425;

Liora N., Poupkou A., Giannaros T.M., Kakosimos K.E., Stein O., Melas D. (2016), Impacts of natural emission sources on particle pollution levels in Europe, Atmospheric Environment, 137, 171-185;

Lund H., Werner S., Wiltshire R., Svendsen S., Thorsen J.E., Hvelplund F., Mathiesen B.V. (2014), 4th Generation District Heating (4GDH), Integrating smart thermal grids into future sustainable energy systems, Energy 68, 1-11;

Lončar, D, Ridjan, I. (2012), Medium term development prospects of cogeneration district heating systems in transition country – Croatian case. Energy 48, 32–39.

Lund R., Van Mathiesen B. (2015), Large combined heat and power plants in sustainable energy systems, Applied Energy, 142, 389–395;

Macdonald R. (2003). Theory and objectives of air dispersion modelling. Modelling Air Emissions for Compliance MME 474A Wind Engineering.

Makaruk A., Miltner M., Harasek M. (2010). Membrane biogas upgrading processes for the production of natural gas substitute. Sep. Purif. Technol. 74 83–92. doi: 10.1016/j.seppur.2010.05.010

Mohan M., Siddiqui T.A. (1998). Analysis of various schemes for the estimation of atmospheric stability classification. Atmos. Environ. Vol. 32, No. 21 3775-3781.

Moretti A.L., Jones C.M. (2012). Advanced emissions control technologies for coal-fired power plants. Babcock & Wilcox Power Generation Group, Inc. Barberton, Ohio, U.S.A. Technical paper.

Oak Ridge National Laboratory (1992). Resources for the future. U.S.– EC Fuel Cycle Study: Background Document to the Approach and Issues, Rep. No. 1, Oak Ridge Natl Lab., TN.

PAEE (2011). National Action Plan for Energy Efficiency. Italian Government (in Italian)

Patterson T., Esteves S., Dinsdale R., Guwy A. (2011). Life cycle assessment of biogas infrastructure options on a regional scale. Bioresour. Technol. 102 7313–7323. doi: 10.1016/j.biortech.2011.04.063

PBL - Netherlands Environmental Assessment Agency (2014). Trends in global CO2 emissions. Report. The Hague, 2014. ISBN: 978-94-91506-87-1.

Perry, S. G., D. J. Burns, R. J. Adams, R. J. Paine, M. G. Dennis, M. T. Mills, D. G. Strimaitis, R. J. Yamartino, and E. M. Insley, (1989): User's Guide to the Complex Terrain Dispersion Model Plus Algorithms for Unstable Situations (CTDMPLUS) Volume 1: Model Description and User Instructions. EPA/600/8-89/041, U.S. Environmental Protection Agency, RTP, NC, 196pp.

Pertl A., Mostbauer P., Obersteiner G. (2010). Climate balance of biogas upgrading systems. Waste Manag. 30 92–99. doi: 10.1016/j.wasman.2009.08.011

Poeschl M., Ward S., Owende P. (2010a) Prospects for expanded utilization of biogas in Germany. Renew. Sustain. Energy Rev. 14 1782–1797. doi: 10.1016/j.rser.2010.04.010

Poeschl M., Ward S., Owende P. (2010b). Evaluation of energy efficiency of various biogas production and utilization pathways. Appl. Energy 87 3305–3321. doi: 10.1016/j.apenergy.2010.05.011

Poeschl M., Ward S., Owende P. (2012a). Environmental impacts of biogas deployment - Part I: life cycle inventory for evaluation of production process emissions to air. J. Clean. Prod. 24 168-183. doi: 10.1016/j.jclepro.2011.10.039

Poeschl M., Ward S., Owende P. (2012b). Environmental impacts of biogas deployment - Part II: life cycle assessment of multiple production and utilization pathways. J. Clean. Prod. 24 184-201. doi: 10.1016/j.jclepro.2011.10.030

Power N.M., Murphy J.D. (2009). Which is the preferable transport fuel on a greenhouse gas basis; biomethane or ethanol? Biomass and Bioenergy 33 1403-1412. doi:10.1016/j.biombioe.2009.06.004

QGIS, Quantum GIS Software, available at: <http://www.qgis.org/> (last accessed 2016-09-13);

Ravina M., Genon G. (2015), Global and local emissions of a biogas plant considering the production of biomethane as an alternative end-use solution, Journal of Cleaner Production, 102, 115-126;

Rezaie B., Rosen M.A. (2012), District heating and cooling: Review of technology and potential enhancements, Applied Energy, 93, 2–10;

Rosen M.A. (2006), An exergy-based method for allocating carbon dioxide emissions from cogeneration systems - Part I: comparison with other methods, in: EIC Climate Change Technology, IEEE, 2006.

Ryckebosch E., Drouillon M., Vervaeren H. (2011). Techniques for transformation of biogas to biomethane. Biomass and bioenergy 35 1633-1645. doi:10.1016/j.biombioe.2011.02.033

Saracco A.M., Antonini M. (2014). From biogas to biomethane an opportunity for agriculture. Turin Agriculture Academy. Report. (in Italian)

Scire J.S., Lurmann F.W., Bass A., Hanna S.R. (1984), User's guide to the MESOPUFF II model and related processor programs. EPA-600/8-84-013, U.S., Environmental Protection Agency, Research Triangle Park, NC;

Senor A. (2016). Environmental compatibility of Turin district heating network related to the cogeneration system. PhD Thesis. Politecnico di Torino. (in Italian)

Singh D., Kumar A., Kumar K., Singh B., Mina U., Singh B.B., Kumar Jain V. (2016), Statistical modeling of O_3, NO_x, CO, $PM_{2.5}$, VOCs and noise levels in commercial complex and associated health risk assessment in an academic institution, Science of the Total Environment, 572, 586–594;

Soltero V.M., Chacartegui R., Ortiz C., Velazquez R. (2016). Evaluation of the potential of natural gas district heating cogeneration in Spain as a tool for decarbonisation of the economy. Energy 115 (2016), 1513-1532. http://dx.doi.org/10.1016/j.energy.2016.06.038

Spath P.L., Mann M.K. (2000). Life cycle assessment of a natural gas combined-cycle power generation system. National Renewable Energy Laboratory, Golden, Colorado.

Starr K., Gabarrell X., Villalba G., Talens L., Lombardi L. (2012). Life cycle assessment of biogas upgrading technologies. Waste Manag. 32 991–999. doi: 10.1016/j.wasman.2011.12.016

Tereshchenko T., Nord N. (2015). Uncertainty of the allocation factors of heat and electricity production of combined cycle power plant. Applied Thermal Engineering 76 (2015) 410-422. http://dx.doi.org/10.1016/j.applthermaleng.2014.11.019

Thomas B., Wyndorps A. (2011). Monitoring of a 192 kW_{el} Biogas CHP unit at the research station "Unterer Lindenhof". Reutlingen University. Report.

Torchio M.F., Genon G., Poggio A., Poggio M. (2009), Merging of energy and environmental analyses for district heating systems, Energy, 34, 220– 227;

Torchio M.F. (2015), Comparison of district heating CHP and distributed generation CHP with energy, environmental and economic criteria for Northern Italy, Energy Conversion and Management, 92, 114–128;

Tree D.R., Svensson K.I. (2007). Soot processes in compression ignition engines. Prog. Energy Combust. Sci. 33 272–309. doi:10.1016/j.pecs.2006.03.002

Tufvesson L.M., Lantz M., Borjesson P. (2013). Environmental performance of biogas produced from industrial residues including competition with animal feed. J. Clean. Prod. 53 214-223. doi: http://dx.doi.org/10.1016/j.jclepro.2013.04.005

Turin Province (2009), Pre-feasibility study for the further development of the district heating network connected to cogeneration in the Turin area, Report (In Italian);

Turin Province (2013). Action plan for sustainable energy in Turin Province. Report. (in Italian).

Turin Province (2012). 8th Energy Report. (in Italian).

Turin Province (2014). 9th Energy Report. (in Italian).

US EPA. United States Environmental Protection Agency. Emission Standards Reference Guide. http://www.epa.gov/otaq/standards [last access 02/09/2014].

US EPA (1998). A Comparison of CALPUFF with ISC3. Office of Air quality Planning and Standards. Report.

US EPA (2011), CALPUFF Modeling System user's manual, Version 6;

van Dijk G.H.J. (2011). Hydrocarbon emissions from gas engine CHP-units 2011 measurement program. KEMA in samenwerking met het Ministerie van Infrastructuur en Milieu. Utrecht, Netherlands. Report.

Vesterlund M., Toffolo A., Dahl J. (2016), Simulation and analysis of a meshed district heating network, Energy Conversion and Management, 122, 63 – 73.

WCED. World Commission on Environment and Development (1987). Our common future, Oxford Univ. Press, Oxford and New York.

WHO World Health Organization (2006). Air quality guidelines for particulate matter, ozone, nitrogen dioxide and sulfur dioxide. WHO/SDE/PHE/OEH/06.02

Web references

www.bing.com

www.google.it/maps

www.ecmwf.it/

http://www.unidata.ucar.edu/software/netcdf/

https://linux.die.net/man/1/ncks

http://www.mingw.org/wiki/msys

http://www.sistemapiemonte.it/cms/privati/ambiente-e-energia/servizi/474-irea-inventario-regionale-delle-emissioni-in-atmosfera

http://www.regione.piemonte.it/ambiente/aria/rilev/ariaday/ariaweb-new/

http://webgis.arpa.piemonte.it/

Appendix 1

Biogas upgrading process design

The dimensioning of the biogas upgrading process system was completed following the approach presented by Brizio (2012), that considered the simultaneous absorption of CO_2 and CH_4.

A schematic representation of the key variables regulating the process is reported in Figure A.1.

Quantities with the superscript refers to methane, otherwise to CO_2; L is the circulating flow of absorbing water; x and y refer to liquid and solid fraction respectively; V_b and V_a are the biogas flow input and output respectively; subscript F_T refers to flash tank and F is the flow of methane-rich gas mixture recirculated at the column input. The five unknown quantities defining the system (x_b, x'_b, L, Z and V_a) were calculated by mean of the following equation system:

CO2) $L_b \cdot x_b = K_y \cdot S \cdot Z \cdot \Delta y_L$ Eq. A1.1

CH4) $L_b \cdot x'_b = K'_y \cdot S \cdot Z \cdot \Delta y'_L$ Eq. A1.2

$V_b \cdot y_b - V_a \cdot y_a = L_b \cdot x_b$ Eq. A1.3

$V_a = V_b \cdot y_b - L_b \cdot x_b + V_b \cdot y'_b - L_b \cdot x'_b$ Eq. A1.4

$L_b = \frac{L_a}{1 - x_b - x'_b}$ Eq. A1.5

where Z is the tower height, S is the cross area of the tower, K_y and K'_y are the overall mass transfer coefficients respectively for CO_2 and CH_4, y_b^* and y_a^* are the mole fractions at equilibrium (according to Henry's law), Δy_L is the logarithmic mean of y_b-y_b^* and y_a-y_a^*. The mass balances reported are all rigorous equations, the only approximation was the use of the logarithmic mean, as solid/liquid equilibrium lines are not straight. To completely define the system flow rate F coming from the flash tank must be known. As a recirculating system is present, quantities are subject to change depending on F itself, so an iterative process must be considered. To do so, equations A.1 to A.5 were coupled to with the following material balance:

$$P = H \cdot x_{FT} = y_{FT} \cdot P^{FT} \qquad \text{Eq. A1.6}$$

$$P' = H' \cdot x'_{FT} = y'_{FT} \cdot P^{FT} \qquad \text{Eq. A1.7}$$

$$L \cdot (x_b - x_{FT}) = F \cdot y_{FT} \qquad \text{Eq. A1.8}$$

$$L \cdot (x'_b - x'_{FT}) = F \cdot y'_{FT} \qquad \text{Eq. A1.9}$$

$$F = L \cdot (x_b - x_{FT} + x'_b - x'_{FT}) \qquad \text{Eq. A1.10}$$

where F is the recirculated molal flow rate (the flashed gas from the flash tank), P and P' are partial pressure of CO_2 and CH_4 in the flash tank, P_{FT} is the total pressure in the flash tank (2-5 atm), H and H' are Henry's law constant for CO_2 and CH_4, x_{FT} and x'_{FT} are respectively CO_2 and CH_4 concentration in the liquid flow leaving the flash tank, y_{FT} and y'_{FT} are respectively CO_2 and CH_4 concentration in the gas flow leaving the flash tank. The equation system was solved numerically trying different configurations, with the objective of obtaining the three different values of x'_b (i.e. the fraction of methane absorbed by the absorbing water) considered in the present study.

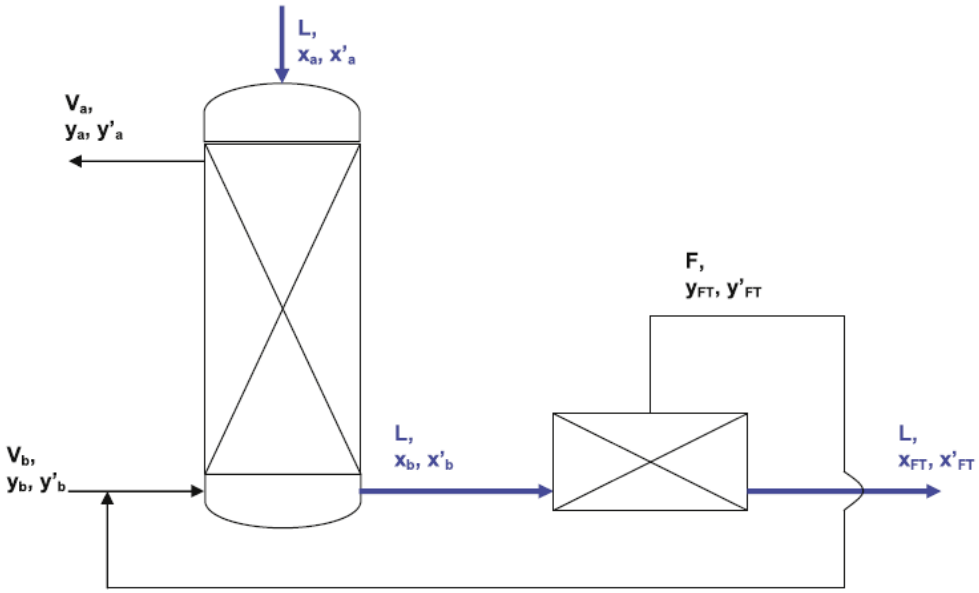

Figure A.1. Schematic representation of biogas absorption with pressurized water

Appendix 2

Description of Gaussian model

The dispersion of gaseous NO_x was estimated using a stationary plume gaussian model, defining the ground level concentration (z_0=0) of pollutant as follows:

$$C(x, y_0, z_0) = \frac{Q}{2\pi u_1 \sigma_y \sigma_z}\left[\exp\left(-\frac{y_0^2}{2\sigma_y^2}\right)\right]\left\{\exp\left[-\frac{(z_0-H)^2}{2\sigma_y^2}\right] + \exp\left[-\frac{(z_0+H)^2}{2\sigma_z^2}\right]\right\}$$

Eq. A2.1

where $C(x,y_0,z_0)$ is the NO_x concentration at a defined distance x, (y_0=0 and z_0=0), Q is the flux of NO_x emitted from the stack, u_1 is the mean wind speed at the source location, σ_y and σ_z are lateral and transversal dispersion coefficients, z_0 is the reference height, H is the height of plume barycenter. Mean wind speed at source location is estimated to be around 3 m/s, according to meteorological data available (ARPA). Plume height H along the axial distance x was calculated by:

$$H(x) = h + \Delta h(x) \qquad \text{Eq. A2.2}$$

where h is the height of the chimney, assumed to be 10 m and $\Delta h(x)$ is the plume contribution, a function of the buoyancy factor F_b:

$$\Delta h(x) = 1.6\frac{F_b^{1/3} x^{2/3}}{U} \qquad \text{Eq. A2.3}$$

$$F_b = w_0 r_0^2 g \frac{T_0 - T_a}{T_0}$$ Eq. A2.4

where U = 3m/s, w_0 is the exhaust gas speed at the stack, r_0 is the radius of the chimney, T_0 is the exhaust gas temperature, T_a is the mean temperature for the considered location. The values of the reported parameters are given in Part 2, Chapter 7.4, Table 2.6 for the two different sources considered.

Dispersion coefficients σ_y and σ_z were calculated as the sum of a term depending on emission conditions (subscript b) and a term depending on dispersion (subscript t):

$$\sigma_y^2(x) = \sigma_{yb}^2(x) + \sigma_{yt}^2(x)$$ Eq. A2.5

$$\sigma_z^2(x) = \sigma_{zb}^2(x) + \sigma_{zt}^2(x)$$ Eq. A2.6

Dispersion terms σ_{yt} and σ_{zt} were calculated using Pasquill-Gifford formulations (Mohan and Siddiqui, 1998):

$$\sigma_y(x) = \frac{k_1 x}{\left[1+\left(\frac{x}{k_2}\right)\right]^{k_5}}$$ Eq. A2.7

$$\sigma_z(x) = \frac{k_4 x}{\left[1+\left(\frac{x}{k_2}\right)\right]^{k_5}}$$ Eq. A2.8

where k_1, k_2, k_3, k_4 and k_5 are fixed coefficients depending on atmospheric stability class.

A different formulation of the stationary gaussian model was used in the calculation of particulate dispersion to take into account the partial deposition of the particles:

$$C(x, y_0, z_0) = \frac{Q}{2\pi u_1 \sigma_y \sigma_z}\left[\exp\left(-\frac{y_0^2}{2\sigma_y^2}\right)\right]\left\{\exp\left[-\frac{(z_0 - H + V_s x/u_1)^2}{2\sigma_{yz}^2}\right]\right\}$$ Eq. A2.9

where V_s is the deposition speed of particles, estimated through Stokes law, considering a mean particle radius of 10 μm.

$$V_s = \frac{2r^2 \rho g}{9\mu}$$ Eq. A2.10

Appendix 3

Description of Torino Nord power plant

The present Appendix reports a general description of the main technical features of Torino Nord power plant. The system is composed by:

- A thermoelectric cogeneration unit combined-cycle of approximately 400 MW_e, fueled by natural gas;
- 4 integration and reserve boilers of 85 MW each, fueled by natural gas;
- A heat accumulation system consisting of 6 accumulators for a total capacity of about 5,000 m^3;
- A pumping, pressurization, water make-up system for the district heating network;
- An electric power station of 220 kV;
- The auxiliary services, such as natural gas measurement station, compressed air production plant, demineralized water production plant and storage, distribution networks for water/air, wastewater treatment plants, offices and parking areas.

Cogenerative combined cycle

The cogenerative combined-cycle unit consists of the following major equipment:

- a gas turbine with a nominal electric power of 270 MW, fueled by natural gas, with alternator;
- a heat recovery steam generator (HRSG), powered by the gas turbine exhaust fumes, which produces steam that is sent to the steam turbine;
- a steam turbine with a nominal electric power of 119 MW, consisting of three turbine bodies (high, medium and low pressure), and alternator;
- a heat production system for the district heating network, by spilling low-pressure steam from the steam turbine, which produces superheated water to 120 °C;
- a condensation unit for the steam turbine, cooled by an air heater.

In continuation, the maximum performance that can be obtained from the combined cycle are reported:

- Electric mode: total gross electrical capacity of 390 MW and gross electrical efficiency of around 56%;
- Cogeneration mode: total gross electrical capacity of 335 MW and thermal power for district heating of around 220 MW.

The gas turbine and the alternator are installed inside a building, for the attenuation of the noise emitted to the outside. The engine room of the gas turbine is equipped with special devices for the maintenance and/or removal and installation of the turbine. The gas turbine alternator is air cooled. The cooling air is in turn cooled in a closed circuit with air/water exchangers.

The steam generator (HRSG) is of the horizontal type, natural circulation and at three steam pressure levels (high, medium and low-pressure levels).

The steam produced by the lower pressure level powers the low-pressure turbine and, in cogeneration mode, the heat exchanger to the district heating network.

The steel chimney reaches a height of 60 m and is connected to the body of the HRSG. The chimney diameter at the exit is 6 m.

The steam turbine and the alternator are installed inside a building for attenuating the noise emitted to the outside. The engine room of the gas turbine is equipped with special devices for the maintenance and/or removal and installation of the turbine.

The steam turbine is composed of a high-pressure, a medium pressure and a low-pressure body. The individual rotors of the three bodies are rigidly coupled. The steam of the steam turbine will be air-cooled.

Integration and reserve boilers

Four integration and reserve boilers will be installed in the power plant, each with a nominal thermal power of 85 MW, for a total power of 340 MW. The fuel used is natural gas. The steam produced by the boilers will be sent to a heat exchanger to produce superheated water at 120 °C for the district heating network.

The boilers have the double function of:

- integration for covering the peak load of the district heating network;
- reserve in case of out of service in the combined cycle thermoelectric unit.

The boilers are of the water-tube type with natural circulation, pressurized, equipped with four burners.

The steam produced by the boilers is used in a superheated water production system, composed by heat exchangers, in which circulates the water of the district heating network.

The key features and technical specifications of boilers are:

- boiling pressure: 16 bar
- design temperature: 250 °C
- working pressure: 12 bar
- start time: from cold (room temperature): 3 hours; from warm (temperature of boiler water 110 °C): 30 minutes.

For the maintenance and handling of the components will be installed special devices.

The chimney of the boilers has a circular cross-section of 8 m in diameter and contains 4 stacks, each with a diameter of about 1.8 m.

The system also contains a heat exchanger, in which the steam produced by the boilers transfers heat to the district heating network. The heat exchangers are of shell and tube type, and main characteristics of each exchanger will be:

- primary and secondary design pressure: 18 bar;
- primary and secondary design temperature: 210 °C;
- primary operating pressure: 12 bar;
- nominal capacity: 3,000 m^3/h;
- supply of district heating water temperature: 120 °C;
- return of district heating water temperature: 70 °C.

Heat storage systems

Six storage system are installed in the plant with the aim of covering the peak demand of thermal energy. The total capacity of the system is about 5,000 m^3.

The storage tanks will be connected, through a pipe system, to the pumping system and to the heat production system for the district heating network.

Auxiliary facilities

The thermoelectric power station is equipped with a pumping station for the superheated water circulation generated by the plant itself, to users through the new district heating network.

The pumping system will be composed of 2 of pumping groups (one on the return from district heating network and one on the supply to the district heating network), each formed by 4 pumps in parallel, each having the following characteristics:

- capacity: 2,500 m^3/h
- prevalence: 8 bar.

The thermoelectric plant is equipped with a system for the pressurization, expansion and filling of the district heating network, capable of performing the following functions:

- maintaining the static pressure of the district heating network;
- storing of the water for the district heating network, to cope with the volume fluctuations due to the temperature variation and with possible losses;
- degassing of the make-up water.

The pressurization pumps are of variable speed type. The metallic water storage vessel has an external hard roof, with an internal floating roof to minimize the contact with the oxygen present in the air. The pressurization pumps and the relief valves are connected to the vessel.

The electric power produced by the combined cycle unit is injected to the national grid through a 220 kV armored electric station, with SF6 insulation, to which the transformers of the gas and steam turbines are connected. The armored power station was built inside a building, which contains the armored equipment at 220 kV, protection and control panels and batteries. The armored electrical station includes, in addition to the turbines' transformer, also two transformers for the power supply to a 6 kV central cabin and for the power supply of the 22 kV cabin serving the integration and reserve boilers.

The plant is governed by an automation system based on distributed control systems (DCS). The district heating network will be controlled by the installed peripheral control units in key points in the network.

The operation takes place by a computerized control room that is head of all distributed control units. The control room will be equipped with two supervision consoles, one for normal operation and another as a reserve. The two consoles are independent and interchangeable among them. The operator interface stations installed in the console are divided according to the main parts controlled:

- thermoelectric group combined cycle;
- integration and reserve boilers;
- armored power station 220 kV;
- district heating network;
    - auxiliary services.

Appendix 4

Algorithm for energy balance calculation

```
%% CENTRALI EMISSIONI PRODOTTE
load('tlr_ton_2014.prn'); %carica richiesta TLR attuale 8760x1
load('profilo1.prn'); %carica profilo di carico 8760x1
a = 626947872 %somma dei kwh dati dai nuovi allacciamenti
(aree_ton_GIULIO_v2.xls)
tlr_futuro=(a/1000)*profilo1; %distribuisce su base oraria
tlr_tot=tlr_ton_2014+tlr_futuro; %valori in MWh
for i=1:8760 %ciclo che assegna i consumi a to_nord, to_est e caldaie
to_nord
 if (tlr_tot(i)<220)
    tlr_ton(i)=tlr_tot(i);
    tlr_toe(i)=0;
    tlr_cald(i)=0;
 else if (tlr_tot(i)<560)
         tlr_ton(i)=220;
         tlr_toe(i)=tlr_tot(i)-220;
         tlr_cald(i)=0;
  else if (tlr_tot(i)>560)
         tlr_ton(i)=220;
         tlr_toe(i)=340;
         tlr_cald(i)=tlr_tot(i)-560;
  end
 end
 end
 end
 %applicazione dei EF
 ef_ton=0.1663; %kg/MWh da storico SME 2014
 ef_cald=0.18; %kg/MWh da storico SME 2014
 ef_toe=0.18; %preso uguale a caldaie ton
 ef_tsp_ton=5.55e-05; %kg/MWh ef tsp da CORINAIR
 ef_tsp_cald=2.47e-04; %kg/MWh ef tsp da CORINAIR
 ef_tsp_toe=2.47e-04;
nox_ton=((tlr_ton*ef_ton*1000))/3600; %calcolo flussi nox emessi
0.05kgNOx/GJ
nox_toe=((tlr_toe*ef_toe*1000))/3600; %valori in g/s
nox_cald=((tlr_cald*ef_cald*1000))/3600;
tsp_ton=((tlr_ton*ef_tsp_ton*1000))/3600; % flussi nox emessi
0.05kgNOx/GJ
tsp_toe=((tlr_toe*ef_tsp_toe*1000))/3600; %valori in g/s
tsp_cald=((tlr_cald*ef_tsp_cald*1000))/3600;
for k=1:8760 %calcola rapporto flusso/velocitÃ  di to_nord
if nox_ton(k)>0 %per assegnare una vel a to_nord futuro
   vel_ton(k)=11.8;
else
    vel_ton(k)=0;
end
if nox_toe(k)>0 %assegna vel a to_est
   vel_toe(k)=11.8;
else vel_toe(k)=0;
end
if nox_cald(k)>0 %assegna vel a caldaie
   vel_cald(k)=11.8;
```

```
else vel_cald(k)=0;
end
end
nox_ton2=nox_ton'; %traspone
nox_toe2=nox_toe';
nox_cald2=nox_cald';
tsp_ton2=tsp_ton';
tsp_toe2=tsp_toe';
tsp_cald2=tsp_cald';
vel_ton2=vel_ton';
vel_toe2=vel_toe';
vel_cald2=vel_cald';
ton_futuro=horzcat(nox_ton2,vel_ton2,nox_toe2,vel_toe2,nox_cald2,vel_cal
                 tsp_ton2,tsp_toe2,tsp_cald2);
dlmwrite('flu_piu_ton.dat',ton_futuro,'delimiter',' ');
%%%%%%%%%%%%%%%%%%%%%%%%%%%%%%%%%%%%%%
%%%%%%%%%%%%%%%%%%%%%%%%%%%%%%%%%%%%%%%%%
% AREE NON ALLACCIATE EMISSIONI PRODOTTE
notlr=[3417 11512 4592 8876 19371 9717]; %kg NOx emessi area NON ALLACCIATA
notlr_tsp=[43 143 57 111 241 121]; %kg TSP emessi area NON ALLACCIATA
a2=notlr*1000; %g NOx emessi da ciascuna area
b2=notlr_tsp*1000; %g TSP emessi da ciascuna area
for j=1:6
nox(:,j)=profilo1*a2(j);
tsp(:,j)=profilo1*b2(j);
end
flux=nox/3600; %g/s nox emessi in ciascuna ora
flupm=tsp/3600; %g/s TSP emessi in ciascuna ora
dlmwrite('nox_piu_aree.dat',flux,'delimiter',' ');
dlmwrite('tsp_piu_aree.dat',flupm,'delimiter',' ');
% AREE ALLACCIATE TLR EMISSIONI EVITATE
tsp_tlr=[106 357 142 275 600 301]; %kg tsp emessi area ALLACCIATA
aree_tlr=[6836 23026 9185 17753 38742 19435]; %kg NOx emessi area ALLACCIATA
a3=aree_tlr*1000; %g NOx emessi da ciascuna area
b3=tsp_tlr*1000; %g tsp emessi da ciascuna area
for j=1:6
nox_meno(:,j)=profilo1*a3(j);
tsp_meno(:,j)=profilo1*b3(j);
end
flux_meno=nox_meno/3600; %g/s nox emessi in ciascuna ora
flupm_meno=tsp_meno/3600; %g/s tsp emessi in ciascuna ora
dlmwrite('flu_meno.dat',flux_meno,'delimiter',' ');
dlmwrite('flupm_meno.dat',flupm_meno,'delimiter',' ');
```

Appendix 5

Algorithm for meteorological input data conversion

```
1         program calcdf
2
3         implicit none
4         integer ncom,nc,numz,numx,numy,nums,nump,numu,tm
5         integer numz_old,numx_old,numy_old,nums_old
6         integer nump_old,numu_old,tm_old
7         parameter (nc=1204)
8         parameter (numz=11)
9         parameter (numx=125)
10        parameter (numy=105)
11        parameter (nums=1)
12        parameter (nump=1)
13        parameter (numu=1)
14        parameter (tm=720)
15
16        parameter (numz_old=10)
17        parameter (numx_old=99)
18        parameter (numy_old=99)
19        parameter (nums_old=5)
20        parameter (nump_old=16)
21        parameter (numu_old=3)
22        parameter (tm_old=4)
23        character*16 DATASET,DATAVER
24        character *64 DATAMOD
25        character*132 COMMENT(nc)
26        character*8 AXTZ,PMAP,DATUM,CLAB1,CLAB2,CLAB3
27        character*8 CLAB4,CLAB5,CLAB6,CLAB7,CLAB8
28        character *8 CLAB9,CLAB10,CLAB11,CLAB12
29        character*12 DATEN
30        character*4 UTMHEM
31        integer i,j,k,h,IBYR,IBMO,IBDY,IBHR,IBSEC
32        integer IEYR,IEMO,IEDY,IEHR,IESEC,IRLG,IRTYPE
33        integer NX,NY,NZ,IWFCOD,NSSTA
34        integer NUSTA,NPSTA,NOWSTA,NLU,IWAT1,IWAT2
35        integer IUTMZN,IDUM,ILANDU_old(numx_old,numy_old)
36        integer NEARS_old(numx_old,numy_old)
37        real DGRID,XORIGR,YORIGR,FEAST,FNORTH
38        real RNLAT0,RELON0,XLAT1,XLAT2,ZFACEM(numz_old+1)
39        real XSSTA_old(nums_old),YSSTA_old(nums_old)
40        real XUSTA_old(numu_old),YUSTA_old(numu_old)
41        real XPSTA_old(nump_old),YPSTA_old(nump_old)
42        real Z0_old(numx_old,numy_old),ELEV_old(numx_old,numy_old)
43        real XLAI_old(numx_old,numy_old)
44        logical LCALGRD
45
46
47         real U_old(numx_old,numy_old,numz_old)
48         real V_old(numx_old,numy_old,numz_old)
49         real W_old(numx_old,numy_old,numz_old)
50         real ZTEMP_old(numx_old,numy_old,numz_old)
51         real USTAR(numx,numy),ZI(numx,numy),EL(numx,numy)
52         real WSTAR(numx,numy),RMM(numx,numy)
53         real TEMPK(numx,numy),RHO(numx,numy),QSW(numx,numy)
54         integer IPGT(numx,numy)
55         integer IRH(numx,numy),IPCODE(numx,numy)
56         integer NDATHRB,NBSEC,NDATHRE,NESEC
57
```

```
58          real U(numx,numy,numz),V(numx,numy,numz),W(numx,numy,numz)
59          real ZTEMP(numx,numy,numz)
60          real z(numz),z_ok(numz+1)
61          integer xy,ILANDU(numx,numy),NEARS(numx,numy),time(tm)
62          real XSSTA(nums),YSSTA(nums)
63          real XUSTA(numu),YUSTA(numu)
64          real XPSTA(nump),YPSTA(nump),Z0(numx,numy)
65          real ELEV(numx,numy),XLAI(numx,numy)
66          character*5 CLABU,CLABV,CLABW,CLABT
67          character*8 CLABUS,CLABZI,CLABSC
68          character*8 CLABL,CLABWS,CLABRMM,CLABTK,CLABD,CLABQ,CLABRH
69          character*8 CLABPC
70          character*3 LABINDEX(numz)
71
72         open (2,FILE='calmet.dat',FORM='unformatted')
73         open (3,FILE='calmet-set.dat',FORM='unformatted')
74
75   c --- Header record #1 - File Declaration -- 24 words
76         read (2) DATASET, DATAVER, DATAMOD
77         write (3) DATASET, DATAVER, DATAMOD
78
79   c --- Header record #2 - Number of comment lines -- 1 word
80         read (2) NCOM
81         write (3) NCOM
82
83   c --- Header record #3 to NCOM+2 (Comment record section) -- 33 words each
84         do i=3,nc+2
85         read (2) comment(i)
86         end do
87
88         do i=3,nc+2
89         write (3) comment(i)
90         end do
91
92   c --- Header record #NCOM+3 - run control parameters -- 39 words
93         read (2) IBYR,IBMO,IBDY,IBHR,IBSEC,
94        *         IEYR,IEMO,IEDY,IEHR,IESEC,AXTZ,IRLG,IRTYPE,
95        *         NX,NY,NZ,DGRID,XORIGR,YORIGR,IWFCOD,NSSTA,
96        *         NUSTA,NPSTA,NOWSTA,NLU,IWAT1,IWAT2,LCALGRD,
97        *         PMAP,DATUM,DATEN,FEAST,FNORTH,UTMHEM,IUTMZN,
98        *         RNLAT0,RELON0,XLAT1,XLAT2
99
100         IBYR=2010
101         IBMO=8
102         IBDY=29
103         IBHR=0
104         IBSEC=0
105         IEYR=2010
106         IEMO=9
107         IEDY=27
108         IEHR=23
109         IESEC=0
110         AXTZ='UTC+0100'
111         IRLG=720
112         NX=125
113         NY=105
114         NZ=11
```

```
115         DGRID=1000
116         XORIGR=1311000
117         YORIGR=4951000
118         NSSTA=1
119         NUSTA=1
120         NPSTA=1
121         NOWSTA=0
122         DATUM='WGS-84'
123         UTMHEM='N'
124         IUTMZN=32
125
126        write (3) IBYR,IBMO,IBDY,IBHR,IBSEC,
127       *          IEYR,IEMO,IEDY,IEHR,IESEC,AXTZ,IRLG,IRTYPE,
128       *          NX,NY,NZ,DGRID,XORIGR,YORIGR,IWFCOD,NSSTA,
129       *          NUSTA,NPSTA,NOWSTA,NLU,IWAT1,IWAT2,LCALGRD,
130       *          PMAP,DATUM,DATEN,FEAST,FNORTH,UTMHEM,IUTMZN,
131       *          RNLAT0,RELON0,XLAT1,XLAT2
132
133 c --- Header record #NCOM+4 - cell face heights (NZ + 1 words)
134       read(2) CLAB1,IDUM,IDUM,IDUM,IDUM,ZFACEM
135
136       open(7,FILE='z_ok.dat')
137       read (7,*) z_ok
138 c      do i=1,numz
139 c       z_ok(i+1)=z(i)
140 c      end do
141 c      z_ok(1)=0
142
143       write(3) CLAB1,IDUM,IDUM,IDUM,IDUM,z_ok
144       close(7)
145
146 c --- Header records #NCOM+5 & 6 - x, y coordinates of surface stations
147 c --- (NSSTA words each record)
148        if(nssta.ge.1)then
149        read (2) CLAB2,IDUM,IDUM,IDUM,IDUM,XSSTA_old
150        read (2) CLAB3,IDUM,IDUM,IDUM,IDUM,YSSTA_old
151        endif
152
153        XSSTA=373000
154        YSSTA=5003000
155
156        if(nssta.ge.1)then
157        write(3) CLAB2,IDUM,IDUM,IDUM,IDUM,XSSTA
158        write(3) CLAB3,IDUM,IDUM,IDUM,IDUM,YSSTA
159        endif
160
161 c --- Header records #NCOM+7 & 8 - x, y coordinates of upper air stations
162 c --- (NUSTA words each record)
163        if(nusta.ge.1)then
164         read (2) CLAB4,IDUM,IDUM,IDUM,IDUM,XUSTA_old
165         read (2) CLAB5,IDUM,IDUM,IDUM,IDUM,YUSTA_old
166         endif
167
168         XUSTA=373000
169         YUSTA=5003000
170
171         if(nusta.ge.1)then
```

```
172         write(3) CLAB4,IDUM,IDUM,IDUM,IDUM,XUSTA
173         write(3) CLAB5,IDUM,IDUM,IDUM,IDUM,YUSTA
174         endif
175
176 c --- Header records #NCOM+9 & 10 - x, y coordinates of precipitation stations
177 c --- (NPSTA words each record)
178         if(npsta.ge.1)then
179         read (2) CLAB6,IDUM,IDUM,IDUM,IDUM,XPSTA_old
180         read (2) CLAB7,IDUM,IDUM,IDUM,IDUM,YPSTA_old
181        endif
182
183         XPSTA=373000
184         YPSTA=5003000
185
186         if(npsta.ge.1)then
187         write(3) CLAB6,IDUM,IDUM,IDUM,IDUM,XPSTA
188         write(3) CLAB7,IDUM,IDUM,IDUM,IDUM,YPSTA
189         endif
190
191
192 c --- Header record #NCOM+11 - surface roughness lengths (NX * NY words)
193
194         read (2) CLAB8,IDUM,IDUM,IDUM,IDUM,Z0_old
195         open(7,FILE='z0.bin',ACCESS='STREAM',FORM='unformatted')
196         read (7) Z0
197         write (3) CLAB8,IDUM,IDUM,IDUM,IDUM,Z0
198         close(7)
199
200 c --- Header record #NCOM+12 - land use categories (NX * NY words)
201       read (2) CLAB9,IDUM,IDUM,IDUM,IDUM,ILANDU_old
202       open (7,FILE='luseok.dat')
203       read (7,*) ILANDU
204       write (3) CLAB9,IDUM,IDUM,IDUM,IDUM,ILANDU
205       close(7)
206
207 c --- Header record #NCOM+13 - elevations (NX * NY words)
208
209       read (2) CLAB10,IDUM,IDUM,IDUM,IDUM,ELEV_old
210         open(7,FILE='rel.bin',ACCESS='STREAM',FORM='unformatted')
211         read (7) ELEV
212        write (3) CLAB10,IDUM,IDUM,IDUM,IDUM,ELEV
213         close(7)
214
215 c --- Header record #NCOM+14 - leaf area index (NX * NY words)
216       read (2) CLAB11,IDUM,IDUM,IDUM,IDUM,XLAI_old
217       open(7,FILE='lai.bin',ACCESS='STREAM',FORM='unformatted')
218       read (7) XLAI
219       write (3) CLAB11,IDUM,IDUM,IDUM,IDUM,XLAI
220       close(7)
221
222 c --- Header record #NCOM+15 - nearest surface station no. to each
223 c --- grid point (NX * NY words)
224        if(nssta.ge.1)then
225        read (2) CLAB12,IDUM,IDUM,IDUM,IDUM,NEARS_old
226        endif
227
228        NEARS=1
```

```
229         if(nssta.ge.1)then
230         write (3) CLAB12,IDUM,IDUM,IDUM,IDUM,NEARS
231         endif
232
233         close(2)
234
235 c --- Read time strings
236       open(7,FILE='tempi_2010_set.dat')
237       read (7,*) time
238       close(7)
239
240 c --- Write label index
241
242         LABINDEX(1)='  1'
243         LABINDEX(2)='  2'
244         LABINDEX(3)='  3'
245         LABINDEX(4)='  4'
246         LABINDEX(5)='  5'
247         LABINDEX(6)='  6'
248         LABINDEX(7)='  7'
249         LABINDEX(8)='  8'
250         LABINDEX(9)='  9'
251         LABINDEX(10)=' 10'
252         LABINDEX(11)=' 11'
253
254         CLABU= 'U-LEV'
255         CLABV= 'V-LEV'
256         CLABW= 'WFACE'
257         CLABT= 'T-LEV'
258         CLABSC= 'IPGT'
259         CLABUS= 'USTAR'
260         CLABZI= 'ZI'
261         CLABL= 'EL'
262         CLABWS= 'WSTAR'
263         CLABRMM= 'RMM'
264         CLABTK= 'TEMPK'
265         CLABD= 'RHO'
266         CLABQ= 'QSW'
267         CLABRH= 'IRH'
268         CLABPC= 'IPCODE'
269
270 c --- Read and write U, V, W wind components
271 c     Loop over vertical layers
272
273         NBSEC=0
274         NESEC=3600
275
276         open(7,FILE='u.bin',ACCESS='STREAM',FORM='unformatted')
277         open(9,FILE='v.bin',ACCESS='STREAM',FORM='unformatted')
278         open(10,FILE='w.bin',ACCESS='STREAM',FORM='unformatted')
279         open(11,FILE='tempk.bin',ACCESS='STREAM',FORM='unformatted')
280         open(12,FILE='pgt.bin',ACCESS='STREAM',FORM='unformatted')
281         open(13,FILE='ustar.bin',ACCESS='STREAM',FORM='unformatted')
282         open(14,FILE='hmix.bin',ACCESS='STREAM',FORM='unformatted')
283         open(15,FILE='l.bin',ACCESS='STREAM',FORM='unformatted')
284         open(16,FILE='wstar.bin',ACCESS='STREAM',FORM='unformatted')
285         open(17,FILE='prec.bin',ACCESS='STREAM',FORM='unformatted')
```

```
286         open(18,FILE='temp1.bin',ACCESS='STREAM',FORM='unformatted')
287         open(19,FILE='rho.bin',ACCESS='STREAM',FORM='unformatted')
288         open(20,FILE='totrad.bin',ACCESS='STREAM',FORM='unformatted')
289         open(21,FILE='irh.bin',ACCESS='STREAM',FORM='unformatted')
290 c        open(22,FILE='ipcode.bin',ACCESS='STREAM',FORM='unformatted')
291
292         h=1
293
294 10     do k=1,numz
295        read (7) ((U(i,j,k),i=1,numx),j=1,numy)
296        write (3) CLABU,LABINDEX(k),time(h),NBSEC,time(h),NESEC,
297       * ((U(i,j,k),i=1,numx),j=1,numy)
298        read (9) ((V(i,j,k),i=1,numx),j=1,numy)
299        write (3) CLABV,LABINDEX(k),time(h),NBSEC,time(h),NESEC,
300       * ((V(i,j,k),i=1,numx),j=1,numy)
301        read (10) ((W(i,j,k),i=1,numx),j=1,numy)
302        write (3) CLABW,LABINDEX(k),time(h),NBSEC,time(h),NESEC,
303       * ((W(i,j,k),i=1,numx),j=1,numy)
304
305        end do
306
307 c --- Read 3-D temperature field
308        if(LCALGRD.and.irtype.eq.1) then
309        do k=1,numz
310        read (11) ((ZTEMP(i,j,k),i=1,numx),j=1,numy)
311        write (3) CLABT,LABINDEX(k),time(h),NBSEC,time(h),NESEC,
312       * ((ZTEMP(i,j,k),i=1,numx),j=1,numy)
313         end do
314         end if
315
316 c --- Read 2-D meteorological fields
317         if(irtype.eq.1) then
318         read (12) IPGT
319         write (3) CLABSC,time(h),NBSEC,time(h),NESEC,IPGT
320         read (13) USTAR
321         write (3) CLABUS,time(h),NBSEC,time(h),NESEC,USTAR
322         read (14) ZI
323         write (3) CLABZI,time(h),NBSEC,time(h),NESEC,ZI
324         read (15) EL
325         write (3) CLABL,time(h),NBSEC,time(h),NESEC,EL
326         read (16) WSTAR
327         write (3) CLABWS,time(h),NBSEC,time(h),NESEC,WSTAR
328         read (17) RMM
329         write (3) CLABRMM,time(h),NBSEC,time(h),NESEC,RMM
330         read (18) TEMPK
331         write (3) CLABTK,time(h),NBSEC,time(h),NESEC,TEMPK
332         read (19) RHO
333         write (3) CLABD,time(h),NBSEC,time(h),NESEC,RHO
334         read (20) QSW
335         write (3) CLABQ,time(h),NBSEC,time(h),NESEC,QSW
336         read (21) IRH
337         write (3) CLABRH,time(h),NBSEC,time(h),NESEC,IRH
338 c       read (22) IPCODE
339         IPCODE=0
340         write (3) CLABPC,time(h),NBSEC,time(h),NESEC,IPCODE
341
342         end if
```

```
343
344         if (h<tm) then
345            h=h+1
346           print *, CLABSC,time(h),NBSEC,time(h),NESEC,IPGT(1,1),h
347            go to 10
348         end if
349
350         close(7)
351         close(9)
352         close(10)
353         close(11)
354         close(12)
355         close(13)
356         close(14)
357         close(15)
358         close(16)
359         close(17)
360         close(18)
361         close(19)
362         close(20)
363         close(21)
364 c        close(22)
365
366 c          do i=1,20
367 c          print *, clabu(i)
368 c          end do
369 c          print *, time
370 c         open(8,FILE='ipgt2.dat')
371 c          write (8,*) ipgt
372         close (3)
373 c        close(8)
374       stop
375       end
```

Appendix 6

Algorithm for source input file creation

As an example, the following is the only text of the algorithm used for the point source emissions generated in the future scenario.

```
      program sources
      implicit none
      integer anno,jul,hour,secini,secfin,i
      character*16 id1,id2,id3,id4,id5
      character*16 idd1,idd2,idd3,idd4,idd5,idd6,idd7,idd8,idd9
      real temp1,vel1,sigy,sigz,flu1,flupm1
      real temp2,vel2,flu2,flupm2
      real temp3,vel3,flu3,flupm3
      real temp4,vel4,flu4,flupm4
      real temp5,vel5,flu5,flupm5
      real temp6,vel6,flu6,flupm6
      real temp7,vel7,flu7,flupm7
      real temp8,vel8,flu8,flupm8
      real temp9,vel9,flu9,flupm9
      real ff1,ff2,ff3,ff4,ff5
      real vv1,vv2,vv3,vv4,vv5
      real tt1,tt2,tt3,tt4,tt5,tempk

      anno=2010
      secini=0
      secfin=3600
      tempk=383
      idd1= 'TOR1'
      idd2= 'TOR2'
      idd3= 'TOR3'
      idd4= 'TOR4'
      idd5= 'TOR5'
      idd6= 'TOR6'
      idd7= 'TON1'
      idd8= 'TON2'
      idd9= 'TOE1'
      open(2,FILE='sources.prn')
      open(3,FILE='ptemarb_ton_toe.dat')
      open(4,FILE='nox_piu_aree.dat')
      open(6,FILE='tsp_piu_aree.dat')
      open(5,FILE='flu_piu_ton.dat')
      temp7=375.0
      temp8=393.0
      temp9=temp8
      do jul=1,365
        do i=1,24
         read (2,*) hour,id1,tt1,vv1,sigy,sigz,ff1
         read (2,*) hour,id2,tt2,vv2,sigy,sigz,ff2
         read (2,*) hour,id3,tt3,vv3,sigy,sigz,ff3
         read (2,*) hour,id4,tt4,vv4,sigy,sigz,ff4
         read (2,*) hour,id5,tt5,vv5,sigy,sigz,ff5
         read (4,*) flu1,flu2,flu3,flu4,flu5,flu6
         read (6,*) flupm1,flupm2,flupm3,flupm4,flupm5,flupm6
         read (5,*) flu7,vel7,flu9,vel9,flu8,vel8,flupm7,flupm9,flupm8
         if (flu8 > 0) then
          vel8=11.8
         else
```

```
53            vel8=0
54           end if
55           if (flu1 > 0) then
56            vel1=5
57           else
58            vel1=0
59           end if
60           if (flu2 > 0) then
61            vel2=5
62           else
63            vel2=0
64           end if
65           if (flu3 > 0) then
66            vel3=5
67           else
68            vel3=0
69           end if
70           if (flu4 > 0) then
71            vel4=5
72           else
73            vel4=0
74           end if
75           if (flu5 > 0) then
76            vel5=5
77           else
78            vel5=0
79           end if
80           if (flu6 > 0) then
81            vel6=5
82           else
83            vel6=0
84           end if
85           if (flu9 > 0) then
86            vel9=11.8
87           else
88            vel9=0
89           end if
90           write (3,*) anno,jul,hour,secini,anno,jul,hour,secfin
91           write (3,*) idd7,temp7,vel7,sigy,sigz,flu7,flupm7
92           write (3,*) idd8,temp8,vel8,sigy,sigz,flu8,flupm8
93           write (3,*) idd9,temp9,vel9,sigy,sigz,flu9,flupm9
94         end do
95       end do
96
97       close(2)
98       close(3)
99       close(4)
100      close(5)
101      close(6)
102      end program
103
```

Appendix 7

Algorithm for calculation of average, maximum and minimum output values

```
clear
load('TSERIES_NOX_1HR_CONC_piu.DAT');
load('TSERIES_NOX_1HR_CONC_meno.DAT');
bil_nox=TSERIES_NOX_1HR_CONC_piu-TSERIES_NOX_1HR_CONC_meno;
con_gen=bil_nox(:,4:9903); %esclude le date
c_gen=reshape(con_gen,[719,100,99]); %riformatta 719=numero ore
c_ass_gen=c_gen; %assegna per il calcolo dei max
c_ass_gen(:); %linearizza
lon=1311500:1000:1435500; %.5 perchÃ¨ Ã¨ al centro cella
lat=4951500:1000:5055500;
for j = 1:5 %impostato per i 5 valori minimi
[m0,i0]=min(c_ass_gen(:)); %fornisce valore e indice
[t0,x0,y0]=ind2sub(size(c_ass_gen),i0); %collega indice a size matrice
xok0=x0+25; %perchÃ¨ la mia griglia parte dalla cella 26
max_gen_abs(j)=m0; %crea matrice  valori minimi
max_gen_abs_tr=max_gen_abs'; %traspone valori minimi
maxpos_gen_abs(j,1)=t0; %crea matrice tempo e posizione dei minimi
maxpos_gen_abs(j,2)=lon(xok0);
maxpos_gen_abs(j,3)=lat(y0);
max_gen_abs_tot=horzcat(max_gen_abs_tr,maxpos_gen_abs);
%unica matrice dei valori minimi
dlmwrite('minpos_nox.dat',max_gen_abs_tot,'delimiter',' ');
%salva su file minimi e posizione
c_ass_gen(t0,x0,y0)=0; %elimina il minimi per trovare il seguente
end
%%Stessa cosa con i MASSIMI
for j = 1:5 %impostato per i 5 valori massimi
[m99,i99]=max(c_ass_gen(:)); %fornisce valore e indice
[t99,x99,y99]=ind2sub(size(c_ass_gen),i99); %collega indice a size
matrice
xok99=x99+25; %perchÃ¨ la mia griglia parte dalla cella 26
mm_gen_abs(j)=m99; %crea matrice  valori massimi
mm_gen_abs_tr=mm_gen_abs'; %traspone valori massimi
mmpos_gen_abs(j,1)=t99; %crea matrice tempo e posizione dei massimi
mmpos_gen_abs(j,2)=lon(xok99);
mmpos_gen_abs(j,3)=lat(y99);
mm_gen_abs_tot=horzcat(mm_gen_abs_tr,mmpos_gen_abs);
%unica matrice dei valori massimi
dlmwrite('maxpos_nox.dat',mm_gen_abs_tot,'delimiter',' ');
%salva su file massimi e posizione
c_ass_gen(t99,x99,y99)=0; %elimina il massimi per trovare il seguente
end
h_max=maxpos_gen_abs(1,1,1);
clear c_ass_gen
clear CONC_gen
clear con_gen
% 2 SALVATAGGIO DELLA CONC MAX COME SURFER GRID
c_max_gen=c_gen(h_max,:,:);
nx=100;
ny=99;
valosum=0; %inizializza le y
lon2=lon(26:125); %estrae solo le coord che ci interessano
```

```
lat2=lat(1:99);
for n=1:ny
 for j=1:nx
valo(j,1)=lat2(n);
 end
valosum=vertcat(valosum,valo); %crea matrice delle y che si ripetono
end
loncat=0; %inizializza le x
for i=1:ny
loncat=horzcat(loncat,lon2); %crea matrice x
end
loncat2=loncat';
consum=0;
con=reshape(c_max_gen,[9900 1]); %linearizza matrice concentr.
consum=vertcat(consum,con); %crea matrice z
xyz_max=horzcat(loncat2,valosum,consum); %crea matrice xyz
xyz_max_ok=xyz_max(2:9901,:); %toglie prima riga
dlmwrite('nox_min.dat',xyz_max_ok,'delimiter',' '); %salva su file
% 3. CALCOLO MEDIA MENSILE E MASSIMI SULLA MEDIA
c_sum_gen=c_gen(1,:,:); %inizializza c_sum
for k=2:719
c_sum_gen= c_sum_gen+c_gen(k,:,:); %somma tutte le celle
end
c_med_gen=c_sum_gen/719; %calcola la media
c_med=c_med_gen; % passa i dati al ciclo per calcolare i max
clear c_sum_gen
c_med(:); %linearizza
for j = 1:5 %impostato per i 5 valori massimi
[m,i]=max(c_med(:)); %fornisce valore e indice
[t,x,y]=ind2sub(size(c_med),i); %collega indice a size matrice
xok=x+25; %perchÃ¨ la mia griglia parte dalla cella 26
maxx_gen_med(j)=m; %crea matrice  valori massimi
maxpos_gen_med(j,1)=t; %crea matrice tempo e posizione dei massimi
maxpos_gen_med(j,2)=lon(xok);
maxpos_gen_med(j,3)=lat(y);
c_med(t,x,y)=0; %elimina il massimo per trovare il seguente
end
maxx_gen_med;
maxpos_gen_med;
% 4. SALVATAGGIO DELLA CONC MEDIA COME SURFER GRID
nx=100;
ny=99;
valosum=0; %inizializza le y
lon2=lon(26:125); %estrae solo le coord che ci interessano
lat2=lat(1:99);
for n=1:ny
 for j=1:nx
valo(j,1)=lat2(n);
 end
valosum=vertcat(valosum,valo); %crea matrice delle y che si ripetono
end
loncat=0; %inizializza le x
```

```
104 for i=1:ny
105 loncat=horzcat(loncat,lon2); %crea matrice x
106 end
107 loncat2=loncat';
108 consum=0;
109 con=reshape(c_med_gen,[9900 1]); %linearizza matrice concentr.
110 consum=vertcat(consum,con); %crea matrice z
111 xyz_med=horzcat(loncat2,valosum,consum); %crea matrice xyz
112 xyz_med_ok=xyz_med(2:9901,:); %toglie prima riga
113 dlmwrite('nox_med.dat',xyz_med_ok,'delimiter',' '); %salva su file
114 % 5. CALCOLO DELLA MEDIA CONSIDERANDO SOLO ORE DIURNE
115 n_ok=6:21; %inizializza serie da estrarre (dalle 6 alle 21)
116 n_ok2=n_ok';
117 for j = 5:4:117 %ciclo che genera array di elementi da estrarre ore
    diurne
118 n=6*j:(6*j)+15;
119 n2=n';
120 n_ok2=vertcat(n_ok2,n2); %accumulo elementi da estrarre
121 end
122 c_gen_day=c_gen(n_ok2,:,:); %matrice conc con solo ore diurne
123 c_sum_gen_day=c_gen_day(1,:,:); %inizializza c_sum_day
124 for h=2:480
125 c_sum_gen_day= c_sum_gen_day+c_gen_day(h,:,:); %somma tutte le celle
126 end
127 c_med_gen_day=c_sum_gen_day/480; %calcola la media
128 c_med_day=c_med_gen_day;
129 clear c_sum_gen_day
130 c_med_day(:); %linearizza
131 for j = 1:5 %impostato per i 5 valori massimi
132 [m2,i2]=max(c_med_day(:)); %fornisce valore e indice
133 [t2,x2,y2]=ind2sub(size(c_med_day),i2); %collega indice a size matrice
134 xok2=x2+25; %perchÃ¨ la mia griglia parte dalla cella 26
135 maxx_gen_day(j)=m2; %crea matrice  valori massimi
136 maxpos_gen_day(j,1)=t2; %crea matrice tempo e posizione dei massimi
137 maxpos_gen_day(j,2)=lon(xok2);
138 maxpos_gen_day(j,3)=lat(y2);
139 c_med_day(t2,x2,y2)=0; %elimina il massimo per trovare il seguente
140 end
141 clear c_gen_day
142 maxx_gen_day;
143 maxpos_gen_day;
144 % 6. SALVATAGGIO DELLA CONC MEDIA DIURNA COME SURFER GRID
145 %nx=100;
146 %ny=99;
147 valosum=0; %inizializza le y
148 %lon2=lon(26:125); %estrae solo le coord che ci interessano
149 %lat2=lat(1:99);
150 for n=1:ny
151  for j=1:nx
152 valo(j,1)=lat2(n);
153  end
154 valosum=vertcat(valosum,valo); %crea matrice delle y che si ripetono
```

```
155 end
156 loncat=0; %inizializza le x
157 for i=1:ny
158 loncat=horzcat(loncat,lon2); %crea matrice x
159 end
160 loncat2=loncat';
161 consum=0;
162 con=reshape(c_med_gen_day,[9900 1]); %linearizza matrice concentr.
163 consum=vertcat(consum,con); %crea matrice z
164 xyz_med_day=horzcat(loncat2,valosum,consum); %crea matrice xyz
165 xyz_med_day_ok=xyz_med_day(2:9901,:); %toglie prima riga
166 dlmwrite('nox_med_day.dat',xyz_med_day_ok,'delimiter',' '); %salva su
    file
167 %%%%%%%%%%%%%%%%%%%%%%%%%%%%%%%%%
168 %%%%%%%%%%%%%%%%%%%%%%%%%%%%%%%%%
169 clear
170 %%STESSA COSA PER LE POLVERI
171 % 1. CALCOLO DEI MASSIMI ASSOLUTI E POSIZIONE
172 load('TSERIES_TSP_1HR_CONC_piu.DAT');
173 load('TSERIES_TSP_1HR_CONC_meno.DAT');
174 bil_tsp=TSERIES_TSP_1HR_CONC_piu-TSERIES_TSP_1HR_CONC_meno;
175 con_gen=bil_tsp(:,4:9903); %esclude le date
176 c_gen=reshape(con_gen,[719,100,99]); %riformatta 719=numero ore
177 c_ass_gen=c_gen; %assegna per il calcolo dei max
178 c_ass_gen(:); %linearizza
179 lon=1311500:1000:1435500; %.5 perchÃ¨ Ã¨ al centro cella
180 lat=4951500:1000:5055500;
181 for j = 1:5 %impostato per i 5 valori minimi
182 [m0,i0]=min(c_ass_gen(:)); %fornisce valore e indice
183 [t0,x0,y0]=ind2sub(size(c_ass_gen),i0); %collega indice a size matrice
184 xok0=x0+25; %perchÃ¨ la mia griglia parte dalla cella 26
185 max_gen_abs(j)=m0; %crea matrice  valori minimi
186 max_gen_abs_tr=max_gen_abs'; %traspone valori minimi
187 maxpos_gen_abs(j,1)=t0; %crea matrice tempo e posizione dei minimi
188 maxpos_gen_abs(j,2)=lon(xok0);
189 maxpos_gen_abs(j,3)=lat(y0);
190 max_gen_abs_tot=horzcat(max_gen_abs_tr,maxpos_gen_abs);
191 %unica matrice dei valori minimi
192 dlmwrite('minpos_tsp.dat',max_gen_abs_tot,'delimiter',' ');
193 %salva su file minimi e posizione
194 c_ass_gen(t0,x0,y0)=0; %elimina il minimi per trovare il seguente
195 end
196 for j = 1:5 %impostato per i 5 valori massimi
197 [m99,i99]=max(c_ass_gen(:)); %fornisce valore e indice
198 [t99,x99,y99]=ind2sub(size(c_ass_gen),i99); %collega indice a size
    matrice
199 xok99=x99+25; %perchÃ¨ la mia griglia parte dalla cella 26
200 mm_gen_abs(j)=m99; %crea matrice  valori massimi
201 mm_gen_abs_tr=mm_gen_abs'; %traspone valori massimi
202 mmpos_gen_abs(j,1)=t99; %crea matrice tempo e posizione dei massimi
203 mmpos_gen_abs(j,2)=lon(xok99);
204 mmpos_gen_abs(j,3)=lat(y99);
```

```
mm_gen_abs_tot=horzcat(mm_gen_abs_tr,mmpos_gen_abs);
%unica matrice dei valori massimi
dlmwrite('maxpos_tsp.dat',mm_gen_abs_tot,'delimiter',' ');
%salva su file massimi e posizione
c_ass_gen(t99,x99,y99)=0; %elimina il massimi per trovare il seguente
end
h_max=maxpos_gen_abs(1,1,1);
clear c_ass_gen
clear CONC_gen
clear con_gen
% 2 SALVATAGGIO DELLA CONC MAX COME SURFER GRID
c_max_gen=c_gen(h_max,:,:);
nx=100;
ny=99;
valosum=0; %inizializza le y
lon2=lon(26:125); %estrae solo le coord che ci interessano
lat2=lat(1:99);
for n=1:ny
 for j=1:nx
valo(j,1)=lat2(n);
 end
valosum=vertcat(valosum,valo); %crea matrice delle y che si ripetono
end
loncat=0; %inizializza le x
for i=1:ny
loncat=horzcat(loncat,lon2); %crea matrice x
end
loncat2=loncat';
consum=0;
con=reshape(c_max_gen,[9900 1]); %linearizza matrice concentr.
consum=vertcat(consum,con); %crea matrice z
xyz_max=horzcat(loncat2,valosum,consum); %crea matrice xyz
xyz_max_ok=xyz_max(2:9901,:); %toglie prima riga
dlmwrite('tsp_min.dat',xyz_max_ok,'delimiter',' '); %salva su file
% 3. CALCOLO MEDIA MENSILE E MASSIMI SULLA MEDIA
c_sum_gen=c_gen(1,:,:); %inizializza c_sum
for k=2:719
c_sum_gen= c_sum_gen+c_gen(k,:,:); %somma tutte le celle
end
c_med_gen=c_sum_gen/719; %calcola la media
c_med=c_med_gen; % passa i dati al ciclo per calcolare i max
clear c_sum_gen
c_med(:); %linearizza
for j = 1:5 %impostato per i 5 valori massimi
[m,i]=max(c_med(:)); %fornisce valore e indice
[t,x,y]=ind2sub(size(c_med),i); %collega indice a size matrice
xok=x+25; %perchÃ¨ la mia griglia parte dalla cella 26
maxx_gen_med(j)=m; %crea matrice  valori massimi
maxpos_gen_med(j,1)=t; %crea matrice tempo e posizione dei massimi
maxpos_gen_med(j,2)=lon(xok);
maxpos_gen_med(j,3)=lat(y);
c_med(t,x,y)=0; %elimina il massimo per trovare il seguente
```

```
257 end
258 maxx_gen_med;
259 maxpos_gen_med;
260 % 4. SALVATAGGIO DELLA CONC MEDIA COME SURFER GRID
261 nx=100;
262 ny=99;
263 valosum=0; %inizializza le y
264 lon2=lon(26:125); %estrae solo le coord che ci interessano
265 lat2=lat(1:99);
266 for n=1:ny
267  for j=1:nx
268 valo(j,1)=lat2(n);
269  end
270 valosum=vertcat(valosum,valo); %crea matrice delle y che si ripetono
271 end
272 loncat=0; %inizializza le x
273 for i=1:ny
274 loncat=horzcat(loncat,lon2); %crea matrice x
275 end
276 loncat2=loncat';
277 consum=0;
278 con=reshape(c_med_gen,[9900 1]); %linearizza matrice concentr.
279 consum=vertcat(consum,con); %crea matrice z
280 xyz_med=horzcat(loncat2,valosum,consum); %crea matrice xyz
281 xyz_med_ok=xyz_med(2:9901,:); %toglie prima riga
282 dlmwrite('tsp_med.dat',xyz_med_ok,'delimiter',' '); %salva su file
283 % 5. CALCOLO DELLA MEDIA CONSIDERANDO SOLO ORE DIURNE
284 n_ok=6:21; %inizializza serie da estrarre (dalle 6 alle 21)
285 n_ok2=n_ok';
286 for j = 5:4:117 %ciclo che genera array di elementi da estrarre ore
    diurne
287 n=6*j:(6*j)+15;
288 n2=n';
289 n_ok2=vertcat(n_ok2,n2); %accumulo elementi da estrarre
290 end
291 c_gen_day=c_gen(n_ok2,:,:); %matrice conc con solo ore diurne
292 c_sum_gen_day=c_gen_day(1,:,:); %inizializza c_sum_day
293 for h=2:480
294 c_sum_gen_day= c_sum_gen_day+c_gen_day(h,:,:); %somma tutte le celle
295 end
296 c_med_gen_day=c_sum_gen_day/480; %calcola la media
297 c_med_day=c_med_gen_day;
298 clear c_sum_gen_day
299 c_med_day(:); %linearizza
300 for j = 1:5 %impostato per i 5 valori massimi
301 [m2,i2]=max(c_med_day(:)); %fornisce valore e indice
302 [t2,x2,y2]=ind2sub(size(c_med_day),i2); %collega indice a size matrice
303 xok2=x2+25; %perchÃ¨ la mia griglia parte dalla cella 26
304 maxx_gen_day(j)=m2; %crea matrice  valori massimi
305 maxpos_gen_day(j,1)=t2; %crea matrice tempo e posizione dei massimi
306 maxpos_gen_day(j,2)=lon(xok2);
307 maxpos_gen_day(j,3)=lat(y2);
```

```
c_med_day(t2,x2,y2)=0; %elimina il massimo per trovare il seguente
end
clear c_gen_day
maxx_gen_day;
maxpos_gen_day;
% 6. SALVATAGGIO DELLA CONC MEDIA DIURNA COME SURFER GRID
%nx=100;
%ny=99;
valosum=0; %inizializza le y
%lon2=lon(26:125); %estrae solo le coord che ci interessano
%lat2=lat(1:99);
for n=1:ny
 for j=1:nx
valo(j,1)=lat2(n);
 end
valosum=vertcat(valosum,valo); %crea matrice delle y che si ripetono
end
loncat=0; %inizializza le x
for i=1:ny
loncat=horzcat(loncat,lon2); %crea matrice x
end
loncat2=loncat';
consum=0;
con=reshape(c_med_gen_day,[9900 1]); %linearizza matrice concentr.
consum=vertcat(consum,con); %crea matrice z
xyz_med_day=horzcat(loncat2,valosum,consum); %crea matrice xyz
xyz_med_day_ok=xyz_med_day(2:9901,:); %toglie prima riga
dlmwrite('tsp_med_day.dat',xyz_med_day_ok,'delimiter',' '); %salva su
file
```